IAHS Publication 318
ISSN 0144-7815

IAHS AISH

Glacier Mass Balance Changes and Meltwater Discharge

Edited by
Patrick Ginot & Jean-Emmanuel Sicart

Glacier Mass Balance Changes and Meltwater Discharge

Edited by:

PATRICK GINOT
IRD Great Ice, La Paz, Bolivia

JEAN-EMMANUEL SICART
IRD Great Ice, Montpellier, France

Proceedings of a workshop on *Andean Glaciology* and a symposium on the *Contribution from Glaciers and Snow Cover to Runoff from Mountains in Different Climates* held during the 7th Scientific Assembly of the International Association of Hydrological Sciences (IAHS) in Foz do Iguaçu, Brazil (4–9 April 2005). The workshop and the symposium were convened by the former IAHS International Commission on Snow and Ice (ICSI), which has since developed into two closely associated organisations: the International Association of Cryospheric Sciences (IACS) and the IAHS International commission on Snow and Ice Hydrology (ICSIH).

IAHS Publication 318
in the IAHS Series of Proceedings and Reports

Published by the International Association of Hydrological Sciences 2007

IAHS Publication 318

ISBN 978-1-901502-39-8

British Library Cataloguing-in-Publication Data.
A catalogue record for this book is available from the British Library.

The papers included in this volume have been peer-reviewed and some were extensively revised by the Editors, in collaboration with the authors, prior to publication.

IAHS is indebted to the employers of the Editors for the invaluable support and services provided that enabled them to carry out their task effectively and efficiently.

Publications in the series of Proceedings and Reports are available from:
IAHS Press, Centre for Ecology and Hydrology, Wallingford, Oxfordshire OX10 8BB, UK
tel: +44 1491 692442; fax: +44 1491 692448; e-mail: jilly@iahs.demon.co.uk

Printed by Alden Group, Oxford, UK.

Preface

Mountain snow cover and glaciers contribute considerably to streamflow in many parts of the world, and modify runoff in terms of quantity, timing and variability. Their role is emphasized in the light of globally increasing freshwater demand and the potential impacts of future climate change. The effect of snow and ice on runoff varies between different climatic regions, such as in the Andes, European Alps or Himalayas. While, for example, in mid and high-latitude areas seasonal snow cover exerts a strong control on runoff variations, in low-latitudes glaciers provide the most dominant source of water during the dry season. Consequently, climate change is expected to trigger different responses in different climatic regimes.

Glaciological investigations in the Andean Cordillera have increased substantially in recent years. A network of glacier mass balance investigations was developed between Ecuador and Southern Patagonia in relation to meteorological and hydrological surveys. Ice core investigations were also performed in various high altitude mountains.

To address these issues, a workshop on Andean Glaciology and a symposium on the Contribution from Glaciers and Snow Cover to Runoff from Mountains in Different Climates were held during the 7th Scientific Assembly of the International Association of Hydrological Sciences (IAHS) in Foz do Iguaçu, Brazil (4–9 April 2005). The workshop and the symposium were convened by the former IAHS International Commission on Snow and Ice (ICSI), which has since developed into two closely associated organisations: the International Association of Cryospheric Sciences (IACS) and the IAHS International commission on Snow and Ice Hydrology (ICSIH).

The importance of these topics was reflected in a large number of contributions to the two events, covering studies in Scandinavia, the Alps, Central and Southern Andes, Asia, North America, Greenland and Antarctica. Selected papers from these meetings have been compiled into: (i) this volume of the IAHS Red Book series, and (ii) a special issue of *Hydrological Processes* (vol. 20, issue 10).

The editors gratefully acknowledge the assistance of the reviewers who made valuable contributions to this volume. We also thank Penny Perrins and Cate Gardner from IAHS Press for their professional approach and help with the processing of the manuscripts.

Patrick Ginot
IRD Great Ice
La Paz, Bolivia

Jean-Emmanuel Sicart
IRD Great Ice
Montpellier, France

Contents

3 Meteorology

1 Hydrology

Glacier Mass Balance Changes and Meltwater Discharge (selected papers from sessions at the IAHS Assembly in Foz do Iguaçu, Brazil, 2005). IAHS Publ. 318, 2007.

Groundwater–surface water exchange in alpine and subalpine watersheds: a review of recent field studies

JAMES WILLIAM ROY* & MASAKI HAYASHI

Department of Geoscience, University of Calgary, Calgary, Alberta T2N 1N4, Canada
jamroy@ucalgary.ca, jim.roy@ec.gc.ca

* now at: *National Water Research Institute, Environment Canada, Burlington, Ontario L7R 4A6, Canada*

Abstract The possibility of a significant role for groundwater exchange with mountain streams and lakes has led to a steadily increasing number of field studies over the past decade. This review is focused on groundwater–surface water (gw–sw) exchange processes in headwater watersheds, mostly in alpine and subalpine areas. It reports on: (i) what field methods have been used or developed over the past decade, and (ii) how field studies over this period have contributed to our understanding of these processes and their effects on hydrology and aquatic ecology. While a number of chemical and thermal methods have been developed, combining these with physical hydrological methods is probably needed to fully realize the finer details of gw–sw exchange in mountainous areas. General conclusions drawn from the assemblage of field studies include that groundwater commonly contributes a substantial amount to alpine streams and that groundwater exchange can also be significant for alpine lakes. Also, locations of gw–sw exchange over many scales tend to be strongly controlled by topography and geology, with coarse deposits (e.g. talus, moraine) playing a dominant role for base flows.

Key words alpine lake; groundwater; headwater; hydrology; mountain

INTRODUCTION

Mountainous areas play an important role in the hydrological cycle throughout the world. These areas typically receive more precipitation than surrounding areas, and thus they can be the initial source of water to rivers and aquifers that supply local communities and those in neighboring lowlands. Additionally, streams descending from the mountains are often used to generate hydroelectric power. The often harsh environmental conditions of alpine and subalpine regions result in unique ecosystems that are sensitive to changes in the hydrological and biogeochemical cycles. The levels of nutrients (e.g. ammonium, silica, and phosphorus) required by algae and aquatic plants, and surface water temperatures, which can affect benthic invertebrate and fish spawning habitat, depend on the pathways and rates of water flow through the watershed. Hauer *et al.* (1997) suggest that mountain streams and lakes may be among the most sensitive indicators of changing global climate.

The interaction between surface water and groundwater has a strong influence on the hydrological and hydrochemical characteristics of mountain streams and lakes, as indicated by the growing body of literature in recent years. This paper presents a review of field studies published mostly within the past decade or so, focusing specifically on the groundwater–surface water (gw–sw) exchange in alpine and subalpine

headwater watersheds; i.e. areas characterized by steep and rugged topography, minimal soil development and forest cover. The hydrology of these areas is generally dominated by snow and glacier ice melt. Some studies conducted at lower elevations will be included where research at higher elevations is lacking. This paper is not intended to be a comprehensive and exhaustive review covering all geological and climatic environments of mountains. Most notably, studies in karstic terrain are excluded, even though a significant body of literature exists on this topic (e.g. Bakalowicz, 2005).

It has taken a long time for hydrologists to focus on mountainous areas, probably because of the many problems of data collection, including accessibility, accuracy, and representativeness (Klemes, 1990). This is especially true for headwater watersheds in alpine areas, where the high relief, rough topography, generally thin overburden materials and high variability in permeability result in a unique set of conditions. The hydrological cycle is further complicated by the many possible water inputs, including rain events, condensation and the melting of snow, glacier ice or permafrost. Additionally, there is the possibility of very fast flow, i.e. shallow flow under large gradients, but also very slow flow, i.e. deep into the Earth with the discharge of geologically old water, and both types may not be under steady-state conditions (Silar, 1990).

In 1990, proceedings were published from two IAHS conferences devoted to the topic of mountain hydrology: Publication 190 (Molnar, 1990) and Publication 193 (Lang & Musy, 1990). Despite the large number of field-based studies reported in these volumes, the role of groundwater was seldom specifically addressed. Meanwhile, Winter & Woo (1990) noted that comprehensive water balance studies of lakes in mountainous areas had not been done.

By 1993, "there [was] growing recognition that watershed process studies should include examination of groundwater" (Goodrich & Woolhiser, 1993, in Winter *et al*., 2003), including the possible exchange with mountain streams and lakes. Consequently, the past decade has witnessed a steadily increasing number of studies on groundwater–surface water (gw–sw) exchange in mountain regions.

The purpose of this review is two-fold. The first section reports on what methods have been used or developed over the past decade to monitor gw–sw exchange processes. The second section addresses how the field studies performed over the past decade have contributed to our conceptual understanding of gw–sw exchange and its effects on hydrology and aquatic ecology of the alpine and subalpine systems. As this review is focused on the past decade of field research in mountainous regions, the reader is directed to reviews by Winter *et al.* (1998), Sophocleous (2002) and Hayashi & Rosenberry (2002) for background on general gw–sw exchange processes, and the work of Winter (1976) and Forster & Smith (1988a,b) for general theory of groundwater flow as applied to watersheds in mountainous regions. Due to the specific focus on gw–sw exchange, this paper does not cover groundwater processes that are not explicitly linked to surface water, such as the possible sources for groundwater (snow, rain, glacier, permafrost) or subsurface storage capacity.

HYDROLOGICAL FIELD METHODS

This section draws primarily from the studies conducted in a few well-instrumented field locations, such as the Rocky Mountains in Colorado (e.g. Loch Vale), the Sierra

Nevada (e.g. Emerald Lake), Californa, USA, the Swiss Alps (e.g. Val Roseg), and our own study at the Lake O'Hara watershed in the Canadian Rockies (Hood *et al.*, this issue).

Physical flow measurements

While the position of ponds or lakes within the hydrological landscape may be used to help delineate discharge and recharge areas (e.g. Campbell *et al.*, 2004), traditional quantitative methods consist of direct head and flow measurements. Rosenberry & Winter (1993) used wells to determine head values and measured flow across the sediment boundary of Mirror Lake using seepage meters. However, unlike the conditions at Mirror Lake, which is underlain by up to 24 m of glacial drift, it is usually difficult to impossible to install common groundwater monitoring devices in high elevation headwater watersheds. In addition, it is difficult to characterize the hydraulic properties of the media, which often consist of fractured rock, partially overlain by rocky till or talus. Researchers rarely have access to geological cores, and geophysical techniques are often plagued by rough topography and rocky surfaces.

As a result, hydrologists have commonly relied upon volumetric balance measurements of surface water bodies (e.g. Kattelmann & Elder, 1991). Any difference in the groundwater inflow and outflow fluxes is calculated from the residual of the surface water inflow and outflows, considering direct precipitation inputs, evapotranspiration outputs and changes in storage. Substantial gw–sw exchange may be masked if the groundwater inflow and outflow are similar. Additionally, Verry (2003) notes that groundwater passing beneath or around surface water control structures and out of the watershed may be significant, but is often overlooked. Over the past decade, direct techniques have generally been replaced or partnered with indirect techniques, such as thermal/chemical balances or tracer methods.

Thermal, chemical, and isotopic tracers

One of the most promising developments in identifying surface waters receiving groundwater is the use of temperature-based methods. The measurements themselves are relatively simple and inexpensive, but can provide continuous data at nearly any location. Their usefulness derives from the fact that surface waters can experience large temperature variations, while groundwater tends to have a more constant temperature. Thus, groundwater is often colder than surface waters in summer, but warmer in winter. Given this trend, diurnal temperature variations in surface waters and vertical temperature gradients in their sediments, have been used to locate groundwater discharge (up-welling) and recharge (down-welling) portions of streams (e.g. Constantz, 1998; Story *et al*., 2003). Also, Katsuyama *et al.* (2005) used changes in stream temperature with a rise in the water table, as one indication of a change in groundwater flow path, from flow through bedrock to predominantly shallow flow along the bedrock surface. Similarly, Uehlinger *et al*. (2003) used thermal patterns to differentiate the streams of a glacial river corridor based on different sources, which included groundwater.

For areas with reasonable access to the upper reaches of the watershed, artificial tracers (usually salts or dyes) can be added to delineate up-welling and down-welling zones and to quantify rates of exchange or timing of flow. Harvey & Bencala (1993) and Morrice *et al.* (1997) used field tracer-tests to explore surface–subsurface water exchange in mountain streambeds, though the sensitivity of this method may be flow-dependent and biased towards zones of fast exchange (Harvey *et al.*, 1996). Alternatively, Clow *et al.* (2003) introduced a tracer into a gaining mountain stream to calculate the groundwater input based on the amount of dilution.

Many naturally-occurring isotopic and chemical tracers have also proven useful for determining sources of water, especially in remote areas (Clow *et al*., 2000). One use of natural tracers is for age-dating. Tritium, chlorofluorocarbons (CFCs), and ^{14}C are useful for ages ranging from years to a thousand years, while ^{35}S derived from atmospheric sources may be better for a year or less (Sueker *et al*., 1999). For example, a reduction in ^{35}S has been used by Sueker *et al.* (1999) and Michel *et al.* (2000) to indicate a greater contribution of groundwater to mountain streams. Meanwhile, Rademacher *et al.* (2005) determined the ages of different springs using CFC concentrations and the ratio of tritium to helium.

A more widespread use of natural tracers is for differentiating sources or pathways based on spatial or temporal changes in the stream/lake chemical signature. Variations in natural isotopes, such as ^{18}O, have been shown to differ for different sources of water. For example, in the Bow Valley, Alberta, Canada, average values for snow, ice, rain and stream base flow were –22.2, –20.9, –12.6 and –20.5, respectively (Hopkinson & English, 2001). Different source areas have also been identified using the chemical character of dissolved organic carbon (Hood *et al.*, 2003; Lafreniere & Sharp, 2003), as plant/soil sources can be separated from algae/microbial sources. Similarly, Sueker *et al.* (2001) found that alkalinity and silica were correlated with old debris and soils, while calcite and nitrogen correlated with new debris and talus slopes (little vegetation and fresh exposure of mineral surfaces).

Other tracers in the water can provide information on groundwater pathways or the relative contribution of groundwater to a stream or lake. Tracers used for this purpose include strontium (especially the ratio $^{87}Sr/^{86}Sr$) (Clow *et al.*, 1997), specific conductance, turbidity, major cations/anions and silica (Ward *et al.*, 1999), and base cations and alkalinity (Clow & Sueker, 2000). More moderated fluctuations in chemical signatures compared to discharge may indicate that shallow groundwater is contributing substantially to stream water during the snow melt (e.g. Campbell *et al*., 1995).

Hydrograph analysis and hydrological modelling

Natural tracers are also used in the hydrograph separation technique – a mass balance approach to separate stream water into different components. Separating two components requires one tracer, while separating three components requires two tracers. Mast *et al.* (1995) used hydrograph separation with ^{18}O and silica, individually, to separate the contributions of snow melt and old water. Sueker *et al*. (2000) stressed the importance of distinguishing between source (snow, rain, groundwater) and path (reacted–slow, unreacted–fast) using different tracers. They used sodium in a two-

component model to distinguish the pathway, and sodium and ^{18}O in a three-component model to distinguish source. However, they found that temporal variability in source concentration probably disrupted their hydrograph separation analysis. They note that this can be accounted for, but the required amount of spatial and temporal data is difficult to obtain over large areas. However, Huth *et al.* (2004) actually measured the changing isotopic signature of melting snow and accounted for it in their hydrograph separation analysis. Liu *et al.* (2004) also had difficulties with their hydrograph separation using ^{18}O and solutes, due to violations of a number of the mixing-model assumptions. They suggested that physical measurements may be needed in future studies, as hydrograph separation may not be able to distinguish the sources and paths on its own. As the scale of analysis increases, the determination of a representative value for ground and soil water will likely become even more problematic due to temporal and spatial variability in the pathways for flow and the rate of transport. The reader is referred to Rice & Hornberger (1998) and Taylor *et al.* (2002) for detailed analyses of problems with hydrograph separation.

Along the same lines as the hydrograph separation technique, chemical mass balances or flux measurements have also been applied to lakes and entire watersheds in the mountains. For instance, Gurrieri & Furniss (2004) calculated the input and output of groundwater for four alpine lakes using a solute tracer mass-balance. Meanwhile, Lafreniere & Sharp (2005) measured total solute fluxes for two watersheds to compare their sources of water and residence times, and to investigate their responses to different weather patterns.

The method that has received new attention recently is the analysis of mountain stream hydrographs. Vitvar *et al.* (2002) describe a method for estimating base flow residence times from the runoff hydrograph recession curve. The analysis is based on an exponential decline in base flow following rainfall as the hydraulic gradients in the surrounding slopes decline. A similar analysis was employed by Tague & Grant (2004). Manga (1999) used input–output models, spectral analysis and time series analysis on spring hydrographs to calculate three different times scales for groundwater flow, which can provide insight into long- and short-term trends in spring discharge. Hydrographs for two streams flowing into Bow Lake, Alberta, Canada, underwent wavelet analysis by Lafreniere & Sharp (2003) to distinguish sources of water and the variability in these sources between years**.** They note that, unfortunately, the analysis could not distinguish changes in flow paths or routes to the stream.

The last major method of analysing field data from studies of gw–sw exchange in mountain environments is computer modelling. Researchers have recently begun using computer models to study hyporheic exchange at the scale of the stream section (e.g. Kasahara & Wondzell, 2003). Additionally, the groundwater component is now routinely included in models addressing watershed-scale hydrology (e.g. Singh & Bengtsson, 2005). However, a full review of these studies is beyond the scope of this paper. It is interesting to note, though, that simulations using simpler, conceptual-based models, following calibration, are still often as good as or better than those using more complicated, physically-based models (Zappa *et al.*, 2003). While useful for prediction, these simpler models do not help improve our understanding of gw–sw exchange processes. However, improvements in these models will likely continue, even though complexity and scale issues make the task quite daunting.

CONCEPTUAL UNDERSTANDING THROUGH FIELD STUDIES

Local-scale exchange of groundwater and surface water

Groundwater–surface water exchange can be considered on a number of spatial scales. We first consider the hyporheic zone exchange of stream water with the surrounding geologic materials along a stream section with relatively homogeneous geology. Along an individual stream, Harvey & Bencala (1993) showed that there is much hyporheic exchange as a result of the rocky beds, steep slopes and rough microtopography. They showed that stream water enters the ground at the downstream end of a pool and returns to the stream at the upstream end of the next pool, bypassing the step section in between (Fig. 1). Morrice *et al.* (1997) compared gw–sw exchange for three mountain streams in alluvial beds and noted a trend of increasing exchange with greater hydraulic conductivity of the bed materials. Similar work on hyporheic exchange of mountain streams flowing in alluvial beds has improved our understanding (e.g. Wondzell & Swanson, 1996; Battin, 1999; Kasahara & Wondzell, 2003; and others). One stream in the study of Morrice *et al.* (1997) had an alluvium consisting of boulders, gravel and sand, more typical of high elevation headwater watersheds. Tracer test data indicated substantial exchange throughout the reach and a discharge threshold above which the effect of gw–sw exchange on solute transport becomes less significant. These findings suggest that the nature of hyporheic exchange for alpine streams in boulder and bedrock beds deserves greater attention.

Research has shown that mountain streams also exhibit both gaining and losing reaches along their length, behaviour that is controlled by larger scale topographic and

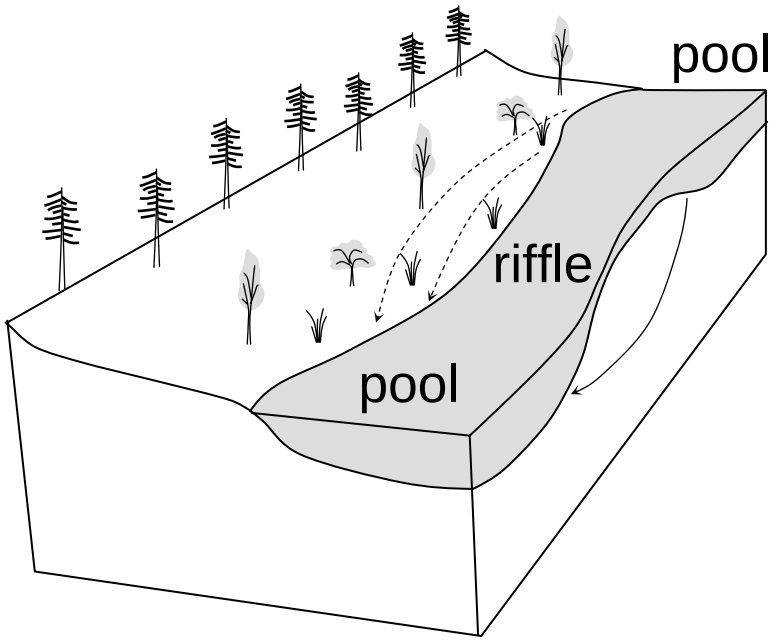

Fig. 1 Schematic diagram of groundwater–surface water exchange within the hyporheic zone, with flow induced by a pool-step sequence. Solid arrow indicates groundwater flow path on vertical cross-section; dashed arrows indicate subsurface flow patterns projected on the surface. (after Hayashi & Rosenberry, 2001, with permission from the Japanese Association of Groundwater Hydrology).

geologic factors. For example, Ward *et al*. (1999) noted that a bedrock constriction (lateral and depth) caused groundwater up-welling into a stream, as indicated by increases in specific conductance and ion concentrations. Subsequent widening of the bedrock valley led to groundwater down-welling. Streams flowing across alluvial fan deposits at the edges of valleys commonly lose water to groundwater (Winter *et al*., 1998). Story *et al*. (2003) noted decreases in temperature linked to groundwater discharge zones, with some evidence of hyporheic exchange. Clow *et al*. (2003) measured increases in stream discharge linked to groundwater discharge from areas with talus slopes. Winter *et al*. (1998) also note that wetlands and springs are commonly found at the base of slopes, an indication of groundwater discharge areas, which we have also observed in the Lake O'Hara watershed.

Groundwater contribution to stream flow

Streams in mountainous areas generally gain more groundwater than they lose due to the large hydraulic gradient from adjacent slopes. Field studies performed over the past decade have proven that the groundwater contribution to these streams is often substantial (Campbell *et al*., 1995; Ward *et al*., 1999; Michel *et al*., 2000; Sueker *et al*. 2000; Clow *et al*., 2003; Huth *et al*., 2004; Liu *et al*., 2004). In addition to dominating base flow (e.g. review by Winter *et al*., 1998; Ward *et al*., 1999), much of the water contributed during high flows following snowmelt or rain events also passes through the ground (Mast *et al*., 1995; Clow *et al*., 2000; Sueker *et al*. 2000; Huth *et al*., 2004). The percentage contribution from groundwater has been reported as high as 60% by Liu *et al*. (2004), greater than 75% during storms and the winter base flow period by Clow *et al*. (2003), and from 80 to 100% for snowmelt in three high-elevation basins (Huth *et al*., 2004). In a study of six basins, Sueker *et al*. (2000) calculated that subsurface water accounted for 37–54% of May–October stream flow in five of the basins, and 89% in the sixth. This last basin had extensive surficial debris and shallow slopes, in comparison to the other basins. Most of these values are based on chemical data sets (often hydrograph separation) and contain a fair amount of uncertainty, but together they are providing a portrait of a strongly groundwater-affected system.

Influence of geology

Geology has also been shown to play a prominent role in the relative contribution of groundwater to mountain streams. Tague & Grant (2004) show that summer baseflows in streams within the Williamette River basin in Oregon are linked to geo-hydrological landscapes, in this case, the proportion of Western Cascade to High Cascade provinces (differentiated based on the age of underlying bedrock). A higher proportion of High Cascade landscape in a stream's watershed results in higher summer base flows. In addition, their stream hydrograph analyses suggest that geology has a strong direct (i.e. via flow path, hydraulic gradient and conductivity) control on long-term stream response throughout the year, with Western Cascade dominated by a well-developed network of shallow groundwater flow paths and High Cascade having a deeper groundwater system with some shallow flow paths activated during high flow periods.

Bedrock is the dominant geologic material, often with substantial surface exposure, in alpine and even sub-alpine areas of the mountains. Hence, it is not difficult to understand why groundwater contributions may have originally been assumed negligible. However, observations of springs and the maintenance of stream base flow suggested the amount could not be zero. Parriaux & Nicoud (1988) analysed the hydrological properties of glacial deposits in mountain areas and suggested that lateral and end moraines would dominate the role of supplying base flow. However, there was a lack of field investigation to support or refute these suggestions. Field studies over the past decade have helped identify the geologic materials contributing to gw–sw exchange. The findings suggest that flow through overburden materials dominates over flow through bedrock (Ward *et al*., 1999; Caballero *et al*., 2002; Clow *et al*., 2003; Winter, 2003), even if fractured. That is not to say that flow in fractured rock is not important, as Katsuyama *et al*. (2005) observed flow through weathered granite, but the discharge to the stream increased markedly when flow through the soil above commenced. Spring flow from rock in the Cascades has also been reported (Manga, 1999).

Subsurface runoff from hillslope to streams

Streams receiving groundwater discharge may respond differently to precipitation or melt events due to the types of groundwater flow paths feeding them. These tend to be designated as “fast” or “slow” for simplicity. For bedrock hillslopes covered by thin soils, fast flow paths likely include pseudo-overland flow within the litter layer on the soil surface; lateral flow along the soil–bedrock interface; and interflow once the water table rises, following vertical infiltration, into the more transmissive soil (fill and spill concept) (Fig. 2, point (a)). Slow flow occurs through the fractured bedrock (Fig. 2, point (c)). This conceptual model for hillslope hydrology (Becker & McDonnell, 1998; Weiler & McDonnell, 2004) is based primarily from field work at lower elevations but likely applies to some areas at higher elevations as well. For areas with substantial talus or moraine materials, Clow *et al*. (2003) provide evidence of a high permeability top layer that can account for fast flow following events (Fig. 2, point (b)), and a low permeability matrix at depth that can release water slowly and maintain base flows (Fig. 2, point (d)). Clow *et al*. (2003) indicate that seepage originating from tarns and ponds, and the melting of ice (glaciers, permafrost) can also help maintain base flows in streams, as suggested by an analysis of the source of local springs. At the Lake O’Hara site, there are a number of small glaciers, yet their melt water does not enter Lake O’Hara directly through surface water routes. Instead, the inlet streams are sourced by smaller lakes up-valley or by groundwater, which in turn are likely sourced through melting snow and glacier ice.

An important development over the past decade is the recognition that the groundwater contribution is usually variable in both time and space and, thus, groundwater signatures are not constant. These changes have been linked to changes in the mixing of different flow paths or in the flow paths themselves (e.g. residence time increasing with declining hydraulic gradient). Ward *et al*. (1999) identified three groundwater aquifer types – sub-glacial, flood plain, tributary (sides) – in a glacial

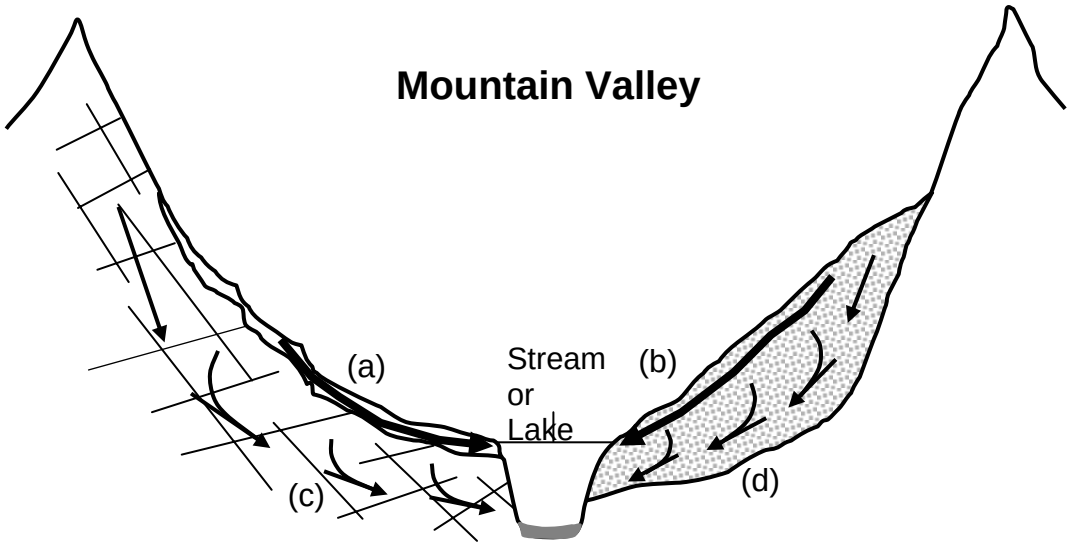

Fig. 2 Schematic diagram representing a conceptual model of the major groundwater sources for streams and lakes formed in bedrock valleys in mountainous headwater catchments. They may receive groundwater quickly from shallow flow paths, which consist of: (a) hillslope flow paths along the top of bedrock, through shallow soils; and (b) the more permeable surface layers of talus or moraine materials. They may receive groundwater slowly (base flow) from deeper flow paths, which consist of: (c) inter-connected bedrock fractures; and (d) the less permeable deep layers of talus or moraine materials.

flood plain in the Swiss Alps, which they differentiated using silica and specific conductance measurements. Katsuyama *et al.* (2005) provided evidence using solute levels and temperature, of groundwater flow originating initially from bedrock, and then with a rising water table, shifting to flow through the soil along the top of the bedrock. Using chemical and age-dating techniques on a stream and nearby springs, Rademacher *et al.* (2005) showed that groundwater properties and residence time varied markedly depending on location on the slope and the season. More research in high elevation headwater watersheds is required to determine how variable groundwater is in areas with minimal soil or alluvial materials, but dominated by talus and bedrock.

The developing conceptual model of gw–sw exchange from the reach to watershed scale provides a framework for improving our simulation of the hydrological behaviour of high elevation mountain watersheds. It does not yet seem sufficient though, especially concerning the role of lakes within the watersheds, to allow for appropriate predictions in ungauged watersheds.

Exchange of groundwater with mountain lakes

Mountain lakes have received much less attention than mountain streams in hydrological studies. Perhaps it has been assumed that any exchange between the lake and groundwater was negligible, since many are cirque lakes occupying a bedrock basin (Winter *et al.*, 1998). However, groundwater piping through moraine dams has been implicated in some dam outbursts (see review by Clague & Evans, 2000). Of the

limited hydrology-based field studies performed, most have been published in the last few years.

Although Mirror Lake in the White Mountains is not located in a high-elevation alpine or sub-alpine zone, it is included in this review because of the scarcity of studies on groundwater exchange with lakes in mountain environments. It is also the site of one of the first hydrological field studies on a mountain lake that explicitly addressed the role of groundwater. Rosenberry & Winter (1993) used head measurements around the lake and seepage measurements along the bottom of the lake to show that Mirror Lake receives groundwater from higher elevations and loses water to the ground at the valley-end of the lake, i.e. it is a flow-through lake. The data also suggested that most of the exchange occurred with the underlying glacial drift sediments, with little flow through the fractured bedrock.

Half a decade later, two reviews of gw–sw exchange (Winter *et al*., 1998; Winter, 1999) covered aspects of groundwater exchange with mountain lakes, but no new studies were reported. However, both stressed the key influences of topography, lake depth, geology and climate (recharge, lake level, transpiration) on the amount and locations of groundwater exchange with mountain lakes.

Over the next few years, studies on a number of mountain lakes indicated that they possess minimal gw–sw exchange. Michel *et al.* (2002) studied two small lakes overlying fractured basalt in the Flattops Wilderness Area, Colorado, USA. They concluded that processes such as groundwater input or evaporation were not important in these lakes because there was no increase in the concentrations of sulphate and other dissolved constituents following the spring freshet. We note that this conclusion is based on an assumption that groundwater should possess higher ion concentrations, though only measurements from a single nearby spring were made. Similarly, in reviewing the hydrological studies on Loch Vale, Colorado, USA, and Emerald Lake, California, USA, both high altitude lakes, Winter (2003) determined both to be surface water dominated (nearly exclusively).

In contrast, during a field study on acidification of subalpine ponds and lakes in northwestern Colorado, Campbell *et al*. (2004) determined that some ponds possessed a higher acid-neutralizing capacity, which they attributed to groundwater inputs. Likewise, in studying four alpine lakes in Montana, USA, using a tracer mass-balance method, Gurrieri & Furniss (2004) suggested that all four possessed gw–sw exchange, with three supposedly being flow-through lakes, and one being a groundwater recharge lake. Unfortunately, neither study contained sufficient data to allow accurate quantification of the groundwater exchange.

The difference in the importance of gw–sw exchange for mountain lakes, as reported in the above studies, suggests substantial variation between locations. Hydrological position within the landscape and the geology bounding the lake are likely key factors. However, a review of these studies also suggests more detailed investigations, combining direct and indirect methods, of the processes and factors involved, are warranted.

Recently, a water balance study was conducted for Lake O'Hara, in British Columbia, Canada (Hood *et al*., this issue). The water balance showed that a large portion of the water output was unaccounted for by storage change and surface water inflow. Evaporation and precipitation were relatively minor components in the water

balance. Assuming that the residual of the water balance represents net groundwater input (i.e. there was no groundwater output), the groundwater input contributed 25–40% of the total input during snowmelt and 35–50% after snowmelt.

Role of groundwater in alpine eco-hydrology

In addition to its role within watershed hydrology, groundwater exchange with mountain streams and lakes has also received attention in many eco-hydrology studies. Surface water properties such as flow, turbidity, temperature, pH, dissolved silica content and alkalinity, among others, can affect the aquatic ecology and can be affected by gw–sw exchange, particularly groundwater discharge, as indicated by the use of chemical/thermal methods described above. For example, Ward *et al*. (1999) differentiated the streams in a glacial flood plain of the Swiss Alps based on the contribution of groundwater. They noted that groundwater streams tended to have higher nitrate levels. They also determined that invertebrate densities were two to six times higher in groundwater-fed channels than all other types. Similarly, Fureder *et al.* (2001) found higher taxa richness and *Chironmid* abundance in a spring-fed stream compared to a glacier-fed stream. Malard *et al*. (2003) found increasing taxonomic abundance downstream of a groundwater up-welling zone. Also in the Alps, Uehlinger *et al*. (2003) observed different temperature patterns for streams with different sources. While the temperature of glacier-fed streams gradually declined over the summer, the groundwater streams warmed. These researchers suggested that thermal heterogeneity on the flood plain may lead to higher biodiversity. This research is primarily focused on alluvial-filled valleys in the Swiss Alps, but it shows how groundwater discharge can affect aquatic ecosystems. More work is needed on eco-hydrology in headwater watersheds to determine if similar groundwater effects are occurring in these sensitive ecosystems.

CONCLUDING REMARKS

Over the past decade, significant strides have been made at identifying and quantifying the key hydrological processes in alpine and subalpine environments. During this time, the importance of groundwater–surface water (gw–sw) exchange has been demonstrated through numerous field studies. Groundwater contributes substantially to mountain streams, both during peak and base flows, and can influence local aquatic ecosystems. Geologic and topographic properties have been shown to control gw–sw exchange both at the local scale (hyporheic exchange) and watershed scale. A conceptual model of fast and slow groundwater flow to adjacent streams from bedrock hillslopes and talus/moraine materials is developing, but needs to be tested at more headwater watershed sites at high elevations. There are far fewer field studies involving gw–sw exchange for mountain lakes, with some reporting negligible exchange and others indicating substantial exchange. For lakes, there is a general lack of understanding of the controlling factors, which suggests that more research is needed.

Despite the difficulty in making measurements in alpine and subalpine watersheds, this literature review indicates that there is a wide range of techniques and analysis

methods available to researchers. A call for more complete data sets and studies that combine physical and chemical/thermal methods has been made to fully realise the finer details of gw–sw exchange. This field-derived data is crucial to our ability to up-scale this behaviour for use in regional hydrological models and, eventually, global climate models.

Acknowledgements Funding was provided by the University of Calgary G8 Chair in Wildlife Ecology and the Natural Sciences and Engineering Research Council of Canada. We thank two anonymous reviewers for valuable comments that greatly improved the manuscript.

REFERENCES

Bakalowicz, M. (2005) Karst groundwater: a challenge for new resources. *Hydrogeol. J.* **13**,148–160.

Battin, T. J. (1999) Hydrologic flow paths control dissolved organic carbon fluxes and metabolism in an alpine stream hyporheic zone. *Water Resour. Res.* **35**(10), 3159–3169.

Becker, A. & McDonnell, J. J. (1998) Topographical and ecological controls of runoff generation and lateral flows in mountain catchments. In: *Hydrology, Water Resources and Ecology in Headwaters* (ed. by K. Kovar, U. Tappeiner, N. E. Peters & R. G. Craig), (HeadWater '98 Conf., Meran/Merano, Italy, April 1998), 199–206. IAHS Publ. 248. IAHS Press, Wallingford, UK.

Caballero, Y., Jomelli, V., Chevallier, P. & Ribstein, P. (2002) Hydrological characteristics of slope in high tropical mountains (Cordillera Real, Bolivia). *Catena* **47**(2), 101–116.

Campbell, D. H., Clow, D. W., Ingersoll, G. P., Mast, M. A., Spahr, N. E. & Turk, J. T. (1995) Processes controlling the chemistry of two snowmelt-dominated streams in the Rocky Mountains. *Water Resour. Res.* **31**(11), 2811–2821.

Campbell, D. H., Muths, E., Turk, J. T. & Corn, P. S. (2004) Sensitivity to acidification of subalpine ponds and lakes in north-western Colorado. *Hydrol. Processes* **18**, 2817–2834.

Clague, J. J. & Evans, S. G. (2000) A review of catastrophic drainage of moraine-dammed lakes in British Columbia. *Quat. Sci. Rev.* **19**, 1763–1783.

Clow, D. W. & Sueker, J. K. (2000) Relations between basin characteristics and stream water chemistry in alpine/subalpine basins in Rocky Mountain National Park, Colorado. *Water Resour. Res.* **36**(1), 49–61.

Clow, D. W., Mast, M. A., Bullen, T. D. & Turk, J. T. (1997) Strontium 87/strontium 86 as a tracer of mineral weathering reactions and calcium sources in an alpine/subalpine watershed, Loch Vale, Colorado. *Water Resour. Res.* **33**(6), 1335–1351.

Clow, D. W., Campbell, D. H., Mast, M. A., Striegl, R. G., Wickland, K. P. & Ingersoll, G. P. (2000) Loch Vale, Colorado: A water, energy, and biogeochemical budgets program site. *US Geological Survey Fact Sheet-164-99*.

Clow, D. W., Schrott, L., Webb, R., Campbell, D. H., Torizzo, A. & Dornblaser, M. (2003) Groundwater occurrence and contributions to streamflow in an alpine catchment, Colorado Front Range. *Groundwater* **41**(7), 937–950.

Constantz, J. (1998) Interaction between stream temperature, streamflow, and groundwater exchange in alpine streams. *Water Resour. Res.* **34**(7), 1609–1615.

Forster, C. & Smith, L. (1988a) Groundwater flow systems in mountainous terrain 1. Numerical modeling technique. *Water Resour. Res.* **24**(7), 999–1010.

Forster, C. & Smith, L. (1988b) Groundwater flow systems in mountainous terrain 2. Controlling factors. *Water Resour. Res.* **24**(7), 1011–1023.

Fureder, L., Schutz, C., Wallinger, M. & Burger, R. (2001) Physico-chemistry and aquatic insects of a glacier-fed and a spring-fed alpine stream. *Freshwater Biol.* **46**, 1673–1690.

Goodrich, D. C. & Woolhiser, D. A. (1993) Catchment hydrology. US National Report to International Union of Geodesy and Geophysics. *Reviews of Geophysics Supplement*, 202–209.

Gurrieri, J. T. & Furniss, G. (2004) Estimation of groundwater exchange in alpine lakes using non-steady mass-balance methods. *J. Hydrol.* **297**, 187–208.

Harvey, J. W. & Bencala, K. E. (1993) The effect of streambed topography on surface-subsurface water exchange in mountain catchments. *Water Resour. Res.* **29**(1), 89–98.

Harvey, J. W., Wagner, B. J. & Bencala, K. E. (1996) Evaluating the reliability of the stream tracer approach to characterize stream-subsurface water exchange. *Water Resour. Res.* **32**(8), 2441–2451.

Hayashi, M. & Rosenberry, D. O. (2001) Effects of groundwater exchange on the hydrology and ecology of surface water. *J. Groundwater Hydrol.* **43**, 327–341.

Hayashi, M. & Rosenberry, D. O. (2002) Effects of groundwater exchange on the hydrology and ecology of surface water. *Groundwater* **40**(3), 309–316.

Hood, J. L., Roy, J. W. & Hayashi, M. (2007) Preliminary assessment of groundwater contribution to the hydrology of an alpine lake in the Canadian Rockies. In: *Proc. VIIth IAHS Scientific Assembly* (3–9 April, 2005, Foz do Iguaçu, Brazil) (this issue).

Hood, E., McKnight, D. M. & Williams, M. W. (2003) Sources and chemical character of dissolved organic carbon across an alpine/subalpine ecotone, Green Lakes Valley, Colorado Front Range, United States. *Water Resour. Res.* **39**(7), 1188, doi:10.1029/2002WR001738.

Hopkinson, C. & English, M. (2001) Spatio-temporal variations of d18O isotope signatures of hydrological components within a glacierised mountainous basin. In: *58th Eastern Snow Conf.* (Ottawa, Ontario, Canada, 14–18 May).

Huth, A. K., Leydecker, A., Sickman, J. O. & Bales, R. C. (2004) A two-component hydrograph separation for three high-elevation catchments in the Sierra Nevada, California. *Hydrol. Processes* **18**, 1721–1733.

Kasahara, T. & Wondzell, S. M. (2003) Geomorphic controls on hyporheic exchange flow in mountain streams. *Water Resour. Res.* **39,** 1, doi:10.1029/2002WR001336.

Katsuyama, M., Ohte, N. & Kabeya, N. (2005) Effects of bedrock permeability on hillslope and riparian groundwater dynamics in a weathered granite catchment. *Water Resour. Res.* **41,** W01010, doi:10.1029/2004WR003275.

Kattelmann, R. & Elder, K. (1991) Hydrologic characteristics and water balance of an alpine basin in the Sierra Nevada. *Water Resour. Res.* **27**(7), 1553–1562.

Klemes, V. (1990) The modelling of mountain hydrology: the ultimate challenge. In: *Hydrology of Mountainous Areas* (ed. by L. Molnar) (Strbske Pleso Workshop, Czechoslovakia, June 1988), 29–43. IAHS Publ. 190. IAHS Press, Wallingford, UK.

Lafreniere, M. J. & Sharp, M. J. (2003) Wavelet analysis of inter-annual variability in the runoff regimes of glacial and nival stream catchments, Bow Lake, Alberta. *Hydrol. Processes* **17**, 1093–1118.

Lafreniere, M. J. & Sharp, M. J. (2005) A comparison of solute fluxes and sources from glacial and non-glacial catchments over contrasting melt seasons. *Hydrol. Processes* **19**, 2991–3012.

Lang, H. & Musy, A. (eds) (1990) *Hydrology in Mountainous Regions. I—Hydrological Measurements; The Water Cycle* (Lausanne, August 1990). IAHS Publ. 193. IAHS Press, Wallingford, UK.

Liu, F., Williams, M. W. & Caine, N. (2004) Source waters and flow paths in an alpine catchment, Colorado Front Range, United States. *Water Resour. Res.* **40,** W09401, doi:10.1029/2004WR003076.

Malard, F., Galasi, D., Lafont, M., Doledec, S. & Ward, J. V. (2003) Longitudinal patterns of invertebrates in the hyporheic zone of a glacial river. *Freshwater Biology* **48**, 1709–1725.

Manga, M. (1999) On the timescales characterizing groundwater discharge at springs. *J. Hydrol.* **219**, 56–69.

Mast, M. A., Kendall, C., Campbell, D. H., Clow, D. W. & Back, J. (1995) Determination of hydrologic pathways in an alpine-subalpine basin using isotopic and chemical tracers, Loch Vale Watershed, Colorado, USA. In: *Biogeochemistry of Seasonally Snow-Covered Catchments* (ed. by K. Tonnessen, M. W. Williams & M. Tranter) (Proc. of the XXI General Assembly of IUGG, Boulder, Colorado), 263–270. IAHS Publ. 228. IAHS Press, Wallingford, UK.

Michel, R. L., Campbell, D. H., Clow, D. W. & Turk, J. T. (2000) Timescales for migration of atmospherically derived sulphate through an alpine/subalpine watershed, Loch Vale, Colorado. *Water Resour. Res.* **36**(1), 27–36.

Michel, R. L., Turk, J. T., Campbell, D. H. & Mast, M. A. (2002) Use of natural 35S to trace sulphate cycling in small lakes, Flattops Wilderness Area, Colorado, USA. *Water, Air and Soil Pollution: Focus* **2**, 5–18.

Molnar, L. (ed.) (1990) *Hydrology of Mountainous Areas*. Strbske Pleso Workshop, Czechoslovakia, June 1988. IAHS Publ. 190. IAHS Press, Wallingford, UK.

Morrice, J. A., Valett, H. M., Dahm, C. N. & Campana, M. E. (1997) Alluvial characterstics, groundwater-surface water exchange and hydrological retention in headwater streams. *Hydrol. Processes* **11**, 253–267.

Parriaux, A. & Nicoud, G. F. (1988) Hydrological behaviour of glacial deposits in mountainous areas. In: *Hydrology of Mountainous Areas* (ed. by L. Molnar) (Strbske Pleso Workshop, Czechoslovakia, June 1988), 291–312. IAHS Publ. 190. IAHS Press, Wallingford, UK.

Rademacher, L. K., Clark, J. F., Clow, D. W. & Hudson, G. B. (2005) Old groundwater influence on stream hydrochemistry and catchment response times in a small Sierra Nevada catchment: Sagehen Creek, California. *Water Resour. Res.* **41,** WO2004, doi:10.1029/2003WR002805.

Rice, K. C. & Hornberger, G. M. (1998) Comparison of hydrochemical tracers to estimate source contributions to peak flow in a small, forested, headwater catchment. *Water Resour. Res.* **34**(7), 1755–1766.

Rosenberry, D. O. & Winter, T. C. (1993) The significance of fracture flow to the water balance of a lake in fractured crystalline rock terrain. In: *Memoires of the XXIVth Congress of IAH* (As, Oslo).

Silar, J. (1990) Surface water and groundwater interactions in mountainous areas. In: *Hydrology of Mountainous Areas* (ed. by L. Molnar) (Strbske Pleso Workshop, Czechoslovakia, June 1988), 21–28. IAHS Publ. 190. IAHS Press, Wallingford, UK.

Singh, P. & Bengtsson, L. (2005) Impact of warmer climate on melt and evaporation for the rainfed, snowfed and glacierfed basins in the Himalayan region. *J. Hydrol*. **300**, 140–154.

Sophocleous, M. (2002) Interactions between groundwater and surface water: the state of the science. *Hydrogeol. J.* **10**, 52–67.

Story, A., Moore, R. D. & Macdonald, J. S. (2003) Stream temperatures in two shaded reaches below cutblocks and logging roads: downstream cooling linked to subsurface hydrology. *Canadian J. Forestry Res.* **33**, 1383–1396.

Sueker, J. K., Turk, J. T. & Michel, R. L. (1999) Use of cosmogenic 35S for comparing ages of water from three alpine–subalpine basins in the Colorado Front Range. *Geomorphology* **27**, 61–74.

Sueker, J. K., Ryan, J. N., Kendall, C. & Jarrett, R. D. (2000) Determination of hydrologic pathways during snowmelt for alpine/subalpine basins, Rocky Mountain National Park, Colorado. *Water Resour. Res.* **36**(1), 63–75.

Sueker, J. K., Clow, D. W., Ryan, J. N. & Jarrett, R. D. (2001) Effect of basin physical characteristics on solute fluxes in nine alpine/subalpine basins, Colorado, USA. *Hydrol. Processes* **15**, 2749–2769.

Tague, C. & Grant, G. E. (2004) A geological framework for interpreting the low-flow regimes of Cascade streams, Williamette River Basin, Oregon. *Water Resour. Res.* **40**, WO4303, doi:10.1029/2003WR002629.

Taylor, S., Feng, S., Williams, M. W. & McNamara, J. P. (2002) How isotopic fractionation of snowmelt affects hydrograph separation. *Hydrol. Processes* **16**, 3683–3690.

Uehlinger, U., Malard, F. & Ward, J. V. (2003) Thermal patterns in the surface waters of a glacial river corridor (Val Roseg, Switzerland). *Freshwater Biol.* **48**, 284–300.

Verry, E. S. (2003) Groundwater and small research basins: An historical perspective. *Groundwater* **41**(7), 1005–1007.

Vitvar, T., Burns, D. A., Lawrence, G. B., McDonnell, J. J. & Wolock, D. M. (2002) Estimation of baseflow residence times in watersheds from the runoff hydrograph recession: method and application in the Neversink watershed, Catskill Mountains, New York. *Hydrol. Processes* **16**, 1871–1877.

Ward, J. V., Malard, F., Tockner, K. & Uehlinger, U. (1999) Influence of groundwater on surface water conditions in a glacial flood plain of the Swiss Alps. *Hydrol. Processes* **13**, 277–293.

Weiler, M. & McDonnell, J. J. (2004) Virtual experiments: a new approach for improving process conceptualization in hillslope hydrology. *J. Hydrol.* **285**, 3–18.

Winter, T. C. (1976) Numerical simulation analysis of the interaction of lakes and groundwater. United States Geological Survey Professional Paper, 1001, p. 45.

Winter, T. C. (1999) Relation of streams, lakes, and wetlands to groundwater flow systems. *Hydrogeology J.* **7**, 28–45.

Winter, T. C. (2003) The hydrology of lakes. In: *The Lakes Handbook, Volume 1 – Limnology and Limnetic Ecology* (ed. by P. E. O'Sullivan & C. S. Reynolds), 61–78. Blackwell Science Ltd., Oxford, UK.

Winter, T. C. & Woo, M.-K. (1990) Hydrology of lakes and wetlands. In: *The Geology of North America*, Vol. O-1, Surface Water Hydrology. The Geological Society of America.

Winter, T. C., Harvey, J. W., Franke, O. L. & Alley, W. M. (1998) Groundwater and surface water: a single resource. US Geological Survey Circular 1139.

Winter, T. C., Rosenberry, D. O. & LaBaugh, J. W. (2003) Where does the groundwater in small watersheds come from? *Groundwater* **41**(7), 989–1000.

Wondzell, S. M. & Swanson, F. J. (1996) Seasonal and storm dynamics of the hyporheic zone of a 4th order mountain stream 1. Hydrologic Processes. *J. N. Am. Benthol. Soc.* **15**, 3–19.

Zappa, M., Pos, F., Strasser, U., Warmerdam, P. & Gurtz, J. (2003) Seasonal water balance of an alpine catchment as evaluated by different methods for spatially distributed snowmelt modelling. *Nordic Hydrol.* **34**(3), 179–202.

Glacier Mass Balance Changes and Meltwater Discharge (selected papers from sessions at the IAHS Assembly in Foz do Iguaçu, Brazil, 2005). IAHS Publ. 318, 2007.

Recent trends in precipitation and streamflow in the Aconcagua River basin, central Chile

FRANCESCA PELLICCIOTTI, PAOLO BURLANDO & KARIN VAN VLIET

Institute of Environmental Engineering, ETH Zurich, CH-8093, Switzerland
pellicciotti@ifu.baug.ethz.ch

Abstract In this paper, trends in streamflow and precipitation at the annual, seasonal and monthly timescales for different periods of records are analysed for the Aconcagua River basin in central Chile. In this mountainous basin in the dry Andes, water resources originate mainly from glaciers and seasonal snowcovers. The Mann-Kendall nonparametric test is used, and statistically significant trends are identified for each station on an annual, seasonal and monthly basis. Trends in streamflow are examined together with changes in precipitation and temperature. Analysis of correlation of the hydroclimatic variables with large-scale atmospheric circulation patterns such as the Southern Oscillation is also carried out. The main identified trend is a decrease in streamflow in the upper section of the basin, which is consistent at both the annual and seasonal scale. Changes in precipitation are not sufficient to explain the observed trend in runoff. Precipitation patterns, however, seem to have changed in the last 30 years, and results of seasonal trend analysis seem to indicate that there has been a shift in precipitation seasonality. Temperature at one station in the basin shows increasing trends at all temporal resolution. We argue that the decreasing trend in runoff might be explained by a decrease in glaciers and snowcover contribution to the total streamflow in the upper basin. Analysis of correlation reveals that both streamflow and precipitation are affected by ENSO events, and in particular that warm ENSO events are associated with an increase in winter and autumn precipitation, and an increase in summer streamflow.

Key words Aconcagua River basin; El Niño events; ENSO; hydroclimatic variability; Mann-Kendall test; SOI; trend analysis

INTRODUCTION

Mountainous catchments are the origin of many of the largest rivers in the world and represent a major source of water availability for many countries. They represent a local resource (local freshwater supply, hydropower generation), but also considerably influence the runoff regime of the downstream rivers. A change of climatic regimes due to the increase of the greenhouse effect as predicted by many studies is expected to affect the river systems originating in mountainous areas (Huber *et al*., 2005).

The debate on climate variability and climate change relies heavily on the detection of trends (or lack thereof) in instrumental records of hydroclimatic variables such as air temperature, precipitation and streamflow. In many parts of the world, and in particular in the United States, Canada and Europe, numerous large-scale analyses of hydroclimatic trends have recently been conducted on precipitation and streamflow data at different time scales (e.g. Lettenmaier *et al.*, 1994; Karl & Plummer, 1995; Lins

& Slack, 1999; Groisman *et al.*, 2001; Molnár & Ramírez, 2001; Zhang *et al.*, 2001; Burn & Hag Elnur, 2002; Kahya & Kalayci, 2004; Birsan *et al.*, 2005). This is not the case for the South American continent, where analyses of trends in instrumental records of streamflow and precipitation are scarce (e.g. Rosenblüth *et al.*, 1997). In this paper, we present a watershed-based analysis of streamflow and precipitation trends in a mountainous watershed in central Chile, the Aconcagua River basin, with emphasis placed on the connection between observed changes in the precipitation and streamflow regimes and possible variations of glaciers in the area. This study is part of a larger investigation aimed to assess past and future variations in water resources in the basin, with special focus on the role played by glaciers and snowcovers. The Aconcagua basin, located in the dry Andes and one of the major Chilean basins, depends heavily on glaciers and seasonal snow covers for its water supply. Precipitation is characterised by a typical annual pattern with very limited rainfall totals during summer and high precipitation during winter. In summer, almost all water supply to the basin, which is used for agriculture, domestic uses and industry, comes from the snow and ice melt in the upper basin. The basin is experiencing increasing pressure on its water resources and competition among different users for water allocation, because of the growing industrialisation, the large intensive agricultural production in the lower watershed, and growing population. In this context, it is crucial to evaluate both future and past changes in the water resources in the basin. The study presented in this paper is a first step in this direction. We conduct a thorough examination of hydroclimatic data from different periods in order to identify seasonality, variability, trends and other properties of precipitation and streamflow at different time scales. Statistically significant trends are identified for each station on an annual, seasonal and monthly basis. Connections to large-scale climate anomalies which are relevant in the region, such as the Southern Oscillation (SO), are also established, and their effect on hydroclimatic variability is examined through correlation analysis.

The goals of this study are: (a) to identify significant trends in observed streamflow data and their occurrence in time and space in the Aconcagua River basin, with particular attention to its upper section; (b) to analyse the connection between observed changes in streamflow, precipitation and air temperature; (c) to analyse the correlation between hydroclimatic variables and global climatic indices representative of large-scale circulation patterns that are active in the region. Results of aims (a) to (c) will be used to attempt a preliminary investigation of the correlation between streamflow trends and watershed properties, in particular glacier coverage. This work complements a couple of previous studies on the Aconcagua basin (e.g. Waylen & Caviedes, 1990; Montecinos & Aceituno, 2003), all of which, however, have focused on the impact of the El Niño–Southern Oscillation (ENSO) phenomenon on the interannual variability of precipitation and streamflow and not on trends analysis.

The methods used in this study are standard. Monthly, seasonal and annual precipitation, temperature and streamflow data were analysed for trends using the Mann-Kendall nonparametric trend test. A limitation of this study is that higher (i.e. daily) resolution data were not available. In order to discriminate trends from stochastic fluctuations and from the influence of serial correlation in time series, the series presenting a positive lag-1 serial correlation after detrending were prewhitened by applying a first order autoregressive filter to the data prior to the trend analysis. The

data used in this study are described, together with the main characteristics of the Aconcagua basin, and the methods used are discussed. The main results are then presented according to the goals of this study: first observed streamflow trends, at the different time scales; then precipitation and temperature trends are shown and linked to the changes in streamflow. The results are then discussed, and further analysis is suggested that should be conducted to complete this first step of the investigation. The main conclusions are then listed.

ACONCAGUA CASE STUDY AND DATA DESCRIPTION

The Aconcagua River is the largest mid-latitude river of Chile, and its characteristics are typical of the temperate latitudes of western South America. Located at the boundary between semi-arid and central Chile, it drains both the ice- and snow-fields of the Andes and Coastal Plain (Fig. 1). The river basin is located about 50 km north of the national capital Santiago, and has a total area of 7.550 km^2. The river has a total length of about 214 km, flowing from east to west from the spring of Juncal to the mouth at Concón bay. Tributaries join along the main stream, maintaining baseflow, and flooding results from intense winter precipitation and summer snowmelt. The upper watershed has several peaks above 5000 m a.s.l. and vegetation is sparse. The Aconcagua upper section is essentially underdeveloped, and uses of economic significance in the upper watershed are limited to mining. In the lower watershed, on the contrary, intensive agricultural production depending almost entirely on irrigation takes place. There are no dams in the basin, but water is used for agriculture and mining. All drinking water in the Aconcagua basin comes from melt water, which also sustains the rich irrigated agriculture in the lower basin. There is also increasing competition for water use and allocation, as water demands from mining and industry are rising. The basin was divided in an upper and lower section, the divide being the meteorological station of San Felipe (DGA station 25), which is considered as part of the upper watershed.

Hydro-climatic records for the basin were obtained from the Chilean Dirección General de Aguas (DGA). Monthly streamflow data from five stations in the upper basin were obtained. Selection of streamflow data was based on two criteria: (1) no substantial influence by water withdrawals for hydropower or other water-use purposes; and (2) at least 30 years of continuous and complete observations. In this way, four stations were identified that were in operation in 2002 and had sufficiently long records. The stations are: Rio Aconcagua at Chacabuquito (14), Rio Juncal at Juncal (16), Rio Aconcagua at Blanco (17), and Rio Blanco at Blanco (18). In brackets is the DGA station number, which will be used throughout this paper to indicate the streamflow gauging stations. Of these stations, two were located directly on the Aconcagua course, and two on the two upper watershed tributaries of Rio Juncal and Rio Blanco. Location of the streamflow stations is shown in Fig. 1 and basic information is given in Table 1. Trend analysis was conducted for two study periods: 1952–2002 for one site (station 14), and 1970–2002 for four sites (stations 14, 16, 17 and 18).

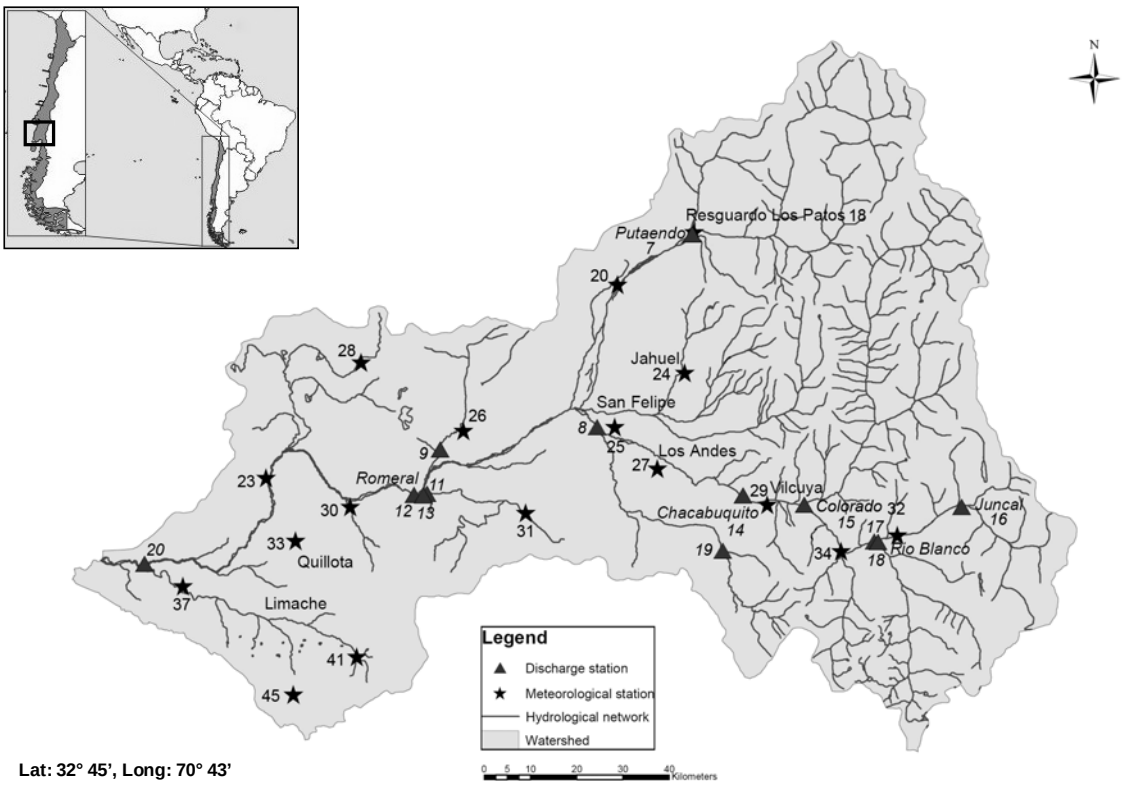

Fig. 1 Aconcagua River basin with the location of the meteorological and streamflow stations. Stations are identified by the numbers of the Dirección General de Aguas (DGA).

Table 1 Streamflow stations used in this study. In bold are the yearly period for stations that are used in this paper for trend analysis. Station 15 is used for analysis of seasonality only.

Name of station	DGA no.	Lat.	Long.	Elevation (m)	Drainage area (km^2)	Observation period
Rio Aconcagua at Chacabuquito	14	32 50	70 34	1030	2400	1950–2002 (**53**)
Rio Colorado at Colorado	15	32 52	70 25	1062	743	1976–2002 (27)
Rio Juncal at Juncal	16	32 53	70 09	1800	233	1970–2002 (**33**)
Rio Aconcagua at Rio Blanco	17	32 54	70 19	1420	875	1970–2002 (**33**)
Rio Blanco at Rio Blanco	18	32 55	70 19	1420	382	1970–2002 (**33**)

Precipitation and temperature records were also analysed. Of the 15 meteorological stations provided by the DGA, nine stations were selected that had sufficiently long records (at least 30 years) (Fig. 1 and Table 2). In contrast to the streamflow stations which are located in the upper basin (Fig. 1), the precipitation stations are situated both in the upper and lower section of the watershed. Throughout this paper, the meteorological stations will be referred to by their DGA station identification number. The analysis on the precipitation records was conducted for five periods: 1929–2004 (one station: 34); 1940–2004 (two stations: 34 and 18); 1954–2004 (three stations: 34, 18 and 26); 1965–2004 (seven stations: 34, 18, 26, 25, 28, 29 and 30); and 1974–2004 (all nine stations).

Table 2 Precipitation stations. In bold are those where long term temperatures were used for trend analysis.

Name of station	Lat.	Long.	Elevation (m)	DGA n.	Observation period
Resguardo Los Patos	32 30	70 36	1220	18	1940–2004
San Felipe	32 45	70 43	640	25	1962–2004
Catemu	32 44	70 56	440	26	1954–2004
Los Andes	32 50	70 36	820	27	1972–2004
Lo Rochas	32 47	71 17	175	28	1964–2004
Vilcuya	**32 52**	**70 28**	**1100**	**29**	**1965–2004**
Rabucco Estero	32 51	71 07	300	30	1965–2004
Riecillos	32 56	70 21	1290	34	1929–2004
Los Aromos	32 57	71 22	100	37	1974–2004

Temperature data were available from four DGA meteorological stations (stations 29, 33, 37 and 45). Of these, only station 29 (Vilcuya), had a number of years of record sufficient for the hydrological investigation (more than 30 years), and was therefore used in this study. The station is located in the upper section of the basin, between streamflow stations 14 and 15.

METHODS

Trend analysis

Trend analyses were conducted using the nonparametric Mann-Kendall (MK) test (Helsel & Hirsch, 1992). This test has been widely used for hydrological data analysis (e.g. Lettenmaier *et al.*, 1994; Molnár & Ramírez, 2001; Zhang *et al.*, 2001; Birsan *et al.*, 2005). It is a rank-based procedure especially suitable for non-normally distributed data, censored data, and nonlinear trends. Its advantages are that it is distribution free, robust against outliers, and has a higher power than many other commonly used tests (e.g. Hess *et al.*, 2001). The null hypothesis of randomness H_0 states that the data (x_1, . . . x_n) are a sample of n independent and identically distributed random variables. The alternative hypothesis H_A is that the distributions of x_k and x_j are not identical for all k, $j \leq n$ with $k \neq j$. The null hypothesis is rejected at a significant level α if $|Z_s| > Z_{crit}$, where Z_{crit} is the value of the standard normal distribution with an exceedence probability of $\alpha/2$. A positive value of Z indicates an upward trend, whereas a negative value indicates a downward trend in the tested time series. Statistically significant trends are generally reported at the 10% significance level ($\alpha = 0.1$, two-tailed test), or confidence level $\beta = 1 - \alpha = 0.90$, in this paper. The trend test statistic Z is used as a measure of trend magnitude, or of its significance. It is not a direct quantification of trend magnitude.

The MK test should be applied to uncorrelated data (Helsel & Hirsch, 1992). It has been demonstrated that the presence of serial correlation decreases the power of the MK test and leads to an erroneous rejection of the null hypothesis (Type II error) (e.g. Kulkarni & von Storch, 1995; Yue *et al.*, 2002; Yue & Wang, 2002; Yue & Pilon, 2003). One of the most common corrections applied in previous studies has been to

remove the serial correlation in the data by *prewhitening*, i.e. by applying the MK test to the series x^*: $x_i^* = x_i - r_1 x_{i-1}$, where r_1 is the lag-1 serial correlation coefficient of the detrended series (e.g. Yue *et al.*, 2002, 2003; Yue & Pilon, 2003). In this paper, detrending was done by removing a linear trend in the data with slope b estimated using the nonparametric Theil-Sen method. This method is suitable for nearly linear trend in the variable x and is less affected by non-normal data and outliers (Helsel & Hirsch, 1992). The slope is computed between all pairs i of the variable x as:

$$\beta_i = \frac{x_j - x_k}{j - k} \quad \text{with} \quad j > k \left(j = 2,...,n; k = 1,...,n-1 \right) \tag{1}$$

where $i = 1 \ldots N$. For n values in the time series x, this will result in $N = n\ (n - 1)/2$ values of β. The slope estimate b is the median of β_i, $i = 1 \ldots N$. Prewhitening was applied only to time series with $r_1 > 0$. To check for the effect of the pre-whitening on the results, we analysed both original data as well as prewhitened data. Because serial correlation coefficients were generally low for the annual and seasonal time series, the differences between the two approaches were not large.

The method was applied to annual, seasonal and monthly data. Four climatological seasons were identified in the region, and analysed separately: winter (June, July and August), spring (September, October and November), summer (December, January and February) and autumn (March, April and May) (see e.g. Waylen & Caviedes, 1990; Montecinos & Aceituno, 2003). The analysis was conducted for streamflow, precipitation and temperature data, and it is reported separately for the three variables.

Correlation analysis with large-scale circulation patterns

In order to investigate the influence of global atmospheric circulation patterns on the hydroclimatic variables, correlation with indices of the general circulation of the atmosphere was carried out. The main natural interannual climatic fluctuation affecting the region under study is the El Niño–Southern Oscillation (ENSO) phenomenon (e.g. Aceituno, 1988; Waylen & Caviedes, 1990; Montecinos *et al.*, 2000; Waylen & Poveda, 2002; Montecinos & Aceituno, 2003; Schneider & Gies, 2004). Using established definitions, El Niño is the warm ocean current frequently observed in the eastern equatorial Pacific off the coast of Ecuador. In contrast to the El Niño, La Niña refers to an anomaly of unusually cold sea surface temperatures found in the eastern tropical Pacific. The large scale fluctuations in air pressure that are associated with the El Niño and La Niña ocean temperature changes are referred to as the Southern Oscillation (SO). The SO phase is negative during El Niño and positive during La Niña episodes. A detail explanation of the generation mechanisms of ENSO and its relation with Sea Surface Temperature (SST) and the thermocline can be found in Waylen & Poveda (2002).

The main effect of ENSO in central Chile is an increase in annual precipitation during El Niño events, which results mainly from an increase in winter precipitation (e.g. Waylen & Caviedes, 1990; Montecinos *et al.*, 2000; Montecinos & Aceituno, 2003). A decrease in rainfall during La Niña events, due to the strengthening of the anticyclone, has also been reported (Rubin, 1955; Aceituno, 1988; Rutllant &

Fuenzalida, 1991). Several indices of the ENSO phenomenon exist (e.g. Waylen & Poveda, 2002). In this study, we employed the Southern Oscillation Index (SOI), defined as the difference of monthly atmospheric pressure anomaly between Tahiti (18S, 150W) and Darwin (12S, 131W), Australia. Prolonged periods of negative SOI values correspond with abnormally warm ocean waters in the eastern tropical Pacific, which is typical of an El Niño event. Conversely, the prolonged positive SOI correspond with abnormally cold ocean waters in the eastern tropical Pacific, which is typical of a La Niña event (e.g. Schneider & Gies, 2004).

The standardised SOI was obtained from the NOAA-CIRES Climate Diagnostics Center, Boulder, Colorado, and was downloaded at http://www.cpc.ncep.noaa.gov. For the details of the calculation the reader is referred to the NOAA website. The SOI has been used in several studies of climatic variation in Chile (e.g. Pittock, 1980; Aceituno, 1988) and in South America in general (e.g. Waylen & Poveda, 2002; Schneider & Gies, 2004). It was selected because of its definition on a monthly basis, its easy updating, and its close relationship to other SO indices (Wright, 1984; Aceituno, 1988).

In this work, we first compared monthly anomaly of streamflow and precipitation with the standardised monthly SOI. Second, we computed the correlation between SOI and monthly, seasonal and annual data. Time lags between time series were incorporated by allowing a lag of up to 12 months.

RESULTS

The main results are reported in three sections. First, trends in streamflow are analysed for different time scales, and their spatial distribution in the upper Aconcagua basin is studied. Second, trends in precipitation and temperature are analysed and their connections with streamflow trends are explored. Third, results of the correlation analysis of streamflow and precipitation with the SOI index are reported.

It is clear that the study period has an impact on trend identification. It has been noted that runoff records may contain large-scale periodic behaviour, and that trend analysis should be conducted on periods that span one or multiple full cycles of this process if it exists (e.g. Pekarova *et al*., 2003). Figure 2 shows annual streamflow anomalies for station 14. It is clear from this figure that both the two study periods contain both high and low flow phases. We can therefore assume that the trend reported here, for even the shortest study period, are not due to low-frequency large-scale behaviour of the data and are representative of changes in the runoff regime.

Streamflow

Seasonality Figure 3 shows the distribution of mean monthly streamflow at the five gauging stations. Runoff peaks in December, at the beginning of the austral summer, and it is very high in November (end of spring) and during summer (DJF). Runoff during summer is almost entirely due to snow- and ice-melt, as precipitation in the basin is very low during DJF. During winter (JJA), streamflow is very low,

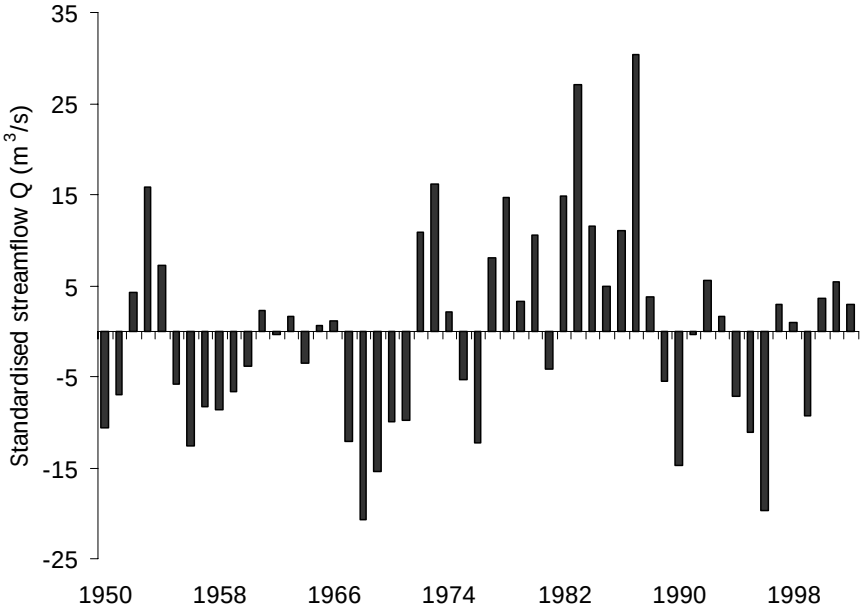

Fig. 2 Standardised annual streamflow *Q* from station 14 in the period 1950–2002. *Q* is computed by subtracting to the annual streamflow its long-term mean.

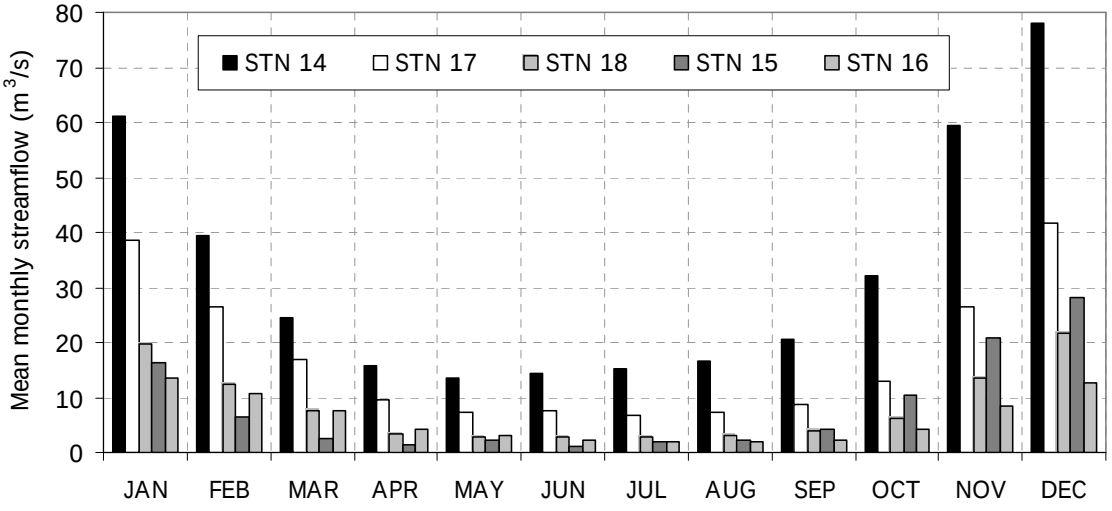

Fig. 3 Mean monthly streamflow distribution over the period of record at the Aconcagua gauges from Table 1. Stations are identified by their DGA number.

varying between 5.6% (at station 15) and 12% (at station 14) of the annual total. There are differences in the streamflow magnitude at the stations, with streamflow being the highest at the most downstream station 14, and decreasing at the upstream stations with higher elevation (Fig. 3). Mean monthly streamflow in the peak month of December ranged from 13 $m^3 s^{-1}$ at station 16 to 78 $m^3 s^{-1}$ at station 14 (Fig. 3). Differences in streamflow magnitude can be observed between station 17 and 18, which are situated in close proximity at the Blanco village. As an example, the mean monthly December streamflow (which is the maximum streamflow at both stations) is 42 $m^3 s^{-1}$ at station 17 and nearly half of this value at station 18 (22 $m^3 s^{-1}$). This is due

to the fact that, although the two sites are very close to each other, station 17 is situated on Rio Aconcagua, while station 18 is on the tributary Rio Blanco, which carries much less water. Seasonality, however, is coherent at all stations (Fig. 3). Nevertheless, while the annual maximum is always in December at all stations, apart from station 16 (maximum in January, but with a minimum difference with respect to the December value), the timing of the annual minimum varies from station to station within the summer months. At the most downstream station (14) the minimum annual is in May, at station 15 is in June, and at the three uppermost stations is in July.

There are also differences in the ratio of the minimum to the annual total from station to station, with station 14, the most downvalley one, having the lowest summer contribution of the five stations (45.5% of the annual total), and the highest winter contribution (11.8% of annual total). This is a clear indication of the fact that the stations higher up in the upper basin, being fed almost solely by snow and glacier fields, have a more pronounced glacio-nival regime.

Trends Results of trend analysis on annual streamflow data for complete records show a decreasing trend at all stations, although the trend is only significant at stations 17 and 18 (Fig. 4). The *Z* statistic for the analysis of trend conducted on the longer period of observations at station 14 is much smaller than the *Z* obtained when analysing the common period of record (1970–2002). This is in agreement with findings of recent research on hydroclimatic trends, which suggest that longer periods of data exhibit fewer and less significant trends than shorter data periods (e.g. Birsan *et al*., 2005). Results of trend analyses on seasonal streamflow data for the four gauging stations are shown in Fig. 5 for the common period of record. There is no common behaviour at the four stations in term of trends in the monthly and seasonal streamflow. While stations 14 and 16 show both increasing and decreasing trends, none of them statistically significant, and with predominance of decreasing trends, stations 17 and 18 exhibit consistently negative trends for all months, and statistically

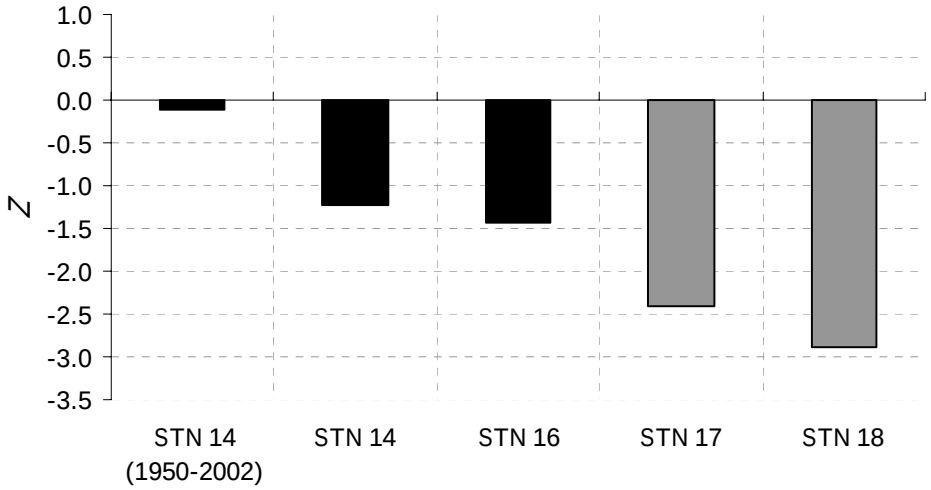

Fig. 4 Trend statistic *Z* for annual streamflow data for the four stations analysed for trends. The sign of *Z* indicates trend direction. Results are shown for the pre-whitened data. Analyses are both for the common period of record (1970-2002) and at station 14 also for the period 1950-2002. In grey are the statistically significant trends, in black the not statistically significant ones.

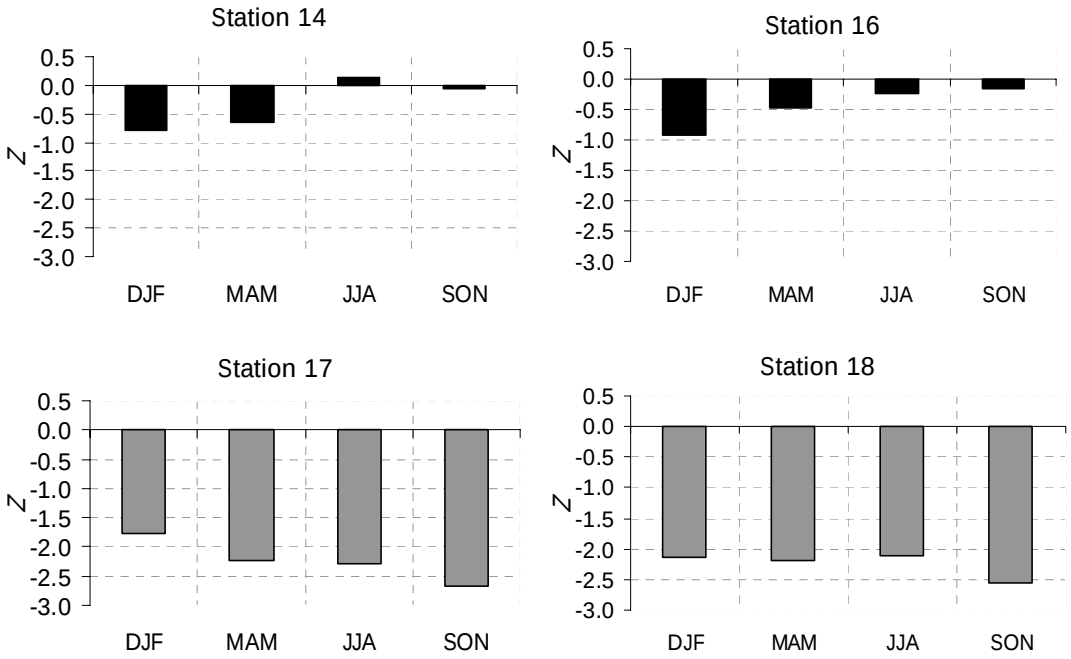

Fig. 5 Trend test statistics for seasonal streamflow totals at the four gauging stations analysed for trends. The sign of *Z* indicates trend direction. In grey are the statistically significant trends, in black the statistically not significant trends. Analyses are for the common period of record (1970–2002).

significant for all months but May at station 17. The observed decreases in annual streamflow have different explanations at stations 14 and 16, and 17 and 18, respectively. At both stations 14 and 16, the observed annual decrease in streamflow comes primarily from a decrease in the high-flow months from December to February. Stations 17 and 18, on the contrary, exhibit a significant decrease throughout the year, with the strongest decreasing trends in spring (SON) (Fig. 5).

Precipitation and temperature

Seasonality of precipitation The monthly distribution of mean precipitation at the main gauges in the Aconcagua basin is shown in Fig. 6. On average, most precipitation occurs between May and August, with 62% of the total occurring during the winter months (JJA) at station 34. June and July are commonly the months with the highest observed precipitation. There is hardly any precipitation in the summer months of December, January and February (Fig. 6), with summer precipitation being less than 2% of annual total at station 34.

Trends Results of trend analyses on *annual* precipitation data show no statistically significant trend at any of the stations and for any of the periods of record considered (Fig. 7). There is, however, an influence of the period of record on the results of the trend analysis. Trends at highest elevation station 34 are positive, although not statistically significant, in the three periods 1940–2004, 1954–2004 and 1965–2004

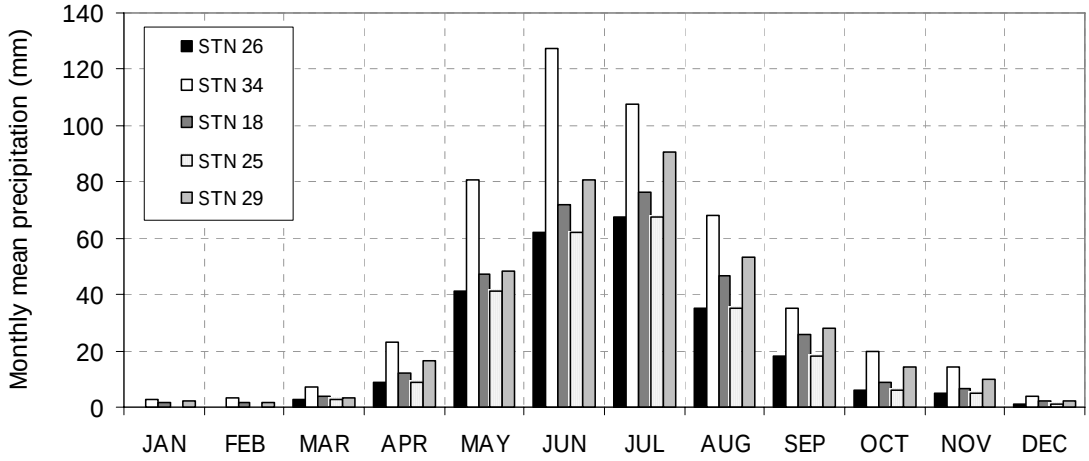

Fig. 6 Distribution of mean monthly precipitation totals over the period of record at five of the nine Aconcagua gauges from Table 2. Stations are indicated by their DGA number.

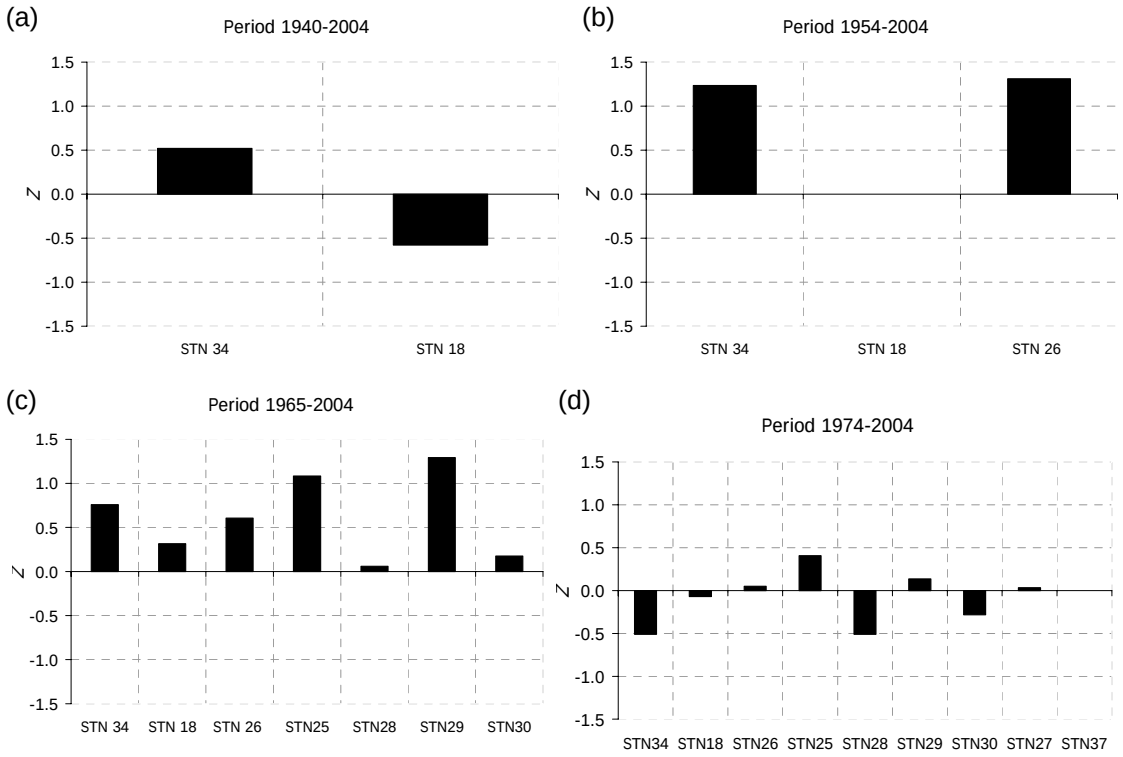

Fig. 7 Trend test statistic *Z* for annual precipitation total at individual stations for the period of records: (a) 1940–2004 (stations 34 and 18); (b) 1954–2004 (stations 34, 18 and 26); (c) 1965–2004 (stations 34, 18, 26, 25, 28, 29 and 30); and (d) 1974–2004 (all stations). The sign of *Z* indicates trend direction. Grey indicates statistically significant trends, black indicates no statistically significant trends.

(Fig. 7(a)–(c). For the period of record 1929–2004, the trend in the annual data at this station is slightly negative and statistically not significant ($Z = –0.1$). Results for the common period of record 1965–2004 (seven stations) show consistently positive trends, although not statistically significant at any of the stations (Fig. 7(c)). Analysis

of trends for the common period of record 1974–2004 (all stations), however, reveals that there is no longer a coherent behaviour at the nine stations examined, with both positive and negative trends (Fig. 7(d)). None of the trends in individual stations is statistically significant (Fig. 7(d)). Figure 7(d) shows both increasing and decreasing trends, with a slight predominance of decreasing trends. Most noteworthy, the increasing trend at station 34 observed in the periods of record 1940–2004, 1954–2004 and 1965–2004 has reverted into a decreasing trend. The same inversion can be observed at stations 28 and 30.

Trend analyses were also conducted on *monthly* and *seasonal* precipitation data for the five periods of records. Results show no statistically significant trend at any station, but few after 1954 (Fig. 8). The increase in annual precipitation observed at station 34 in the period 1940–2004 is caused by an increase in winter (JJA) and spring (SON) precipitation totals, which compensate the decrease in summer precipitation (Fig. 8(a)). It has to be kept in mind, however, that summer has a much smaller contribution to total precipitation than both the winter and spring totals.

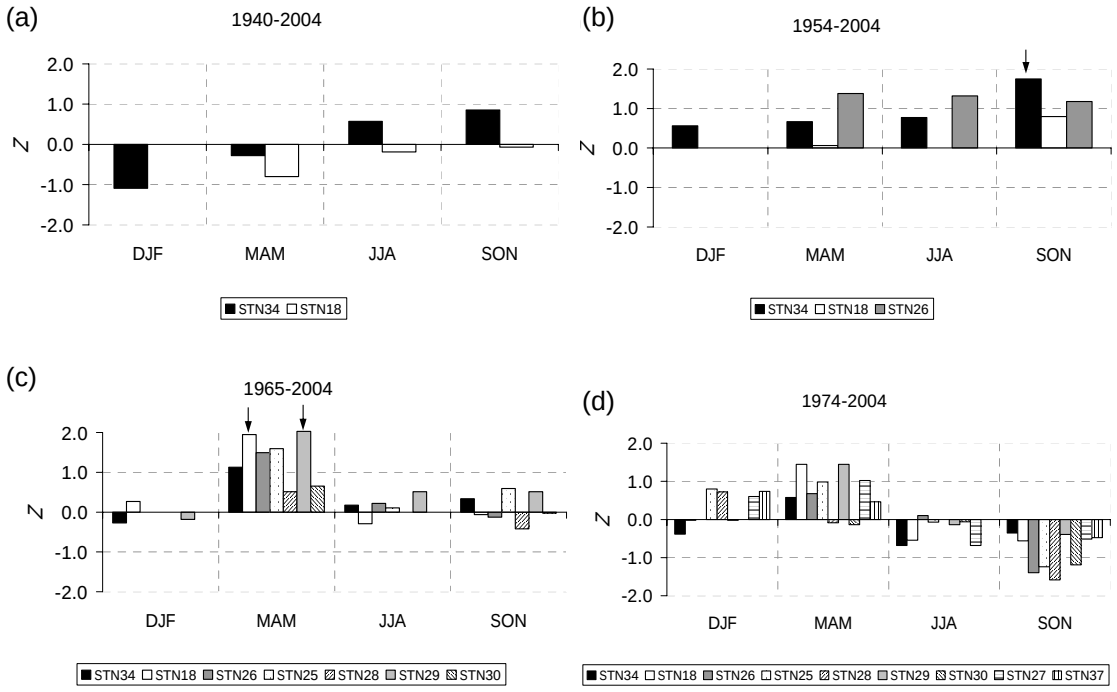

Fig. 8 Trend test statistic *Z* for seasonal precipitation totals at individual stations for the period of records: (a) 1940–2004 (stations 34 and 18); (b) 1954–2004 (stations 34, 18 and 26); (c) 1965–2004 (stations 34, 18, 26, 25, 28, 29 and 30); and (d) 1974–2004 (all stations). Statistically significant trends are indicated by an arrow.

Seasonal trends at individual stations in the period 1954–2004, although not statistically significant, are consistently positive, in agreement with the results of annual data trend analysis (Fig. 8(b)). Analysis of trend results in the period of record 1965–2004 shows that the annual increase in precipitation, which was observed at all stations, comes primarily from an increase in autumn (MAM) precipitation, which is

consistent at all stations and significant at stations 18 and 29 (Fig. 8(c)). On the other hand, results of analysis of trends on seasonal precipitation totals in the period of record 1974–2004 clearly indicate that there has been a consistent decrease in the spring (SON) precipitation amount at all stations (Fig. 8(d)), this effect being stronger at stations 28, 30, 25 and 26. No major changes have occurred in the periods 1965–2004 (seven stations) and 1974–2004 (nine stations) to the winter precipitation total (Fig. 8(c),(d)), which represents the main contribution to the annual total at all stations in the basin (see Fig. 6).

Air temperature plays a crucial role in the water cycle of the upper Aconcagua, because of the impact it has on the occurrence of snowfalls and snowmelt in this highly mountainous basin. Analysis of trends in annual, seasonal and monthly temperature data conducted at meteorological station 29 for the period of record 1965–2004 showed a statistically significant increase in temperature at annual, monthly and seasonal scales (Table 3 and Fig. 9). At the annual scale, the increasing trend is significant at the 1% significance level. Trends in monthly temperature data are consistently positive in all months, and statistically significant in summer (December to February), in March, June, August and October–November (Fig. 9).

Table 3 Trend statistic Z for seasonal and annual temperature data at station 29, for the period of record 1965–2004. In bold are statistically significant trends. All significant trends are at 1% significance level.

DJF	MAM	JJA	SON	Annual
2.74	1.54	**3.16**	**3.03**	**2.94**

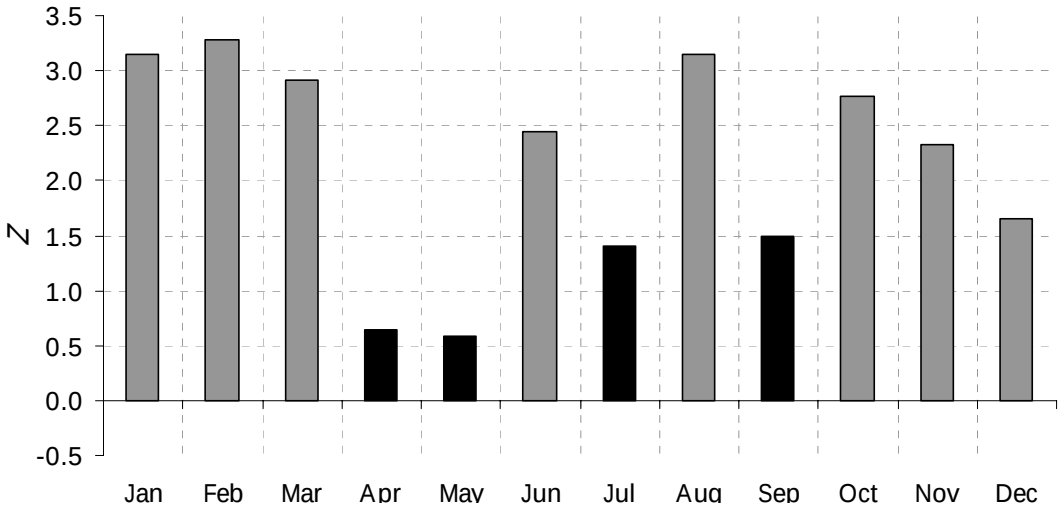

Fig. 9 Trend test statistic *Z* for monthly mean temperature at station 29. The sign of *Z* indicates trend direction. Grey indicates statistically significant trends; black indicates no statistically significant trends.

Correlation with global climatic signals Comparison of the time series of monthly mean streamflow anomalies at station 14 and standardised monthly SOI is shown in Fig. 10. It is evident from Fig. 10 that there is a strong inverse correlation

between SOI and standardised streamflow during ENSO events. Maxima in the monthly streamflow record coincide with warm phase ENSO years (negative SOI) at all stations in the Aconcagua basin (see for instance the event of 1977–1978, of 1982–1983 and of 1987–1988 in Fig. 10). In some years, runoff peaks can be observed in both the ENSO and ENSO-plus-one year, such as in the warm phase events of 1977–1978 and 1982–1983 (Fig. 10). This might be explained by the increase in winter precipitation associated with warm phase ENSO events, which has been both documented by previous research (e.g. Waylen & Caviedes, 1990; Rutllant & Fuenzalida, 1991; Montecinos & Aceituno, 2003) and revealed by the analysis conducted in this study (see below in this section). Increased winter precipitation at high elevations leads to increased winter accumulation, which results in turn in an increase in summer melt and therefore runoff in the following summer. This mechanism has been reported by, among others, Cerveny *et al.* (1987), Waylen & Caviedes (1990) and Schneider & Gies (2004).

Correlation coefficients at time lag 0, ρ, were computed between the time series of annual, seasonal and monthly streamflow at the five gauging stations and the SOI, and are listed in Table 4 for the seasonal time scale. Correlation coefficients are in general negative, in agreement with results of previous studies (e.g. Pittock, 1980; Schneider & Gies, 2004). At the monthly time scale, correlation coefficients vary from $\rho = -0.18$ at station 16 to $\rho = -0.28$ at station 14. Correlation analyses conducted on a seasonal basis between streamflow and SOI reveals a number of characteristics. First, correlation is always negative in all seasons and at all stations (Table 4), which is also in agreement with findings of the current literature that have shown that SOI is

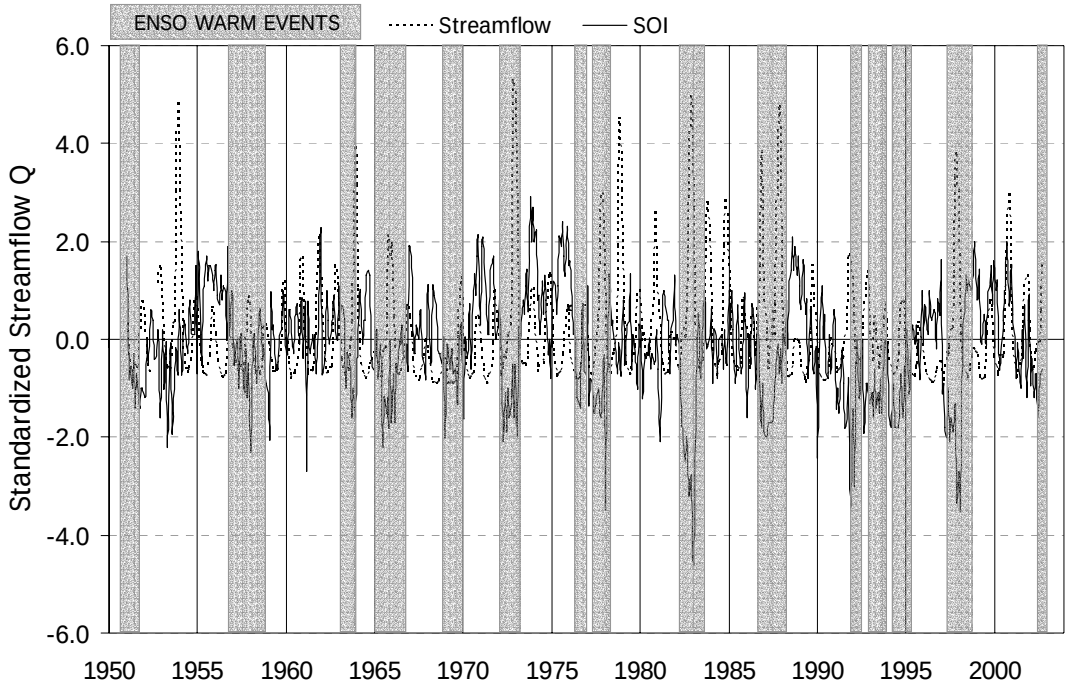

Fig. 10 Time series of the standardised monthly South Oscillation Index (SOI) and of standardised monthly mean streamflow *Q* at station 14, for the period 1951–2002. Positive values of SOI indicate cold phase ENSO events (La Niña) and negative values warm phase ENSO events (El Niño). The grey boxes indicate warm ENSO events.

inversely correlated to streamflow. Second, in summer (DJF), when runoff is high and the contribution to annual total runoff is the highest, correlation coefficients are also high, varying between ρ = –0.47 at station 18 and ρ = –0.63 at station 15 (Table 4). This can be explained by increased temperature associated with the ENSO warm phase events (see below), and might also indicate that ENSO phenomena cause an increase in summer precipitation. Third, winter (JJA) correlation coefficients are also high, revealing the well documented increase in winter precipitation reported by several studies (see Waylen & Caviedes, 1990; Montecinos & Aceituno, 2003), which results in turn in an increase of winter runoff. Values of winter correlation coefficients are very high at station 14 (ρ = –0.58) and 15 (ρ = –0.52), which are situated in the lower part of the upper basin. Stations 17, 18 and 16, however, show smaller correlation coefficients (Table 4). At these sites, winter precipitation falls mainly as snow, and has therefore a limited effect on the winter runoff. It creates, however, a storage of water in the form of winter accumulation which will melt in the following summer season. This effect is particular evident at the highest station 16, which has the lowest correlation coefficient of all stations (ρ = –0.17, Table 4).

Time series of mean annual, seasonal and monthly precipitation records were also correlated to the SOI. The results reveal that correlation coefficients are negative at both the annual and seasonal scale at almost all stations (Table 5). Annual correlation coefficients vary between ρ = –0.40 (station 37) and ρ = –0.55 (station 27), indicating that a stronger connection between precipitation and SOI at the annual scale exists than between streamflow and SOI. This was expected, given that runoff is an integrated variable that is affected by the transformation of rainfall into runoff operated by the watershed. The three highest ρ are found at station 34, 29 and 27, which are located in

Table 4 Correlation coefficients between mean seasonal streamflow and mean seasonal standardised SOI at the five streamflow stations.

Station	DJF	MAM	JJA	SON
14	–0.49	–0.30	–0.58	–0.37
15	–0.63	–0.22	–0.52	–0.41
16	–0.52	–0.16	–0.17	–0.12
17	–0.54	–0.09	–0.30	–0.28
18	–0.47	–0.13	–0.24	–0.28

Table 5 Correlation coefficients between mean seasonal precipitation and mean seasonal standardised SOI at the meteorological stations. In bold the seasonal correlation coefficients higher than 0.5.

Station	Annual	DJF	MAM	JJA	SON
18	–0.48	–0.13	–0.36	**–0.60**	–0.03
25	–0.47	–0.17	–0.43	**–0.60**	–0.06
26	–0.49	–0.21	–0.33	**–0.62**	–0.05
27	**–0.55**	–0.23	–0.42	**–0.65**	–0.23
28	–0.45	0.02	–0.36	**–0.55**	–0.01
29	**–0.54**	–0.09	–0.41	**–0.62**	–0.23
30	–0.41	0.26	–0.36	**–0.55**	–0.02
34	**–0.51**	–0.15	–0.38	**–0.57**	–0.31
37	–0.40	0.06	–0.38	**–0.54**	–0.21

the upper section of the Aconcagua basin. At the annual scale, results seem to suggest that the effect of ENSO is more marked at the stations located in the upper section of the basin. Seasonal correlation coefficients also reveal a couple of interesting features. First, very strong correlation between precipitation and SOI can be observed in winter (JJA) at all stations (Table 5). As mentioned above, this funding agrees with the evidence produced by a number of other studies that looked at the effect of ENSO events on the hydroclimatic variability of the region. The order of magnitude of the correlation coefficient is very similar to that found by Aceituno (1988). Second, correlation coefficients in autumn (MAM) are also consistently negative and important. Less conclusive is the evidence about the summer (DJF) and spring (SON) seasons, which show both negative and positive ρ of different, but always limited, magnitude.

Analyses of lags correlations for both streamflow and precipitation did not bring any insight into the relation of streamflow and precipitation with the SOI.

Mean monthly, annual and seasonal temperature was also correlated to the SOI, and results of the correlation analysis show a consistent negative correlation at all time scale. On a seasonal basis, the stronger negative correlation was found in autumn (MAM).

DISCUSSION

The analyses of recent trends in streamflow, precipitation and temperature in the Aconcagua basin has revealed several interesting features of this mountainous basin in the dry Andes. Analysis of annual, seasonal and monthly trends in streamflow has revealed the existence of significant decreasing trends in the period 1970–2002 at stations 17 and 18 in the upper section of the basin. Decreasing trends, although not significant, were observed at all time scales at the remaining streamflow stations. This decrease in runoff observed in the uppermost stations suggests that progressively lower annual runoff is produced in the basin, especially in its upper section. In contrast to streamflow, annual and seasonal precipitation records do not show the same significant decreasing trends in recent decades. For the 40 years common period from 1965, none of the studied gauges in Table 2 exhibited a statistically significant trend in annual precipitation. We did not find significant trends in seasonal precipitation except in the spring (SON) precipitation at station 34 for the period of record 1954–2004 (positive); and in autumn (MAM) total at station 18 and 29 for the period of record 1965–2004 (positive) (Fig. 8(c)). Most notable is that there are no significant trends in the precipitation amount in recent winter seasons, which represent the highest contribution to the annual precipitation totals. However, analyses of seasonal precipitation in the shortest and most recent period of record (1974–2004) showed an inversion in trend tendency at some stations, with stations 34, 28 and 30 seeing negative trends in both annual (Fig. 7(d)) and spring mean runoff time series (Fig. 8(d)). However, none of these trends is statistically significant. The results of this analysis show that trends in precipitation and streamflow in the Aconcagua basin in recent periods are not well correlated, and that changes in spring (and to a less degree winter) precipitation measured at some raingauges can only partly explain the trends in streamflow observed in the upper basin since 1972.

A factor that needs to be considered when studying the relationship between driving climatic factors such as temperature and precipitation and their effect on the integrated catchment variable streamflow are the characteristics of the watershed. In this case, a predominant characteristic of the basin is the presence of glaciers and extensive snow covers. The decrease in streamflow observed in the upper basin could be explained by a progressive change in glacier area and volume in the basin, corresponding to the retreat of the glaciers. This would explain the decrease in runoff observed at the two gauging stations that are closest to the glacier-covered area of the basin (statistically significant decreasing trends), which is reflected to a lesser extent in the time series records at the stations downvalley (15 and 14, statistically not significant decreasing trends). Evidence of glacier retreat and thinning in central Chile during the 20th century has been provided by Casassa (1995) and Rivera *et al.* (2002). Rivera *et al.* (2002) examined glacier surface and thickness variations for 95 Chilean glaciers, and concluded that a general glacier recession has occurred in central Chile, with an average estimate of 12.8% of area loss in the last 51 years from 1945 to 1996. The hypothesis that glaciers have been retreating in the recent past in the Aconcagua upper section and are therefore contributing less to the downvalley streamflow is corroborated by the results of temperature trends, which showed a statistically significant increase in monthly, seasonal and annual temperature in the common period of record 1965–2004. This result is in agreement with findings of previous studies on temperature trends (Rosenblüth *et al.*, 1997; Carrasco *et al.*, 2005), which have indicated statistically significant warming since the end of the 19th century to the end of the 20th century in central Chile. Carrasco *et al.* (2005) obtained an overall warming of 1.3–2.1°C in minimum near-surface air temperature in central Chile during the period from 1961 to 2001, and a warming of 0.2–1.5°C in maximum temperature. A sustained positive change in air temperature will likely affect both the summer snowmelt, by enhancing it, and the phase of the winter precipitation, by increasing the amount of precipitation that falls as liquid precipitation, thus decreasing glacier storage. This seems to be confirmed by the fact that the negative temperature trend reported is due to changes in minimum temperature rather than in maximum temperature (Rosenblüth *et al*., 1997; Carrasco *et al*., 2005). For the same reasons, it is likely that the extension and depth of the seasonal snow covers in the area have also been decreasing, as it might also be inferred from the results of Carrasco *et al.* (2005), which showed an increase of the snow line elevation of 127 m in central Chile in the last quarter of the 20th century. Glacier changes in the Aconcagua basin, however, are difficult to document because of limited data (e.g. Rivera *et al*., 2002). A new mapping of the glacier extension in the area is currently being undertaken by the authors in cooperation with Centro de Estudios Cientificos, Chile, using images from the ASTER satellite. They will allow comparison of the actual glacier extent with that derived from the older maps of the Instituto Geografico Militar of the Chilean Army that were made during the 1970s, and therefore assessment of changes in the intervening 30 years. It is evident from the analysis in this paper that this is a key step to be carried out to interpret the observed hydroclimatic trends in the context of recent glacier cover changes in the basin.

Analysis of hydroclimatic variability has often been conducted at the monthly and annual time scale for the South American region (e.g. Pittock, 1980; Aceituno, 1988;

Montecinos *et al.*, 2000; Schneider & Gies, 2004). This is partly due to the fact that data are often only available at this time resolution. In this respect, our study is standard. However, in order to completely understand the observed variability in hydroclimatic factors in the basin, it will be crucial to perform the analysis of trends at higher time resolution. Several recent studies have shown that analysing trends in annual or monthly streamflow totals cannot provide the complete picture of runoff behaviour (e.g. Chiew & McMahon, 1996; Molnár & Ramírez, 2001; Birsan *et al.*, 2005). Comprehensive trends analysis conducted in the United States (e.g. Lettenmaier *et al.*, 1994; Lins & Slack, 1999; Groisman *et al.*, 2001) and Canada (e.g. Zhang *et al.*, 2001; Burn & Hag Elnur, 2002) have shown that both precipitation and streamflow records exhibit a complex behaviour in which trends significance depends on flow magnitude and season. Shifts in the distribution were observed, with high and low frequency exhibiting different behaviour in different seasons. The results of these and other studies have demonstrated that, in many cases, only detailed examination of high resolution (i.e. daily) streamflow data can identify the complex changes that may have occurred in the instrumental record (e.g. Chiew & McMahon, 1996). The analysis conducted in this paper has already highlighted differences in trend behaviour between seasons. This needs to be complemented by analyses of trends in event frequency, event intensity in different quantiles, and in particular, in precipitation and streamflow maxima, in wetness (number of wet days), etc., as has been done in recent contributions for watersheds in Europe and North America (e.g. Molnár & Ramírez, 2001; Birsan *et al.*, 2005).

There is a lack of trends analysis conducted in the South American region and in particular in central Chile (Rosenblüth *et al.*, 1997), and this paper intended to contribute to explore this issue in the region. Most of the studies conducted in the region have focused on the impact of the ENSO on hydroclimatic variability (e.g. Waylen & Caviedes, 1990; Montecinos & Aceituno, 2003). The results of our analysis of SOI correlation with streamflow, precipitation and temperature records are in agreement with previous findings. Winter precipitation has been shown to increase during El Niño years (e.g. Montecinos & Aceituno, 2003).This was confirmed by our analysis, which has shown that winter (JJA) precipitation correlates very well with SOI (high negative correlation coefficients at all stations). Correlation coefficients between mean seasonal runoff and SOI were also high in winter at the stations at the lower elevation in the upper basin, reflecting the increase in precipitation that causes an increase in runoff at lower elevation. At higher elevation, precipitation falls as snow and does not affect the runoff in that season (while it will in the following summer). Summer streamflow also correlates well with SOI, probably because of an increase in temperature associated with El Niño events. In addition to confirming previous findings, our study has provided evidence for correlation between SOI and autumn (MAM) precipitation (Table 5), suggesting that warm-phase ENSO years cause an increase not only in winter, but also in autumn precipitation.

Results of trend analysis on seasonal precipitation data in the period of records 1965–2004 and 1974–2004 reveal an interesting feature of the precipitation pattern in the recent decades. Figure 8(d) shows that in the most recent period of record (1974–2004), autumn (MAM) precipitation totals have consistently increased and spring (SON) totals have consistently decreased at all stations, while no major changes have

occurred in winter precipitation totals (no trends at all or small negative trends, such as at stations 34, 28 and 27, see Fig. 8(d)). This might suggest that from 1974 a shift in precipitation seasonality has occurred in the Aconcagua basin, with more precipitation falling in autumn and less in spring. This is likely going to impact the glacier's mass balance, in that precipitation falling as snow at the onset of the melt season covers the glacier with a highly reflecting layer with high albedo that slows down the melt process by reducing absorption of shortwave incoming radiation. The effect of fresh snowfalls on the glacier albedo and melt at the onset of the ablation season has been demonstrated by Brock *et al.* (2000). Less precipitation falling as snow in the upper basin in spring, together with increased temperature, might have contributed to shift the onset of the melt season. This might suggest an earlier start of the melt season in the last 30 years. Such a precipitation pattern was observed for the period of record 1974–2004, which corresponds to the period analysed for streamflow trends in which statistically significant decreasing trends in mean runoff at the two stations, 17 and 18, in the upper basin were observed.

A contribution of this paper has been to highlight a decrease in streamflow in the recent decades in the upper section of the Aconcagua basin. Recent literature suggests that increasing runoff trends are found in many parts of the world (e.g. Birsan *et al.*, 2004), associated with increasing precipitation and/or temperature. The preliminary results presented here, however, seem to suggest that no increase in runoff took place in the upper section of the Aconcagua basin from 1972. This is to connect with the hydrological character of the basin, which has a glacio-nival regime dominated by snow- and ice-melt, and in which, therefore, glaciers and snow cover play a crucial role in determining the streamflow regime. Decrease in glacier and snow cover extension, which has been documented for this region by a recent study (Rivera *et al.*, 2002), could counteract the effect of increased precipitation and determine an overall decrease in streamflow. The finding of this paper should be supported by further analysis with more complete data sets.

In order to interpret the observed hydroclimatic trends in the context of recent glacier cover changes, therefore, this investigation needs to be complemented by two further steps of analysis: (1) analysis of high resolution (i.e. daily) data; and (2) a more complete analysis of changes in the glacier volume and area and in the snowcover extension. Both steps have been already undertaken by the authors, and results will be published in a follow-up paper.

CONCLUSIONS AND OUTLOOK

This paper has provided a first assessment of the hydroclimatic variability in the Aconcagua River basin, and in particular in its upper section, as it was reconstructed from monthly means of streamflow, precipitation and temperature records. Two types of analysis were conducted. First, the impact of global climatic signals on the interannual variability of streamflow was investigated through correlation analysis in order to gain a complete picture of the factors affecting the variability of streamflow. Second, analysis of trends was conducted to detect changes in the hydroclimatic variables on the long term.

With respect to the first part of the analysis, this study has confirmed the findings of previous studies conducted in the region suggesting that ENSO has an effect on the streamflow and precipitation regimes during both its warm and cold phase, and that increased winter precipitation is associated with warm phase ENSO events. In addition to previous findings, our work has also shown that the increase in winter precipitation associated with warm phase ENSO years is also accompanied by an increase in autumn (MAM) precipitation. On a longer time scale, this work has provided initial evidence of a consistent decrease in annual, seasonal and monthly streamflow at the stations in the upper basin in the most recent period of record 1970–2004, which might be attributed to a change in glacier streamflow contribution. Seasonal snowcovers, on the other hand, might also have been decreasing in the last decades, as it might be inferred by the decrease (although statistically not significant) in precipitation observed in the same period at some stations and the consistent increase in temperature exhibited by station 29 and observed at other stations in central Chile (Rosenblüth *et al*., 1997; Carrasco *et al*., 2005).

This evidence will have to be confirmed by further research, including both analysis of longer and higher resolution data records and analysis of changes in glacier runoff. This study is part of an ongoing extensive investigation aimed at assessing the past and future variations of water resources in the upper Aconcagua basin, with emphasis put on the role played by glaciers and snow cover. The analysis conducted in this paper is a first step towards the identification of the causes of the recent hydro-climatic variations. The two next steps that need to be taken are: (1) analysis of trend of daily data and quantiles of the distribution at all stations in the basin (these data have been very recently made available by DGA to the authors); and (2) connection of observed changes in streamflow with recent changes in glacier cover and extension in the basin. Evidence of glacier shrinkage in central Chile has been provided by Casassa (1995) and Rivera *et al*. (2002). These studies have shown that from 1945 onwards glaciers in the area have been thinning and retreating, with an average rate of surface loss higher than in the other regions of Chile. In this context, it would be appropriate to investigate when the glacier shrinkage, and consequent contribution to runoff, have taken place most intensely in association with the increase in minimum and maximum temperature suggested by some authors (Rosenblüth *et al*., 1997; Carrasco *et al*., 2005). The results of this investigation seem to suggest that the increase in the melt water production from the glaciers in the upper section of the Aconcagua basin took place earlier, and that the glaciers are actually in a phase of lesser contribution to the basin streamflow than before. Accordingly, a new mapping of glacier extension is currently being undertaken by the authors, which could be used in the future to relate the observed trends, or lack thereof, in streamflow to the basin's attributes and in particular to the presence of glaciers and their extension. Analysis of daily data and in particular of the quantiles distribution is currently under investigation, and will be published in a following paper.

Acknowledgements The Chilean Dirección General de Aguas (DGA) is gratefully acknowledged for providing the hydroclimatic data for this analysis. We would like to thank Marius Birsan for his help with trend analysis, and Peter Molnar for useful

discussions about this article. We thank Lars Ribbe for providing the original Fig. 1. FP would like to thank José Araos for support when FP was in Chile. We gratefully acknowledge the comments of two anonymous reviewers that considerably improved the final manuscript.

REFERENCES

Aceituno, P. (1988) On the functioning of the Southern Oscillation in the South America Sector. Part I: Surface climate. *Mon. Weath. Rev.* **116**, 505–524.

Birsan, M. V., Molnár, P., Burlando, P. & Pfaundler, M. (2005) Streamflow trends in Switzerland. *J. Hydrol.* **314**(1–4), 312–329.

Brock, B. W., Willis, I. C., Sharp, M. J. & Arnold, N. S. (2000) Modelling seasonal and spatial variations in the surface energy balance of Haut Glacier d'Arolla, Switzerland. *Ann. Glaciol.* **31**, 53–62.

Burn, D. H. & Hag Elnur, M. A. (2002) Detection of hydrologic trends and variability. *J. Hydrol.* **255**, 107–122.

Carrasco, J. F., Casassa, G. & Quintana J. (2005) Changes of the 0°C isotherm and the equilibrium line altitude in central Chile during the last quarter of the 20th century. *Hydrol. Sci. J.* **50**(6), 933–948.

Casassa, G. (1995) Glacier inventory in Chile: current status and recent glacier variations. *Ann. Glaciol*. **21**, 317–322.

Cerveny, R. S., Skeeter, B. R. & Dewey, K. F. (1987) A preliminary investigation of a relationship between South American snow cover and the southern oscillation. *Mon. Weath. Rev.* **115**, 620–623.

Chiew, F. H. S. & McMahon, T. A. (1996) *Trends in Historical Streamflow Records. Regional Hydrological Response to Climate Change* (ed. by J. A. A. Jones), 63–68. Kluwer, Doredrecht, The Netherlands.

Groisman, P. Y., Knight, R. W. & Karl, T. R. (2001) Heavy precipitation and high streamflow in the contiguous United States: trends in the twentieth century. *Bull. Amer. Met. Soc.* **82**(2), 219–246.

Helsel, D. R. & Hirsch, R. M. (1992) *Statistical Methods in Water Resources.* Elsevier, Amsterdam, The Netherlands.

Hess, A., Iyer, H. & Malm, W. (2001) Linear trend analysis: a comparison of methods. *Atmos. Environ.* **35**, 5211–5222.

Huber, U. M, Bugmann, H. K. M. & Reasoner, A. M. (eds) (2005) *Global Change and Mountain Regions: An Overview of Current Knowledge*. Advances in Global Change Research series, Vol. 23. Springer, New York, USA.

Kahya, E. & Kalayci, S. (2004) Trend analysis of streamflow in Turkey. *J. Hydrol.* **289**, 128–144.

Karl, T. R. & Plummer, N. (1995) Trends in high-frequency climate variability in the twentieth century. *Nature* **377**, 217–220.

Kulkarni, A. & von Storch, H. (1995) Monte Carlo experiments on the effect of serial correlation on the Mann-Kendall test of trend. *Meteorol. Z.* **4**(2), 82–85.

Lettenmaier, D. P., Wood, E. F. & Wallis, J. R. (1994) Hydro-climatological trends in the continental United States, 1948–88. *J. Climate* **7**, 586–606.

Lins, H. F. & Slack, J. R. (1999) Streamflow trends in the United States. *Geophys. Res. Lett.* **26**(2), 227–230.

Molnár, P. & Ramírez, J, G. (2001) Recent trends in precipitation and streamflow in the Rio Puerco basin. *J. Climate* **14**, 2317–2328.

Montecinos, A. & Aceituno, P. (2003) Seasonality of the ENSO-related rainfall variability in central Chile and associated circulation anomalies. *J. Climate* **16**, 281–296.

Montecinos, A., Díaz, A. & Aceituno, P (2000) Seasonal diagnostic and predictability of rainfall in subtropical South America based on tropical pacific SST. *J. Climate* **13**, 746–758.

Pekarova, P., Miklanek, P. & Pekar, J. (2003) Spatial and temporal runoff oscillation analysis of the main rivers of the world during the 19th–20th centuries. *J. Hydrol.* **274**, 62–79.

Pittock, A. B. (1980) Patterns of climatic variations in Argentina and Chile. Part I: Precipitation, 1931–1960. *Mon. Weath. Rev*. **108**, 1347–1361.

Rivera, A., Acuña, C., Casassa, G. & Bown F. (2002) Use of remote sensing and field data to estimate the contribution of Chilean glaciers to the sea level rise. *Ann. Glaciol*. **34**, 367–372.

Rosenblüth, B., Fuenzalida, H. A. & Aceituno, P. (1997) Recent temperature variations in Southern South America. *Int. J. Climatol.* **17**, 67–85.

Rubin, M. J. (1955) An analysis of pressure anomalies in the Southern Emisphere. *Notos* **4**, 11–16.

Rutllant, J. & Fuenzalida, H. (1991) Synoptic aspects of the central Chile rainfall variability associated with the Southern Oscillation. *Int. J. Climatol*. **11**, 63–76.

Schneider, C. & Gies, D. (2004) Effects of El Niño-Southern Oscillation on Southernmost South America precipitation at 53 S revealed from NCEP_NCAR reanalyses and weather station data. *Int. J. Climatol.*, **24**, 1057–1076.

Waylen, P. R. & Caviedes, C. N. (1990) Annual and seasonal streamflow fluctuations of precipitation and streamflow in the Aconcagua River basin, Chile. *J. Hydrol*. **120**, 79–102.

Waylen, P. R. & Poveda, G. (2002) El Nino–Southern Oscillation and aspects of western South American hydro-climatology. *Hydrol. Processes* **16**, 1247–1260.

Wright, P. B. (1984) Relationships between the indices of the Southern Oscillation. *Mon. Weath. Rev*. **112**, 1913–1919.

Yue, S. & Wang, C. Y. (2002) Applicability of prewhitening to eliminate the influence of serial correlation on the Mann-Kendall test. *Water Resour. Res*., **38**(6), doi:10.1029/2001WR000861.

Yue, S. & Pilon, P. (2003) Interaction between deterministic trend and autoregressive process. *Water Resour. Res*. **39**(4), doi:10.1029/2001WR001210.

Yue, S., Pilon, P. & Cavadias, G. (2002) Power of the Mann-Kendall and Spearman's rho tests for detecting monotonic trends in hydrological series. *J. Hydrol.* **259**, 254–271.

Yue, S., Pilon, P. & Phinney, B. (2003) Canadian streamflow trend detection: impacts of serial and cross-correlation. *Hydrol. Sci. J*. **48**(1), 51–63.

Zhang, X., Harvey, K. D., Hogg, W.D. & Yuzyk, T. R. (2001) Trends in Canadian streamflow. *Water Resour. Res*. **37**(4), 987–998.

Glacier Mass Balance Changes and Meltwater Discharge (selected papers from sessions at the IAHS Assembly in Foz do Iguaçu, Brazil, 2005). IAHS Publ. 318, 2007.

Preliminary assessment of groundwater contribution to the hydrology of an alpine lake in the Canadian Rockies

JAIME LYNN HOOD, MASAKI HAYASHI & JAMES W. ROY*

Department of Geoscience, University of Calgary, 2500 University Drive NW, Calgary, Alberta T2N 1N4, Canada
jlhood@ucalgary.ca

* now at: *National Water Research Institute, Environment Canada, Burlington, Ontario L7R 4A6, Canada*

Abstract Groundwater storage and pathways in alpine headwater regions of the Canadian Rockies have not been well understood, although these processes may play a significant role in controlling the amount and timing of runoff in mountain streams. A field study was initiated in 2004 at the Lake O'Hara watershed in Yoho National Park, British Columbia, to examine the role of groundwater in the alpine hydrological cycle. The main objective of the first year of this study was to quantify the groundwater input to Lake O'Hara using a water balance approach, which consisted of weekly field measurements of inflow and outflow streams and lake water level, along with local meteorological data. Of all measurable terms in the water balance, surface water inflow and outflow were by far the largest components, while direct precipitation and evaporation were almost negligible. Surface water outflow was substantially greater than inflow, indicating that the groundwater residual (i.e. net groundwater inflow minus outflow) was a major component. Taking the groundwater residual as a minimum estimate of groundwater inflow to the lake, it was estimated that groundwater contribution was approximately 25–40% of total water inputs to the lake during the peak flow period (late June to early July) and 35–50% toward the end of the summer. This preliminary finding implies that groundwater processes play a much more important role in the hydrological cycle of alpine headwater regions than previously thought.

Key words glacier; Lake O'Hara; mountain hydrology; water balance

INTRODUCTION

Rivers originating in the Rocky Mountains are an important source of water for the majority of the population, as well as industrial and agricultural activities, in the prairie region of Canada. Alpine glaciers in the Canadian Rockies are perceived by the public as the dominant source of water during summer months, and hence there is a growing concern about the effects of climate warming on glaciers and mountain streams and lakes. While the glaciers are clearly shrinking in response to climate warming, the snowpack is an additional and significant contributor to annual streamflow. The effect of snow and ice melt on the hydrological cycle of alpine watersheds, including diurnal changes in streamflow (Singh *et al.*, 2004; Lundquist & Dettinger, 2005) and lag times between meteorological forcing and glacier melt response (Shea *et al.*, 2005) have been extensively studied. However, the pathway by which melt water reaches streams and lakes in alpine terrain is not well understood. The routing and transit time of

subsurface flow pathways will affect how alpine streams respond to precipitation and melt events; therefore, it is imperative to understand the effects of both seasonal melting and groundwater flow pathways. An improved understanding of the storage and flow mechanisms is necessary for reliable model predictions of the response of mountain streams and lakes to climate warming.

Recent studies in Colorado and California, USA, have indicated that much of the rain and melt water passes through the ground before entering nearby streams, both quickly through shallow groundwater (Campbell *et al.*, 1995; Michel *et al.*, 2000; Sueker *et al.*, 2000) and more slowly through drainage of overburden materials such as talus fields (Clow *et al.*, 2003). In headwater zones of the Canadian Rockies, first- and second-order streams typically go through lakes before they feed higher-order streams. Therefore, the exchange of groundwater with alpine lakes may play an important role in the response of mountain streams to melt-water inputs from glaciers and seasonal snowpack. However, there have been few published studies on this topic. Groundwater exchange was considered negligible for two small lakes overlying fractured basalt, in the Flattops Wilderness Area, Colorado (Michel *et al.*, 2002) and for Loch Vale, Colorado, and Emerald Lake, California (Winter *et al.*, 2003) both overlying granitic bedrock. Other researchers working with ponds or lakes in Colorado (Campbell *et al.*, 2004) and Montana (Gurrieri & Furniss, 2004) have suggested groundwater played a significant role. However, a direct quantification of the groundwater exchange was not made in these two studies.

In an effort to further understand the hydrological processes in the alpine headwater region of the Canadian Rockies, a field study was initiated in 2004 at the Lake O'Hara watershed. The main objective of the first year of this study was to quantify the groundwater input to Lake O'Hara using a water balance approach. This paper reports a preliminary assessment of the data collected in 2004, which was presented at a symposium on the *Contribution from Glaciers and Snow Cover to Runoff from Mountains in Different Climates* at the 7th Scientific Assembly of the International Association of Hydrological Sciences in Foz do Iguaçu, Brazil, in April 2005. A more comprehensive analysis including the 2005 data was subsequently reported by Hood *et al.* (2006).

SITE DESCRIPTION

The Lake O'Hara study area is located in a 14 km^2 watershed in the Canadian Rockies, in Yoho National Park, British Columbia (Fig. 1). The watershed encompasses rugged terrain, ranging in elevation from 2010 m to 3490 m, of which approximately 20% is sub-alpine coniferous forest and 80% is alpine. The Oesa and Opabin sub-watersheds are partially glaciated, containing small pocket glaciers (Fig. 1). Glaciers cover approximately 6% of the watershed. Mean annual precipitation is estimated to be 1100–1500 mm, depending on elevation, based on the archived data from meteorological stations in the area around Lake O'Hara (MSC, 2005). Much of the watershed becomes snow-covered by early October. Snowmelt normally starts in late April, and the watershed becomes mostly snow free by late July, except around the glaciers. The geology consists primarily of early Cambrian sedimentary quartzite, sandstone and shale, while some Middle Cambrian limestone and dolostone are present

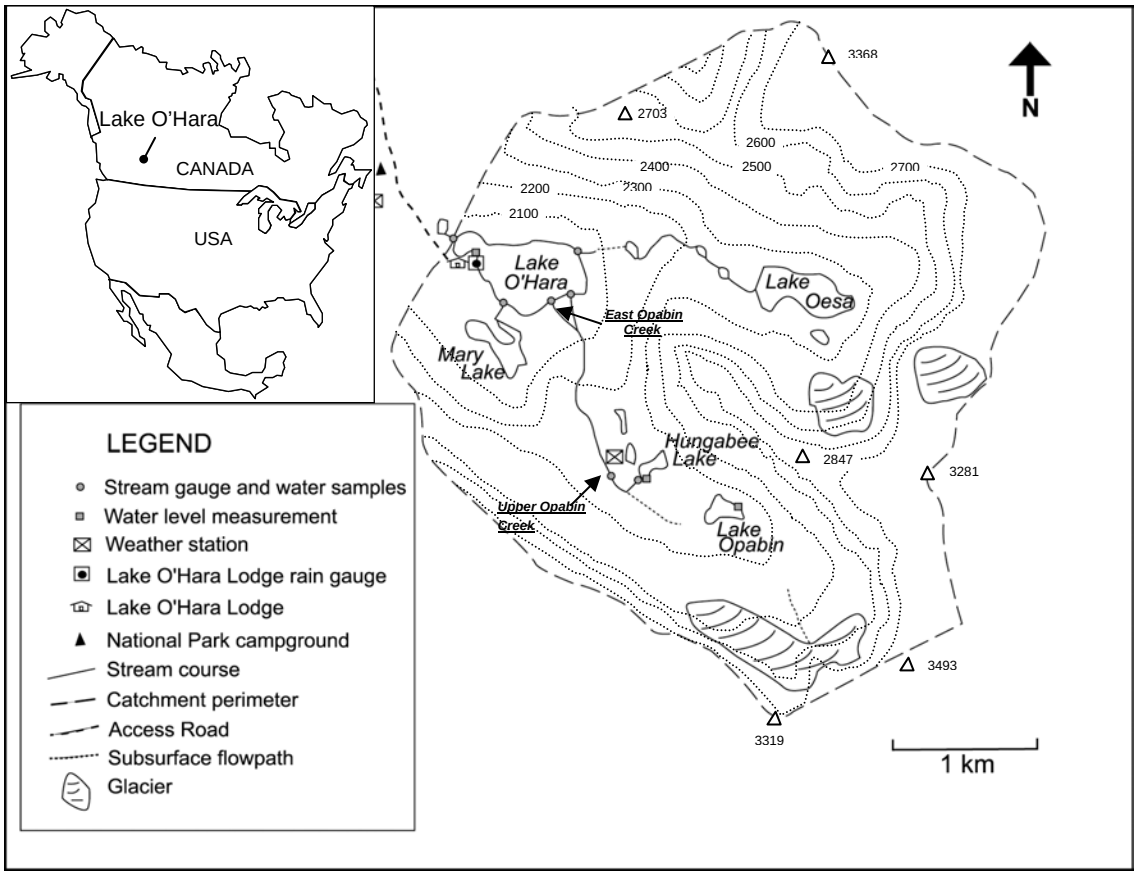

Fig. 1 Lake O'Hara location and topographic map. Contour interval is 100 m.

at elevations above 2900 m on the east side of the watershed and above 2600 m on the west side (Price, 1980). In the basin there are many areas with extensive surficial cover, including large terminal moraines, ablation moraines, talus fields and talus cones. The talus in the area is comprised of siliclastics and carbonate material that has been transported from higher elevations.

Lake O'Hara is 0.26 km^2 in area and has a maximum depth of 42 m. The lake is ice-free from June until October. It is a relatively simple system fed by four inflowing creeks from three sub-watersheds (Mary, Opabin and Oesa) and drained by a single outlet (Fig. 1). Direct input of overland flow to the lake occurs as the snowpack around the lakeshore melts early in the melt season, but it is rarely observed during summer months. Like many other alpine lakes in the region, its outflow continues through the winter while all surface water sources are frozen, implying groundwater contribution, but the amount of groundwater inputs and its seasonal variability have never been quantified.

METHODS

Discharge measurement and water sampling and analysis

Discharge in the four inflowing creeks (Fig. 1) and single outflow was measured with the area–velocity method on a weekly basis from 8 June to 4 September 2004, and at

longer intervals until 13 November. A propeller flow meter (Global Water FP101) was used to measure flow velocity. To assess the magnitude of stream gauging errors, discharge was measured at three different sections within a 100-m stream reach located in the Opabin sub-watershed (Upper Opabin Creek – Fig. 1) seven times between 18 July and 31 August 2005 (Hood *et al.*, 2006). This stream reach represents a typical condition of stream channels measured in this study. The coefficient of variability for these discharge measurements ranged between 4% and 9% over these seven dates, with an average of 6%. Therefore, the magnitude of gauging error is expected to be 10% or less. Errors may also result from the "spot" measurements of discharge, because alpine streams typically have short-term fluctuations caused by the variability in the melting rate of glacier ice and snowpack (Singh *et al.*, 2004; Lundquist & Dettinger, 2005). A continuous water-level recorder (*in situ* Mini-Troll) was installed at the East Opabin Creek (Fig. 1) and a stage–discharge rating curve was established to address this issue (see below for results).

During the spring melt, bulk snow samples were collected weekly at two locations around the lake and three locations higher in the watershed. Snow samples were melted at room temperature and then bottled and stored at 4°C until analysis. Additionally, rain samples were collected weekly from a rain collector located near Hungabee Lake at 2250 m (Fig. 1). Hand-held meters were used to measure the pH, temperature, and electrical conductivity (EC) of snow and rain samples in the laboratory and of stream water at all gauging stations in the field. EC values were standardized to 25°C (Hayashi, 2004).

Lake storage

The water level of Lake O'Hara was measured manually on a concrete abutment of the Lake O'Hara Lodge dock on a weekly basis from 6 to 30 June 2004. From 30 June to 16 October, 2004, the water level was measured every 10 minutes with a pressure transducer (*in situ*, Mini-Troll) housed in a stilling well. Ten-minute data were later averaged to obtain hourly values. Water depths from the pressure transducer were compensated for long-term drift (Rosenberry, 1990) using manually measured data. Estimated error of water level measurement is less than 1 cm. Lake storage changes were calculated from water level changes assuming that changes in the lake area were negligible.

Precipitation and evaporation

Two sources of precipitation data were used in this study. Data from a manual gauge operated by the Lake O'Hara Lodge was used for the period 8 June to 26 August, 2004. Subsequently, data were collected by a meteorological station equipped with a Campbell Scientific CR10X data logger and located 500 m northwest of Lake O'Hara (Fig. 1). At the meteorological station, precipitation was measured using a tipping-bucket raingauge (Hydrological Services TB4) during summer months and a vibrating-wire raingauge equipped with a wind shield (Geonor T-200) after the first snowfall on 18 September. Cumulative precipitation during 25 August–17 September was 132 mm

measured by the tipping bucket, and 126 mm reported by the Lodge, and daily values were very similar between the two data sets.

As described below, evaporation is a very minor component of the water balance of Lake O'Hara. Meteorological data necessary for physically-based methods of evaporation estimates were not available until early September. Therefore, an attempt was made in this study to obtain a crude estimate of lake evaporation using the Thornthwaite temperature index method, as outlined in Rosenberry *et al.* (2004). Temperature data reported by Lake O'Hara Lodge were used when available; otherwise, data from the Wapta Lake meteorological station (MSC, 2005) were used. Wapta Lake is located 5 km north of Lake O'Hara at an elevation of 1650 m. Heat storage in lakes can be a significant factor affecting the evaporation flux (Blanken *et al.*, 2000). However, insufficient lake temperature data were collected to determine the extent of seasonal heat storage at Lake O'Hara.

Water balance calculation

The lake water balance equation was used to determine if a significant groundwater flux exists at Lake O'Hara:

$$\Delta S/\Delta t = \sum Q_{in} + P - E - Q_{out} + Q_{GWin} - Q_{GWout} \quad (1)$$

where $\Delta S/\Delta t$ is the rate of storage change ($m^3\ s^{-1}$), $\sum Q_{in}$ is the total discharge ($m^3\ s^{-1}$) of the four inflow creeks, P is precipitation ($m^3\ s^{-1}$), E is evaporation ($m^3\ s^{-1}$), Q_{out} is the discharge of the outflow stream ($m^3\ s^{-1}$), Q_{GWin} is the total flow rate of incoming groundwater ($m^3\ s^{-1}$), and Q_{GWout} ($m^3\ s^{-1}$) is the total flow rate of outgoing groundwater. Volumetric rates of precipitation and evaporation were calculated from the data measured in depth unit (mm day^{-1}) assuming a constant area of the lake. Separate values of groundwater inflow and outflow cannot be determined, only the difference between the two. As such, the water balance equation becomes:

$$\Delta S/\Delta t = \sum Q_{in} + P - E - Q_{out} + Q_{res} \quad (2)$$

where Q_{res}, the groundwater residual, is a net flow rate ($m^3\ s^{-1}$) of groundwater inflow to the lake (positive) or outflow (negative) from the lake.

RESULTS

Stream discharge and lake water level

Snowmelt began in May, prior to the first field visits, and the peak seasonal flow occurred around 1 July (Fig. 2(a)). The total discharge of the four inflow streams during the peak was 1.9 $m^3\ s^{-1}$. The discharge measured at the Lake O'Hara outlet varied from 0.11 $m^3\ s^{-1}$ to a maximum of 3.1 $m^3\ s^{-1}$ during the peak of snowmelt (Fig. 2(a)). Inflow and outflow generally decreased following the peak, but isolated maxima corresponding to storm events, as indicated by the precipitation data (Fig. 2(b)), occurred throughout the observation period. The lake water level reached its peak around 1 July (Fig. 2(c)), and followed a similar pattern to that of stream discharge (Fig. 2(a)).

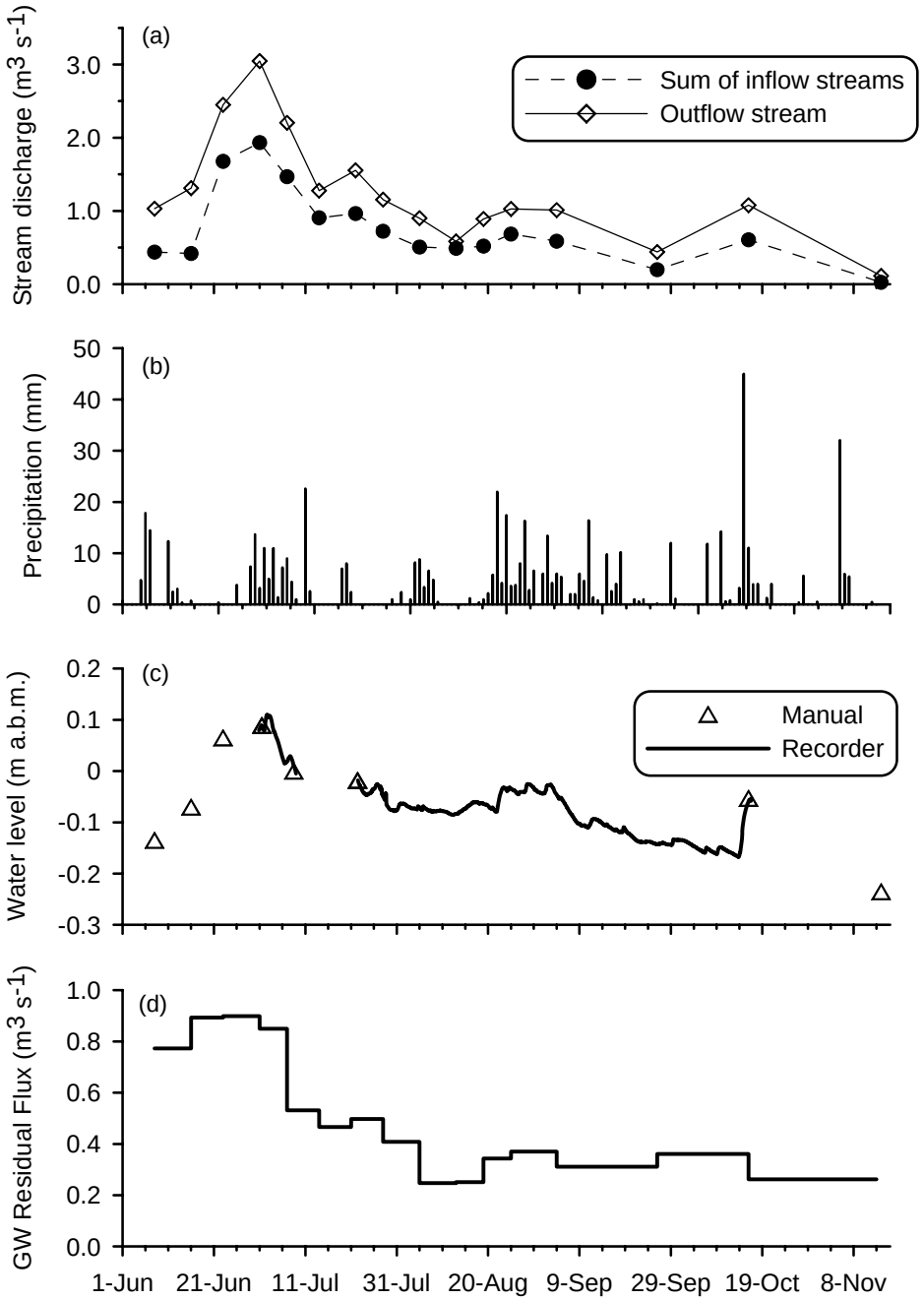

Fig. 2 (a) Total discharge of the four inflow streams and the Lake O'Hara outflow in 2004. (b) Daily precipitation. (c) Lake water level. (d) Groundwater residual (Q_{res}) in equation (2).

At the East Opabin Creek, the hourly discharge, estimated from the continuous water level data and the stage–discharge rating curve, had diurnal fluctuations as well as some peaks that were not captured by the manual measurements (Fig. 3(a)). In order to assess the errors resulting from using the spot measurements, average discharge values were calculated for each period (e.g. 14 July–22 July), by taking an arithmetic mean of the two end values (e.g. 14 July and 22 July) for manual data and of all hourly values for the hourly data. When average values are compared, the two methods were

reasonably similar (Fig. 3(b)) with a root-mean-squared (RMS) difference of 0.015 $m^3 s^{-1}$, which is approximately 7% of average discharge. Therefore, the expected magnitude of error resulting from the spot measurement is less than 10%. When the gauging error of 10% (see Methods above) is added to this value, the maximum error in discharge estimate is expected to be less than 20%.

Lake water balance

The water balance (equation (2)) for Lake O'Hara was calculated for the period of 1 July to 13 November, 2004. Since stream discharge data were available on discrete dates, the period was subdivided into weekly or longer intervals. The water balance for each interval was calculated using the arithmetic mean of the two end points for stream discharge, total value divided by the length of the interval for precipitation and evaporation, and the difference between the initial and final values for the storage change. Monthly summary of the water balance (Table 1) indicates that stream inflow and outflow were the dominant terms in equation (2), while evaporation, precipitation and storage change were minor components.

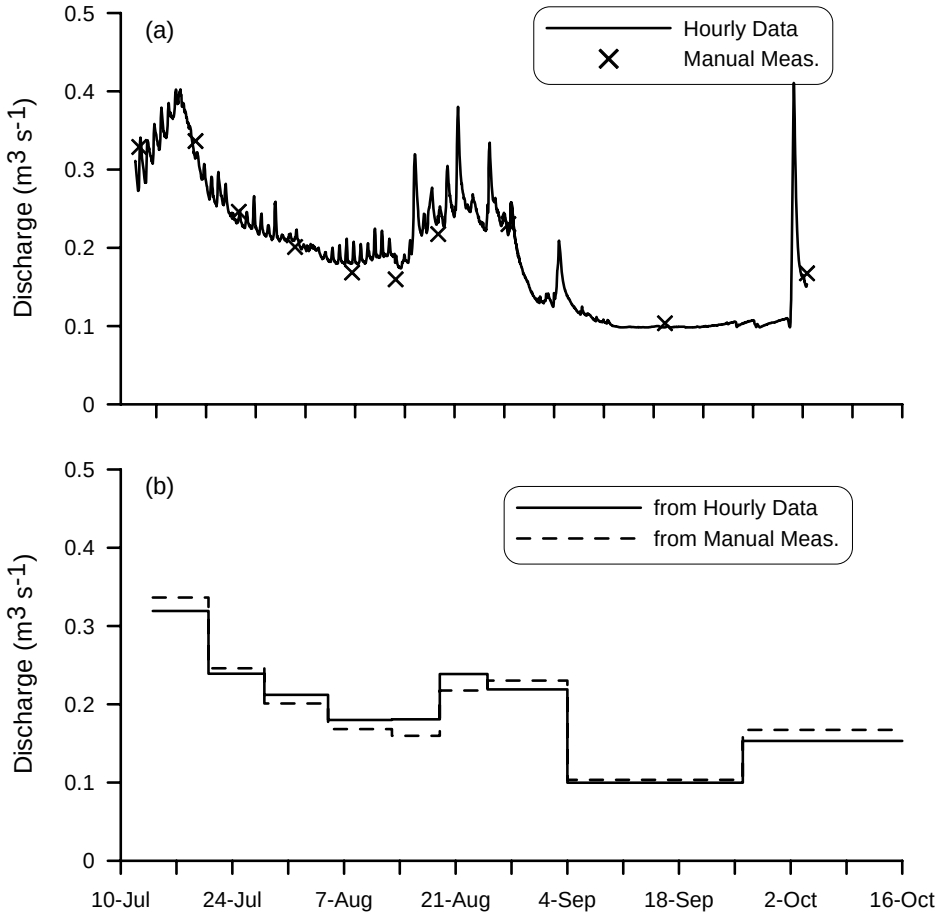

Fig. 3 Discharge at the East Opabin Creek in 2004. (a) Hourly discharge estimated from water level data (solid line) and manually measured values (crosses). (b) Weekly or longer-interval average calculated from hourly values and manual measurements.

Table 1 Summary of the water balance for Lake O'Hara on an approximately monthly-basis, for 2004.

Month	Lake Storage Increase	Stream Inflow	Precipitation	Stream Outflow	Evaporation	GW Residual
	mm	mm	mm	mm	mm	mm
Jun 8–Jul 1	224	7500	48	12970	70	5270
Jul 1–Jul 28	–154	9450	93	14440	79	5140
Jul 28–Aug 25	13	4780	95	7460	77	2650
Aug 25–Sept 26	–108	4570	135	7720	47	3170
Sept 26–Nov 13	–40	3870	164	7610	9	3630

At all times, the groundwater residual was positive (Table 1, Fig. 2(d)), indicating that groundwater inflow was much greater than groundwater outflow. It is impossible to quantify the groundwater inflow and outflow separately using the water balance alone. Therefore, the groundwater residual is considered a minimum estimate of groundwater inflow in this study. Noting that the surface water inflow and outflow are the dominant terms in equation (2) and that these terms have estimated errors of less than 20%, the error in groundwater residual is expected to be about 30% or less, using the standard method for error propagation (Harris, 1991). Adding these errors to the water balance calculation, Fig. 2(d) shows that groundwater contributed 0.90 ± 0.27 m^3 s^{-1} of water inputs to the lake during the peak flow and 0.25 ± 0.075 m^3 s^{-1} towards the end of the summer. This is equivalent to approx. 25–40% of surface outflow from the lake during the peak flow and 35–50% towards the end of the summer.

Electrical conductivity of stream and lake water

Electrical conductivity (EC) of surface inflows to Lake O'Hara provides a valuable insight into the potential role of groundwater pathways from the source (glacier, snowpack, and summer rain) to the creeks. The EC of snow and rain samples ranged from 1.5 to 19 μS cm^{-1}, indicating little interaction with minerals. The EC in the inflowing creeks was 100 μS cm^{-1} before the peak flow (Fig. 4) and gradually increased to 170 μS cm^{-1} by the late autumn. The latter value is relatively high for a headwater alpine system compared to 7 μS cm^{-1} reported by Gurrieri & Furniss (2004), 10–30 μS cm^{-1} by Richards & Moore (2003), 20–50 μS cm^{-1} by Ward *et al.* (1999). The relatively high value of EC indicates that the water flowing in the creeks in the late autumn had been in contact with minerals for a sufficiently long time to dissolve them, implying the importance of subsurface pathways, such as soil water and groundwater, in the source areas of the creeks. The lower EC values in June and July (Fig. 4) were probably caused by the mixing of relatively mineral-rich water with dilute snowmelt water rapidly reaching the creek via surface or near-surface pathways.

The EC of the outflow from Lake O'Hara had a much narrower range than that of the inflow water (Fig. 4), indicating that the seasonal variability is buffered by the lake. Considering the small distance of only a few kilometres between the drainage divide, which is also the continental divide of North America, and the lake outlet, the data shown in Fig. 4 indicate that mineral dissolution can alter the chemistry of melt water at the very top of mountain river watersheds.

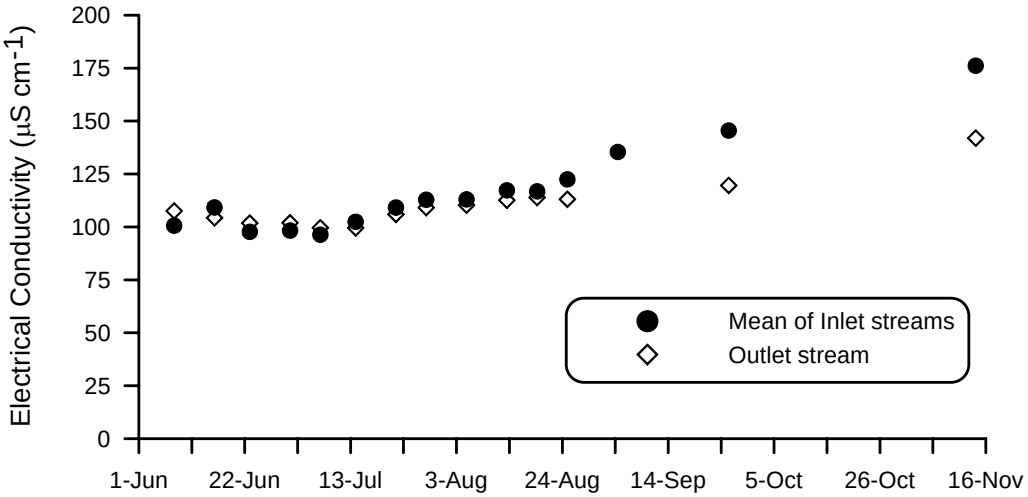

Fig. 4 Electrical conductivity of Lake O'Hara inflow and outflow streams. Inflow stream data are the discharge-weighted mean of the four inflow streams.

CONCLUSION

Of all measurable terms in the water balance of Lake O'Hara, surface water inflow and outflow were by far the most dominant components, while direct precipitation and evaporation were almost negligible. The water balance calculation in the summer of 2004 revealed that groundwater residual (i.e. net groundwater inflow minus outflow) was also a major component. Taking the groundwater residual as a minimum estimate of groundwater inflow to the lake, it was estimated that the groundwater contribution was approximately 25–40% of total water inputs to the lake during the peak flow period (late June to early July) and 35–50% toward the end of the summer. This preliminary finding implies that groundwater processes play a much more important role in the hydrological cycle of alpine headwater regions than previously thought. Therefore, further studies are warranted to examine the role of groundwater storage and pathways as these may significantly alter the amount and timing of ice- and snow-melt runoff and potentially affect the chemistry of water in alpine lakes and streams. Such studies should include the spatial and temporal distribution of snow accumulation and melt within the watershed, the mass balance of glaciers, detailed mapping of moraine and talus materials, and chemical and isotopic compositions of source waters.

Acknowledgements We thank Joanne Williams and Gloria Sundbo of Parks Canada for logistical support; Bruce Millar of Lake O'Hara Lodge for providing meteorological data; Craig Smith of the Meteorological Service of Canada for arranging a long-term loan of weather stations; Michael Toews, Jaclyn Schmidt, and Lisa Grieef for field assistance; and Susan Watson for introducing us to Lake O'Hara. Constructive comments by two anonymous reviewers greatly improved the manuscript. The funding for this study was provided by the University of Calgary G8 Chair in Wildlife Ecology, Environment Canada Science Horizons Program, the Natural Sciences and Engineering Research Council of Canada, and the Alberta Ingenuity Studentship to JLH.

REFERENCES

Blanken, P. D., Rouse, W. R., Culf, A. D., Spence, C., Boudreau, L. D., Jasper, J. N., Kochtubajda, B., Schertzer, W. M., Marsh, P. & Verseghy, D. (2000) Eddy covariance measurements of evaporation from Great Slave Lake, Northwest Territories, Canada. *Water Resour. Res.* **36**(4), 1069–1077.

Campbell, D. H., Clow, D. W., Ingersoll, G. P., Mast, M. A., Spahr, N. E. & Turk, J. T. (1995) Processes controlling the chemistry of two snowmelt-dominated streams in the Rocky Mountains. *Water. Resour. Res.* **31**(11), 2811–2821.

Campbell, D. H., Muths, E., Turk, J. T. & Corn, P. S. (2004) Sensitivity to acidification of subalpine ponds and lakes in north-western Colorado. *Hydrol. Processes* **18**(15), 2817–2834.

Clow, D. W., Schrott, L., Webb, R., Campbell, D. H., Torizzo, A. & Dornblaser, M. (2003) Ground water occurrence and contributions to streamflow in an alpine catchment, Colorado Front Range. *Ground Water* **41**(7), 937–950.

Gurrieri, J. T. & Furniss, G. (2004) Estimation of groundwater exchange in alpine lakes using non-steady mass-balance methods. *J. Hydrol.* **297**, 187–208.

Harris, D. C. (1991) *Quantitative Chemical Analysis*, 3rd edn. W. H. Freeman, New York, USA.

Hayashi, M. (2004) Temperature-electrical conductivity relation of water for environmental monitoring and geophysical data inversion. *Environ. Monit. Assess*. **96**, 119–128.

Hood, J. L., Roy, J. W. & Hayashi, M. (2006) Importance of groundwater in the water balance of an alpine headwater lake. *Geophys. Res. Lett.* **33**, L13405, doi:10.1029/2006GL026611.

Lundquist, J. D. & Dettinger, M. D. (2005) How snowpack heterogeneity affects diurnal streamflow timing. *Water Resour. Res*. **41**, W05007, doi:10.1029/2004WR003649.

Meteorological Service of Canada (MSC) (2005) National climate data archive of Canada. Environment Canada, Dorval, Quebec, Canada.

Michel, R. L., Campbell, D. H., Clow, D. W. & Turk, J. T. (2000) Timescales for migration of atmospherically derived sulphate through an alpine/subalpine watershed, Loch Vale, Colorado. *Water Resour. Res*. **36**(1), 27–36.

Michel, R. L., Turk, J. T., Campbell, D. H. & Mast, M. A. (2002) Use of natural ^{35}S to trace sulphate cycling in small lakes, Flattops Wilderness Area, Colorado, USA. *Water, Air & Soil Pollut.* **2**, 5–18.

Price, R. A., Cook, D. G., Aitken, J. D. & Mountjoy, E. W. (1980) Geology, Lake Louise, Alberta and British Columbia, Map 1483A, Scale 1:50 000, Geol. Survey of Canada, Ottawa, Ontario, Canada.

Richards, G. & Moore, R. D. (2003) Suspended sediment dynamics in a steep, glacier-fed mountain stream, Place Creek, Canada. *Hydrol. Processes* **17**(9), 1733–1753.

Rosenberry, D. O. (1990) Effect of sensor error on interpretation of long-term water-level data. *Ground Water* **28**, 927–936.

Rosenberry, D. O., Stannard, D. I., Winter, T. C. & Martinez, M. L. (2004) Comparison of 13 equations for determining evapotranspiration from a prairie wetland, Cottonwood Lake area, North Dakota, USA. *Wetlands* **24**(3), 483–497.

Singh, P., Haritashya, U. K. & Kumar, N. (2004) Seasonal changes in meltwater storage and drainage characteristics of the Dokriani glacier, Garhwal Himalayas (India). *Nordic Hydrol.* **35**(1), 15–29.

Shea, J. M., Anslow, F. S. & Marshall, S. J. (2005) Hydrometeorological relationships on Haig Glacier, Alberta, Canada. *Annals Glaciol.* **40**, 52–60.

Sueker, J. K., Ryan, J. N., Kendall, C. & Jarrett, R. D. (2000) Determination of hydrologic pathways during snowmelt for alpine/subalpine basins, Rocky Mountain National Park, Colorado. *Water Resour. Res.* **36**(1), 63–75.

Ward, J. V., Malard, F., Tockner, K. & Uehlinger, U. (1999) Influence of ground water on surface water conditions in a glacial flood plain of the Swiss Alps. *Hydrol. Processes* **13**, 277–293.

Winter, T. C. (2003) The hydrology of lakes. In: *The Lakes Handbook*, vol. 1 – *Limnology and Limnetic Ecology* (ed. by P. E. O'Sullivan & C. S. Reynolds), 61–78. Blackwell Science Ltd., Oxford, UK.

Glacier Mass Balance Changes and Meltwater Discharge (selected papers from sessions at the IAHS Assembly in Foz do Iguaçu, Brazil, 2005). IAHS Publ. 318, 2007.

Hydrological regime characteristics due to the development of proglacial lakes at Glacier Soler, Northern Patagonia Icefield, Chile

TAKANE MATSUMOTO[1], HIROSHI FUKAMI[2], FERNANDO ESCOBAR[3], SATORU YAMAGUCHI[4] & RENJI NARUSE[5]

1 *Department of Natural History Sciences, Faculty of Science, Hokkaido University, Kita 10, Nishi 8, Kita-ku, Sapporo 060-0810, Japan*
mtakane@nature.sci.hokudai.ac.jp

2 *Geological Survey of Hokkaido, Kita 19, Nishi 12, Kita-ku, Sapporo 060-0819, Japan*

3 *Dirección General de Aguas, Ministerio de Obras Públicos, Morandé 59, Santiago, Chile*

4 *Snow and Ice Research Center, National Research Institute for Earth Science and Disaster Prevention, Suyoshi-machi, Nagaoka, 940-0821, Japan*

5 *Institute of Low Temperature Science, Hokkaido University, Kita 19, Nishi 8, Kita-ku, Sapporo 060-0819, Japan*

Abstract Comparing the hydrological regimes of a stream from Glacier Soler in Patagonia, which were observed before (1985) and after (1998) the onset of proglacial lake development (1992) due to the large-scale retreat of the glacier, the following differences were found: (a) an increase in glacier flow speed; (b) advance in occurrence time of the daily maximum discharge; (c) steepening of the diurnal rising and falling limbs of hydrographs; (d) occurrence of a flood due to sudden drainage from the lakes; (e) decrease in the range of variation in electric conductivity; and (f) positive correlation between discharge and electric conductivity within each day of the period. The differences in glacier flow and stream discharge variation may have resulted from the change in the hydraulic features of the subglacial drainage system due to thinning of the glacier and/or the development of lakes. The complexity of flow paths of meltwater within the glacier owing to the development of lakes may have caused the differences in chemical features of the stream water.

Key words Glacier Soler; hydrograph; meltwater; Northern Patagonia Icefield; proglacial lake; specific electric conductivity; stream discharge

INTRODUCTION

Most outlet glaciers from the Northern Patagonia Icefield (NPI) and the Southern Patagonia Icefield (SPI) retreated throughout the latter half of the 20th century (e.g. Warren & Sugden, 1993; Aniya, 1999). According to Rignot *et al*. (2003), the largest 63 glaciers in Patagonia lost ice at a rate equivalent to a sea level rise of 0.105 mm $year^{-1}$ between 1995 and 2000. The thinning and retreating of glaciers into overdeepened troughs, which are commonly found in Patagonia, should lead to the formation of proglacial lakes. Thus, many proglacial lakes have developed in this region, and 71% and 58% of outlet glaciers from NPI and SPI, respectively, have lacustrine-calving termini (Warren & Aniya, 1999). Previous studies have discussed the process of development and limnological characteristics of proglacial lakes (Kirkbride, 1993; Chikita *et al*., 1997; Sakai *et al*., 2000), and resultant outburst floods

(Yamada, 1998; Richardson & Reynolds, 2000). However, there have been few reports on the influence of glacier shrinkage and lake development on the runoff processes of proglacial streams.

In the summer of 1998, we carried out hydrological observations at Glacier Soler, an outlet glacier from NPI where proglacial lakes have been expanding due to a large retreat in recent decades, in order to determine the hydrological regime characteristics during the period of lake development. In this study, by comparing the results of the observations in 1998 and those in 1985, before the onset of lake development (e.g. Fukami & Escobar, 1987), we identify differences in the hydrological regime of a proglacial stream from Glacier Soler between the two periods. The possible causes of these differences in the pattern of discharge variation, the hydrochemical features, and other parameters are then discussed.

STUDY AREA

Glacier Soler is an outlet glacier that flows southeastward from NPI (Fig. 1). According to Naruse *et al*. (2000), the present terminus position is located at about 300 m a.s.l. The area of the glacier is 50.9 km^2, with a length of 16.6 km, of which the lowest 7 km is the outlet part. The ELA was estimated from a 1985 survey as 1350 m a.s.l.

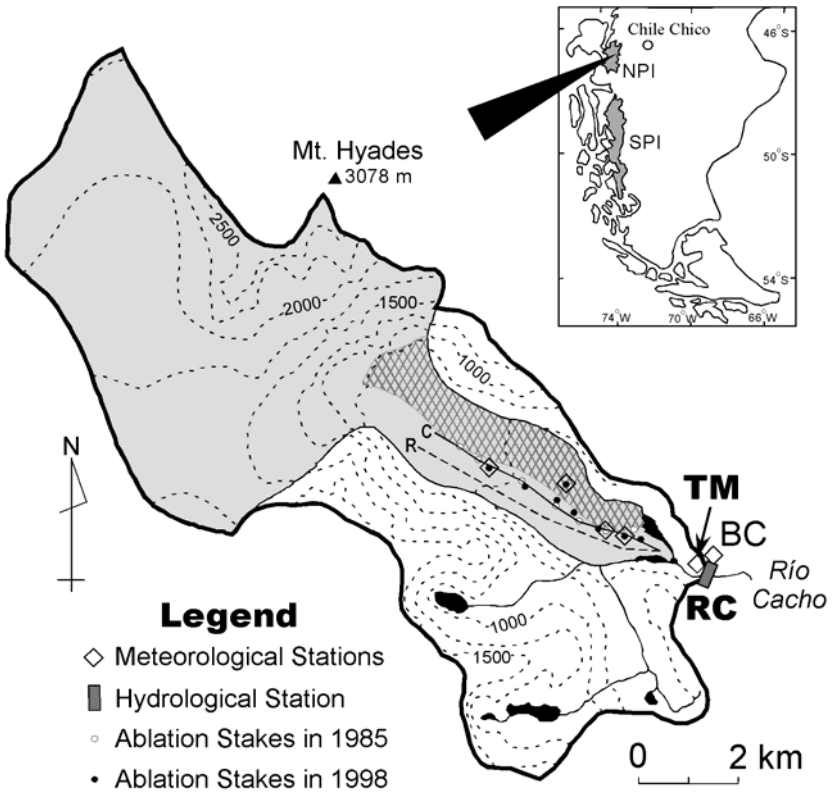

Fig. 1 Map of the Glacier Soler drainage basin. The shaded area and meshed area indicate Glacier Soler and the debris-covered part of the glacier, respectively. Lines C and R indicate positions of the surface and the bedrock profiles along the central flow line and the bedrock profile on the right-bank side, respectively.

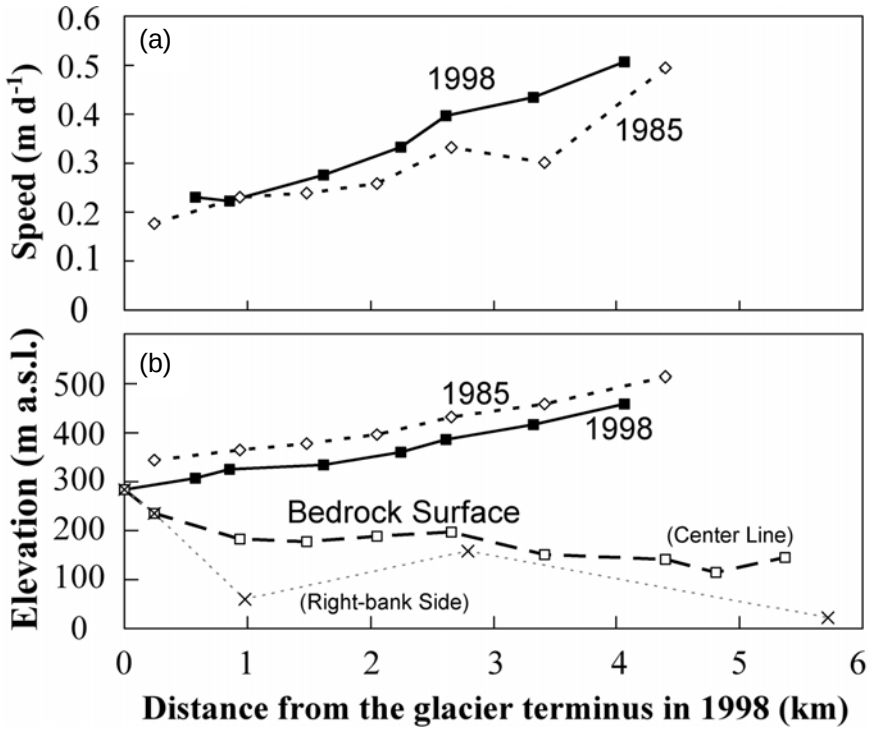

Fig. 2 Changes in: (a) distribution of the surface flow speed of the glacier along the central flow line, and (b) surface and bedrock profiles along the flow line (modified from Yamaguchi *et al*., 2003). The flow speed, surface and bedrock profiles were measured along the central flow line (Line C in Fig. 1), and the bedrock profile on the right-bank side was measured along Line R in Fig. 1 during the 1985 period. The flow speed and surface profile were measured at sites along Line C during the 1998 period.

(Casassa, 1987). The drainage basin containing Glacier Soler consists of granitic rock, and its area is 81.0 km^2. A survey of ice thickness deduced from gravity anomalies (Casassa, 1987) showed that the bedrock beneath the outlet part of the glacier declines toward the northwest; that is, the opposite of the flow direction (Fig. 2). A proglacial stream, Río Cacho, flows eastward from the terminus and then southward into Lago Plomo (a part of Lago General Carrera).

In recent decades, especially between 1985 and 1998, a number of changes have occurred in Glacier Soler and the surrounding landforms. This glacier has been retreating at least since 1945, and has made a relatively large retreat between 1996 and 1999 because of the diminished ice supply from the icefield, coupled with calving in proglacial lakes (Aniya, 2001). Between 1985 and 1998, the glacier terminus retreated from about 200 m to 550 m, and surface lowering of the glacier in the ablation area was found to be about 42 m on average (Naruse *et al*., 2000). Based on Digital Elevation Models generated from a 1975 map and from a 2001 satellite (ASTER) image, Rivera *et al*. (2007) have estimated the thinning rate of the ablation area between these two years as 2.5 ± 0.97 m $year^{-1}$.

Due to the retreat of the glacier, the surface topography of the glacier forefield around the terminus in 1998 shows significant differences from that in 1985 (Fig. 3). Between the position of the terminus in 1985 and that in 1998, several rows of ice-cored moraine ridges and a low moraine ridge consisting of granulated gravel and

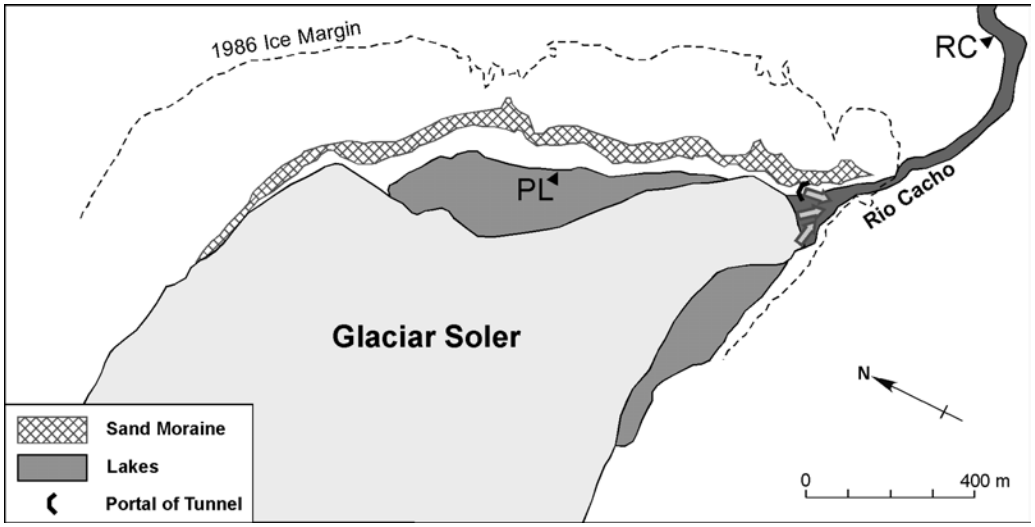

Fig. 3 The terminal area of Glacier Soler in 1998 (modified from Glasser & Hambrey, 2002). Grey arrows indicate meltwater drainage into Río Cacho from the glacier and the lakes. Solid triangles indicate hydrological stations during the 1998 period.

coarse sand, referred to as a "sand moraine" by Glasser & Hambrey (2002) and Glasser *et al*. (2002), were found. Two proglacial lakes touching both sides of the glacier terminus have been expanding since about 1992 (Aniya, 2001); in 1998, they had an area of about 0.2 km^2. Both lakes were dammed by glacier ice in 1998, however, they were partly connected to Río Cacho through subsurface pathways. A tunnel beneath a ridge of debris-covered ice was found as an outlet from the lake on the left-bank side near the terminus. In addition, direct discharge of meltwater from the glacier into Río Cacho was also found at the central part of the terminus. On the right margin and about 1 km upglacier from the terminus, we found a large area of depression and collapse of ice, in which a lake was located.

We have only a limited number of data on mass balance components of NPI. Escobar *et al*. (1992) estimated the annual precipitation on the icefield as 6000–7000 mm based on the water balance of a drainage basin including the eastern part of NPI. In the accumulation area of Glacier Nef (1500 m a.s.l.) adjacent to Glacier Soler on the south, the annual accumulation and ablation were estimated from a firn core as 5.6 and –3.4 m w.e., respectively (Matsuoka & Naruse, 1999).

FIELD OBSERVATIONS

At Glacier Soler and its drainage basin, hydrological, meteorological and glaciological observations were carried out over three summers as follows:

- **1983 period**: 17 December 1983–2 January 1984 (e.g. Kobayashi & Saito, 1985; Saito & Kobayashi, 1985)
- **1985 period**: 20 October 1985–8 December 1985 (e.g. Fukami & Escobar, 1987; Fukami *et al*., 1987; Naruse *et al*., 1992)
- **1998 period**: 16 November 1998–8 December 1998 (e.g. Naruse *et al*., 2000; Yamaguchi *et al*., 2003)

In this study, we use the results of observations of the 1985 and 1998 periods in order to compare the hydrological regimes during the periods before and after the onset of the development of the proglacial lakes in 1992.

The sites of field observations during the 1985 and 1998 periods are shown in Fig. 1. Measurements of various weather conditions, including air temperature, global radiation and precipitation (shown in Fig. 4) were carried out on the glacier forefield at

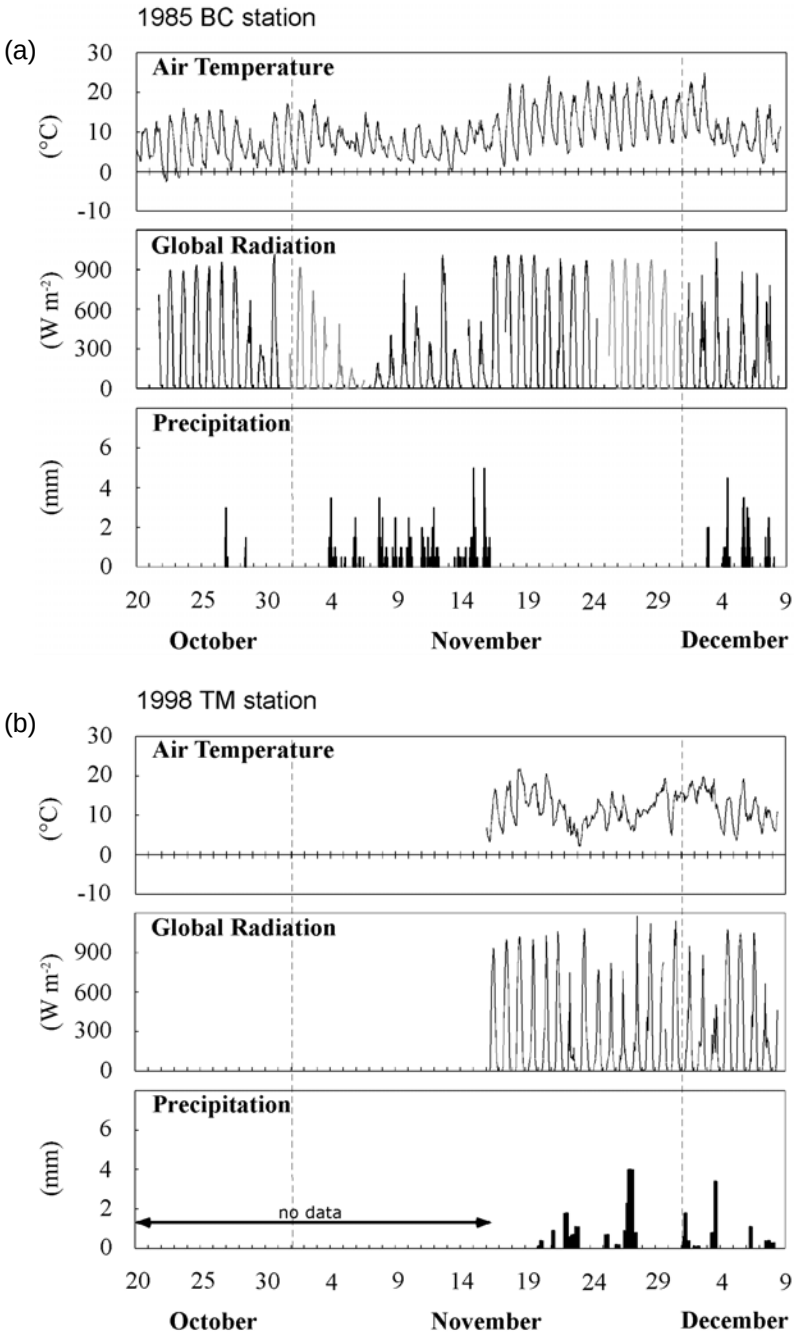

Fig. 4 Meteorological components observed (a) at BC station during the 1985 period, and (b) at TM station during the 1998 period (precipitation was measured at BC station in 1998). Global radiation measured on the glacier near the terminus during the 1985 period is shown as a grey line.

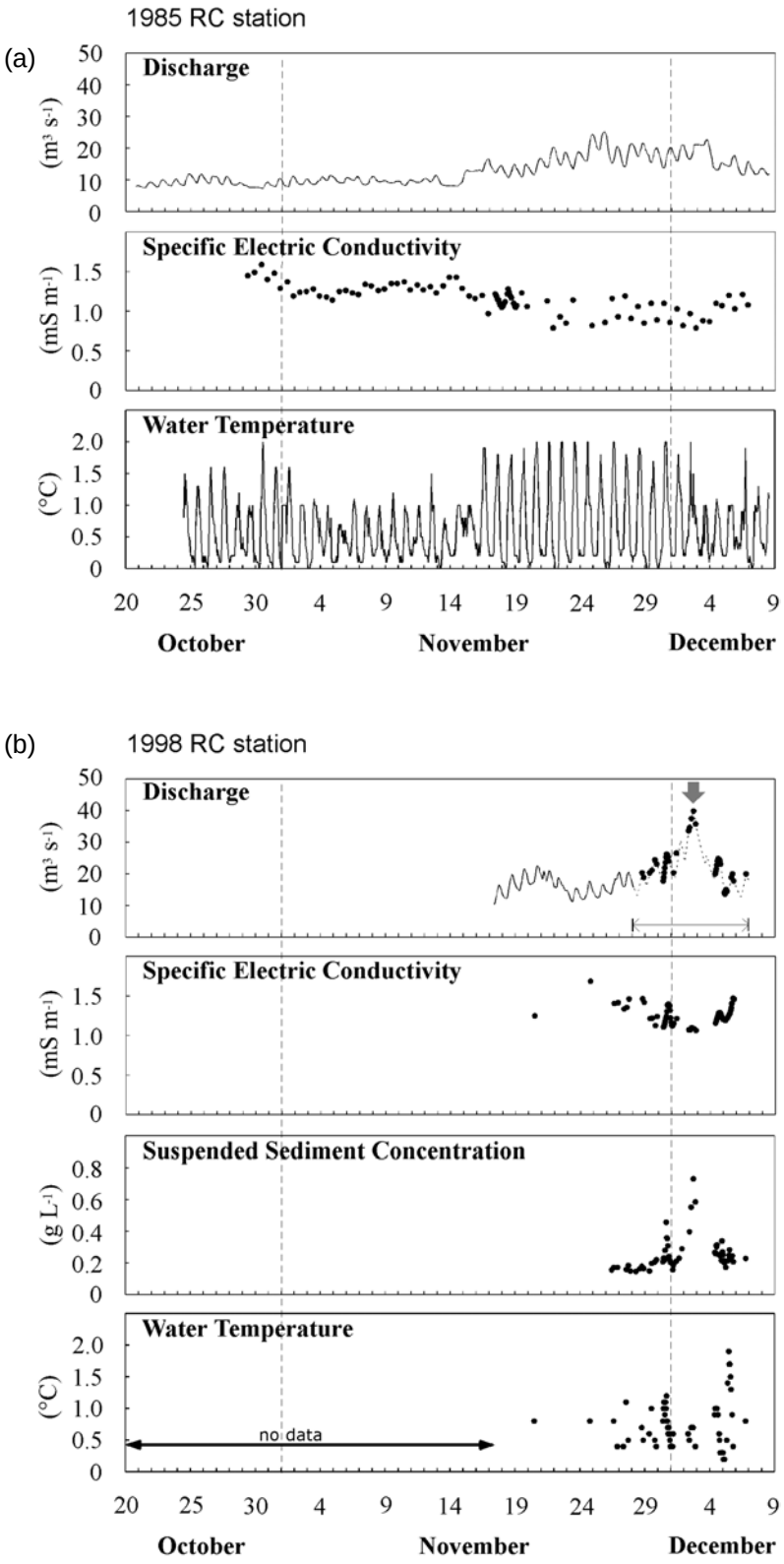

Fig. 5 Hydrological components observed at RC station during (a) the 1985 period and (b) the 1998 period. The dotted line indicates the rough estimate of discharge variation during the latter half of the 1998 period (the period of this estimation is shown by a thin arrow). The thick grey arrow shows a flood event in 2 December 1998.

BC station in 1985 and TM station in 1998. Air temperature and global radiation were measured 1.5 m above the ground and recorded at 1-hour intervals. Air temperatures at the BC and TM stations were well correlated with those observed in the ablation area of the glacier (e.g. GL station of Fukami *et al*. (1987)) during each observation period. Precipitation was measured at BC station during both periods using a tipping bucket raingauge in 1985 and a simple raingauge composed of a bottle and a 21-cm-diameter funnel (Ushiyama & Matsuyama, 1995) in 1998. Measurement during the 1998 period was carried out several times for each rainstorm and the hourly precipitation rate was obtained assuming uniform rainfall intensity between the two measurements. Detailed information on meteorological observations during the 1985 period has already been reported by Fukami *et al*. (1987).

Daily melt rates of the glacier were measured at 11 sites during the 1985 period (Fukami & Naruse, 1987) and at seven sites during the 1998 period (Yamaguchi *et al*., 2003). A significant difference in ice density was found between 1985 (850 kg m^{-3}) and 1998 (920 kg m^{-3}). However, even if the ice density was correctly measured during each period, it is hard to believe that there was a difference of this magnitude across the whole glacier. Thus, in order to obtain melt rates during both periods in this paper, we assume that the ice density was 900 kg m^{-3}, although Yamaguchi *et al*. (2003) calculated melt rates during both periods using each of the reported densities.

Hydrological observations of Río Cacho were carried out at RC station during both periods (Fig. 5). The water level was measured and recorded at 1-hour and 10-minute intervals in 1985 and 1998, respectively. Hourly discharge was calculated from the water level and stage-discharge curves obtained from seven and five discharge measurements during the 1985 and the 1998 periods, respectively. We had to fill gaps in the data record of discharge due to trouble with the water level gauge in the latter half of the 1998 period using manually measured values, the averaged gradients of the diurnal rising and falling limbs of the hydrograph (see Fig. 6), and the averaged occurrence times of daily maximum and minimum discharges during the early half of the period. Moreover, the specific electric conductivity (SEC) and temperature of meltwater were observed during the 1985 period (Fukami & Escobar, 1987), while SEC, water temperature and suspended sediment concentration (SSC) were measured during the 1998 period at RC station. *In situ* measurements of SEC and water temperature were carried out at RC station several times a day in both periods. To measure SSC, stream water was sampled at RC station and then filtered at the camp using a handy vacuum pump and glass fibre filters (pore size = 0.6 μm). The value of SSC was obtained by measuring the weights of these filter papers in a laboratory in Japan. In addition, the water level, water temperature and SEC of the surface layer of the proglacial lake on the left-bank side were measured 9 times from 2 to 6 December, 1998 at PL station, and the results are shown in Fig. 3. Other details on the observations during the 1985 period have been described by Fukami & Escobar (1987).

RESULTS

Weather conditions and glacier ablation

Temporal variations in air temperature, global radiation and precipitation in the glacier forefield (at BC or TM) during the 1985 and the 1998 periods are shown in Fig. 4.

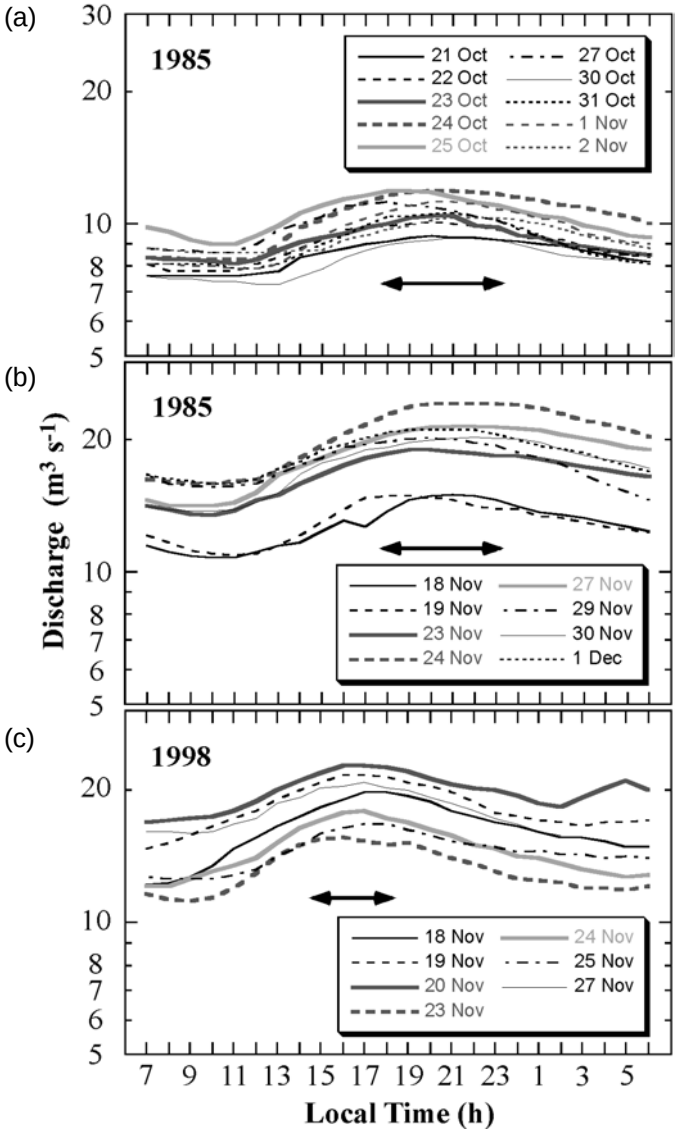

Fig. 6 Patterns of diurnal discharge variations of Río Cacho during (a) the early half and (b) latter half of the 1985 period, and during (c) the 1998 period. Black arrows indicate periods of occurrence of the maximum discharge.

Table 1 shows the summary of observed meteorological and hydrological elements and daily melt rate in the ablation area during the early half (20 October – 15 November) and the latter half (16 November – 8 December) of the 1985 period and the 1998 period.

During the 1985 period, the general condition alternated between fine and rainy weather, with each condition lasting for about two weeks (Fukami *et al*., 1987). On the other hand, during the 1998 period, the duration of each of the weather condition was much shorter. Air temperature at BC station varied between –3 and 18°C in the early half of the 1985 period; then, in the latter half, after a two-week-long rainy period, the air temperature clearly increased and ranged between 1 and 25°C. No significant difference could be found between air temperatures during the 1998 period and the

latter half of the 1985 period. Moreover, air temperatures at Chile Chico, a town about 120 km east of the glacier, which are known to an indicator of the temperature conditions around Glacier Soler, showed that there was no substantial difference between the two years from the preceding winter to the respective observation period (Fig. 7), although a strong ENSO event has occurred from 1997 to 1998. In the latter half of the 1985 period, total rainfall was 59 mm due to clear days in late November; total rainfall during the same period in 1998 was 151 mm.

Table 1 Mean or total values (with standard deviations) of meterological and hydrological elements and daily melt rate measured at Glacier Soler during the early and latter halves of the 1985 period.

	Air temperature (°C)		Global radiation (W m^{-2})		Precipitation (mm)		Melt rate (mm day^{-1})		Electric Conductivity (mS m^{-1})		Water temperature (°C)	
	Mean	SD	Mean	SD†	Total	Mean‡	Mean	SD	Mean	SD	Mean	SD
1985 (early)	7.2	4.0	189	98	127	20.3	9.5	1.2	1.3	0.1	0.5	0.4
1985 (latter)	12.2	5.3	300	103	59	41.5	16.5	3.3	1.0	0.1	0.7	0.6
1998	11.8	4.1	250	87	151	45.0	17.3#	4.1#	1.3	0.1	0.7	0.4

Observation periods 1985 (Early) 20 October – 15 November 1985 (Latter) and 1998: 16 November–8 December.
†Standard deviation of daily mean global radiation in each period.
‡Averaged value of melt rate at 3 sites (1985 (early) and 1998) or 2 sites (1985 (Latter)) in the ablation area between 0.5 and 3.0 km upglacier from the terminus.
#Rough estimates of discharge indicated by dotted line in Fig. 5(b) are excluded.

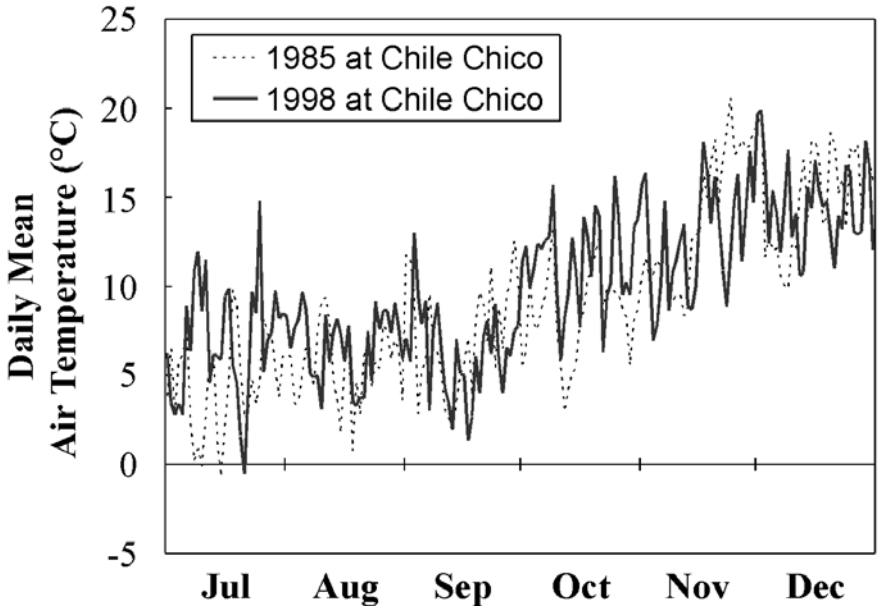

Fig. 7 Daily mean air temperature at Chile Chico from July to December in 1985 and 1998.

Mean daily melt rates at two or three sites on the glacier ice without debris between 0.5 and 3 km upglacier from the terminus were 20 mm during the early half of the 1985

period, 42 mm during the latter half of the 1985 period, and 45 mm during the 1998 period (Table 1). Thus, we could find no significant difference in the meltwater supply into the glacier between the two years from mid-November to early December.

Changes in stream discharge variation

Temporal variations in discharge, SEC and SSC of Río Cacho at RC station during the 1985 and the 1998 periods are shown in Fig. 5 (including rough estimates of discharge after 28 November 1998). In addition to air temperature, a difference was found in the pattern of diurnal discharge variation between the early and latter halves of the 1985 period. The early half-period was characterized by a small discharge amount (ranging from 7 to 13 $m^3 s^{-1}$) and small diurnal variation, and the latter half-period by a large discharge amount (ranging from 11 to 25 $m^3 s^{-1}$) and large diurnal variation (Fukami & Escobar, 1987). In Fig. 6, diurnal discharge variations of the days without severe rainfall during the early and latter halves of the 1985 period and the 1998 period are shown with a log-normal scale. In spite of changes in the amount of discharge, no clear difference was found in the patterns of diurnal variations between the early and latter halves of the 1985 period.

During most of the 1998 period, the discharge of Río Cacho varied, showing a diurnal cycle between 10 and 31 $m^3 s^{-1}$. Regarding the amount and the amplitude of diurnal variations, the runoff regime during the 1998 period was quite similar to that in the same season in 1985. However, a remarkable flood event with a discharge of about 40 $m^3 s^{-1}$, which was not observed during the 1985 period, occurred on 2 December 1998. No significant increase in melt rate was observed before the flood, and after the flood the water level of the lake on the left-bank side was found to be much lower. As can be seen in Fig. 8, the lake level clearly correlated with variations in stream discharge after the flood (unfortunately, no measurements were available before the flood). Because no collapse of the glacier or moraines was observed, the sudden development of a subsurface pathway beneath the debris-covered ice may have caused this flood event.

Two other differences between the two periods in the same season were found in Fig. 6. First, the daily maximum discharge in the 1998 period usually occurred between 15:00 and 18:00 h, whereas in the same season in 1985, the maximum was usually observed between 18:00 and 22:00 h. Second, the gradients of the diurnal rising and falling limbs of the hydrograph shown in log-normal scale were larger during the 1998 period than those in the 1985 period. As a result, the shapes of the hydrographs for the 1998 period are much steeper than those for 1985.

Changes in the chemical and physical features of meltwater

The SEC of meltwater in Río Cacho varied between 0.7 and 1.6 mS m^{-1} during the 1985 period, and between 1.1 and 1.7 mS m^{-1} during the 1998 period (Fig. 5). In general, SEC during the 1998 period was higher than that in the same season, that is, the latter half of the 1985 period (Table 1). However, the data on the stream discharge and SEC shown in Fig. 9 indicate that the range of SEC variation was much smaller

during the 1998 period, whereas the range of discharge variation was larger than that during the 1985 period. One further interesting difference was found in the relationship between stream discharge and SEC (Fig. 9). During the 1998 period, SEC varied in phase with discharge diurnally; nevertheless, the relationship for the whole period shows an inverse correlation. On the other hand, SEC varied simply, showing inverse correlation with discharge throughout the 1985 period. Paying attention to diurnal variations during the 1998 period, a larger increase in SEC can be found on days with a smaller discharge. We believe that this cannot be a measurement artefact, because we did not find any evidence of this kind of relationship in the 1985 period and because the measurements were made at the same place under the same condition of water temperature using a similar instrument. Such a strange relationship between discharge and SEC has never been reported, at least for proglacial streams, anywhere in the world.

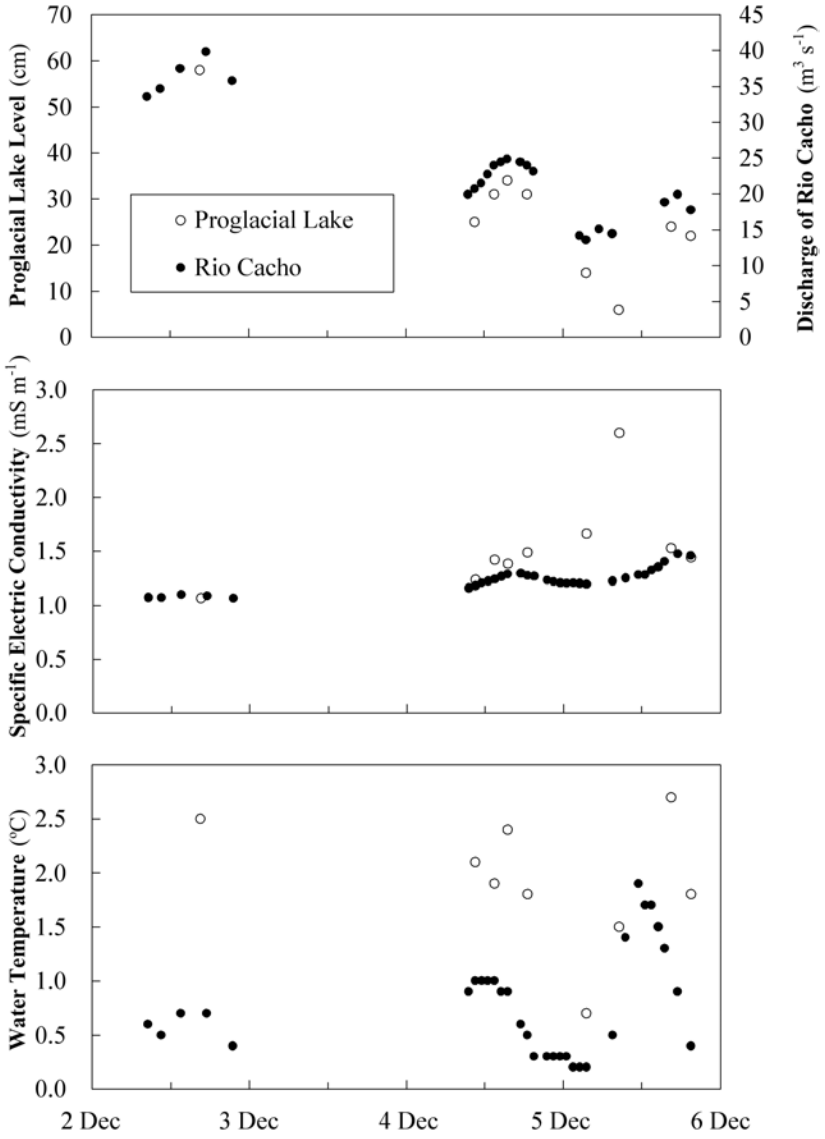

Fig. 8 Temporal variations in water level, SEC and water temperature of the proglacial lake on the left-bank side at PL station (solid circles) and discharge, SEC and water temperature of Río Cacho at RC station (open circles) in early December 1998.

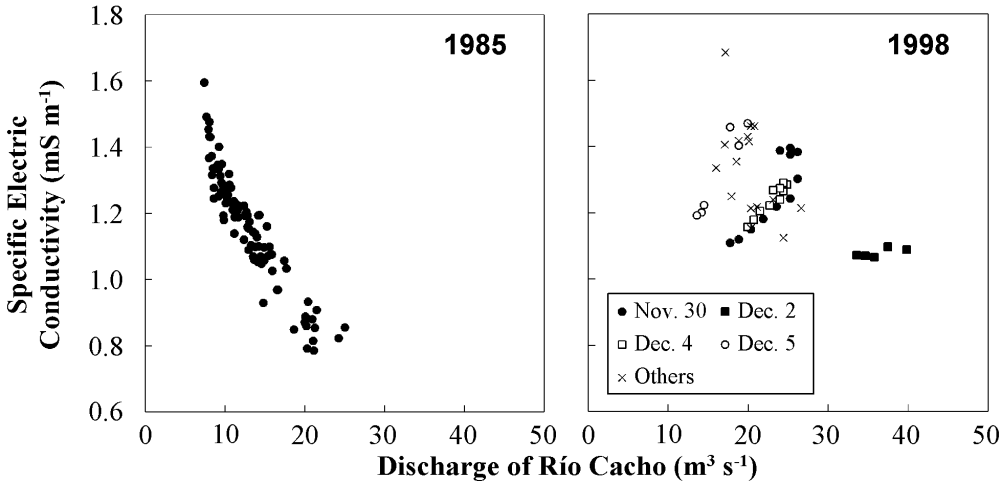

Fig. 9 The relationship between discharge and specific electric conductivity of Río Cacho at RC station during the 1985 and 1998 periods.

SSC was only measured in 1998, and showed variation between 0.1 and 0.8 g L^{-1} in phase with discharge. The relationship between discharge (Q in m^3 s^{-1}) and SSC (C in g L^{-1}) was found to be the following:

$$C = 0.0016Q^{1.60} \quad (r^2 = 0.80) \tag{1}$$

It seems unlikely that there would be a significant difference between the discharge-SSC relationship during the 1998 period and that during the 1983 period (Saito & Kobayashi, 1985), although it is hard to compare the two directly due to the differences in the method of measurement. The water temperature varied between 0 and 2°C, with clear diurnal cycles in both years (Fig. 5).

DISCUSSION AND CONCLUSIONS

Glacier Soler shrank throughout the latter half of the 20th century. Based on the results of the above-described hydrological observations, and on previously published glaciological observations at this glacier (Naruse *et al*., 1992; Yamaguchi *et al*., 2003), we conclude that the 1998 hydrological regime of Glacier Soler differed from the 1985 regime in the following ways:

(a) increase in surface flow speed of the glacier (Fig. 2(a): Yamaguchi *et al*., 2003);
(b) advance in time of occurrence of the daily maximum discharge;
(c) increase in gradient of the diurnal rising and falling limbs of hydrographs;
(d) occurrence of a flood event due to sudden drainage from the proglacial lakes;
(e) decrease in the range of SEC variation during the observation period;
(f) positive correlation between discharge and SEC within each day.

In order to clarify the causes of these differences in hydrological regime, it is necessary to consider the influence of the possible changes in the drainage systems within the glacier, along with the difference in weather conditions between the two periods. Unfortunately, we do not have enough information to accurately estimate the

hydraulic conditions of the glacier drainage systems, that is, the configuration of englacial and subglacial drainage pathways (e.g. Hooke, 1989; Fountain & Walder, 1998), the basal water pressure, the detailed distribution of the ice thickness, the depth of the proglacial lakes, etc. Nevertheless, we can speculate on the possible causes of these differences.

The higher flow speed, despite the thinner ice, indicates that the basal sliding was much greater in the 1998 period than in the 1985 period due to a decrease in the subglacial effective pressure. Both the changes in the configuration and the hydraulic features of glacier drainage systems and temporal changes in meltwater supply into these systems should affect the effective pressure. On the other hand, the changes in the patterns of diurnal discharge variations (b and c) imply an increase in the flow velocity of meltwater, and thus the changes in the configuration and the hydraulic features of glacier drainage systems, because the hydrographs in a specific period show the same shape regardless of discharge (Fig. 6). As already described in the previous section, we believe that there was no significant difference in meltwater supply between the latter half of the 1985 period and the 1998 period. If there was a significant difference in ice density between the two periods, that is, 850 kg m^{-3} in 1985 and 920 kg m^{-3} in 1998, the mean melt rates in the lower ablation area during the latter half of the 1985 period and the 1998 period were 39 mm day^{-1} and 46 mm day^{-1}, respectively. In such a case, the difference in melt rate between the two periods may have partly contributed to the decrease in effective pressure, and then to the increase in basal sliding. However, it would be very difficult to explain the other differences in hydrological regime, such as differences (b) and c) above, solely in terms of a temporal difference in the meltwater supply. Therefore, we suppose that some changes in glacier drainage systems have a greater influence on the changes in discharge variation of Río Cacho. Possible causes of the change in the configuration and the hydraulic features of the drainage systems within Glacier Soler include:

(i) Differences in the meltwater supply during the season from the preceding winter to the respective observation period, which can affect the degree of seasonal development of drainage systems;
(ii) Thinning of the glacier ice which would leads to a decrease in overburden pressure; and
(iii) The development of proglacial lakes.

As already shown in Fig. 7, there was no clear difference in air temperature at Chile Chico from the preceding winter to October between the two years. Even in the case that air temperature and discharge were clearly increased between the early and the latter halves of the 1985 period (Table 1), no significant change arose in the time of occurrence of the daily maximum discharge or in the gradient of the limbs of the hydrographs. Therefore, differences in the water supply during the season before each observation period could not be the major cause of such changes in the patterns of diurnal discharge variation.

Distribution of ice thickness is one of the factors controlling the configuration and the hydraulic features of drainage systems within glaciers (e.g. Röthlisberger, 1972). Thinning of glacier ice may influence the flow velocity of meltwater and other features of drainage systems. The available ice thickness and bedrock profile measurements may offer interesting information that can help to describe the water flow processes

within and beneath the glacier. Indeed, according to the results of gravity measurements by Casassa (1987), the bedrock along the central flow line generally slopes in the upglacier direction for about 5 km from the terminus, creating a large overdeepening (indicated by the open squares and broken line in Fig. 2(b)). However, another measurement procedure by Casassa (1987) shows that this profile lies on a subglacial ridge along the flow line; thus, a much greater overdeepening can be located between the central flow line and the lateral margins. The bedrock profile indicated by the crosses and dotted thin line in Fig. 2(b) shows that the slope for about 1 km from the terminus in the right-bank side might be much steeper than that in the central part. According to the theory of subglacial water flow by Röthlisberger (1972), the water pressure would be higher than the overburden pressure under the topographical condition.

$$\tan \alpha < 0.46(\rho_w/\rho_i) \tan \beta = 0.59 \tan \beta \quad (2)$$

where α and β are surface slope and bed slope (assuming to be equal to the grade of subglacial conduit), respectively, and ρ_w and ρ_i are the densities of water at 0°C and ice, respectively. Röthlisberger (1972) suggested that under such conditions, the subglacial conduit is unstable and the water spreads out at the contact between ice and bedrock and moves in a thin film or sheet as proposed theoretically by Weertman (1964, 1969). The bedrock slope on the right-bank side of Glacier Soler can partly fulfill equation (2); thus, it is possible for a complicated drainage network including water film beneath the glacier to exist near the terminus. Bindschadler (1983) pointed out that such a condition of water flow as a thin film decoupling the ice from the bed probably exists in the area near the terminus of Columbia Glacier, a tidewater glacier in Alaska that has a bedrock profile similar to that of Glacier Soler. It is difficult to quantitatively evaluate the influence of ice thinning on water flow velocity within the glacier and on changes in discharge variation. However, we can conclude that the increase in the surface flow speed of the glacier results partly from the decrease in the effective pressure due to the thinning of glacier ice, as Meier & Post (1987) explained for the increase in flow speed of Columbia Glacier. This decrease in the effective pressure may have resulted in an increase of water flow velocity.

The development of proglacial lakes may also strongly affect hydraulic features within the glacier due to the high water pressure at the terminus. Besides, lake development can make flow paths within the glacier much shorter, thereby shortening the transit time of meltwater from the glacier surface to Río Cacho.

Changes in the stream hydrochemical characteristics should also be discussed. Mixing of some meltwater components with various solute concentrations in the proglacial lakes before drainage into Río Cacho should significantly affect the decrease in the range of SEC variation at RC station. On the other hand, it is more difficult to explain the strange relationship between discharge and SEC in the 1998 period. It would be impossible to simulate such a combination of relationships with normal and inverse correlations based on the assumption of the mixing of two flow components, i.e. delayed flow (chemically concentrated) and quick flow (chemically diluted) which can be modelled with two linear reservoirs (e.g. Hannah & Gurnell, 2001), whereas it is possible to simulate the discharge-SEC relationship in the 1985 period under this assumption. We hypothesize that there were at least three major components of meltwater which flowed through different pathways from the glacier to Río Cacho:

chemically diluted englacial water draining directly into the river, diluted englacial water draining into the proglacial lakes, and concentrated subglacial water draining into the proglacial lakes. The second and the third components should be mixed in the lakes and then drain into Río Cacho. Comparing the water level and SEC of meltwater in the proglacial lake at PL station with those of Río Cacho at RC station in Fig. 8, it is clear that SEC at PL station was much higher than that at RC station only when lake level was lower than 20 cm; when the lake water level was higher than 20 cm, the SEC valued at the two stations were almost identical. This result implies that a temporal change in lake level leads to a change in the proportion of the three water components in stream water at RC station. In a warm period with a high melt rate (e.g. during the daytime on 2 and 4 December) an increase in the meltwater supply into the lake would result in a reduction of the SEC at PL station (and an increase in the surface water temperature). A higher lake level would lead to an increase in the drainage of lake water to Río Cacho, and when lake water, which has a much higher SEC than diluted englacial water, becomes dominant in the bulk meltwater, the SEC variation in the lakes will control SEC at RC station. On the other hand, during a cool period with low melt rate (e.g. the morning of 5 December), SEC at PL station would be higher owing to a decrease in the supply of diluted englacial water, and thus an increase in the proportion of concentrated subglacial water in the lake. However, the release of lake water into Río Cacho would be diminished when the lake level dropped below a certain depth. In such a situation, the proportion of the diluted water from the glacier would increase, and discharge and SEC at RC station would decrease. This explanation looks consistent with the inverse relationship between water level and SEC of the lake found in Fig. 8. If this strange relationship during the 1998 period resulted from such a combination of drainage processes of meltwater, the discharge-SEC relationship would be expected to return to a simpler one once the proglacial lakes expanded to cover the entire glacier tongue, that is, once all of the meltwater was flowing into the lake before the drainage into Río Cacho.

Glacier shrinkage and development of proglacial lakes are now commonly found in Patagonia. According to Glasser *et al*. (2002), geological evidence indicates that a proglacial lake also existed at Glacier Soler before the advance in the Little Ice Age. Thus, to clarify how glacier drainage systems change with glacier variation will be important for the reconstruction of hydrological conditions in glacierized basins during the Holocene, and also for the assessment of future changes around the icefields in Patagonia. Because of the difficulty of direct measurements of drainage systems beneath the thick ice of glaciers in this region, we propose that modelling approaches to simulate the effect of hydraulic features of glacier drainage systems that arise from changes in ice thickness and development of proglacial lakes should be useful for further study.

Acknowledgments We would like to express our gratitude to Kaoru Izumi, Niigata University, Hiroshi Ohno, Hokkaido University and Masamu Aniya, Tsukuba University for their help in the field in 1998 and for giving us valuable suggestions. We are also grateful to Jorge F. Carrasco, Dirección Meteorologica de Chile, for providing us meteorological data at Chile Chico. We would also like to thank Anselmo

Soto for his logistical support in the field during both the 1985 and the 1998 periods. Precise comments and suggestions from Jean-Emmanuel Sicart and anonymous reviewers led to major improvement in the manuscript. Part of this study was supported by a Grant-in-Aid from the Ministry of the Education, Science, Sport and Culture of Japan (No. 10041105) and a grant from the 21st century Center of Excellence (COE) Program on “Neo-Science of Natural History“ (Program Leader: Hisatake Okada) at Hokkaido University.

REFERENCES

Aniya, M. (1999) Recent glacier variations of Hielo Patagónicos, South America, and their contribution to sea-level change. *Arctic Antarctic Alpine Res.* **31**, 165–173.

Aniya, M. (2001) Glacier variations of Hielo Patagónico Norte, Chilean Patagonia, since 1944/1945, with special reference to variations between 1995/1996 and 1999/2000. *Bull. Glaciol. Res.* **18**, 55–64.

Bindschadler, R. (1983) The importance of pressurized subglacial water in separation and sliding at the glacier bed. *J. Glaciol.* **29**, 3–19.

Casassa, G. (1987) Ice thickness deduced from gravity anomalies on Soler Glacier, Nef Glacier and the Northern Patagonia Icefield. *Bull. Glacier Res.* **4**, 43–57.

Chikita, K., Yamada, T., Sakai, A. & Ghimire, R. P. (1997) Hydrodynamic effects on the basin expansion of Tso Rolpa Glacier Lake in the Nepal Himalaya. *Bull. Glacier Res.* **15**, 59–69.

Escobar, F., Vidal, F., Garin, C. & Naruse, R. (1992) Water balance in the Patagonia Icefield. In: *Glaciological Researches in Patagonia, 1990* (ed. by R. Naruse & M. Aniya), 109–119. Japanese Society of Snow and Ice, Nagoya, Japan.

Fountain, A. G. & Walder, J. S. (1998) Water flow through temperate glaciers. *Rev. Geophys.* **36**, 299–328.

Fukami, H. & Escobar, F. (1987) Hydrological characteristics of Soler Glacier drainage, Patagonia. *Bull. Glacier Res.* **4**, 91–96.

Fukami, H., Escobar, F., Quiteros, J., Casassa, G. & Naruse, R. (1987) Meteorological measurements at Soler Glacier, Patagonia, in 1985. *Bull. Glacier Res.* **4**, 31–36.

Fukami, H. & Naruse, R. (1987) Ablation of ice and heat balance on Soler Glacier, Patagonia. *Bull. Glacier Res.* **4**, 37–42.

Glasser, N. & Hambrey, M. (2002) Sedimentary facies and landform genesis at a temperate outlet glacier: Soler Glacier, North Patagonian Icefield. *Sedimentol.* **49**, 43–64.

Glasser, N., Hambrey, M. & Aniya, M. (2002) An advance of Soler Glacier, North Patagonian Icefield, at c. AD 1222–1342. *The Holocene* **12**, 113–120.

Hannah, D. M. & Gurnell, A. M. (2001) A conceptual, linear reservoir runoff model to investigate melt season changes in cirque glacier hydrology. *J. Hydrol.* **246**, 123–141.

Hooke, R. LeB. (1989) Englacial and subglacial hydrology: a qualitative review. *Arctic Alpine Res.* **21**, 221–233.

Kirkbride, M. P. (1993) The temporal significance of transitions from melting to calving termini at glaciers in the central Southern Alps of New Zealand. *The Holocene* **3**, 232–240.

Kobayashi, S. & Saito, T. (1985) Meteorological observations on Soler Glacier. In: *Glaciological Studies in Patagonia Northern Icefield 1983-1984* (ed. by C. Nakajima), 32–36. Data Center for Glacier Research, Japanese Society of Snow and Ice, Nagoya, Japan.

Matsuoka, K. & Naruse, R. (1999) Mass balance features derived from a firn core at Hielo Patagónico Norte, South America. *Arctic Antarctic Alpine Res.* **31**, 333–340.

Meier, M. F. & Post, A. (1987) Fast tidewater glaciers. *J. Geophys. Res.* **92**(B9), 9051–9058.

Naruse, R., Fukami, H. & Aniya, M. (1992) Short-term variations in flow velocity of Glacier Soler, Patagonia, Chile. *J. Glaciol.* **38**, 152–156.

Naruse, R., Yamaguchi, S., Aniya, M., Matsumoto, T. & Ohno, H. (2000) Recent thinning of Soler Glacier, northern Patagonia, South America. *Data Glaciol. Studies* **89**, 150–155.

Richardson, S. D. & Reynolds, J. M. (2000) An overview of glacial hazards in the Himalayas. *Quaternary Int.* **66**, 31–47.

Rignot, E., Rivera, A. & Casassa, G. (2003) Contribution of the Patagonia Icefields of South America to sea level rise. *Science* **302**, 434–437.

Rivera, A., Benham, T., Casassa, G., Bamber, J. & Dowswell, J (in press) Ice elevation and areal changes of glaciers from the Northern Patagonia icefield, Chile. *Global Planetary Change* (in press).

Röthlisberger, H. (1972) Water pressure in intra- and subglacial channels. *J. Glaciol.* 11, 177–203.

Sakai, A., Chikita, K. & Yamada, T. (2000) Expansion of a moraine-dammed glacial lake, Tso Rolpa, in Rolwaling Himal, Nepal Himalaya. *Limnol. Oceanogr.* **45**, 1401–1408.

Saito, T. & Kobayashi, S. (1985) Hydrological observations at Soler Glacier. In: *Glaciological Studies in Patagonia Northern Icefield 1983-1984* (ed. by C. Nakajima), 57–63. Data Center for Glacier Research, Japanese Society of Snow and Ice, Nagoya, Japan.

Ushiyama, M. & Matsuyama, H. (1995) A trial manufacture of simple raingauge and comparison with the traditional observation. *J. Japan Soc. Hydrol. Water Resour.* **8**, 492–498 (in Japanese with English Abstract).

Warren, C. & Aniya, M. (1999) The calving glaciers of southern South America. *Global Planetary Change* **22**, 59–77.

Warren, C. R. & Sugden, D. E. (1993) The Patagonian icefields: A glaciogical review. *Arctic Antarctic Alpine Res.* **25**, 316–331.

Weertman, J. (1964) The theory of glacier sliding. *J. Glaciol.* **5**, 287–303.

Weertman, J. (1969) Water lubrication mechanism of glacier surges. *Can. J. Earth Sci.* **6**, 929–942.

Yamada, T. (1998) *Glacier lake and its outburst flood in the Nepal Himalaya*. Data Center for Glacier Research, Japanese Society of Snow and Ice, Tokyo, Japan.

Yamaguchi, S., Naruse, R., Matsumoto, T. & Ohno, H. (2003) Multiday variations in flow velocity at Glacier Soler, northern Patagonia, Chile. *Arctic Antarctic Alpine Res.* **35**, 170–174.

Glacier Mass Balance Changes and Meltwater Discharge (selected papers from sessions at the IAHS Assembly in Foz do Iguaçu, Brazil, 2005). IAHS Publ. 318, 2007.

Variations of a low latitude Andean glacier according to global and local climate variations: first results

ERIC CADIER[1], MARCOS VILLACÍS[1], ANTINEA GARCÉS[1], PIERRE LHUISSIER[1], LUIS MAISINCHO[2], RÉMY LAVAL[1], DIEGO PAREDES[3], BOLIVAR CÁCERES[2] & BERNARD FRANCOU[1]

1 *Institut de Recherche pour le Développement (France), IRD, UR032 Greatice, Casilla 17.12.857 Quito Ecuador*
cadier@ird.fr

2 *Instituto Nacional de Meteorología e Hidrología, INAMHI, Proyecto "Glaciares" Iñaquito 700 y Correa Quito Ecuador*

3 *Empresa Metropolitana de Alcantarillada y Agua Potable de Quito, EMAAP-Q, Casilla 17.12.857 Quito Ecuador*

Abstract We have 10 years of mass balance, meteorology and precipitation data on glacier 15 of Antizana, located in Ecuador, very close to the equator. Starting with the results of Francou *et al.* (2004), we studied the relation of monthly ablation zone volume variations of the glacier with 20 variables chosen to represent the global and local climate. The statistical model provided explains 58% of the melt variance. This model implicates the Niño3+4 index, as well as precipitation anomalies at the foot of Antizana. Excess (lack) of precipitation during the nine previous months corresponds to a decrease (increase) of melting. A warm (cool) anomaly of the ENSO oscillation corresponds to an increase (decrease) of melting 4 months later.

Key words Andes; Ecuador; El Niño; glacier melting modelling; tropical glacier

INTRODUCTION

Tropical glaciers are valuable indicators of low latitude climate variations. Their generalised retreat, which has been accelerating since the end of the 1970s, is probably linked to global warming (Francou *et al.*, 2005). We shall try to link glaciers variations to those of the current climate, expecting to contribute to the reconstruction of climatic variations. The processes of glacier variations are complex and dependent on several variables. Ice loss (melting and sublimation) is dependent on temperature, air humidity, wind, cloud cover, incident and reflected solar radiation on the glacier surface (thus of albedo), while its maintenance depends upon precipitation. Furthermore, the entire glacier moves downwards.

Francou *et al.* (1995a,b) and Ribstein *et al.* (1995) highlighted the links between variations of the global climate (ENSO) and that of the Zongo glacier in Bolivia (16°S). In Bolivia, Wagnon *et al.* (1999, 2001) and Sicart (2002) studied the mechanisms of Bolivian glaciers, showing that their melting depended both on the ENSO and temperatures, and also on the importance of the snow cover, which directly influences albedo.

In Ecuador, Antizana Glacier 15, as labelled and registered by Hastenrath (1981), is located about 30 km to the south of the equator. The mass, hydrological and elements of energetic balances monitoring began in 1994 and have been published in eight reports by Sémiond *et al.* (1998), Bontron *et al.* (1999), Favier *et al.* (2000) and Cáceres *et al.* (2001, 2002, 2003, 2005). Rossel (1997), Villacis (2001), Bendix (2000), Francou *et al.* (2000) and Vuille *et al.* (2000a,b) studied the links between climate anomalies in the tropical Pacific and Atlantic oceans and those of the Ecuadorian Andes. They highlighted an increase (decrease) in air temperatures in the Andes linked to warm (cold) phases of the ENSO, and an increase in wind during cold phases. However, the influence of these anomalies on precipitation is less evident. Later, Favier *et al.* (2004), Menegoz (2004) and Favier (2004) studied the mechanics of melting and sublimation in relation to findings from Bolivia. They showed that, despite a weak seasonality in terms of temperatures and incident radiation, the increase in winds between June and September produced an increase in sublimation, to the detriment of melting. These authors confirmed the fundamental role of the albedo of the glacier surface in the radiative balance and melting control.

Objectives and methods

We now have 10 years of mass balance data concerning a glacier of the Antizana. We shall compare on a monthly scale the relations between glacier variations, and those of the local, regional, and global climate, in order to find the climatic variables which better explain the melting variations of the last 10 years. We shall try to develop the results recently presented by Francou *et al.* (2004), which display an important relationship between the glacier volume variation and the Niño4 index temperature anomalies observed 3 months earlier about 11 000 km to the west of Antizana. This relation shows that there is a link between global climate and this glacier. Its quick variations show its sensitivity and the importance of this type of glacier in the investigation of climatic oscillations (Kaser & Osmaston, 2002).

We shall begin by analysing the relationship of the glacier ablation zone volume variations, represented by the variable “Bal” and: (i) Global climate variations (SOI, ENSO indices, etc.), starting from the results of Francou *et al.* (2004). (ii) Local and regional climate variations: climatic variables provided by NCEP-NCAR reanalysis of climatic variables close to Antizana (Kalnay *et al.*, 1996). (iii) Precipitation anomalies measured close to glacier 15. (iv) Meteorological measurements taken on the surface of the glacier. We shall then choose the most pertinent variables and propose a melting model.

ANTIZANA VOLCANO, ITS GLACIERS AND ITS MONITORING NETWORK

Antizana (0°28′S; 78°09′W) is located in Ecuador, about 30 km south of the equator. Despite being close to the Pacific Ocean, located 200 km to the west, it is mainly subject to easterly air flow, principally responsible for precipitation.

Antizana's climate description

In these regions, close to the equator, temperature, radiation and extraterrestrial radiation vary little throughout the year. The wind, cloud cover and precipitation vary much more. Favier *et al.* (2004) observed two major weather types throughout 2003: (i) Type P1 occurring generally between June and September–October characterized by strong winds (6.6 ms^{-1}), low cloud cover (0.37) and reduced precipitation levels. (ii) Type P2, from October to May, presents weaker winds (3.6 ms^{-1}), but higher cloud cover (0.59), precipitation, temperature and humidity.

Principal climatic variations from 1995 to 2004

Throughout the last 10 years, we observed several climatic episodes (Fig. 1):

(a) Several "El Niño" periods inducing temperature increases and a glacier retreat acceleration (weak and long Niño in 1994–1995, very strong in 1997–1998, latent Niño with prolonged deficit of precipitation in 2002–2004).
(b) A strong "La Niña" period between September 1998 and October 2000, which was cool, windy and wet, throughout which was observed a stabilization or slight glacier advance.
(c) But also distinct variations of precipitation with long periods of excess (1996–1997; 1999–2001) or deficit (1995; 2002–2004) (Lhuissier, 2005).

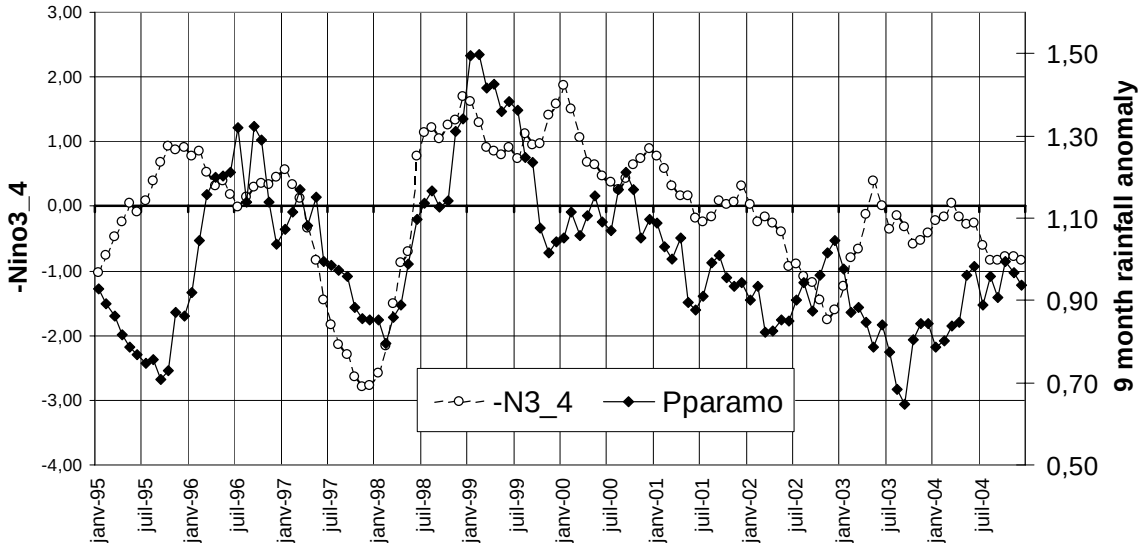

Fig. 1 Indices (Niño3+4) and rainfall anomalies for 9 months. Note, ENSO index is inversed.

Monitoring network

Figure 2 displays the position of glacier 15, of the meteorological and rain gauges stations. A stake network allows measurement of the melting between 4850 m a.m.s.l.

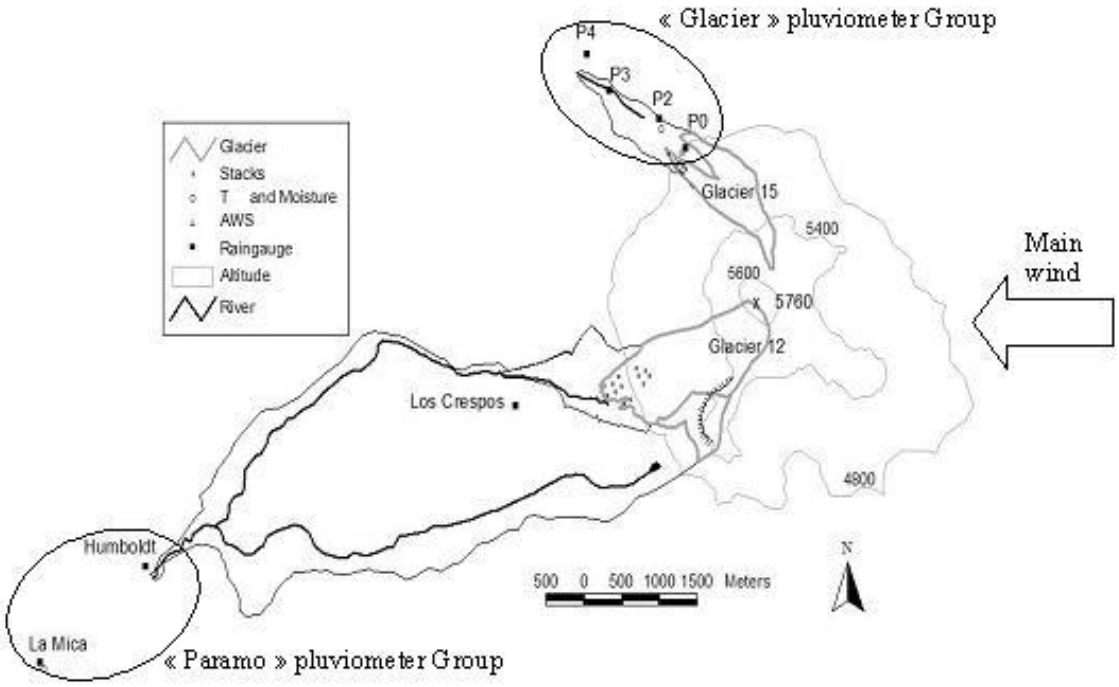

Fig. 2 Map of glacier position, monitoring network and pluviometric groups.

and the glacier equilibrium line (ELA) placed on average at 5100 m a.m.s.l. The automatic meteorological station, close to the rain gauge P0, is located on glacier 15 at an altitude close to 4900 m a.m.s.l.

DATA

In this first study, we analyse the monthly values of the climatic and glaciological variables with complete series during the period 1995–2004. We seek to explain and model the glacier's volume variation using the variable "Bal" defined by Francou *et al.* (2004) as: the volume variation of glacier ablation zone, divided by the ablation surface, expressed in mm of water per month. Negative (positive) values correspond to a glacier retreat (accumulation in ablation zone).

For this modelling, we used:

(a) Variables characteristic of global climate. We have selected the classic global indices linked to ENSO oscillations on the Pacific Ocean: SOI, indices Niño1+2, Niño3, Niño4, OLR, etc. The Niño 4 zone is located west of the Pacific between 5°N and 5°S and 160°E and 150°W, being close to 11 000 km further west.

(b) Variables linked to local and regional climate: (i) variables (temperature, wind, humidity, radiation, OLR) resulting from NCEP/NOAA reanalysis in the east sector of Antizana at levels 500, 600, and 700 hPa. (ii) Precipitation in the zones close to the glacier base (Pglacier between 4500 and 4900 m a.m.s.l.) and in lower zones (Pparamo around 4000 m a.m.s.l).

RELATIONSHIP BETWEEN GLACIER VARIATION AND CLIMATE VARIABLES

Relationship between precipitation and glacier volume variations

We have calculated the means of anomalous precipitation over *n* preceding months in the two climatic zones of the glacier and the Páramo. Thus Pglacier2 is the mean of the anomalies of precipitation in the "glacier" zone for the two preceding months, Pparamo9 in the "Páramo" zone for the nine preceding months, etc.

The best correlations are obtained for rainfall anomalies of the nine preceding months for the zone "Páramo" (r = 0.69, r2 = 0.47). (Table 1). This table shows that an excessive (insufficient) precipitation corresponds to a decrease (increase) of glacier melting, corroborating the results of Wagnon *et al.* (2001), Sicart (2002) and Favier *et al.* (2004).

Relationship between melting and global climate variables

Global climate variables directly linked to ENSO oscillation like SOI, ocean temperature anomalies of Niño3+4 block, etc. are correlated to glacier balances. The best correlation (r = –0.59, r2 = 0.35) is obtained between "Bal" and "N3+4" observed 4 months before, suggesting that a positive anomaly of western Pacific ocean temperatures is followed 4 months later by an acceleration of glacier ablation during the 120 months studied period (Table 2).

Table 1 Correlations between the glacier volume variations (Bal) and the averaged rainfall anomalies over the last n month of the two pluviometric groups.

Month number	1	2	4	6	9	12
Pglacier	0.34	0.51	0.54	0.59	0.61	0.56
Pparamo	0.36	0.55	0.58	0.65	0.69	0.64

Table 2 Correlations between the glacier volume variations (Bal) and the main global climatic variables for different time lag.

Variable	N3+4	N3+4	N3+4	N3+4	N3+4	N3+4	SOIMb	OLR	T600	Humed
Lag (month)	0	3	4	5	6	7	0	0	0	0
Correlation	–0.38	–0.58	–0.59	–0.58	–0.56	–0.52	0.51	–0.44	–0.57	0.53

The variables coming from NCEP-NCAR reanalysis close to Antizana present slightly lesser correlations. The most significant is the temperature at 600 hPa (r = –0.57). Time lag attempts for these temperatures have worsened this relationship. The relationship between "Bal" and the other NCEP-NCAR reanalysis variables are not as good. Note the correlation of –0.44 with "OLR" and 0.53 with "Humed".

STATISTICAL MODELLING OF GLACIER VOLUME VARIATIONS

We shall try to model the glacier volume variations using all these variables. The multiple linear regressions model calculated by the Stagraphics ® software selects and proposes a minimum amount of variables, which better explain the variance.

Complete model

The rainfall anomalies concerning the 9 and 2 previous months in the Páramo zone some 10 km west of the glaciers (variables Pparamo9 and Pparamo2) and the anomalous values of Pacific ocean temperatures 4 months earlier (Niño3+4 index) were selected for the best model construction. This complete model (Fig. 3) explains 58% of the "Bal" variance by the following equation:

Bal = 478*Pparamo9 + 180*Pparamo2 – 73*N3+4(lag of 4 months) –943 (r2 = 0.58; r = 0.76)

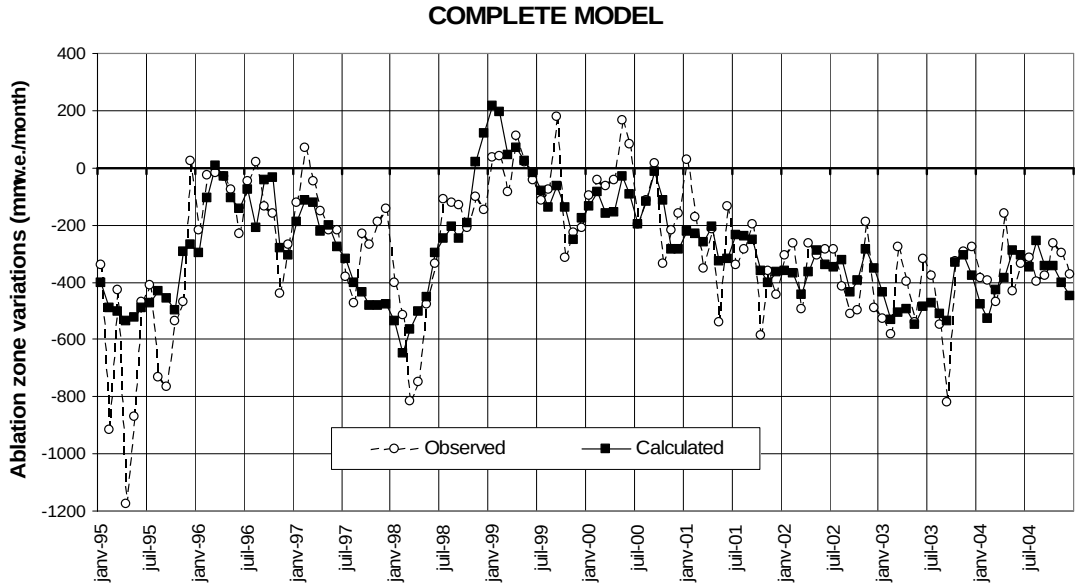

Fig. 3 Complete ablation zone mass variation model on Antizana glacier15. Time series comparison: Observed values = open circles; Calculated values = solid squares.

According to the proposed equation an ablation increase is linked to an increase in the Niño3+4 index (thus a warm ocean temperature anomaly) and/or a period of prolonged lack of precipitation over the 9 and 2 previous months. This lack of precipitation is generally accompanied by an elevation of the temperature, of the rain–snow limit, of the snow line altitude, and an albedo diminution, thus acceleration in the ablation. The opposite occurs with excessive rainfall.

The model correctly reproduces the melting variations throughout the concerned period. Note the systematic under estimation of the ablation in year 1995, and of some of the high-melting months.

Component effect: partial melting models

To better appreciate the variables role, we adjusted one model using only the global variable N3+4(lag of 4 months), and another using only the local variables Pparamo9 and Pparamo2

First model This model (Bal = –138*N3+4 (lag of 4 months) –279; r = 0.59) now explains only 35% of the variance. The Niño index, which varies slowly, correctly reproduces the ablation tendencies over several months, but cannot reproduce quick variations.

Second model This model (Bal = 716*Pparamo9+ 170*Pparamo2 –1175; r = 0.67) explains 45% of variance. It seems that it better reproduces quick ablation variations, but does not reproduce accurately the acceleration observed during the strong Niño of 1997–1998.

We have not presented here the component effects of variables not selected by the model.

DISCUSSION AND CONCLUSION

The complete model allowed us to explain close to 60% of the variance of Glacier 15's ablation using only two variables:

The first is the anomaly, 4 months prior, of sea surface temperature in block Niño3+4 at over 11 000 km further west, which represents the climate's oscillations for several months' amplitude. A warm (cool) anomaly of ENSO oscillation will result in an increase (decrease) in melting or glacier ablation 4 months later.

The second is a precipitation anomaly index throughout the nine previous months, representing the local climate's influence on the glacier, which influences the snow cover protecting the glacier and controls its global albedo. Excessive precipitation during the nine previous months in the Antizana region will result in a reduction in ablation.

Limitations

Note the linear statistical modelling technique used is fast and effective, but has its weaknesses: (i) It cannot correctly represent phenomenon that are probably non-linear. (ii) The model's variable selection is based upon the variance reduction that each variable adds to the model. However, we must check (in the present work and in its future developments) that the model stays compatible with the melt's physical mechanics. (iii) These models have been adjusted with monthly values. Yet, one same month could contain periods where meteorological conditions and melt mechanisms have been very different.

The data may contain errors. Moreover, it may be that exceptional conditions may occur (such as a volcanic eruption), which would require other models and equations.

Prospects

These first results are promising, and they confirm and complement the conclusions of Francou *et al.* (2004). We show, as a new complementation, a local precipitation influence on ablation reduction in addition to the Niño4 index effect already demonstrated. We now continue the work: (i) By the same method, we shall analyse the modelling of other glaciers and melting floods. (ii) We shall soon validate these models by observations of the glacier melt for 2005. (iii) We are analysing the mechanisms and modelling of the glacier melt using more precise time steps (hourly or daily) (Favier, 2004; Villacis, in press). (iv) Continuing the research for the melt's explicative variables under tropical conditions.

The high proportion of explained variance by this first model opens up perspectives to work on the glaciers and water resources evolution, in association with other more sophisticated and physically based models. For instance, IPCC scenarios could be considered, using the recent past LIA glacier regression (Little Ice Age), which is well documented in the Antizana region, to try to adjust and validate this simple kind of linear model to different global climate conditions.

REFERENCES

Bendix, J. (2000) Precipitation dynamics in Ecuador and northern Peru during the 1991/92 El Niño: A remote sensing perspective. *Int. J. RemoteSens*. **21**(3), 533–548.

Bontron, G., Francou, B., Ayabaca, E., Cáceres, B., Maisincho, L., Chango, R., de la Cruz, A., Garzón, L. A. & Neubert, D. (1999) El Glaciar 15 del Antizana – Mediciones glaciológicas, hidrométricas y topográficas (años 1997–1998), Informe n^0 2 IRD-INAMHI-EMAAP-Q.

Cáceres, B., Maisincho, L., Favier, V., Francou, B., Ramírez, J., Vargas, A., Chango, R., Cruz, F. & Neubert, D. (2001) Glaciar 15 del Antizana (Ecuador). Balance de masa, topografía, prospección geofísica, meteorología, hidrología y balance de energía. Año 2000. Informe 3, IRD, INAMHI, EMAAP-Quito, INGEOMINAS-COLOMBIA: 110 p.

Cáceres, B., Maisincho, L., Taupin, J. D., Tachker, P., Chazarin, J. P., Francou, B. & Favier, V. (2002) Glaciar 15 del Antizana (Ecuador). Balance de masa, topografía, meteorología, hidrología y balance de energía. Año 2001. Informe 4, IRD, INAMHI, EMAAP-Quito 91p.

Cáceres, B., Maisincho, L., Taupin J. D.; Favier, V., Tachker, P., Chazarin, J. P., Francou, B., Cadier, E., & Cruz, F. (2003) Glaciar 15 del Antizana (Ecuador). Balance de masa, topografía, meteorología, hidrología y balance de energía. Año 2002. Informe 5, IRD, INAMHI, EMAAP-Quito, 111 p.

Cáceres, B., Maisincho, L., Taupin, J. D., Bucher, R., Paredes, D., Villacís, M., Chazarin, J. P., Francou, B., Cadier, E. (2004) Glaciar 15 del Antizana (Ecuador). Balance de masa, topografía, meteorología e hidrología. Año 2003. Informe 6, IRD, INAMHI, EMAAP-Quito, 77 p.

Cáceres, B., Maisincho, L., Taupin, J. D., Francou, B., Cadier, E., Delachaux, F., Bucher, R., Villacis, M., Paredes, D., Chazarin, J. P., Garces, A. & Laval, R. (2005) Glaciares del Ecuador: Antizana y Carihuyarzo, balance de masa, topografía, meteorología & hidrología. Informe del Año 2004. IRD, EMAAP-Q, INAMHI Quito 176 p.

Favier, V., Cáceres, B., Maisincho, L., Francou, B., de la Cruz, A., Chango, R. & Neubert, D. (2000) El Glaciar 15 del Antizana (Ecuador). Mediciones glaciológicas, hidrométricas, meteorológicas y topográficas (año 1999). Informe NGT-Ecuador, 3, IRD, EMAAP-Quito, INAMHI 97 p.

Favier, V., Wagnon, P., Chazarin, J. P., Maisincho, L. & Coudrain, A. (2004) One-year measurements of surface heat budget on the ablation zone of Antizana Glacier 15, Ecuadorian Andes. *J. Geophys. Res.* **109**, D18105, doi:10.1029/2003JD004359.

Favier, V. (2004) Etude du bilan d'énergie de surface et de la production des écoulements de fonte d'un glacier des Andes d'Equateur, relation glacier - climat en zone tropicale, PhD Thesis, Univ. de Montpellier II, France.

Francou, B., Ribstein, P. Sémiond, H., Portocarrero, C. & Rodríguez, A. (1995a) Balance de glaciares y clima en Bolivia y Perú. Impactos de los eventos ENSO. *Bull. Inst. Fr. études andines* **24**(3), 643–654.

Francou, B., Ribstein, P. Tiriau, E. & Saravia, R. (1995b) Monthly balance and water discharge on an inter tropical glacier. The Zongo glacier, Cordillera Real, Bolivia, 16_S. *J. Glaciol.* **42**(137), 61–67.

Francou, B., Ramirez, E., Cáceres, B. & Mendoza, J. (2000) Glacier evolution in the tropical Andes during the last decades of the 20th century. Chacaltaya, Bolivia, and Antizana, Ecuador. *Ambio* **29**(7), 416–422.

Francou, B., Vuille, M., Favier, V. & Cáceres, B. (2004) New evidence for an ENSO impact on low latitude glacier: Antizana 15, Andes of Ecuador, 0°28′S. *J. Geophys Res.* **109**, D18106.

Francou, B., Ribstein, P., Wagnon, P., Ramirez, E. & Pouyaud, B. (2005) Glaciers of the Tropical Andes, indicators of the global climate variability. In: *Global Change and Mountain Regions: A State of Knowledge Overview* (ed. by U. Huber, K. M. Harald & M. A. Reasoner). Springer, New York, USA.

Hastenrath, S. (1981) *The Glaciation of the Ecuadorian Andes*. Balkema, Rotterdam, The Netherlands.

Kalnay, E., Kanamitsu, M., Kistler, R., Collins, W., Deaven, D., Gandin, L., Iredell, M., Saha, S., White, G., Woollen, J., Zhu, Y., Leetmaa, A., Reynolds, B., Chelliah, M., Ebisuzaki, W., Higgins, W., Janowiak, J., Mo, K.C., Ropelewski, C., Wang, J., Jenne, R. & Joseph, D. (1996) The NCEP/NCAR 40–year reanalysis project. *Bull. Am. Meteorol. Soc*. **77**(3), 437–471.

Kaser, G. & Osmaston, H. A. (2002) *Tropical Glaciers*. Cambridge Univ. Press, New York, USA.

Lhuissier, P. (2005) Mise en évidence de modèles de comportement pluviométrique sur le volcan Antizana. IRD, Quito, Ecuador.

Menegoz, M. (2004) Etude de la couche limite atmosphérique sur le glacier de l'Antizana (Equateur) et estimation des flux turbulents. MSc Thesis, Univ. Grenoble, France.

Ribstein, P., Francou, B,. Tiriau, E. & Saravia, R. (1995) Tropical climate and glacier hydrology. A case study in Bolivia. *J. Hydrol*. **165**, 221–234.

Rossel, F. (1997) Influence du Niño sur les régimes pluviométriques de l'Equateur. PhD Thesis, Univ. de Montpellier II, France

Sémiond, H., Francou, B., Ayabaca, E., de la Cruz, A., & Chango, R. (1998) El Glaciar 15 del Antizana (Ecuador): investigaciones glaciológicas 1994–1997. ORSTOM-IFEA-EMAAP-Q-INAMHI, Quito.

Sicart, J. E. (2002) Contribution à l'étude des flux d'énergie, du bilan de masse et du débit de fonte d'un glacier tropical: Le Zongo, Bolivie. PhD Thesis, Univ. de ParisVI, Paris, France.

Villacis, M. (2001) Influencia de El Niño-Oscilación del Sur sobre la precipitación en los Andes centrales del Ecuador. Tesis de grado, 199pp., Esc. Pol. Nac., Quito, Ecuador.

Vuille, M., Bradley, R. S. & Keimig F. (2000a) Interannual climate variability in the central Andes and its relation to tropical Pacific and Atlantic forcing. *J. Geophys. Res.* **105**(12), 447.

Vuille, M., Bradley, R. S. & Keimig F. (2000b) Climatic variability in the Andes of Ecuador and its relation to tropical Pacific and Atlantic sea surface temperature anomalies. *J. Climate* **13**, 2520–2535.

Wagnon, P., Ribstein, P., Francou, B. & Pouyaud B. (1999) Annual cycle of energy balance of Zongo glacier, Cordillera Real, Bolivia. *J. Geophys. Res.* **104**, 3907–3923.

Wagnon, P., Ribstein, P., Francou, B.& Sicart, J. E. (2001) Anomalous heat and mass budget of Zongo glacier Bolivia, during the 1997–98 El Niño year. *J. Glaciol.* **47**(156), 21–28.

Glacier Mass Balance Changes and Meltwater Discharge (selected papers from sessions at the IAHS Assembly in Foz do Iguaçu, Brazil, 2005). IAHS Publ. 318, 2007.

Changes in quantity and variability of runoff from Alpine basins with climatic fluctuation and glacier decline

DAVID N. COLLINS

Alpine Glacier Project, School of Environment & Life Sciences, University of Salford, Salford Crescent, Manchester M5 4WT, UK
d.n.collins@salford.ac.uk

Abstract Impacts of climatic fluctuation on amount and year-to-year variability of runoff were assessed for four sub-basins with between ~1.8 and ~70% glacier cover within the upper Rhône catchment, Switzerland, during a period of sustained glacier recession. Runoff in the most highly-glacierised sub-basin mimicked annual mean summer air temperature through two warming cycles. In the least glacier-covered basin, the pattern of runoff variation was inverse, reflecting changes in total annual precipitation. Coefficients of variation were used to characterise runoff variability, which increased with level of discharge in only the most highly glacierised sub-basin. Overall, variability of runoff was negatively related to percentage glacierisation despite variability increasing slightly in basins with between 40 and 70% ice cover. Variability was enhanced in the more glacierised, but reduced in the less-glacierised basins during the warmer drier 1980s through 2000s, by comparison with the cooler wetter 1960s through 1970s.

Key words climatic fluctuation; coefficient of variation; glacier recession; glacierised basin; meltwater discharge; percentage glacierisation; runoff

INTRODUCTION

Year-to-year variations in discharge tend to be moderated in glacierised basins, making glaciers reliable water resources. Even limited ice cover in a mountain basin reduces the variability of annual total runoff with respect to that of annual total precipitation (Kasser, 1959). Year-to-year variability of discharge reduces with increasing percentage basin glacierisation (e.g. Fleming & Clarke, 2005) to a minimum between 20 and 50%, before remaining constant or increasing (Krimmel & Tangborn, 1974; Tvede, 1982; Fountain & Tangborn, 1985; Röthlisberger & Lang, 1987; Collins, 1988).

Runoff from a glacierised basin arises both from the ice-free area and from the glacier itself, and opposing responses of these two portions of the basin to the same hydrometeorological input provide the moderating effect. Total annual runoff from the ice-free zone is always less than but directly proportional to annual total precipitation over that area, having year-to-year variability close to that of precipitation. Annual runoff from the glacierised area essentially depends on the interaction between snowfall and the amount of heat energy available for melt. The sooner and higher the rise of the transient snowline in summer, the thicker the layer of ice melted, as a larger area of ice is exposed to melt for longer. The meltwater contribution from the glacier, therefore, augments basin runoff in years in which warm summers following dry winters lead to relatively low flow from the ice-free area. As glaciers have declined in

area, such offsetting of low flow may have been reduced, warmer summers notwithstanding. Thermal energy availability for melt more strongly influences runoff variability in more highly-glacierized basins, ice-free areas predominantly located at lower elevations producing limited runoff from less precipitation.

Although compensating responses may well reduce year-to-year variability in discharge from glacierised basins, runoff from such basins in the European Alps has responded to two cycles of warming since the mid-19th century, the underlying patterns of flow having fluctuated considerably (Collins, 2005). However, the same climatic fluctuations led to generally sustained loss of mass and reduction in glacier size from dimensions attained during the Little Ice Age (e.g. Maisch *et al*., 1999). Glacier recession will have added a component of flow to runoff in excess of that related to contemporary levels of precipitation. That additional component of flow can not be sustained indefinitely, for, should glaciers ultimately disappear, flow will be reduced, and runoff variability increased to reflect solely the then contemporary amounts and variability of precipitation. Reduction of glacierised area, resulting in decreasing percentage basin glacierisation, might be expected to lead to year-to-year variability in runoff in more highly-glacierised basins being diminished but being enhanced in basins with low percentage ice cover, given the U-shaped relationship between runoff variability and glacierisation. Depending on relative rates of increase in energy availability and associated decrease of glacierised area, annual totals of runoff might first be expected to increase before decreasing as glacier geometry translates loss of ice mass into glacier area depletion and reduced surface area for heat exchange and melt.

The aim of this paper is to examine how runoff from four Alpine sub-basins of the upper Rhône, in Valais, Switzerland, with differing percentages of glacier cover (Fig. 1), varied through a period of climatic fluctuation and sustained glacier recession. The hydrometeorological and discharge records now available for these basins extend by 20 years the series analysed by Collins (1989a), to include the warm period towards the end of the twentieth and into the 21st century. These records allow investigation of questions concerning reliability of runoff as air temperature warms and glaciers decline. How climatic fluctuation influenced runoff quantity, how runoff variability varied with percentage glacierisation and amount of discharge, and hence whether warmer air temperatures led to more or less year-to-year variability in runoff are assessed for basins which in 2002 had ice-covers ranging between 1.8% and 65.9%. The long record for the Massa allows comparison of runoff through two warming cycles through which glacier area declined by about 6%. Both Kasser (1981) and Chen & Ohmura (1990) considered that reduction in glacierised area had contributed to downward trend in runoff from Alpine glacierised basins in the period 1922–1972. Elsewhere, in western Canada, depletion of glacier storage was insufficient to offset generally declining discharge irrespective of percentage glacierisation (for the period indicated) (e.g. Hopkinson & Young, 1998 (1951–1993); Moore & Demuth, 2001 (1969–1989)).

STUDY BASIN CHARACTERISTICS AND CHANGES IN GLACIERISED AREAS

Dimensions and vertical extents of the selected basins and included glacierised areas are shown in Table 1 and Fig. 2, respectively. Fig. 2 indicates that percentage

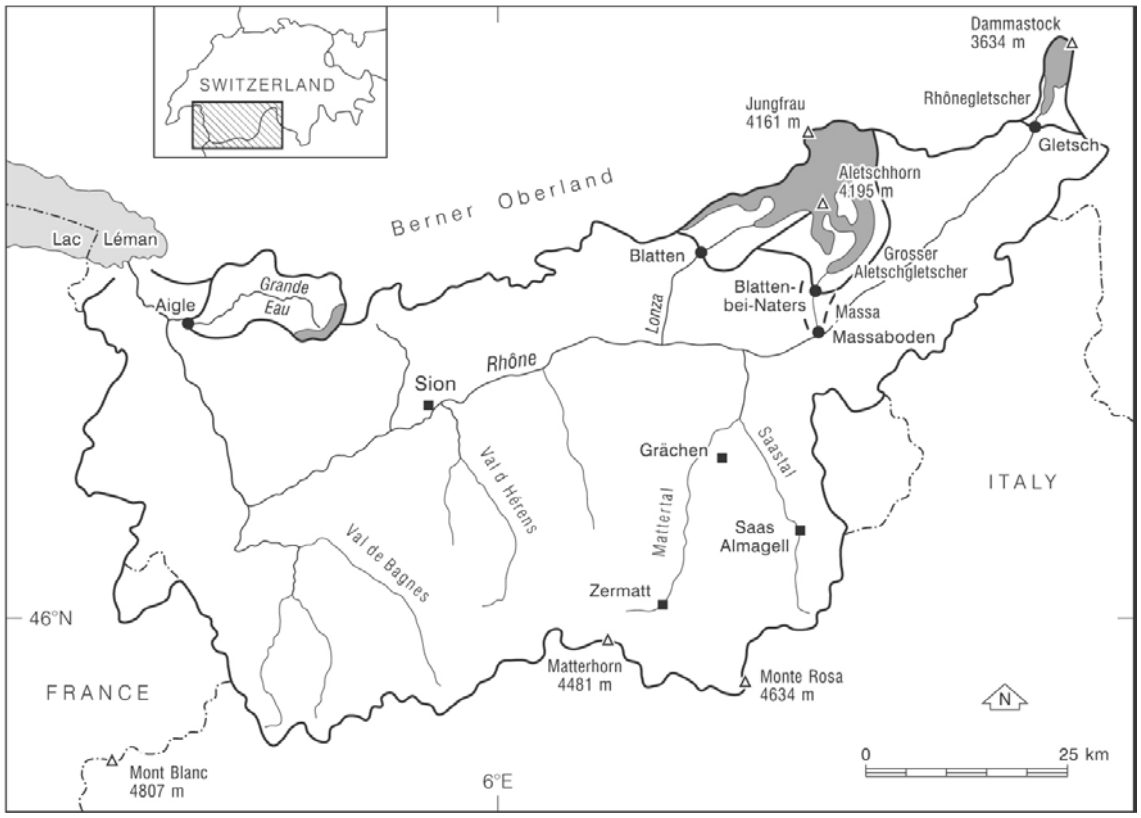

Fig. 1 Locations of study basins nested in the upper Rhône basin, Valais, Switzerland. Gauging and meteorological stations are indicated by circles and squares, respectively. Glacierised areas within the study basins are shaded.

Table 1 Characteristics of drainage basins, glacierised areas and runoff.

River/Gauging station	Basin area (km^2)	Basin glacierisation (year)	(%)	Mean runoff 1956–2005 (m)
Grande Eau/Aigle	132.0	1977	1.9	1.190
		2002	1.8	
Lonza/Blatten	77.8	1977	40.6	1.905
		2002	36.5	
Rhône/Gletsch	38.9	1977	56.4	2.218
		2002	52.2	
Massa/Massaboden	202.0	1934	67.6	2.112
		1957	64.1	
Massa/Blatten-bei-Naters	195.0	1934	70.0	
		1957	66.4	
		1977	66.6	
		2002	65.9	

glacierisation of basin is essentially an arbitrary condition, dependent on distance downstream from glacier terminus to gauging station location. Areal dimensions, hypsometry and elevations of glaciers, which actually influence meltwater production, are not simple derivatives of percentage glacierisation. Percentage glacierisation of

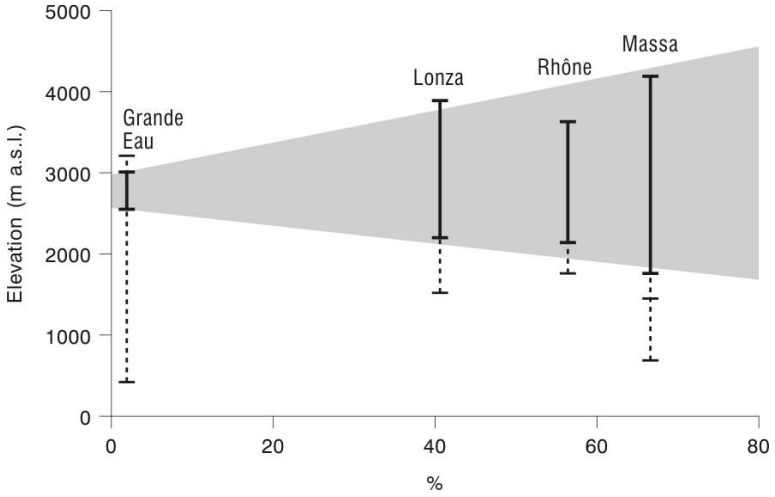

Fig. 2 Elevations of upper and lower limits of glacierised areas (solid lines) and basins (broken lines) plotted against percentage basin glacierisation. The shaded area shows schematically the ranges of elevations within which glaciers are distributed in the upper Rhône basin.

total basin area was taken from the contemporary annual *Hydrologisches Jahrbuch der Schweiz* (e.g. Bundesamt für Wasser und Geologie, 2006). All four basins are subject to the same pattern of climatic influences.

Small discontinuous glaciers, such as Glacier de Pierredar (1.25 km^2 in 1973), which receded slightly between 1977 and 2002, exist on the eastern rim of the Grande Eau basin. Since 1942, some water has been transferred each year to the basin from storage in the Arnensee, which has a contributing area of 7.1 km^2, 5.10% of the combined basin areas. Total glacier-covered areas of about 32 and 22 km^2 in the Lonza and Rhône basins declined by about 10% and 7.5%, respectively, during the same period. Following construction of a dam, from 1965 the Massa was gauged at Blatten-bei-Naters, upstream of the former station at Massaboden, reducing basin area by 3.47%. Percentage glacierisation of the Massa basin, recalculated to take into account catchment area change (Table 1), reflects loss of total ice-covered area of about 8 km^2 (6%) from 136.6 km^2 between 1934 and 2002, of which about 75% had disappeared by 1957. With the exception of the Grande Eau, flow conditions are natural.

MEASUREMENTS

Mean summer air temperature for the months May to September ($T_{5–9}$) is used to indicate energy availability for melting. Such means from the long record at Sion (Couvent des Capucins) (1865–1977) correlate well with values from other stations in the upper Rhône, and with runoff from glacierised sub-basins (Collins, 1987, 1989b). Since measurements ceased in 1977, subsequent values of $T_{5–9}$ for Sion have been estimated from observations at Grächen (1966–2005). Total annual precipitation between November and October ($P_{11–10}$) reflects both build up of winter snow pack before subsequent contribution to runoff on melting in spring, and the liquid precipitation contribution in summer. $P_{11–10}$ was derived from the precipitation record for Zermatt (1893–2005).

Annual runoff from a basin is represented by $Q_{1–12}$, the total discharge in a calendar year. Records for the Massa have not been adjusted for the basin area change resulting from gauge relocation in 1965. Subsequent runoff in the Massa is unlikely to have decreased *pro rata* with the 3.47% reduction in basin area, as the portion of basin excluded was ice-free, with below average precipitation being at low elevation.

CLIMATIC FLUCTUATIONS AND RUNOFF

From the 1860s, summer air temperature first decreased, to a minimum in 1888, before rising to the late 1940s, with a peak in 1947. $T_{5–9}$ then declined until the late 1970s, before generally rising to the start of the 21st century, with the warmest summer in the record in 2003, on an underlying gently rising linear trend from the 1880s (Fig. 3). $P_{11–10}$ varied roughly inversely with $T_{5–9}$, on a weak linear downward trend, being relatively low from the late 1920s to the 1950s, with 1942/1943 the driest year of the 20th century, before rising from the late 1950s through to the early 1980s as summers became cooler. 1979/1980 was the wettest year since 1913/1914. Precipitation was then generally below average for much of the warmer period from the 1980s, on a steep falling trend, with a minimum in 2003/2004, the driest $P_{11–10}$ since 1892/1893.

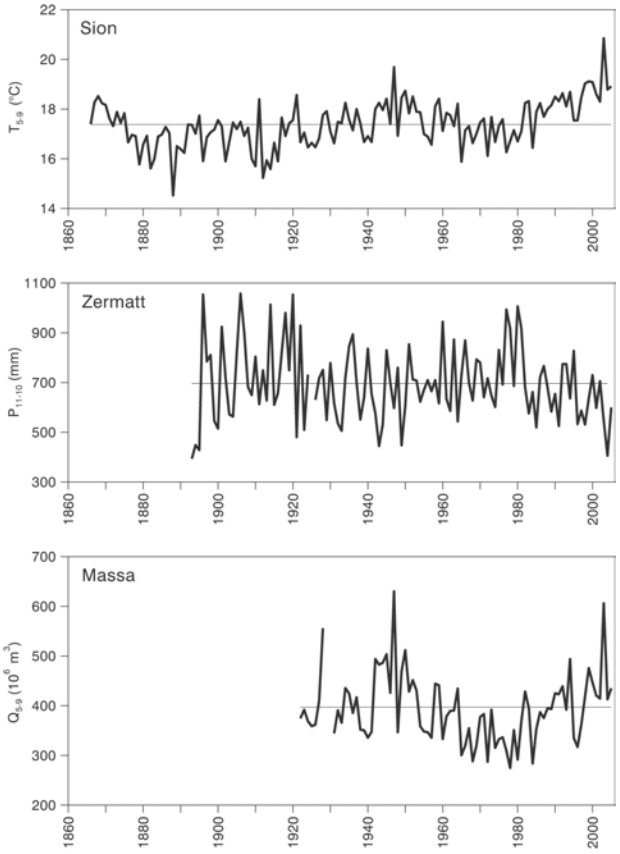

Fig. **3** Year-to-year variation and series average (horizontal line) of mean summer air temperature ($T_{5–9}$) at Sion, annual total precipitation between November and October ($P_{11–10}$) at Zermatt, and discharge of the Massa (annual totals in the ablation season months May through September ($Q_{5–9}$)) in the period 1865–2005. From 1978 to 2005, ($T_{5–9}$) at Sion was estimated from records at Grächen and Saas Almagell.

Discharge of the Massa ($Q_{1–12}$), which drains the most highly-glacierised basin, mimicked the cyclical pattern of variation in $T_{5–9}$ (correlation coefficient of 0.88 for 1936–2005). Flows in the warmer 1990s–2000s ($T_{5–9}$ 18.87°C, $Q_{1–12}$ 469.33 × 10^6 m^3 for 1996–2005) just failed to exceed those of the 1940s–1950s ($T_{5–9}$ 18.07°C, $Q_{1–12}$ 473.09 × 10^6 m^3 for 1946–1955), decrease in glacierisation notwithstanding (Figs 3 and 4). 1947 and 2003 stand out as peak runoff years ranked first and second, with $T_{5–9}$ 19.77 and 20.85°C, respectively. In the least-glacierised basin, $Q_{1–12}$ of the Grande Eau generally reflected the pattern of precipitation not thermal conditions, rising to a maximum in the 1960s, declining in the early 1970s, before increasing again in the late 1970s/early 1980s (Fig. 4). In the second warming cycle runoff declined by 15.93% from 1976–1985 to 1996–2005 (Table 2), reflecting below average precipitation and high evaporation. Particularly wet years (1965/1966, 1969/1970 and 1994/1995) stand out in the record. The pattern of flow in the Rhône, $Q_{1–12}$ at Gletsch, up by 23% from 1966–1975 to 1986–1995, paralleled that of the Massa until a divergence in the late 1990s–early 2000s, when runoff from the Rhône basin declined by 8.57% to 1996–2005, whilst the Massa was further augmented by 6.75% between 1986–1995 and 1996–2005. Temporal variation of runoff in the Lonza was to an extent intermediate between that in Grande Eau and Rhône, but declined much less than both between 1986–1995 and 1996–2005. Runoff in the Lonza was lower in warmer 2003 than in 1994, whereas in the more highly-glacierised Rhône and Massa basins, runoff in 2003 exceeded that in 1994.

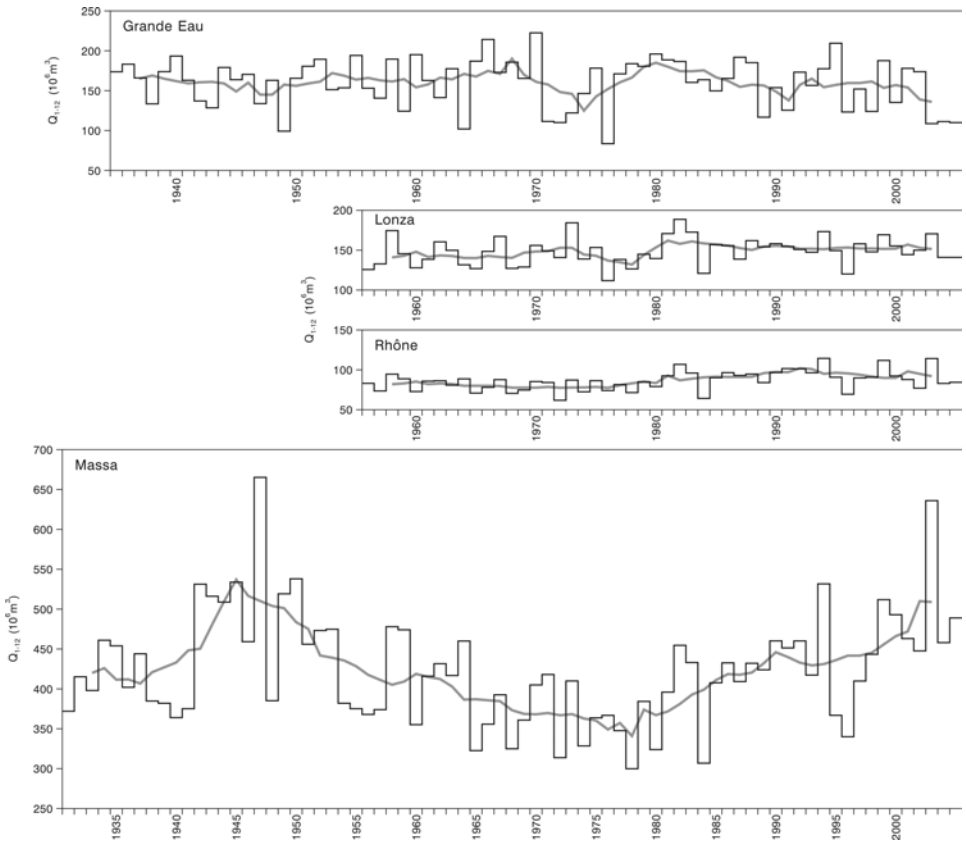

Fig. 4 Year-to-year variations and nine-year moving averages of annual total discharge ($Q_{1–12}$) of the Grande Eau, Lonza, Rhône and Massa in the period 1930–2005.

Table 2 Mean annual runoff and variability of flow (as coefficient of variation) for selected periods.

Period	Length of period years	Basin Grande Eau ($\times 10^6$ m^3)	Lonza ($\times 10^6$ m^3)	Rhône ($\times 10^6$ m^3)	Massa ($\times 10^6$ m^3)
1936–1945	10	161.74	–	–	444.61
		(0.131)			(0.152)
1946–1955	10	159.54	–	–	473.09
		(0.168)			(0.176)
1956–1965	10	156.52	140.50	82.57	409.76
		(0.184)	(0.106)	(0.090)	(0.123)
1966–1975	10	162.38	148.77	78.89	368.90
		(0.238)	(0.111)	(0.106)	(0.099)
1976–1985	10	164.50	147.01	84.22	372.19
		(0.189)	(0.159)	(0.142)	(0.136)
1986–1995	10	163.39	154.42	97.00	439.67
		(0.170)	(0.057)	(0.077)	(0.094)
1996–2005	10	138.29	149.82	90.96	469.33
		(0.208)	(0.094)	(0.128)	(0.154)
1936–2005	70	158.10	–	–	425.36
		(0.193)	–	–	(0.168)
1931–1955	25	–	–	–	456.28
		–	–	–	(0.158)
1956–1980	25	159.95	142.15	80.25	380.50
		(0.223)	(0.114)	(0.095)	(0.129)
1981–2005	25	154.21	154.06	93.20	443.44
		(0.190)	(0.099)	(0.120)	(0.142)
1956–2005	50	157.05	148.10	86.41	411.97
		(0.208)	(0.114)	(0.134)	(0.157)

Records are available for all four basins for the period 1956–2005, which can be divided into two sub-periods of equal length (25 years), 1956–1980 and 1981–2005. The former period was predominantly cooler and wetter than the second ($T_{5–9}$ of 17.23 and 18.23°C, and $P_{11–10}$ of 729 and 646 mm, respectively). The warmer summers and relatively dry winters characterising the second period resulted from sustained high pressure anomalies over Central Europe (Beniston & Jungo, 2002). As indicated in Table 2, mean discharge increased between the first and second sub-periods in the three more highly glacierised basins, but decreased in the Grande Eau basin. Within the second sub-period, however, runoff in the Lonza and Rhône decreased between 1986–1995 and 1996–2005.

YEAR-TO-YEAR VARIABILITY OF RUNOFF

For the purposes of comparison of variability of runoff between basins, coefficient of variation (ratio of standard deviation to mean) is used to indicate relative dispersion of

flow. For the 70-year period 1936–2005, which includes both periods with warmer summers and higher levels of runoff in the Massa, runoff variability of the Massa was much reduced by comparison with that of the Grande Eau (Table 2), reflecting the moderation of flow by the large glacierised area. During the 50-year period 1956–2005, for which data are available for all four basins, runoff variability was greatest in the Grande Eau (CV = 0.208), least in the Lonza (~39% glacierised, CV = 0.114), but then increased with increasing glacierisation to a CV of 0.157 in the Massa (~66% glacierised), a typical asymmetric U-shaped pattern of variation of variability of stream flow with percentage glacierisation in the Alps (Fig. 5).

In the sub-period 1956–1980, generally wet years with cool summers, the difference in range of variability of flow between least in the Rhône (~55% glacierised) and most in the Grande Eau was wider than in the full 50-year period (Table 2, Fig. 5). In the drier and warmer sub-period 1981–2005, the range of difference between least (Lonza) and most (again Grande Eau) variability narrowed, CV for each river being less, respectively, than during the full period. Variability of flow in the two more highly-glacierised basins, Rhône and Massa, was increased, whilst in the Lonza and Grande Eau CV was reduced in comparison with 1956–1980.

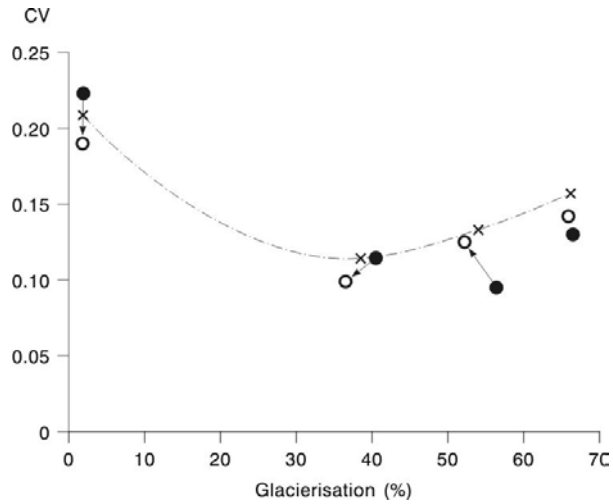

Fig. 5 Coefficients of variation (CV) of annual total discharge ($Q_{1–12}$) of the Grande Eau, Lonza, Rhône and Massa plotted against respective basin percentage glacierisation for the period 1956–2005 (crosses, connected by pecked line), and changes in CV between wetter and cooler (1956–1980) (closed circle) and drier and warmer (1981–2005) (open circle) sub-periods indicated by arrows.

DISCUSSION

The underlying slightly declining linear trend in runoff in the Massa between the late 1920s and mid-2000s was strongly dominated by the two cycles of warming (Figs 3 and 4), the rise to the second maximum of which, between the late 1970s and 2000s, paralleled the upward trend in runoff detected by Birsan *et al.* (2005) in basins in Switzerland having more than 10% glacier cover. From the 1940s to the 1970s, runoff in the Massa declined, ablation reducing with falling energy availability and shrinking

glacierised area. Accumulation of winter precipitation must have been insufficient to offset even reduced ablation, so failing to maintain glacier mass. The temporal pattern of runoff from the <2%-glacierised Grande Eau basin tended to be the inverse of that from the highly-glacierised Massa basin. High summer energy availability for melt in the 1990s–2000s over the tiny glacier area made no impact against low precipitation over the large ice-free zone. Underlying linear trend in runoff from the late 1930s to the mid-2000s was slightly negative, in contrast to generally positive trends identified in basins across Switzerland. The downward trend accelerated from the 1970s, as was the case in general for summer runoff in basins in Switzerland with less than 10% glacierisation (Birsan *et al.*, 2005).

Flow in the Rhône at Gletsch showed a rising linear trend from the 1970s to a maximum in 1994, before runoff started to decline, high energy availability being unable to make up for declining glacier area and reduced precipitation. Runoff in the Lonza followed precipitation over the ice-free 60% of the basin area during the 1960s and 1970s. However, in the 1990s and 2000s, flow was maintained, total discharge being just higher in exceptionally-warm 2003 than in 1999, although lower than in 1994.

Although runoff in glacierised basins was moderated, runoff quantities varied considerably from year to year. Maximum $Q_{1–12}$ in the Massa in 1947 was 1.22 times greater than the minimum in 1978 on a temperature difference of 3.33°C, whereas in the Grande Eau, the highest annual runoff in 1970 was 1.75 times larger than the lowest in 1976, for a difference in $T_{5–9}$ of 0.18°C. and in $P_{11–10}$ of 105 mm. Correlation between CV and mean discharge for each river during the five decadal periods for which data are available for all four basins is mixed (r = +0.34 Massa, –0.33 Rhône, –0.52 Lonza and –0.18 Grande Eau). Variability of flow was enhanced at higher discharges in the Massa for which r = +0.61 over all seven decadal periods of the record. For those seven decades, correlation for the Grande Eau was r = –0.27. Nonetheless, between the two 25-year periods 1956–1980 and 1981–2005, runoff variability decreased in the two least glacierised basins, as mean discharge in the Grande Eau declined by 3.6% in the warmer drier conditions. Mean discharge increased by 8.4% in the Lonza, however, despite glacier area decline (Table 2, Fig. 5). In the two most glacierised basins, runoff variability increased between the two periods as discharge in the Rhône and Massa was enhanced by 16.1% and 16.5%, respectively.

Negative correlation between runoff variability and percentage basin glacierisation is generally stronger in other mountain ranges than in the Alpine sub-basins of the upper Rhône. For example, for nine basins (four ice-free and five partially-glacierised) in southwest Yukon and northwest British Columbia, over records 22 to 47 years in length, Spearman rank correlation (r_S) between runoff variability and glacierisation was –0.71, but percentage glacierisation was described as "relatively small" and the basins as "large", terms which were undefined (Fleming & Clarke, 2005). Spearman correlation does not require linearity in a relationship and can be applied to CV $Q_{1–12}$ – percent glacierisation curves for the four upper Rhône sub-basins. For the 50-year period 1956–2005, r_S was –0.50. For these basins, presumably small in comparison with those in the Yukon and British Columbia, the upturn in runoff variability at levels of ice-cover greater than ~40% reduces the degree of negative correlation. Precipitation levels appear to have been insufficient to contribute enough runoff from the small non-glacierised portions of the more highly-glacierised basins to offset

variations in the quantities of meltwater produced from the glacierised area by year-to-year fluctuations in energy availability. In the cooler wetter period 1956–1980, r_S was –0.75, falling in warmer drier 1981–2005 to –0.50.

CONCLUSION

Percentage glacierisation of basin influenced the response of runoff from the four Alpine study basins to the same pattern of climatic variation. Runoff from the highly-glacierised Massa basin followed mean summer air temperature rising through the warm 1940s–1950s, declining in the cool 1970s before increasing again in the 1990s–2000s. The temporal pattern of runoff from the near ice-free Grande Eau basin, on the other hand, was broadly the inverse. Influenced by precipitation, runoff increased during the cool wet late 1960s–1970s before declining into the warm dry 1990s–early 2000s, with glacier melt insufficient to offset low precipitation in dry warm years. Precipitation levels, too low to maintain glacier mass against summer energy input, were insufficient in highly-glacierised basins to moderate the quantities of meltwater produced from large glacierised areas by fluctuations in energy availability. Depletion of glacierised area led to runoff in warm years in the 1990s–2000s being marginally reduced by comparison with the first warming period. At middle levels of glacierisation, runoff declined during the later part of the second warm period.

Overall, year-to-year variability of flow was negatively correlated with percentage basin glacierisation despite the upturn in runoff variability at levels of ice-cover greater than ~40%. In warmer drier conditions, runoff variability was increased with enhanced flow in more highly glacierised basins, but reduced with declining flow in less glacierised basins, and *vice versa* during cooler wetter conditions. Variability of flow increased directly with runoff, however, in only the most highly-glacierised basin, decreasing in the other three basins. Should warmer air temperatures and drier conditions be sustained, and glaciers continue to decline, runoff will ultimately be reduced irrespective of basin glacierisation but runoff variability may either increase or decrease depending on basin glacier cover.

Acknowledgements The assistance of Bundesamt für Wasser und Geologie, and MeteoSchweiz, in making available discharge and meteorological records, respectively, and of Nick Scarle, in producing the diagrams, is gratefully acknowledged.

REFERENCES

Beniston, M. & Jungo, P. (2002) Shifts in the distributions of pressure temperature and moisture and changes in the typical weather patterns in the Alpine region in response to the behaviour of the North Atlantic Oscillation. *Theoretical & Appl. Climatol.* **71**, 29–42.

Birsan, M. -V., Molnar, P., Burlando, P. & Pfaundler, M. (2005) Streamflow trends in Switzerland. *J. Hydrol.* **314**, 312–329.

Bundesamt für Wasser und Geologie (2006) *Hydrologisches Jahrbuch der Schweiz 2004.* Bern, Switzerland.

Chen, J. & Ohmura, A. (1990) On the influence of Alpine glaciers on runoff. In: *Hydrology in Mountainous Regions. I–Hydrological Measurements; The Water Cycle* (ed. by H. Lang & A. Musy), 117–125. IAHS Publ. 193. IAHS Press, Wallingford, UK.

Collins, D. N. (1987) Climatic fluctuations and runoff from glacierised Alpine basins. In: *The Influence of Climate Change and Climate Variability on the Hydrologic Regime and water Resources* (ed. by S. I. Solomon, M. Beran & W. Hogg), 77–89. IAHS Publ. 168. IAHS Press, Wallingford, UK.

Collins, D. N. (1988) Influences of climatic fluctuations and changes in glacierised area on runoff from Alpine basins. In: *Proc. Seventh Northern Research Basins Symposium*, 77–86.

Collins, D. N. (1989a) Influence of glacierisation on the response of runoff from Alpine basins to climate variability. Conference on Climate and Water. *Publ. Academy of Finland* 9/89 Vol. 1, 319–328.

Collins, D. N. (1989b) Hydrometeorological conditions, mass balance and runoff from Alpine glaciers. In: *Glacier Fluctuations and Climatic Change* (ed. by J. Oerlemans), 235–260. Kluwer, Dordrecht, The Netherlands.

Collins, D. N. (2005) Climatic variation and runoff in mountain basins with differing proportions of glacier cover. In: *Proc. Fifteenth Northern Research Basins Symposium*, 21–30.

Fleming, S. W. & Clarke, G. K. C. (2005) Attenuation of high-frequency interannual streamflow variability by watershed glacial cover. *J. Hydraul. Engng* **131**, 615–618.

Fountain, A. G. & Tangborn, W. V. (1985) The effects of glaciers on stream flow variations. *Water Resour. Res.* **21**, 579–586.

Hopkinson, C. & Young, G. J. (1998) The effect of glacier wastage on the flow of the Bow River at Banff, Alberta, 1951–1993. *Hydrol. Processes* **12**, 1745–1762.

Kasser, P. (1959) Der Einfluss von Gletscherruckgang und Gletschervorstoss auf den Wasserhaushalt. *Wasser- und Energiewirtschaft* **6**, 155–168.

Kasser, P. (1981) Rezente Gletscherveraenderungen in den Schweizer Alpen. *Jahrbuch der Schweizerischen Naturforschenden Gesellschaft wissenschaftlicher Teil 1978*, 106–138. Birkhauser, Basel, Switzerland.

Krimmel, R. M. & Tangborn, W. V. (1974) South Cascade Glacier: the moderating influence of glaciers on runoff. In: *Proc. Western Snow Conf.* **42**, 9–13.

Maisch, M., Wipf, A., Denneler, B., Battaglia, J. & Benz, C. (1999) Die Gletscher der Schweizer Alpen. Gletscherhochstand 1850. Aktuelle Vergletscherung. Gletscherschwund-Szenarien. *Schlussbericht NFP 31*, Vdf Hochschulverlag ETH Zürich, Switzerland.

Moore, R. D. & Demuth, M. N. (2001) Mass balance and streamflow variability at Place Glacier, Canada, in relation to recent climate fluctuations. *Hydrol. Processes* **15**, 3473–3486.

Röthlisberger, H. & Lang, H. (1987) Glacial hydrology. In: *Glaciofluvial Sediment Transfer* (ed. by A. M. Gurnell & M. J. Clark, 207–284. John Wiley, Chichester, UK

Tvede, A. M. (1982) Influence of glaciers on the variability of long runoff series. In: *Proc. Fourth Northern Research Basins Symp.*, 179–189.

Glacier Mass Balance Changes and Meltwater Discharge (selected papers from sessions at the IAHS Assembly in Foz do Iguaçu, Brazil, 2005). IAHS Publ. 318, 2007.

Analysis on the facts of runoff increase in the Urumqi River basin, China

TIANDING HAN, YONGJIAN DING, CHANGWEI XIE, BAISHENG YE, YONGPING SHEN & KEQIN JIAO

Tianshan Glaciological station/Key Laboratory of Cryosphere and Environment, Cold and Arid Regions Environmental and Engineering Research Institute, CAS, Lanzhou, Gansu 730000, China
tdhan@lzb.ac.cn

Abstract This paper systematically analyses the runoff changes at three stations in the headwater, middle and low basins of the Urumqi River in the Tianshan Mountains of China during 1958–2003. The runoff in the Urumqi River basin has shown a remarkable positive trend during the past several decades, responding to the climatic change in Xinjiang regions, particularly since the mid 1980s. All runoff of three hydrological stations, Glacier No. 1 at the Urumqi River headwater (hereafter Glacier No. 1 hydrological station), the Yuejinqiao in the middle basin (hereafter YJQ) and Yingxiongqiao in the low basin (hereafter YXQ), increase strongly, although the timing of runoff increases were not concurrent among the stations. Furthermore, the records show that an abrupt increase in runoff at the Glacier No. 1 hydrological station occurred in 1997, which was probably caused by both the rapid ablation of glaciers in response to the intense climate warming processes and the precipitation increase in the basin. Results also show that the trends of annual runoff at the YJQ are consistent with that at Glacier No. 1. Preliminary analysis indicates that the runoff increase in the Urumqi River basin mostly resulted from the significant precipitation increase in the high altitude mountain regions.

Key words climatic transition; precipitation; runoff; Tianshan mountains; Urumqi River

INTRODUCTION

A climatic transition from warm-dry to warm-wet had been reported in the Xinjiang regions of China, particularly the western part of the Tianshan Mountains, since 1987 (Shi *et al.*, 2002; Zhang *et al.*, 2003). Both increasing precipitation and glacial ablation rates have occurred under the climatic transitional regime (Shi *et al.*, 2002; Han *et al.*, 2003a; Li *et al.*, 2003). As a result, the high-altitude Asian glaciers have been significantly retreating since the 1990s, in particular those smaller than 2 km^2, which are much more sensitive to climate warming (Meier, 1984; Oerlemans & Fortuin, 1992; Yao *et al.*, 2004). It is estimated that glacier runoff has increased by over 5.5% due to the ablation of glaciers in the western region of China (Shi, 2001). The hydrological and meteorological observations during the past decades indicated that both precipitation and runoff have generally shown a rising trend over the whole Urumqi River basin, particularly in the headwater area, although the differences in changes are very obvious between the upper and lower reach of the river (Han *et al.*, 2003b; Li *et al.*, 2003). The hydrological and climatic variables have obvious regional patterns over the Urumqi River basin.

This research is based on the runoff variations in the Urumqi River basin, Tianshan Mountains, China, to identify the regional differences of the Urumqi River runoff in response to climate change.

SITE DESCRIPTION, DATA AND METHODS

The Urumqi River is one of the main water sources for Urumqi City, capital of Xinjiang, The studied area in this research only refers to the part of the drainage basin above the YXQ hydrological station which generates nearly all water resources of the river (Fig. l). The river originates from the Glacier No. 1 (43.05°N, 86.49°E), which is on the north slope of the Tianger peak in the middle Tianshan Mountains, China (Fig. 1).

Comprehensive observations of the glacier mass balance, alpine snow cover, and permafrost in the river source area have been conducted by the Tianshan Glaciological Station (hereafter TGS), Chinese Academy of Sciences, since 1959.

The discharge data of three hydrological stations in the basin are available (Fig. 1). The Glacier No. 1 hydrological station with 3.34 km^2 drainage area is located in Urumqi River source at the elevation of 3659 m a.s.l, about 300 m downstream from

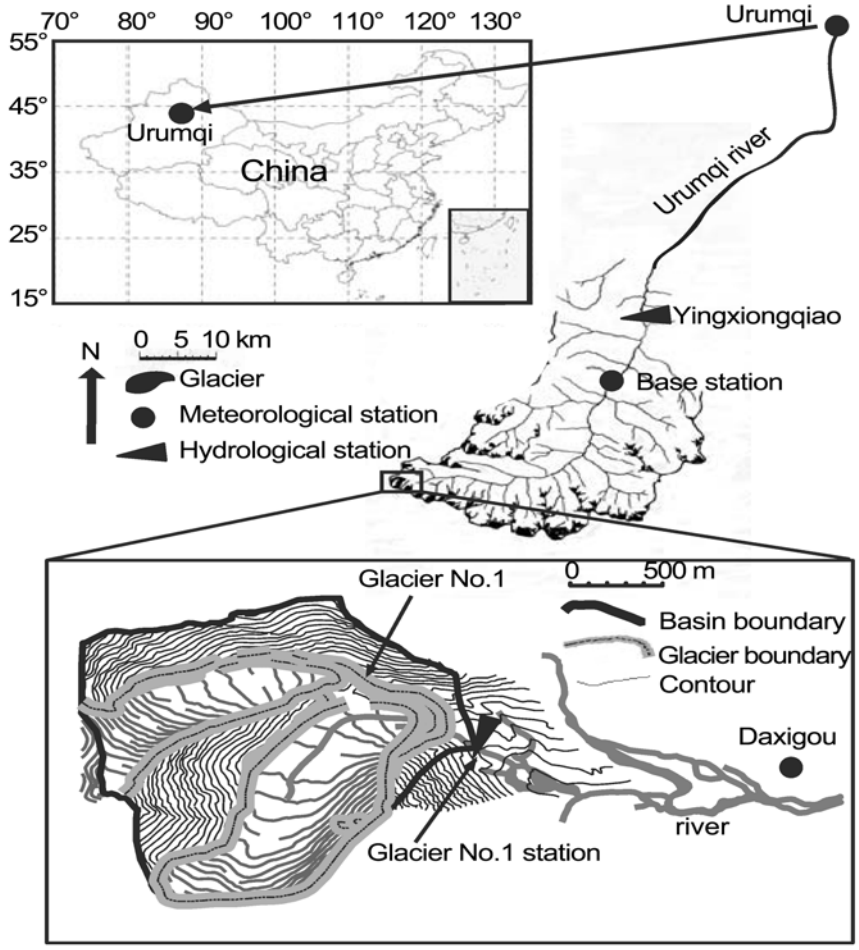

Fig. 1 Sketch map of the Urumqi River basin.

Table 1 List of the hydrological and meteorological stations in the Urumqi River basin.

Station type	Name	Data period	Catchment area (km^2)	Altitude (m)
Hydrological	Glacier No.1	1980–2003	3.34	3659
	YJQ	1983–2003	310	2336
	YXQ	1958–2001	924	1920
Meteorological	DXG	1959–2003		3539
	TGS	1986–2003		2134
	Urumqi	1951–2000		918

the tongue of Glacier No. 1 (Fig. 1). The discharge has been observed during the melting period (May–September) from 1980 to 2003. The YJQ and YXQ hydrological stations are located in the middle and lower reach of the river part in the mountains, respectively. The catchment area is 310 km^2 and 924 km^2, respectively. The glacier area coverage is about 8.9% above the YJQ station and 4.0% above the YXQ station (Glacier Inventory of China, 1986).

The meteorological data at two meteorological stations in the study basin and one meteorological station in the downstream of Urumqi River and the YXQ hydrological station (including meteorological observation) has been employed. Relevant information about the hydrological and meteorological data used in this study, such as the data period, catchment area and altitude, are listed in Table 1. The Daxigou meteorological station at the headwater of Urumqi River (hereafter DXG) was set up in 1958. The TGS meteorological station at Houxia, a small town below the YJQ hydrological station, has observed data from 1982 to 2003; and meteorological data have been collected at the Urumqi meteorological station during 1951–2003, in Urumqi city where the piedmont plain regions are found (Fig. 1).

The trend analyses are carried out by the linear regression for the long-term meteorological, hydrological and glacier data collected at the basin of Urumqi River, and used the Parameter Testing method (signal-to-noise ratio) to examine the characteristics of runoff variation at all three hydrological stations. The relationships among precipitation, glacier mass balance and runoff are also analysed to quantify the impact of climate change on runoff at the outlet of the basin.

RESULTS

Variations of temperature, precipitation in the Urumqi River basin

The observed data show strong temperature increases during 1959–2003, at the Urumqi and DXG meteorological stations in the basin of Urumqi River, particularly since 1997 (Fig. 2). The annual mean temperature has increased by about 0.8°C (95% significance level) in the DXG meteorological station over the last five decades (Ye *et al.*, 2005), and every month there have also been increase trends in temperature, for example, in the summer (June–August) mean temperatures ranged from 3.0 to 4.6°C during 1959–1996, and from 4.4 to 5.8°C, since 1997 (Ye *et al.*, 2005).

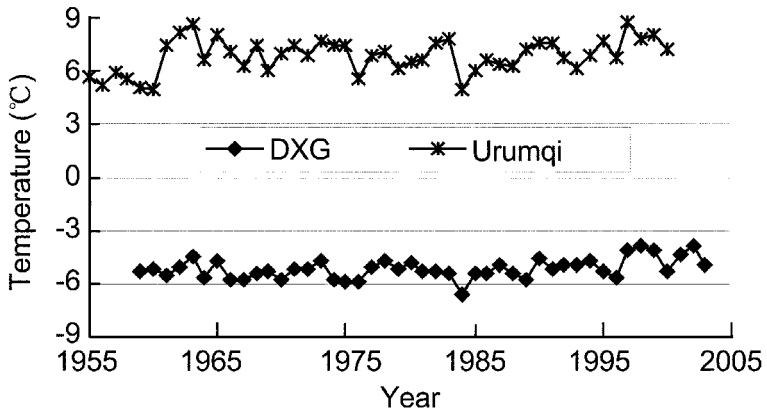

Fig. 2 Variations of temperature in the Urumqi River basin.

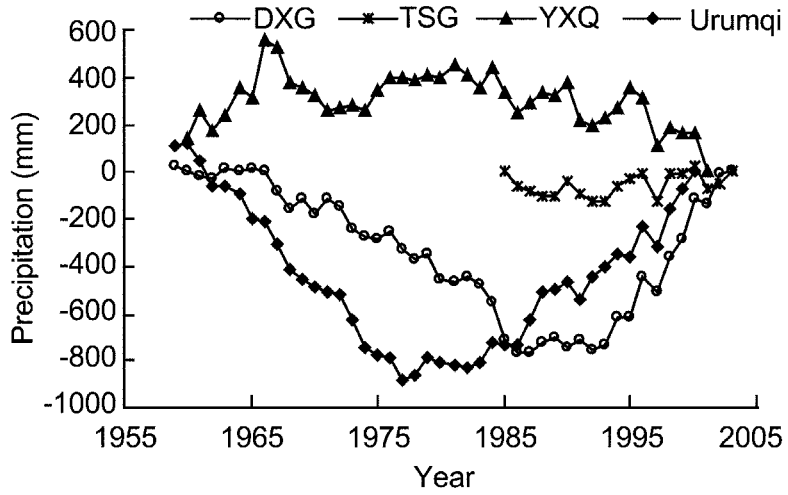

Fig. 3 Accumulated anomaly curve of precipitation in the Urumqi River basin.

The long-term annual precipitation data at the Urumqi and DXG meteorological stations indicate that the annual precipitation at both stations has a negative trend from the mid-1950s to the early 1980s, with an obvious positive trend after the early 1980s. The positive trend of precipitation at the TGS is also obvious in this period. The positive trends in precipitation are statistically significant at the 95% confidence level. The statistics on the accumulated precipitation anomalies indicate that precipitation shifts from negative to positive anomaly in 1978 and 1986 at the Urumqi and DXG stations, respectively. This may imply that precipitation at the piedmont plain (at the Urumqi station) is earlier by 10 years than that at the headwater of the river (at the DXG station) (Fig. 3). The shift time of the precipitation at the headwater of the river from negative to positive anomaly has been reported (Han *et al.*, 2003a). The annual mean precipitation is 294 mm during 1978–2000 and 231 mm during 1951–1977, respectively, at Urumqi station and the difference is 63 mm or 27.3% during the study period. The annual mean precipitation at the DXG station is 492 mm during 1986–2003 and 426 mm during 1958–1985, having increased by 15.5%. However, the trend of precipitation at the YXQ station is even negative from the mid 1980s to 2001, which

is inconsistent with the DXG and TGS and Urumqi stations. This inconsistency in precipitation may be caused by the YXQ station topography, which is in a narrow gorge, so the precipitation data is not used here.

Glacier No. 1 change

The fluctuation of the glacier in response to climate change is one of the important factors responsible for the runoff variation. The mass balance measurement in Glacier No. 1 was conducted from 1959 up to now, but the observation was interrupted during 1967–1979 and the data has been reconstructed (Annual Report of Tianshan Glaciological Station, 2002). Glacier mass balance shows a decrease, almost monotonically, in the last 45 years, especially in the most recent 10 years. The annual mean mass balance amount is –74.5 mm during 1959–1984 and –423 mm during 1985–2003. The glacier was divided into two independent branches in 1993 (Jiao *et al.*, 2000). Analysis shows that cumulative mass balance reached –9982 mm over the study period, equivalent to glacier thinning of about 10 m. The ablation of the glacier became very strong since 1997 (Fig. 4) and the annual mean mass balance amount is –689 mm during 1997–2003. Li *et al.* (2003) reported that the general variation of Glacier No. 1 can be attributed to the ablation in accumulation area since the 1980s, and they also found that the glacier decreased strongly in accumulation area from 1997 to 2002.

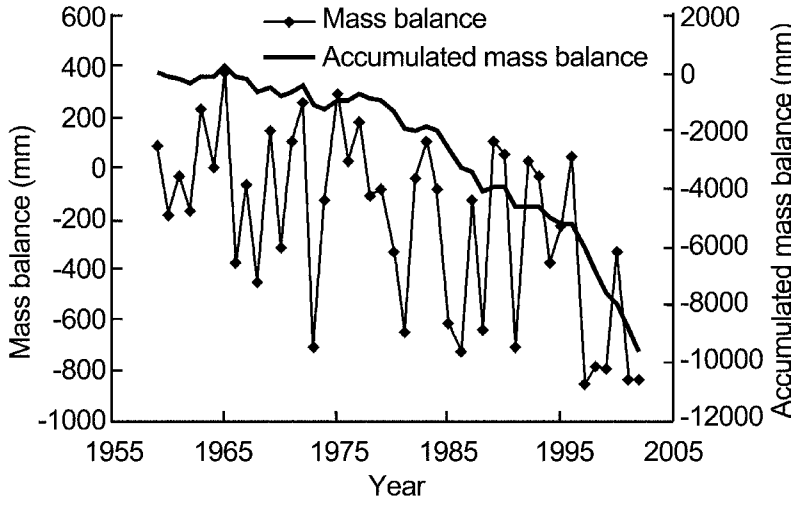

Fig. 4 Mass balance of Glacier No. 1 at the headwater of the Urumqi River.

The changes of precipitation and temperature affect the glacier mass balance differently. Precipitation increases enhance accumulation, and temperature-warming enlarges ablation. The negative mass balance is associated with temperature warming and precipitation increase over the study area. A 1°C increase in summer temperature leads to an increase of 486 mm glacier mass loss (Ye *et al.*, 2005). It is reasonable to conclude that the ablation due to warming has also consumed the contribution of precipitation increase to the glacier.

Runoff variation

In general, the seasonal melting of glacier and seasonal precipitation regulate the river runoff; and climate change impacts the hydrological regime from glacier down to the lower reach. Figure 5(a) shows the accumulated anomaly variations of runoff at the Glacier No. 1 and YXQ hydrological stations. Results demonstrate that the runoff at the Glacier No. 1 hydrological station does not show a significant abrupt increase, although the measured precipitation at the DXG meteorological station indicated an obvious increase since the mid-1980s. This reveals that the precipitation is not the unique factor controlling the glacier runoff, and in fact other factors, such as air temperature, and solar radiation, controlling the melting of the glacier, are also critical to the runoff variation of the headwater. Data show that the runoff of Glacier No. 1 has significantly increased, mainly after the mid-1990s when climate warming was indicated by considerable air temperature increases (Han *et al.*, 2003b; Li *et al.*, 2003). Other relevant studies have been conducted to investigate the influences of the precipitation in the river source area, alpine snow accumulation, and groundwater due to the degradation of permafrost on the runoff in the Experimental Cirque located near the northern part of Glacier No. 1. The results show that the runoff in the Experimental Cirque increased after the mid-1980s (Han *et al.*, 2003b), which was mainly attributed to the precipitation increase since 1985; however, other factors, such as the degradation of permafrost and consequently melted ground ice and increased groundwater activities could also partly contribute to the runoff increase.

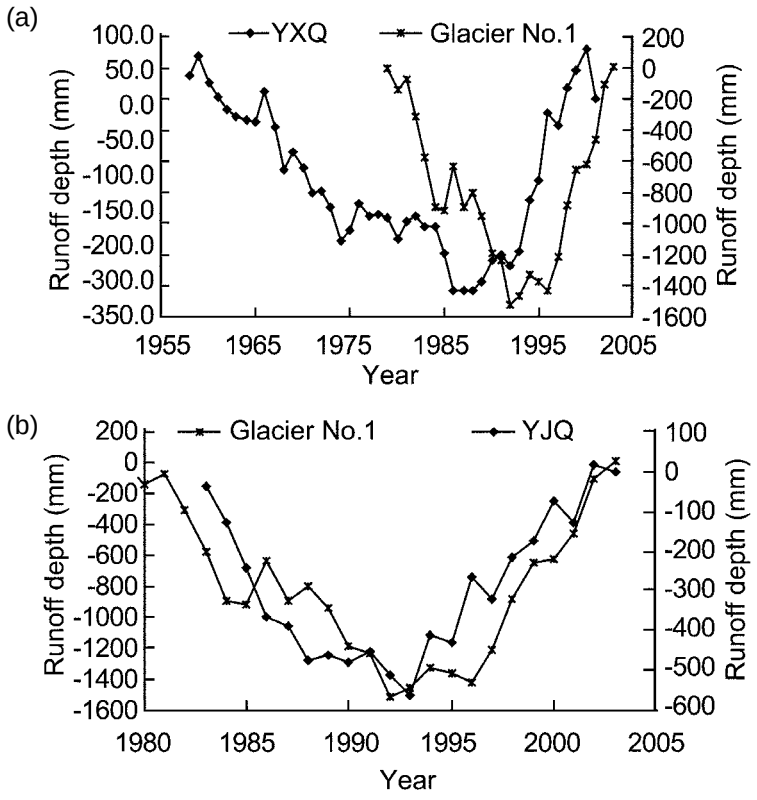

Fig. 5 Accumulated anomaly diagram of runoff in the Urumqi River ((a) Glacier No.1 –YXQ; (b) Glacier No.1 –YJQ).

In this study, the Parameter Testing method (signal-to-noise ratio) (Yamamoto *et al.*, 1985) was used to examine the characteristics of runoff variation at three hydrological stations. Results show that the runoff at the Urumqi River headwater greatly increased after 1997, and the annual mean glacial runoff depth increased from 585 mm during 1980–1996 to 874 mm during 1997–2003, or by about 49.4%.

Although the runoff at the YJQ hydrological station does not show a great increase, the process of interannual variation is much more similar to that at the Glacier No. 1 hydrological station (Fig. 5(b)); furthermore, the positive trend of runoff is remarkable since 1994, and the inter-annual variation amplitude of runoff becomes more obvious, but this is not significantly correlated with the precipitation variation in the area. No abrupt runoff increase occurred at the YXQ hydrological station in 1997, although the runoff kept increasing. The runoff increase started in 1987, with a remarkable trend (Fig. 5(a)), which marked the time of increased precipitation. The annual mean runoff at the YXQ hydrological station increased from $7.37 \times 10^8 m^3$ during 1958–1986 to $8.28 \times 10^8 m^3$ during 1987–2001, or about 12.3%.

DISCUSSION AND CONCLUSION

The air temperature at the DXG meteorological station showed a positive trend since the mid-1980s; in particular, the air temperature during 1997–1999 was unusually warm. The annual mean air temperature was –5.4°C during 1959–1986 and –4.9°C during 1986–2003, respectively, increasing by 0.5°C. The mean mass balance of Glacier No. 1 was –689 mm during 1997–2003; theoretically it consumed all the total yearly supply from precipitation. The unusual warm thermal conditions resulted in the abrupt increase of runoff on Glacier No. 1 since 1997. It is reasonable to conclude that the abrupt runoff increase at Glacier No. 1 hydrological station was caused mainly by the intense ablation of the glacier in response to the unusual warming thermal conditions. However, with a greater increase of the precipitation relative to the long term mean during 1997–1999, the precipitation also made a certain contribution to the increase of the runoff.

The runoff at the YJQ and YXQ hydrological stations did not show an abrupt increase in 1997. The runoff at the YXQ station showed an obvious positive trend since the mid 1980s, earlier than the timing of runoff increase at Glacier No. 1 hydrological station at the headwater of the Urumqi River and the YJQ station. It was found that the characteristics of runoff variation at the YXQ station were roughly synchronous with the precipitation variation at the DXG station in the high mountain area (Fig. 6). As the contribution of glacier melt water to the runoff accounts for only 8.0% of the runoff at the YXQ station (Yang & Han, 1994), the runoff changes in the mountain region mainly depend on the precipitation variation across the entire region. Furthermore, the glacier runoff is mainly dependent on the thermal conditions, for instance, the abrupt glacier runoff increase since 1997. The glacier runoff contributes more to the runoff at the YJQ station than that at the YXQ station. Both the glacier runoff and precipitation in the high altitude mountain regions are responsible for the river runoff variation at the YJQ station. It is worth noting that the time when runoff started to increase was earlier at the YXQ station than that at the YJQ station.

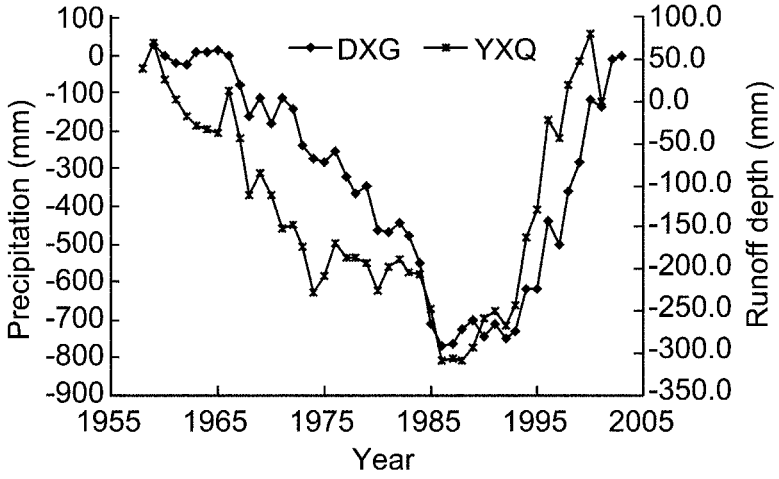

Fig. 6 Anomalies sum curves of precipitation and runoff in the Urumqi River basin.

Generally, the runoff variations in the Urumqi River basin depend mainly on the changes of precipitation in the high mountain regions; the contribution of glacier runoff to the river runoff depends on the ratio of glaciers' coverage to area. As the variation of glacier runoff at Glacier No. 1 hydrological station at the Urumqi headwater is roughly consistent with that at YJQ station, but inconsistent with that at YXQ station, it is reasonable to conclude that the ratio of glaciers coverage and spatial variation of precipitation are two main factors responsible for the different characteristics in runoff variation along the river.

The precipitation also showed a positive trend in the basin, however, at the YXQ station no abrupt increase occurred in the whole period. The precipitation data at the YXQ station even showed a clear negative trend. The inconsistencies of runoff and precipitation variations at different elevations in the mountain region show that there is a clear difference in precipitation variation between the piedmont plain and mid-high mountain region. As the precipitation at the YXQ station exhibits an obvious negative trend, we guess that the runoff increase at the outlet (the YXQ hydrological station) of the mountain valley could be attributed to the variation of the precipitation in the mid-high mountain regions, in addition to glacier runoff variation.

The following conclusions can be drawn from the foregoing discussion. In the process of climatic transition from the warm-dry to warm-wet, the runoff at the YXQ hydrological station exhibited a strong positive trend since 1987, the annual mean runoff increased by about 12.3% from the period 1987–2001 to 1958–1986. The runoff increase is mainly attributed to the precipitation increase in the high mountain regions.

Since 1997 an abrupt increase in the runoff at Glacier No. 1 hydrological station occurred in the headwater area of the Urumqi River; the annual mean glacier runoff depth increased from 585 mm during 1980–1996 to 874 mm during 1997–2003, or by about 50%. Such a strong increase in glacier runoff is mainly due to the intense ablation of glaciers in response to unusual warming and increasing precipitation. The variation of runoff at the YJQ station is consistent with the variation at the headwater of the Urumqi River.

The remarkable increase of precipitation occurred in the high mountain regions and piedmont plain in the Urumqi River basin, but the increase in the high mountain

regions did not result in an abrupt increase of runoff at the mountain outlet (the YXQ hydrological station). The precipitation at the headwater area of Urumqi River has started a strong positive anomaly since 1987, which is about 10 years later than that in the piedmont Urumqi. The annual mean precipitation at the Urumqi meteorological station has increased from 231 mm during 1951–1977 to 294 mm during 1978–2000, or by 27.3%. The annual mean precipitation at the DXG meteorological station has increased from 426 mm during 1958–1985 to 492 mm during 1986–2003, or by 15.5%. No abrupt increase occurred in precipitation in the study periods.

Acknowledgements This work was supported by National Basic Research Program of China (973 Program) no. 2007CB411500, the Knowledge-Innovation Program of Chinese Academy Sciences (KZCX3-SW-345) and the project of Key Open Laboratory of Atmospheric Chemistry of China Meteorological Bureau (CCSF2005-3-DH17).

REFERENCES

Han, P., Xue, Y. & Su, H. (2003a) Precipitation signal of the climatic shift in Xinjiang Region. *J. Glaciol. & Geocryol*. **25**(2), 179–182.

Han, T., Li, Z. & Ye, B. (2003b) Increasing in runoff in the Ice-free Cirque at the headwaters of the Urumqi River. *J. Glaciol & Geocryol*. **25**(4), 389–393.

Jiao, K., Wang, C. & Han, T. (2000) A strong negative mass balance appeared in the Glacier No. 1 at the headwater of the Urumqi River. *J. Glaciol. & Geocryol*. **22**(1), 62–64.

Lanzhou Institute of Glaciology and Geocryology, CAS (1986) *Glacier Inventory of China*. Science Press, Beijing, China.

Li, Z., Han, T., Jin, Z., Yang, H. & Jiao, K. (2003) A summary of 40-year observed variation facts of climate and Glacier No. 1 at Headwater of Urumqi River, Tianshan, China. *J. Glaciol. & Geocryol*. **25**(2), 117–123.

Meier, M. F. (1984) Contribution of small glaciers to global sea level. *Science* **51**, 49–62.

Oerlemans, J. & Fortuin, J. P. F. (1992) Sensitivity of glaciers and small ice caps to greenhouse warming. *Science* **258**, 115–117.

Shi, Y. (2001) Estimation of the resources affected by climatic warming and glacier shrinkage before 2050 in west China. *J. Glaciol. & Geocryol*. **23**(4), 333–341.

Shi, Y., Shen, Y. & Hu, R. (2002) Preliminary study on signal, impact and foreground of climate shift from warm-dry to warm-humid in northwest China. *J. Glaciol. & Geocryol*. **24**(3), 219–226.

TianShan Glaciological Station (2002) Annual Report of Tianshan Glaciological Station, Lanzhou: Lanzhou Institute of Glaciology and Geocryology, CAS, Vol. 1–16.

Yamamoto, R., Iwashima, T. & Sanga, N. K. (1985) Climatic jump, a hypothesis in climate diagnosis. *J. Met. Soc. Japan* **63**, 1157–1160.

Yang, X. & Han, T. (1994) Climate characteristic and glacial runoff in the source of Urumqi River. *J. Glaciol. & Geocryol*. **16**(2), 147–155.

Yao, T., Liu, S., Pu, J., Shen, Y. & Lu, A. (2004) The recent retreat of glacier in High Asia and its effect on water resources in Northwest China. *Sci. China, Ser. D* **34**(6), 535–543.

Ye, B., Yang, D., Jiao, K., Han, T., Jin, Z., Yang, H. & Li, Z. (2005) The Urumqi River source Glacier No. 1, Tianshan, China: Changes over the past 45 years. *Geophys. Res. Lett*. **32**, L21504, doi: 10.1029/2005GL024178.

Zhang, G., Wu, S. & Wang, Z. (2003) The signal of climate shift in Northwest China deduced from river runoff change in Xinjiang region. *J. Glaciol. & Geocryol*. **25**(2), 183–187.

Glacier Mass Balance Changes and Meltwater Discharge (selected papers from sessions at the IAHS Assembly in Foz do Iguaçu, Brazil, 2005). IAHS Publ. 318, 2007.

Extensive hydrological monitoring of a small, highly glacierized watershed in the Hohe Tauern region, Austrian Alps

GERNOT KOBOLTSCHNIG[1], WOLFGANG SCHÖNER[2] & HUBERT HOLZMANN[1]

1 *Department of Water, Atmosphere and Environment, University of Natural Resources and Applied Life Sciences (BOKU), Vienna, Austria*
gernot.koboltschnig@ktn.gv.at

2 *Department of Climatology, Central Institute of Meteorology and Geodynamics (ZAMG), Vienna, Austria*

Abstract This paper gives an overview of the various measurement techniques used for the monitoring of snow- and glacier melt in a small but highly glacierized watershed in the Austrian Alps. An alpine meteorological observatory is located in the catchment area of glacier Goldbergkees, which has recorded climatological data since 1886. The equipment of the observatory and the network of totalizers and snow stakes used for glaciological purposes are described. The existing network has been extended by additional temperature measurements at different elevations and by a rainfall tipping bucket at the catchments outlet. Snow pack investigations (distribution of snow depth and density) have been conducted once a year, and more often during special campaigns. Annual mass balance measurements and runoff observations at the outlet of the watershed make the calculation of the water balance possible.

Key words alpine observatory; glacier melt; ice ablation; runoff gauging

INTRODUCTION

Monitoring meteorological and hydrological parameters, which describe melt processes, has gained more and more interest in recent years. Even the permanent glacier retreat in the Alps since the beginning of the 1980s (Dyurgerov, 2002) makes an efficient monitoring programme for some well observed glacierized watersheds indispensable.

At the observatory at mount Hoher Sonnblick (Austrian Alps) permanent meteorological measurements are conducted. Since 1886 meteorological measurements have included air temperature, precipitation, moisture, snow depth, depth of fresh fallen snow, global radiation, wind speed, wind direction, sunshine duration, and air pressure. The permanent network has been expanded, with additional air temperature measurements at different elevations, temporary energy balance stations and a discharge gauge, which continuously measures runoff during a part of the melt season. The catchment area of glacier Golbergkees is defined as a complex type of basin (definition by Singh & Bengtsson, 2005) as it receives the contribution to streamflow from rainfall, snowmelt, and glacier melt. Hence runoff formation is described by several sub-processes. The results of an extensive glacier monitoring are used for the calibration of water balance models requiring high temporal and spatial resolution.

INVESTIGATION AREA

Mount “Hoher Sonnblick” (47°03′16″N, 12°57′25″E), as one peak of the Hohe Tauern region in the Austrian Alps, is well known for the meteorological observatory on its top at about 3106 m a.m.s.l. The observatory is part of the worldwide GAW (global atmosphere watch) network and offers a broad spectrum of meteorological and climatological measurements. Sonnblick observatory is the highest and oldest permanently staffed observatory in the Alps, existing since 1886. One of the nearby glaciers is Goldbergkees, directly beneath the observatory (see Fig. 1). The watershed is 2.7 km² in area, more than 50% glacierized (about 1.5 km^2, computed for 1998) and elevation ranges between 2350 and 3106 m a.m.s.l. Topographically, the basin consists of three major units.

The upper part comprises south and southeast facing areas with typical slopes of about 24°, ranging from nearly flat to 50°. The middle part faces east and northeast and has quite flat slopes round about 10° including steeper slopes next to the ridges. The

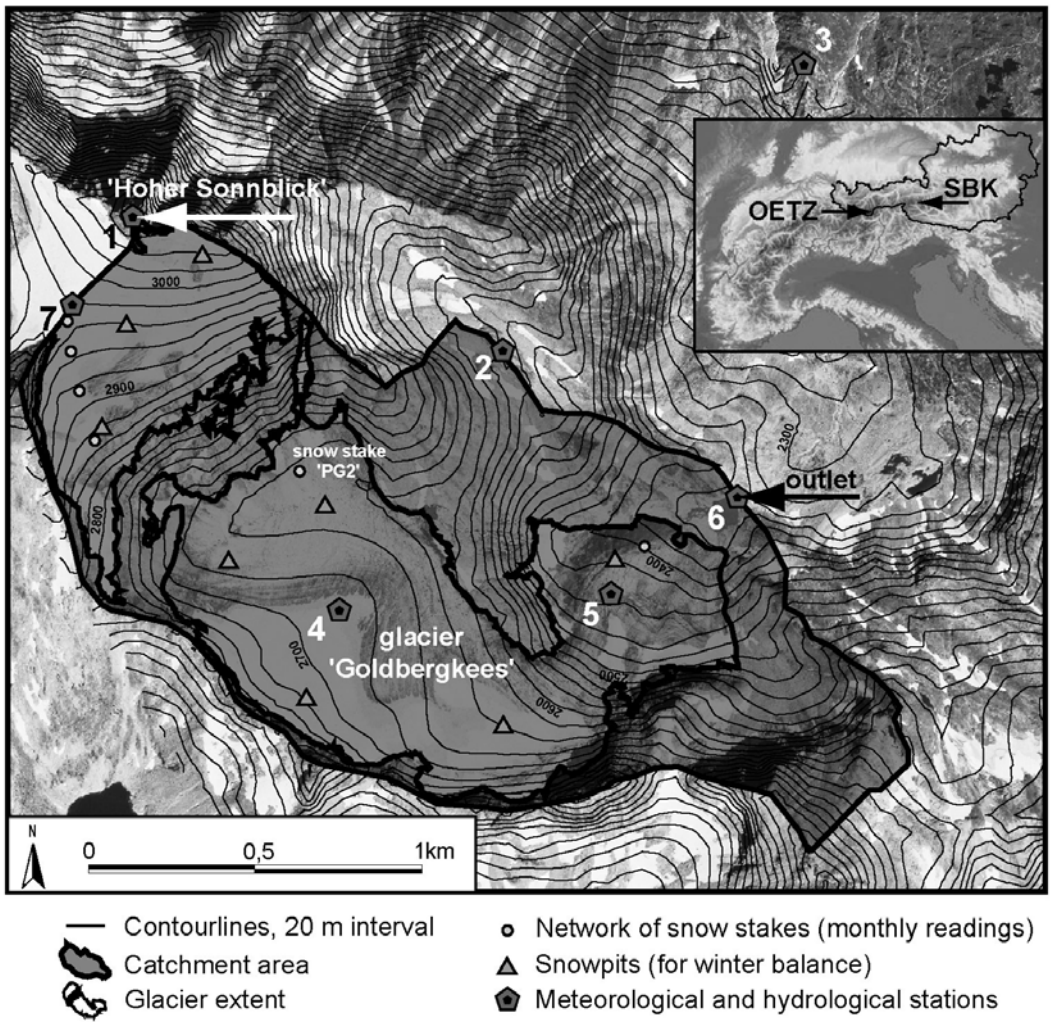

Fig. 1 Aerial photograph of Goldbergkees watershed showing the location of the hydrological and meteorological monitoring network.

lower part comprises the tongue of the glacier which faces north and northeast. No part of the catchment is lower than the timber line. The dominant land cover is rock, gravel and ice, with partial firn cover. The whole area of Goldbergkees watershed is part of the "National Park Hohe Tauern". Field works have to be planned carefully because of the sensitive high alpine ecosystem. Equipment has to be transported by foot or otherwise by cable car, which connects Sonnblick observatory at 3106 m a.m.s.l. with the station in the valley at 1620 m a.m.s.l.

The mean air temperature at Sonnblick observatory is about –5.7°C. The annual precipitation at Sonnblick observatory averages about 2680 mm, with 89% as snow (climate normals 1961–1990, see Fig. 2). Lowest monthly sums of precipitation are in October, the highest are during the winter period. The annual precipitation of the middle part of the Goldbergkees watershed can be estimated using the totalizer at about 2580 m a.m.s.l. (see Fig. 1, no. 2), which shows 2530 mm on annual average (Auer *et al.*, 2002).

MONITORING NETWORK

The major part of the meteorological and glaciological monitoring network is traditionally driven by the staff of Sonnblick observatory. The network of the totalizers next to the Goldbergkees watershed (see Fig. 1, no. 1, 2 and 3) has existed since the early 1930s. Four stakes of the network of monthly read snow stakes were installed in 1928, two further stakes in 1971 (see Fig. 1). Since 1987 the mass balance of glacier Goldbergkees is measured using the glaciological method (Hoinkes, 1970; Østrem & Brugman, 1991), both for winter and annual net balance (Auer *et al.*, 2002).

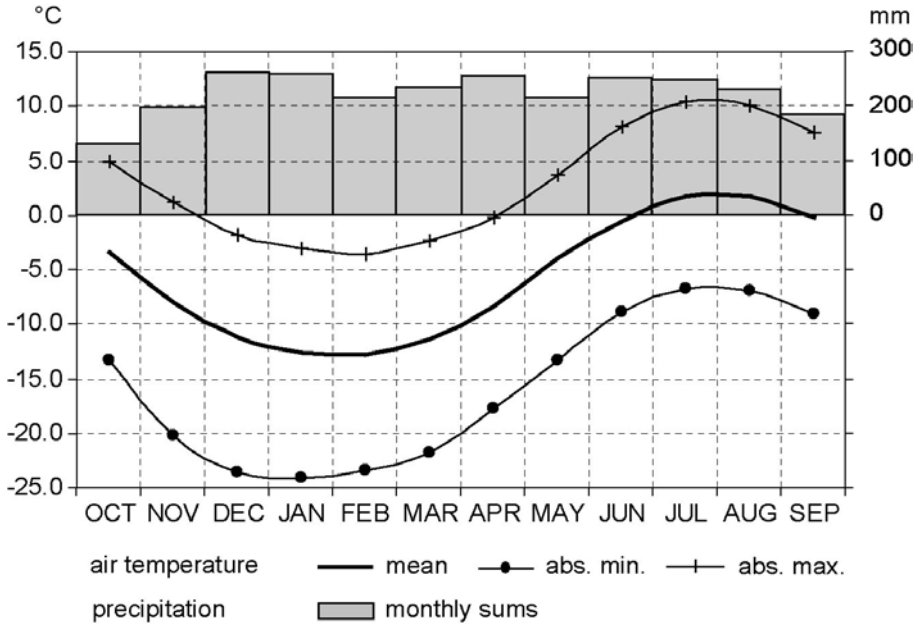

Fig. 2 Comparison of monthly mean, absolute maximum and minimum air temperature and monthly precipitation (averaged for the period 1961–1990) at Sonnblick observatory 3106 m a.m.s.l.

Air temperature

Air temperature is the main parameter for temperature index based ice- and snowmelt simulations (Anderson, 1973; Hock, 1999). At Sonnblick observatory (see Fig. 1, no. 1) the ventilated air temperature is measured for records of one hour resolution. Maximum and minimum thermometers are used for the estimation of extreme temperatures. Additional measurements have been established at the locations of the totalizers (see Fig. 1, no. 2 and 3) and at the discharge gauge (see Fig. 1, no. 6). The temperature sensors are protected using radiation shields mounted at the tripod of the totalizers at the standpipe of the discharge gauge, respectively. Data is recorded at one hour intervals.

Precipitation

At Sonnblick observatory (see Fig. 1, no. 1) rainfall gauges with different temporal resolutions are available. Totalizers collect precipitation (liquid and solid) on a monthly time scale. For the daily precipitation rainfall buckets are used. The main disadvantage of this instrument is that it is not provided with a windshield. This can result in large measurement errors. Hourly precipitation is measured using a weighing system, for both liquid and solid precipitation (available since 1991). An additional tipping bucket was temporarily installed next to the discharge gauge during the 2005 melt season (see Fig. 1, no. 6). This type of instrument is only able to record rainfall events (liquid). It is used to get a better insight of the regional variability of precipitation during the summer season. Totalizers give the best information about the total amount of precipitation, but do not allow temporal resolutions of less than one month (Auer *et al.*, 2002).

Snow

Estimations for snow accumulation are the most complicated tasks for hydrological balancing in mountainous areas. Snow drift by wind as well as vertical displacement by avalanches enhance the spatial variability of the snow pack. Whereas variability of the snow depth is high, the distribution of the snow density is rather uniform over different elevations (Auer *et al.*, 2002). Since the beginning of mass balance measurements at glacier Goldbergkees in 1987, extensive snow courses were enforced every year around 1 May to obtain field data for the winter balance. During a special field campaign in early summer of 2005, additional snow depth measurements combined with snow density measurements at selected snow pits were taken at the beginning of June and the beginning and end of July. These time series of measurements should give a better database for the spatial calibration of snow accumulation and snowmelt models.

Snow depth

Snow depth is measured at about 100 points covering the entire glacier. These data are needed to spatially extend the comprehensive measurements at the snow pits. For

further use the SWE (snow water equivalent) is calculated. Snow depth is measured along contour lines, at approximately every 100 m, using an aluminium probe of up to 7 m in length. Depth transects are located using portable GPS. During the special field campaigns the number of depth measurements was increased to 170 points all over the Goldbergkees watershed. The total coverage of the watershed was limited because of the danger of avalanches in some areas.

Furthermore, the data of the network of monthly-read snow stakes at glacier Goldbergkees are available (see Fig. 1). For SWE (snow water equivalent) calculations the mean snow density for a given particular time has to be estimated.

An automated ultrasonic system, which measures the change of snow depth is installed at about 100 m of elevation below Sonnblick observatory (see Fig. 1, no. 7). This snow depth gauge is driven by the regional Avalanche Warning Service. Snow depth for this location is available with hourly resolution.

Snow density

About seven snow pits are dug into the snow pack for snow density measurements (see Fig. 1). Depending on the location (avalanches, accumulated wind drifted snow) the snow pits can be up to 7 m of depth. Every 20 cm a sample is taken vertically and weighed using an aluminium cylinder. Samples are taken until the firn horizon or glacier ice is reached. Additionally, the stratigraphy and snow temperature is taken (see Kaser *et al.*, 2003).

Snow cover patterns

Snow cover patterns are mapped in the field using a DGPS system walking along the snowline. There is an analogy of snow cover patterns from year to year. The shapes depend on topographical properties (elevation, exposition and shading).

Ice melt

The monitoring of ice melt is part of the mass balance studies. For this purpose, a network of 25 ice ablation stakes in total is driven at glacier Goldbergkees. Ablation stakes are drilled into the ice using the “Heucke Ice Drill” (Heucke, 1999). The depths of ablation stakes in snow free areas is measured for discrete time steps, hence the ice melt for this given period can be calculated using the estimated area of bare ice.

Runoff

Discharge is the most typical parameter to be observed for hydrological studies. Runoff time series of glacierized catchments with a high temporal resolution make studies on diurnal and seasonal variability possible (Hannah *et al.*, 1999, 2000; Swift *et al.*, 2005).

Figure 3 shows the relation between precipitation, snow depth, depth of fresh fallen snow, air temperature, and discharge. Precipitation and air temperature were measured at Sonnblick observatory at 3106 m a.m.s.l., snow depth at the ultrasonic gauge at 2975 m a.m.s.l. and runoff at the catchment outlet at 2350 m a.m.s.l. The hydrograph shows typical signals depending on the actual processes contributing to discharge.

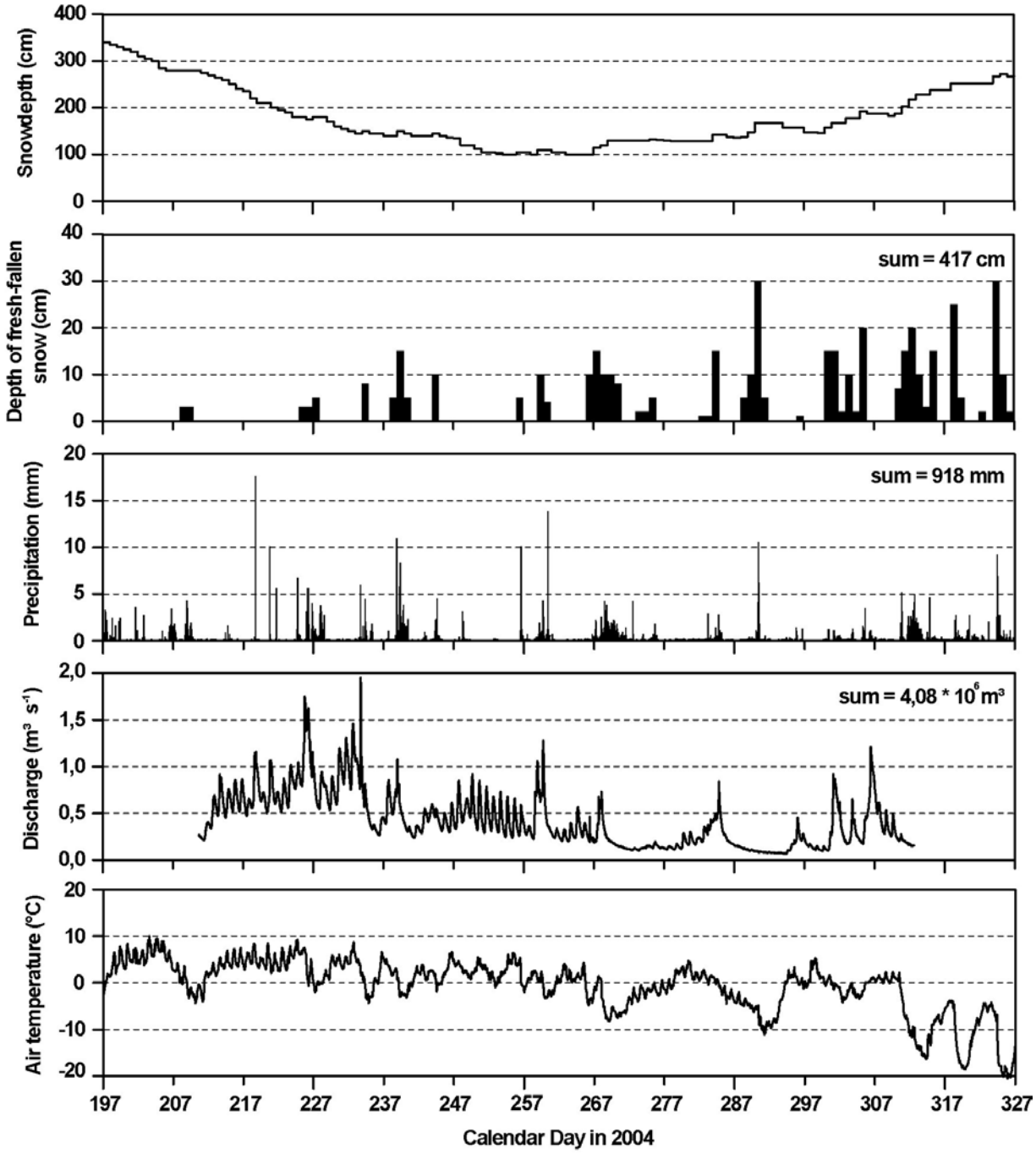

Fig. 3 Hourly time series of discharge at catchment outlet, air temperature and precipitation at Sonnblick observatory and daily time series of snow depth and depth of fresh fallen snow at ultrasonic snow depth gauge for the 2004 melt season.

Gauging station

At Goldbergkees watershed an automatic discharge gauging station (OTT Nimbus), with internal GSM-modem for remote data enquiry, was installed about 250 m downstream of the glacier tongue (see Fig. 1, no. 6). The station uses a bubble sensor. Thus the logger is galvanically isolated from the water. Water stages are registered in 5-min intervals, and the 15-min average is recorded to the data logger. The gauging station was installed for the first time in autumn 2002 and afterwards in 2003, 2004, and 2005. During the winter period the gauging station has to be removed because of high snow pressure, which might possibly damage the equipment. The beginning of discharge records in the summer period strongly depends on climatic conditions. The date of installation of the instrumentation is due to the actual snow cover situation. Hence, the entire melt seasons were not observed. Jansson *et al.* (2003) reported: "A problem with all field studies is that they do not cover the entire hydrological year and in some cases cover only a part of the melt season".

Discharge measurements

Measurements at different water stages are needed to derive discharges from recorded water levels. For discharges of more than 500 L s^{-1} the hydrometric propeller is used to measure flow velocities in a natural cross section at the outlet of the glacier lake. Discharges are calculated by applying the velocity-area method (Herschy, 1985). Lower discharges were measured using the salt dilution gauging method. Five to eight discharge measurements are needed every year to obtain the rating curve.

Special and additional monitoring

During the ablation period in the summer of 2003, two temporary meteorological stations were installed in the watershed. One was at the middle part (see Fig. 1, no. 4) and the other at the tongue of glacier Goldbergkees (see Fig. 1, no. 5), both fixed directly on bare ice. One station (no. 5) recorded radiation (long and short wave), wind speed and direction, air temperature, vapour pressure and air turbidity; the other station (no. 4) recorded only radiation. Air temperature was measured in a vertical profile and the effect of the glacier wind was investigated (Hynek, 2007).

RESULTS AND DISCUSSIONS

Glacier Goldbergkees is part of the north facing region of the Alpine main ridge, which means that this glacier earns more precipitation compared to glaciers south of the Alpine main ridge or glaciers in drier regions in the western part of Austria at Oetztal. Three well known glaciers, Hintereisferner, Kesselwandferner and Vernagtferner, with long time series of mass balance and hydro-meteorological investigations (Span *et al.* 1997; Braun *et al.*, 2004) are related to Oetztal. The main differences between the

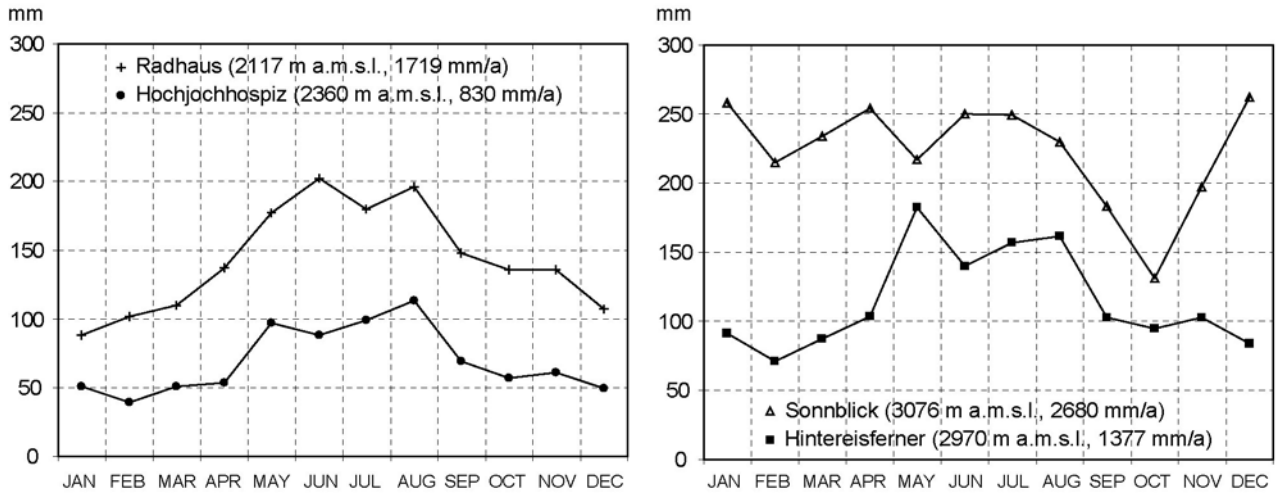

Fig. 4 Comparison of the monthly precipitation (averaged for the period 1961–1990) of two stations at Oetztal (near Hintereisferner) and two stations at Sonnblick area.

Oetztal and the Sonnblick area can be found by comparing precipitation depths. Figure 4 shows the comparison of the monthly precipitation of two stations at lower altitude on the left, and two stations at higher altitude on the right. Station “Radhaus” can be found in Fig. 1 named no. 3 and the station “Sonnblick” can be found in Fig. 1 named no. 1. Both stations in the Sonnblick area show more than two times more precipitation than the stations at Hintereisferner. Station Sonnblick shows quite balanced precipitation quantities over the year, despite autumn, with the lowest rates of about 130 mm in October.

For the period 1891–2003 a decreasing trend for the solid precipitation share during the summer season can be seen in Fig. 5 (Auer *et al*., 2002). Minimum values of about 60% were observed in 1982 and maximum values of about 97% were observed in 1913, 1914 and 1919. Decreasing solid precipitation during the summer season has a direct influence on glaciers and permafrost areas: the albedo is lowered, the fewer glaciers get covered by fresh fallen snow, and more bare ice is exposed to radiation.

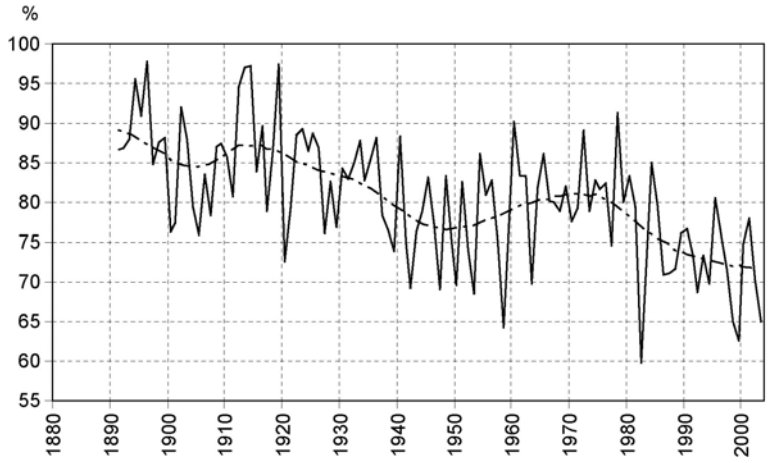

Fig. 5 Solid precipitation as a portion of the total precipitation at Sonnblick observatory, summer season 1891 to 2003.

Decreasing solid precipitation share and increasing melt rates during the summer period result in a temporal shift of the maximum ablation. Figure 6 shows snow stake readings at every 1 August for the period 1928–2003.

Another long-term time series is the mean monthly sum of positive temperatures for the ablation periods starting in 1886 (see Fig. 7). This time series shows a slight trend whereas the positive temperature sums increase.

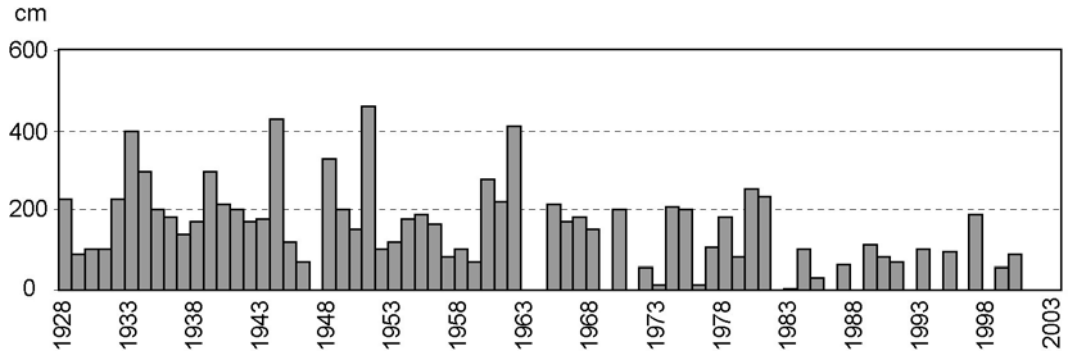

Fig. 6 Snow depths on 1 August at snow stake "PG2" in 2670 m a.m.s.l.

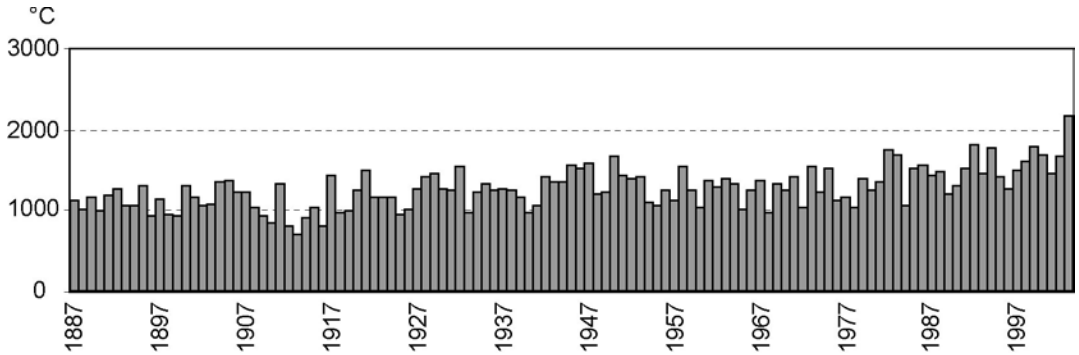

Fig. 7 Monthly sum of positive air temperatures, averaged for the ablation period (May–September), 1887–2003.

Focusing on the results of the observations for the ablation period of 2004 (see Fig. 3) the longest constant melt period started at the beginning and terminated at the end of August (day 210–225). The strongest discharge peaks were superposed by rainfall events. Typical diurnal variations of the discharge were observed at the beginning of September (day 245–256), whereas dry weather conditions dominated. At day 266 10 cm of fresh-fallen snow were measured, and on the days after more snow falls occurred. Because of a short temperature rise, the discharge at the catchment outlet increased. After that time, runoff peaks were only occasionally developed.

SUMMARY AND CONCLUSIONS

The longest time series of meteorological data at Hoher Sonnblick observatory are of about 120 years. Snow depth observations in the mountainous surroundings have existed for more than 80 years. These long-term data sets were expanded by

continuous mass balance investigations starting in the mid-1980s. Finally, melt runoff observations have been forced for the last 4 years. These excellent data sets are used for detailed analyses and modelling (snow pack models, distributed hydrological models, and for the estimation of index based models). Even the hydrological research on ungauged basins needs well observed reference watersheds to test and adopt melt and water balance models. The results of the annual winter balance measurements represent a solid possibility to validate distributed snow accumulation and snow melt models. Using long-term meteorological observations the reaction of glaciers to past climatological events can be simulated.

Acknowledgements This ongoing research was supported by a grant from the Austrian Academy of Sciences under the project SNOWTRANS HOE29, part of the IHP PUB (International Hydrological Program, Prediction in Ungauged Basins).

REFERENCES

Anderson, E. A. (1973) National weather service River Forecast System – snow accumulation and ablation model. Silver Spring, Maryland, US Department of Commerce. (NOAA Technical Memorandum NWS Hydro-17).

Auer, I. & Böhm, R. (1998) Schneepegel und Totalisatoren im Sonnblickgebiet. 94. und 95. Jahresbericht des Sonnblickvereines für die Jahre 1996 und 1997, S 42–87, Eigenverlag des Sonnblickvereines, Wien, Austria.

Auer, I., Potzmann, R. & Schöner, W. (2000) Welchen Beitrag leisten Totalisatoren für die Klimaforschung im Hochgebirge? – gezeigt mit Hilfe des Totalisatorenmessnetzes im Sonnblickgebiet. 96. und 97. Jahresbericht des Sonnblickvereines für die Jahre 1998 und 1999, S 22–30, Eigenverlag des Sonnblickvereines, Wien, Austria.

Auer, I., Böhm, R., Leymüller, M., Schöner, W., Kaiser, A., Scheifinger, H., Langer, M., Scheider, St. & Häberli, Ch. (2002) Das Klima des Sonnblicks. Klimaatlas und Klimatographie der GAW Station Sonnblick einschließlich der umgebenden Gebirgsregion. Österreichische Beiträge zu Meteorologie und Geophysik. Heft 28, Zentralanstalt für Meteorologie und Geodynamik, Wien, Austria. ISSN 1016-6254.

Braun, L. N., Escher-Vetter, H., Heucke, E., Siebers, M. & Weber, M. (2004) Experiences with the new "Vernagtbach" hydro-meteorological station. In: *Automatic Weather Stations on Glaciers* (ed. by J. Oerlemans & C. H. Tijm-Reijmer**)**, 38–44 (Pontresina, 28–31 March 2004, IMAU).

Dyurgerov, M. (2002) Glacier mass balance and regime: data of measurements and analysis. Occasional Papers no. 55, Inst. of Arctic and Alpine Research, University of Colorado, USA.

Hannah, D. M., Gurnell, A. M. & McGregor, G. R. (1999) A methodology for investigation of the seasonal evolution in proglacial hydrograph form. *Hydrol. Processes* **13**, 2603–2621.

Hannah, D. M., Smith, B. P. G., Gurnell, A. M. & McGregor, G. R. (2000) An approach to hydrograph classification. *Hydrol. Processes* **14**, 317–338.

Herschy, R. W. (1985) *Stream Flow Measurement*. Elsevier Applied Science Publishers, UK.

Heucke, E. (1999) A light portable steam-driven ice drill suitable for drilling holes in ice and firn. *Geografiska Annaler: Series A, Physical Geography* **81**(4), 603.

Hock, R. (1999) A distributed temperature-index ice- and snowmelt model including potential direct solar radiation. *J. Glacol.* **45**(149), 101–111.

Hoinkes, H. (1970) Methoden und Möglichkeiten von Massenhaushaltsstudien auf Gletschern. Ergebnisse der Meßreihe Hintereisferner (Ötztaler Alpen) 1953–1968. *Zeitschrift für Gletscherkunde und Glazialgeologie* **6**, 37–90.

Hynek, B. (2007) Energiebilanz des Goldbergkees während des Sommers 2003. Diplomarbeit am Institut für Meteorologie der Universität Wien, Austria.

Jansson, P., Hock, R. & Schneider, Th. (2003) The concept of glacier storage: a review. *J. Hydrol.* **282**, 116–129.

Kaser, G., Fountain, A. & Jansson, P. (2003) A manual for monitoring the mass balance of mountain glaciers. IHP-VI. Technical Documents in Hydrology, no. 59, UNESCO, Paris, France.

Østrem, G. & Brugman, M. (1991) Glacier mass-balance measurements – a manual for field and office work: Environment Canada, National Hydrology Research Institute Science Report no. 4, and Norwegian Water Resources and Energy Administration.

Singh, P. & Bengtsson, L. (2005) Impact of warmer climate on melt and evaporation for the rainfed, snowfed and glacierfed basins in the Himalayan region. *J. Hydrol.* **300**, 140–154.

Span, N., Kuhn M. & Schneider H. (1997) 100 years of ice dynamcs of Hintereisferner, Central Alps. *Annals Glaciol.* **24**, 297–302.

Swift, D. A., Nienow, P. W., Hoey, T. B. & Mair, D. W. F. (2005) Seasonal evolution of runoff from Haut Glacier d'Arolla, Switzerland and implications for glacial geomorphic processes. *J. Hydrol.* **309**, 133–148.

2 Mass Balance

Glacier Mass Balance Changes and Meltwater Discharge (selected papers from sessions at the IAHS Assembly in Foz do Iguaçu, Brazil, 2005). IAHS Publ. 318, 2007.

Mass balance of the Amitsulôq ice cap, West Greenland

ANDREAS P. AHLSTRØM[1], CARL EGEDE BØGGILD[2], OLE B. OLESEN[2], DORTHE PETERSEN[3] & JOHAN J. MOHR[1]

1 *Ørsted-DTU, Technical University of Denmark, Ørsteds Plads, Building 348, DK-2800 Kgs. Lyngby, Denmark*
now at: *Geological Survey of Denmark and Greenland, Øster Voldgade 10, DK-1350 Copenhagen K, Denmark*
apa@geus.dk

2 *Geological Survey of Denmark and Greenland, Øster Voldgade 10, DK-1350 Copenhagen K, Denmark*
now at: *Dept. of Geophysics, The University Centre in Svalbard, PB 156, N-9171 Longyearbyen, Norway*

3 *ASIAQ Greenland Survey, Qatserisut 8, Postbox 1003, DK-3900 Nuuk, Greenland*

Abstract We present detailed mass balance measurements from the Amitsulôq ice cap in West Greenland spanning from 1982 to 1990. The data includes summer and winter balances from 26 stake locations distributed over five transects covering the whole ice cap. The mass balance measurements are combined with a recent satellite-derived digital elevation model to calculate the specific balance, which is in turn compared to discharge data from the adjacent Tasersiaq basin. The correlation between specific summer balance and discharge is $R^2 = 0.93$ indicating that the basin discharge is dominated by glacial meltwater, linking the hydropower potential of the basin closely to the fate of the adjoining Greenland ice-sheet margin.

Key words glaciated; Greenland; hydropower; local ice cap; mass balance; Tasersiaq basin

INTRODUCTION

Apart from the Greenland ice sheet, approx. 20 000 local glaciers and ice caps are found in Greenland. Of these, roughly 5000 are located in West Greenland (Weidick *et al.*, 1992). These local ice masses are of interest in connection with hydropower feasibility studies, as well as for their possible contribution to global sea level change. Moreover, glaciers are widely recognized as excellent indicators of climate change (Church *et al.*, 2001). However, local ice masses in Greenland are often considered part of the Greenland ice sheet when assessing global changes in the cryosphere (Zuo & Oerlemans, 1997; de Woul & Hock, 2005) even though there are fundamental differences in their climatology, and they might be more comparable to, for example, the Alaskan glaciers, which have retreated dramatically (Arendt *et al.*, 2002). Therefore, it is important to make the sparse data collected from local glaciers and ice caps in Greenland available. The Geological Survey of Denmark and Greenland has carried out a number of mass balance programmes in Greenland to assess the hydropower feasibility of individual basins since the mid-1970s. In this study, we present mass balance measurements from such a programme covering from 1981 to 1990 on the Amitsulôq ice cap, a local ice cap situated at 66°08′N, 50°20′W between an ice sheet outlier to the south, the Sukkertoppen ice cap to the west and the

Greenland ice sheet proper to the east (see Fig. 1). The Amitsulôq programme was initiated to evaluate the glacial meltwater contribution to the adjacent Tasersiaq basin and simultaneous gauging of the basin discharge was carried out by the Greenland Technical Organization (now ASIAQ Greenland Survey). These data, along with a more recent digital elevation model derived from repeat-track interferometric synthetic aperture radar analysis of ERS-1 and -2 data from 1995/1996 (Ahlstrøm *et al.*, 2002) will be used to calculate the specific mass balance of the Amitsulôq ice cap from 1982 to 1990 and compare them to concurrent discharge data from the Tasersiaq basin.

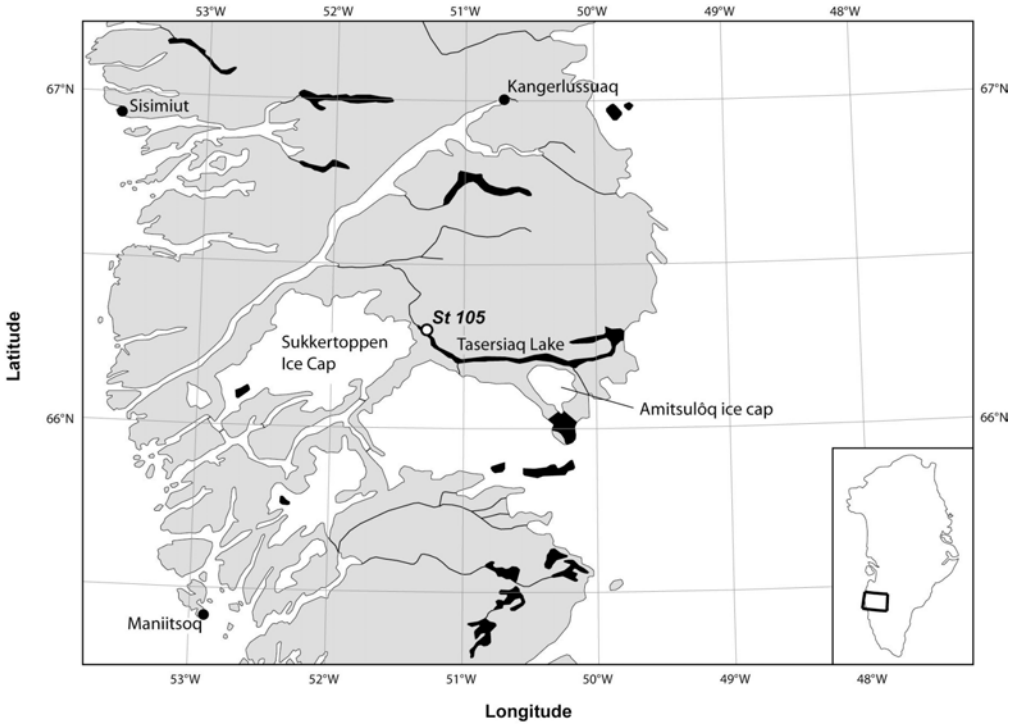

Fig. 1 The regional setting of the Amitsulôq ice cap in West Greenland. The outlet of the Tasersiaq basin considered for hydropower exploitation is by the automatic climate and discharge station labelled "St 105".

MEASUREMENTS

The summer balance measurements were made on single stakes, using a 1-m crossbar to avoid the ablation hollow around the stake tube, i.e. the straight-edge method. The stakes were visited several times during the summer, making it possible to keep track of superimposed ice formation. At the last visit of the summer period, a thin layer of red tennis court dust was sprinkled over a specific area at some distance from the stake, to make it easier to locate the summer surface on the first visit next year. The summer surface was then located stratigraphically from a snow pit at the first measurement next year to account for any additional ablation since the last visit, meaning that the mass-balance measurements were collected according to the stratigraphic method (the reader is referred to Østrem & Brugman (1991) for mass-balance measurement terms). The summer balance measurements are listed in Table 1.

Table 1 Water equivalent specific summer balance in centimetres observed at Amitsulôq ice cap from 1982 to 1990. SD is standard deviation and Alt. is altitude in metres a.s.l.

Stake*	1982	1983	1984	1985	1986	1987	1988	1989	1990	Mean	SD	Alt.
900	–	41.6	87.4	325.6	168.3	217.0	220.7	–	354.5	202.2	106.3	895
950	168.5	25.0	77.9	–	–	–	–	–	–	90.5	59.3	950
951	–	–	–	247.1	148.0	218.1	135.2	–	–	187.1	46.9	955
1050	65.3	25.4	40.0	94.7	80.2	87.6	100.7	104.6	–	74.8	27.1	1040
1100	51.5	10.7	36.4	99.7	50.9	87.7	57.4	78.3	99.2	63.5	28.4	1085
1150	38.4	32.1	47.6	66.6	43.9	78.3	51.8	55.2	–	51.7	14.1	1145
1250	21.3	–	28.7	–	27.4	59.5	29.8	33.5	72.4	38.9	17.7	1250
1350	12.5	10.8	23.3	37.9	18.6	42.9	–	34.4	64.8	30.7	17.0	1350
1400	2.9	8.5	17.3	23.9	15.4	34.3	18.2	23.8	48.0	21.4	12.7	1415
1	122.3	35.5	63.3	305.5	171.3	172.6	153.1	–	288.6	164.0	89.6	900
2	140.5	18.6	56.6	148.4	144.7	128.7	146.1	159.5	208.0	127.9	53.4	1060
3	43.3	13.0	45.8	60.3	45.7	74.0	52.5	51.3	85.1	52.3	19.2	1130
4	42.0	4.6	42.3	75.9	46.5	82.3	55.3	48.7	73.1	52.3	22.2	1145
5	44.5	14.9	–	63.4	39.2	71.6	53.6	49.5	81.5	52.3	19.3	1190
6	25.9	7.1	32.4	38.3	31.2	49.7	33.0	39.3	71.2	36.5	16.4	1310
7	17.8	1.5	–	31.0	20.4	54.8	32.7	34.5	–	27.5	15.4	1310
8	29.1	–	–	–	–	–	–	–	–	29.1	0.0	1185
8.1	–	–	–	–	49.0	61.0	–	49.9	82.5	60.6	13.5	1205
9	119.5	19.3	58.5	187.8	90.2	128.2	110.3	137.6	–	106.4	48.0	1065
10	118.3	35.2	64.8	231.6	118.4	–	124.9	169.0	219.4	135.2	64.4	1000
11	28.8	9.8	33.8	50.1	16.8	58.1	34.0	35.6	72.6	37.7	18.6	1295
12	43.9	15.8	23.4	–	–	–	51.3	47.2	76.3	43.0	19.7	1190
13	57.3	–	41.0	75.7	–	–	67.4	92.0	–	66.7	17.1	1110
14	83.9	26.1	64.4	111.8	99.4	156.2	105.2	129.2	170.9	105.2	42.1	1000
15	121.8	58.9	105.1	166.3	116.2	–	132.1	186.0	220.5	138.4	47.5	885
16	34.8	–3.6	21.1	52.2	38.7	75.7	31.7	54.4	69.6	41.6	23.2	1300
17	49.5	20.2	43.0	79.0	61.7	100.1	53.5	51.0	89.2	60.8	23.4	1195
18	81.7	35.7	71.6	119.8	134.1	–	93.0	129.2	170.6	104.5	39.6	1090

* Individual stake numbers relate to the transects of each ice-cap segment of Fig. 2 as follows, starting from the margin of the ice cap: NW-transect: 18, 17, 16, 1400; N-transect: 15, 14, 13, 12, 11, 1400; NE-transect: 10, 9, 8/8.1, 7; E-transect: 900, 950/951, 1050, 1100, 1150, 6; S-transect: 1, 2, 3, 4, 5, 1250, 1350, 1400.

To get a measure of the uncertainty of the summer balance measurement as derived from a single stake, a stake farm of five stakes, positioned within a few metres of each other, were maintained for a number of years at the site of Stake 950/951 near the base camp. An analysis of the data from 10 June to 31 August 1985, shows a mean value of 2.434 m ice equivalent with a standard deviation of 0.139 m ice equivalent, or less than 6%. The absolute difference in the ablation measurements varies from –5.7% to +10.5%. This corresponds well with the more thorough investigation by Braithwaite *et al.* (1998) of errors in ablation measurements in northeast Greenland which yielded a ±10% difference in mean ablation between nine stakes in 1993 and eight stakes in 1994 at two different sites.

The winter balance measurements were taken as a mean of 11 probings: one at the stake, two on each side of the stake and eight probings at a uniform distance of 10 m from the stake in a complete circumference. The density profile was derived from snow pit sampling. Last year's summer surface was located by digging the pit in the

Table 2 Water equivalent specific winter balance in centimetres observed at Amitsulôq ice cap from 1982 to 1990. 'SD' is standard deviation and 'Alt.' is altitude in metres a.s.l.

Stake*	1982	1983	1984	1985	1986	1987	1988	1989	1990	Mean	SD	Alt.
900	–	60.8	63.4	1.3	18.9	48.1	27.7	10.3	22.4	31.6	21.7	895
950	31.8	31.8	47.7	3.7	–	–	–	–	–	28.8	15.9	950
951	–	–	–	17.7	25.5	44.9	54.6	–	–	35.7	14.7	955
1050	63.0	75.0	77.4	41.1	24.2	59.8	60.1	35.3	–	54.5	17.8	1040
1100	55.3	56.4	70.0	37.0	62.4	49.7	66.5	38.7	59.1	55.0	10.8	1085
1150	69.6	84.8	83.1	62.7	84.8	60.6	99.2	57.7	–	75.3	13.8	1145
1250	63.6	71.3	73.3	31.2	43.7	61.9	73.7	50.1	66.5	59.5	13.9	1250
1350	47.9	70.9	73.3	27.5	48.8	58.7	–	46.9	58.2	54.0	13.8	1350
1400	23.9	43.9	53.8	20.2	33.2	26.5	45.9	32.8	37.4	35.3	10.4	1415
1	45.3	54.5	66.5	12.0	54.8	89.8	52.1	46.3	63.1	53.8	19.5	900
2	20.8	42.8	52.7	20.5	26.3	40.3	35.3	29.4	48.2	35.1	11.0	1060
3	47.9	63.1	73.5	14.2	32.5	67.6	61.0	44.9	64.1	52.1	18.1	1130
4	68.7	74.0	83.1	32.2	62.8	92.7	98.0	50.9	78.7	71.2	19.4	1145
5	52.0	67.7	–	30.2	57.3	60.6	68.2	50.5	75.6	57.8	13.1	1190
6	27.5	42.4	52.4	2.3	17.8	40.2	36.7	29.9	35.3	31.6	13.9	1310
7	57.2	66.1	–	9.4	36.0	36.5	45.9	38.5	–	41.4	16.8	1310
8	82.5	–	–	–	–	–	–	–	–	82.5	–	1185
8.1	–	–	–	–	49.0	86.2	–	24.5	48.2	52.0	22.1	1205
9	34.3	50.6	65.9	30.1	56.9	93.5	63.5	42.2	66.0	55.9	18.3	1065
10	53.3	77.6	74.5	53.4	74.7	73.1	60.5	47.0	84.4	66.5	12.4	1000
11	53.0	66.7	55.4	28.5	45.2	51.1	87.7	45.8	70.2	56.0	16.1	1295
12	45.1	40.6	41.0	–	25.1	53.3	67.0	25.3	42.3	42.5	12.9	1190
13	98.5	–	64.5	12.3	47.1	–	–	29.9	–	50.5	29.6	1110
14	58.4	106.2	69.6	76.3	47.6	63.0	84.0	50.0	93.5	72.1	18.7	1000
15	55.9	106.5	77.8	80.7	90.5	69.6	91.1	69.4	93.6	81.7	14.5	885
16	19.4	36.5	42.5	19.0	46.5	34.9	38.1	20.7	36.2	32.6	9.8	1300
17	44.2	76.8	69.5	70.6	72.6	73.4	79.1	50.0	65.0	66.8	11.3	1195
18	40.4	74.4	55.2	54.8	50.8	55.1	79.0	50.4	72.9	59.2	12.3	1090

* Individual stake numbers relate to the transects of each ice-cap segment of Fig. 2 as follows, starting from the margin of the ice cap: NW-transect: 18, 17, 16, 1400; N-transect: 15, 14, 13, 12, 11, 1400; NE-transect: 10, 9, 8/8.1, 7; E-transect: 900, 950/951, 1050, 1100, 1150, 6; S-transect: 1, 2, 3, 4, 5, 1250, 1350, 1400.

undisturbed snow on the border of the dusted area mentioned above. It was then possible to track stratigraphic features in the undisturbed snow, using the dust-marked horizon as reference. The winter balance measurements are listed in Table 2.

Various climate parameters were recorded manually and on paper rolls in the base camp near the ice-cap margin, and for brief periods on the ice cap itself. These measurements encompassed daily values of mean, minimum and maximum air temperature, precipitation, wind speed and direction, cloudiness, sunshine hours, radiation energy, relative humidity, evaporation and firn temperature. A detailed analysis of the correlation of climate parameters with stake measurements is out of the scope of this work and the following analysis will therefore be restricted to an attempt at calculating the specific mass-balance from the sparse stake network followed by a correlation with the discharge curve of the adjacent Tasersiaq basin. A preliminary analysis of the climate and mass balance data can be found in Ahlstrøm (2003), giving

a tentative equilibrium line altitude variation from roughly 1300 m a.s.l. in 1985 to below the lowest elevation of the ice cap, i.e. less than 800 m a.s.l. in 1983.

SPECIFIC MASS BALANCE

The stake observations have been separated into five transects referring to their geographical orientation: NW-, N-, NE-, E- and S-transect, as shown in Fig. 2. Each

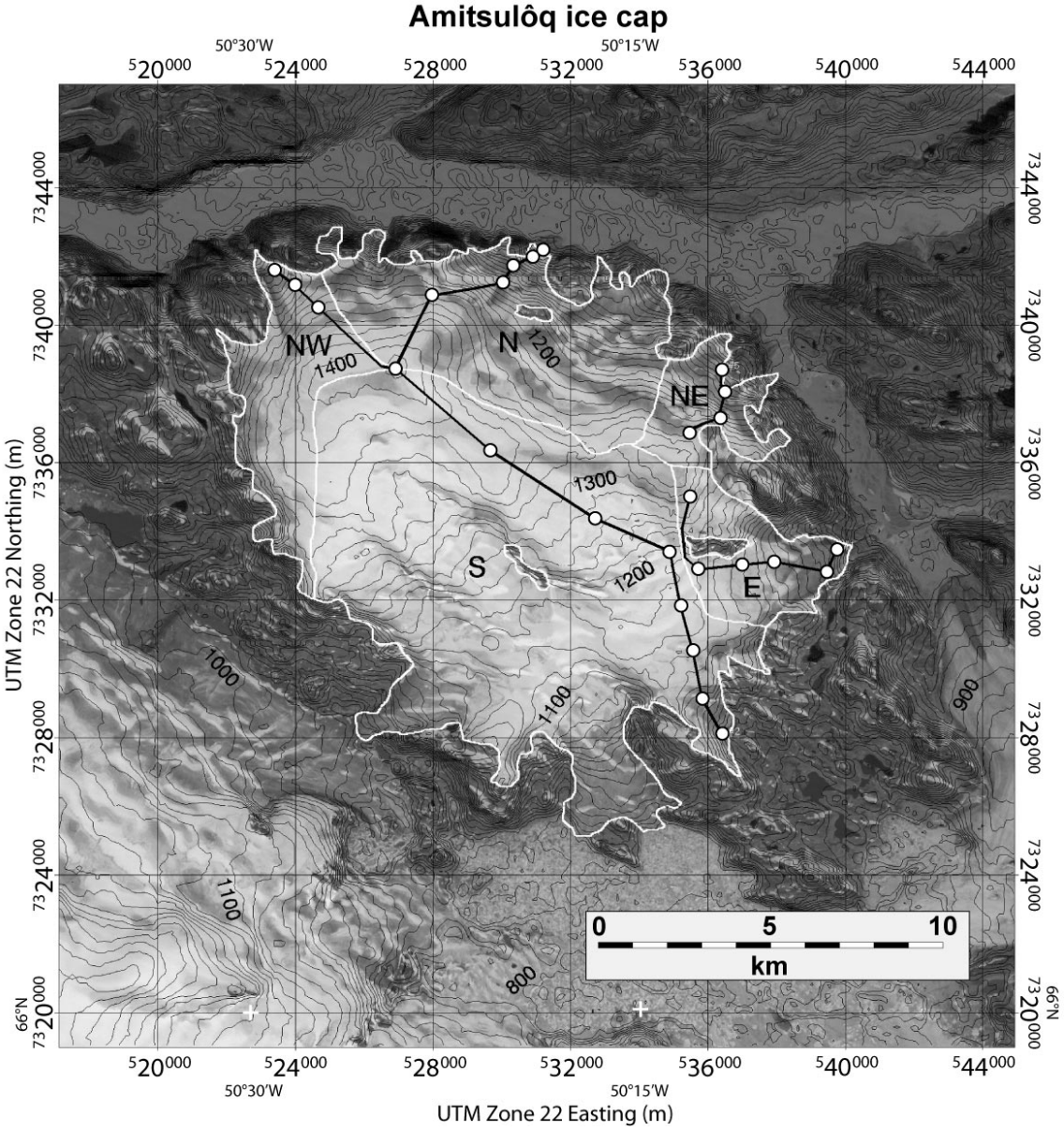

Fig. 2 Map of the Amitsulôq ice cap in UTM projection (Zone 22N), with 20 m elevation contours (m a.s.l.) based on the 1995/1996 elevation model of Ahlstrøm *et al.* (2002) overlaid on a panchromatic Landsat 7 ETM$^+$ image from 14 August 1999. The white boundaries separate the ice cap into five segments labelled N, NE, NW, S and E, respectively, according to their orientation. Each segment has a transect (black line) with individual stakes (white dots).

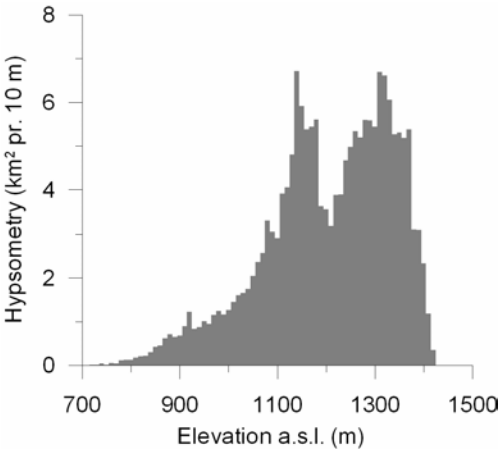

Fig. 3 The distribution of area with elevation for the Amitsulôq ice cap calculated in km^2 for altitude intervals of 10 m. The total area of the Amitsulôq ice cap was 185.4 km^2 in August 1999, at the acquisition time of the Landsat 7 ETM^+ image used to delineate between ice and land.

transect was considered representative for its segment in the calculation of the mass balance which is based on the detailed hypsometry shown in Fig. 3, available from a digital elevation model of the ice cap in 1995/1996 described in Ahlstrøm *et al.* (2002). The discrepancy in time between the field measurements (1981–1990) and the elevation model from 1995/1996 is a source of error that is difficult to quantify. However, a comparison between the elevation model used here and the barometric altitude measurements made from a helicopter during the fieldwork shows that the elevation has probably not changed much in the intervening years. The resulting specific summer-, winter- and mass-balance is shown in Table 3 and illustrated in Fig. 4. As mentioned previously, the division between summer and winter periods was defined through the stratigraphic method. This method is superior to a fixed-date method in regions with a pronounced annual temperature cycle, since the summer- and winter-balances are separated through direct observations of the transition (the hardened summer surface) as it is seen in the snow pit. A reasonable question to ask is how representative the mass balance measurements from Amitsulôq ice cap are for the discharge of the Tasersiaq basin as a whole. Apart from receiving meltwater from a 25 km stretch of the Greenland ice-sheet margin, the Tasersiaq basin also includes approx. 2000 km^2 of non-glaciated land. Initially, the Amitsulôq mass balance programme was established because it was not feasible to have a similar programme on the nearby Greenland ice-sheet margin due to difficulties with relocating the stake network and the necessity of accessing stakes by helicopter. The Amitsulôq ice cap, with its strategic position and altitude range, was a full scale, yet manageable, ice margin laboratory. When comparing the Tasersiaq basin discharge with the Amitsulôq data of Table 3, it turns out that the best correlation is obtained with the specific summer balance, with $R^2 = 0.93$ as illustrated in Fig. 5. There is no significant correlation between discharge and specific winter balance. It is reasonable to assume that the ablation on the Amitsulôq ice cap is comparable to the ablation on the neighbouring part of the Greenland ice-sheet margin, as they are only separated by a few kilometres of ice-free land and are positioned in the same precipitation shadow.

Table 3 The specific winter-, summer-, and mass-balance of Amitsulôq ice cap from 1982 to 1990, shown graphically in Fig. 4, based on observations from 26 stakes.

Year	Winter (10^6 m^3)	Summer (10^6 m^3)	Total (10^6 m^3)
1982	91	–86	5
1983	116	–27	90
1984	121	–69	51
1985	52	–147	–95
1986	85	–96	–11
1987	108	–150	–42
1988	120	–105	15
1989	78	–137	–59
1990	111	–186	–75

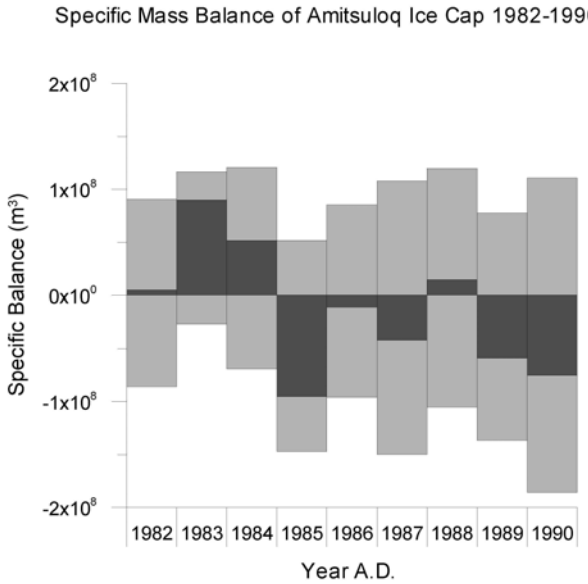

Fig. 4 The specific mass-balance calculated for Amitsulôq ice cap (dark grey) with the specific summer- and winter-balance (light grey).

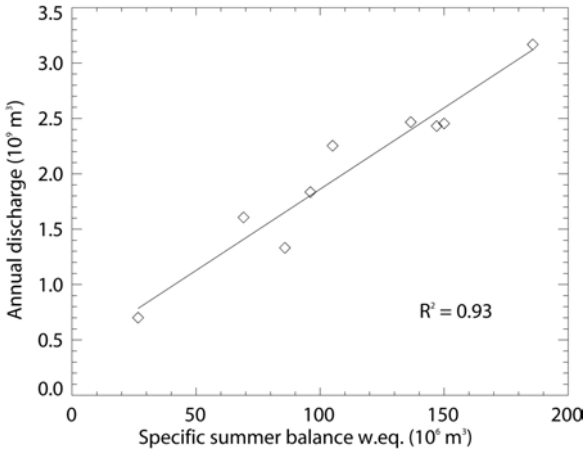

Fig. 5 The relationship between specific summer balance of the Amitsulôq ice cap and annual discharge from the Tasersiaq basin from 1982 to 1990. The two extreme points are 1983 for the low extreme and 1990 for the high extreme, respectively.

Thus, the high correlation between the summer balance of the Amitsulôq ice cap and the discharge of the Tasersiaq basin gives a strong indication of the dominating role of meltwater from the Greenland ice sheet over the water availability compared to precipitation in this dry and sunny region. The future hydropower potential of the Tasersiaq basin is therefore closely connected to the fate of the adjacent Greenland ice-sheet margin rather than fluctuations in the precipitation.

DISCUSSION AND CONCLUSION

The mass balance measurements presented from the Amitsulôq ice cap provide a first step in the assessment of the state of the local ice masses in Greenland. The sensitivity to climate fluctuations is apparent in Fig. 4 for the year 1983, which yielded an abnormally low summer balance also seen in other records of glacier mass balances in Greenland (Braithwaite, 1985; Olesen, 1986). The cause of the low summer balance was most likely the surface cooling caused by the eruption of the Mexican volcano El Chichón in March and April 1982, which is clearly evident in West and South Greenland temperature records (Box, 2002) and has been shown to have had a significant impact on the Greenland ice sheet runoff (Hanna *et al*., 2005).

Fluctuations in the summer balance dominate the variance in the mass balance of Amitsulôq ice cap, as is evident when comparing the correlations of specific mass balance with specific summer balance ($R^2 = 0.87$) and specific winter balance ($R^2 = 0.43$), respectively. The ice cap is situated in a precipitation shadow in a continental setting with large differences in air temperature between summer and winter. The northern part of the Tasersiaq basin completely lacks glaciers although the elevations are comparable, indicating that the Amitsulôq ice cap could be very sensitive to minor changes in the ambient climate. Indeed, the mass balance measurements show that the entire ice cap experiences a net loss in particular warm years.

When considering the hydropower aspect, the correlation between the summer balance and the discharge curve of the adjacent Tasersiaq basin illustrates the dominance of glacial meltwater on the hydropower potential of basins near the Greenland ice sheet. Utilizing the hydropower resources available in Greenland represents a formidable logistical challenge due to the remoteness of the larger basins and the harsh climate. The Tasersiaq basin has the largest hydropower potential in West Greenland, amounting to 2000 GWh per year or 300 MW (Weidick & Olesen, 1978) and could potentially make Greenland self-sufficient with energy if it could be distributed or alternatively used for an energy-demanding industry such as aluminium production. The demonstrated dominance of the glacial meltwater on the water supply underlines the need for studies of ice-marginal changes and their potential impact when assessing the future hydropower potential of partially glaciated basins in Greenland.

Acknowledgements The authors wish to thank the numerous people who participated in the field programme. Thanks to the two anonymous reviewers for their constructive suggestions and to Regine Hock for useful discussions. This work was funded by the

Danish Technical Research Agency under contract 2058-03-0035 (Forsyningssikkerhed for det største vandkraftpotentiale i Vestgrønland - FORSYN). This paper is published with the permission of the Geological Survey of Denmark and Greenland.

REFERENCES

Ahlstrøm, A. P. (2003) Ice sheet ablation assessed by observation, remote sensing and modelling. PhD Thesis, University of Copenhagen. Geological Survey of Denmark and Greenland Report 2003/49.

Ahlstrøm, A. P., Bøggild, C. E., Mohr, J. J., Reeh, N, Christensen, E. L., Olesen, O. B. & Keller, K. (2002) Mapping of a hydrological ice-sheet drainage basin on the West Greenland ice-sheet margin from ERS-1/-2 SAR interferometry, ice-radar measurement and modelling. *Ann. Glaciol.* **34**, 309−314.

Arendt, A., Echelmeyer, K., Harrison, W., Lingle, C. & Valentine, V. (2002) Rapid wastage of Alaska glaciers and their contribution to rising sea level. *Science* **297**, 382−386.

Braithwaite, R. J. (1985) Glacier-climate investigations in 1984 at Qamanârssûp sermia, West Greenland. *Rapp. Grønlands geol. Undersøg.* **125**, 108−112.

Braithwaite, R. J., Konzelmann, T., Marty, C. & Olesen, O. B. (1998) Errors in daily ablation measurements in northern Greenland, 1993−94, and their implications for glacier climate studies. *J. Glaciol.* **44**(148), 583−588.

Church, J. A., Gregory, J. M., Huybrechts, P., Kuhn, M., Lambeck, K., Nhuan, M. T., Qin, D. & Woodworth, P. L. (2001) Changes in sea level. In: *Climate Change 2001: The Scientific Basis. Contribution of Working Group I to the Third Assessment Report of the Intergovernmental Panel on Climate Change* (ed. by J. T. Houghton, Y. Ding, D. J. Griggs, M. Noguer, P. J. van der Linden, X. Dai, K. Maskell & C. A. Johnson). Cambridge University Press, Cambridge, UK.

de Woul, M. & Hock, R. (2005) Static mass balance of Arctic glaciers and ice caps using a degree-day approach. *Ann. Glaciol.* **42**, 217−224.

Olesen, O. B. (1986) Fourth year of glaciological field work at Tasersiaq and Qapiarfiup sermia, West Greenland. *Rapp. Grønlands geol. Undersøg.* **130**, 121−126.

Østrem, G. & Brugman, M. (1991) Glacier mass-balance measurements. NHRI Science Report no. 4.

Weidick, A. & Olesen, O. B. (1978) Hydrologiske bassiner i Vestgrønland. Grønlands Geologiske Undersøgelse (in Danish, with map and abstract in English).

Weidick, A., Bøggild, C. E. & Knudsen, N. T. (1992) Glacier inventory and atlas of west Greenland. *Rapp. Grønlands geol. Undersøg.* **158**.

Zuo, Z. & Oerlemans, J. (1997) Contribution of glacier melt to sea-level rise since AD 1865: a regionally differentiated calculation. *Clim. Dyn.* **13**, 835−845.

Glacier Mass Balance Changes and Meltwater Discharge (selected papers from sessions at the IAHS Assembly in Foz do Iguaçu, Brazil, 2005). IAHS Publ. 318, 2007.

Recent snow cover fluctuations in the mountainous areas of Japan

SATURO YAMAGUCHI[1], OSAMU ABE[2], SENTO NAKAI[1] & ATSUSHI SATO[1]

1 *Snow and Ice Research Center, National Research Institute for Earth Science and Disaster Prevention, Suyoshi, Nagaoka, Niigata, 940-0821, Japan*
yamasan@bosai.go.jp

2 *Shinjo Branch of Snow and Ice Research Center, National Research Institute for Earth Science and Disaster Prevention, 1400 Tokamachi, Shinjo, Yamagata 996-0091, Japan*

Abstract Meteorological data from mountainous areas of Japan have been collected by the National Research Institute for Earth Science and Disaster Prevention (NIED) for over 10 years. We found good correlations between the maximum snow depth and winter air temperature at all sites. Also the gradient of variation in maximum snow depth compared with variation in mean winter air temperature at all sites was close to the mean value of 17% $°C^{-1}$. According to this relationship, snow cover in Japanese mountainous areas is estimated to decrease by 23% in the next 100 years. In the central part of Honshu a given change of winter temperature had a relatively large direct effect on the maximum snow depth in low elevation areas, but not at higher elevation mountain sites.

Key words Japanese mountainous area; meteorological conditions; snow cover; water resource

INTRODUCTION

The two largest islands of Japan, Honshu and Hokkaido, are located on the east side of the Eurasian continent and heavy snowfalls are carried by the northwesterly monsoon to areas of the Sea of Japan. Japan has a large spatial extent of mountainous areas with winter snow, and the amount of snow and other properties of the snow cover range widely due to the extent in latitude and altitude (Ishizaka, 1998). Gaining a better understanding of these snow cover properties is important because the demand for water has been increasing every year in Japan, and the use of dams to moderate the fluctuation in mountain water runoff is widespread.

Melt water from snow is a very important water resource for Japan and therefore it is very important to determine the mass of snow cover in Japanese mountainous areas. To know the amount of snow and to predict future snow cover condition in mountainous areas, information on the present meteorological conditions and trend in snowpack fluctuations is necessary. However, until recently, there were few continuously operating meteorological stations in Japanese mountain areas due to severe weather conditions. Thus, a little over 10 years ago, the National Research Institute for Earth Science and Disaster Prevention (NIED) constructed a mountainous weather and snow station network (Mount-Net) to measure meteorological and snow conditions. The primary aims of Mount-Net are to obtain basic information on meteorological conditions in Japanese mountainous areas and to determine the sensitivity of snowpack properties to climate changes, in particular to global warming.

In this paper, we discuss the recent fluctuations of meteorological and snow cover conditions in Japanese mountainous areas and compare the results with similar measurements obtained at flatter regions with lower elevations, hereafter referred to as flatland sites.

OBSERVATION SITES

NIED began building mountain stations in 1990 and seven stations were established by 1995 (Nakamura *et al.*, 1997; Shimizu & Abe, 2001). The mountain stations are distributed to cover all Japanese snowy mountain areas from 35°N to 43°N with less than 2° intervals. The mountain stations are located on the representative mountain of the local region, which is generally the mountain with the largest snowpack in the region (Fig. 1). The measurements depend on the situation at each site. All stations record data on air temperature, snow depth and snow mass (snow weight), but in addition, stations MS5 and MS7 (station labels are defined in Fig. 1) collect precipitation data.

Each station of Mount-Net was paired with a nearby flatland station (from Pair 1 to Pair 7) that has records of air temperature, precipitation, and snow depth (Fig. 1, Table 1). Most of the flatland stations are managed by the Japan Meteorological Agency (JMA); the two exceptions are FS3 and FS4, which instead belong to NIED. FS3 and FS4 maintain snow mass data because they are part of NIED. The location and elevation of all stations are in Table 1.

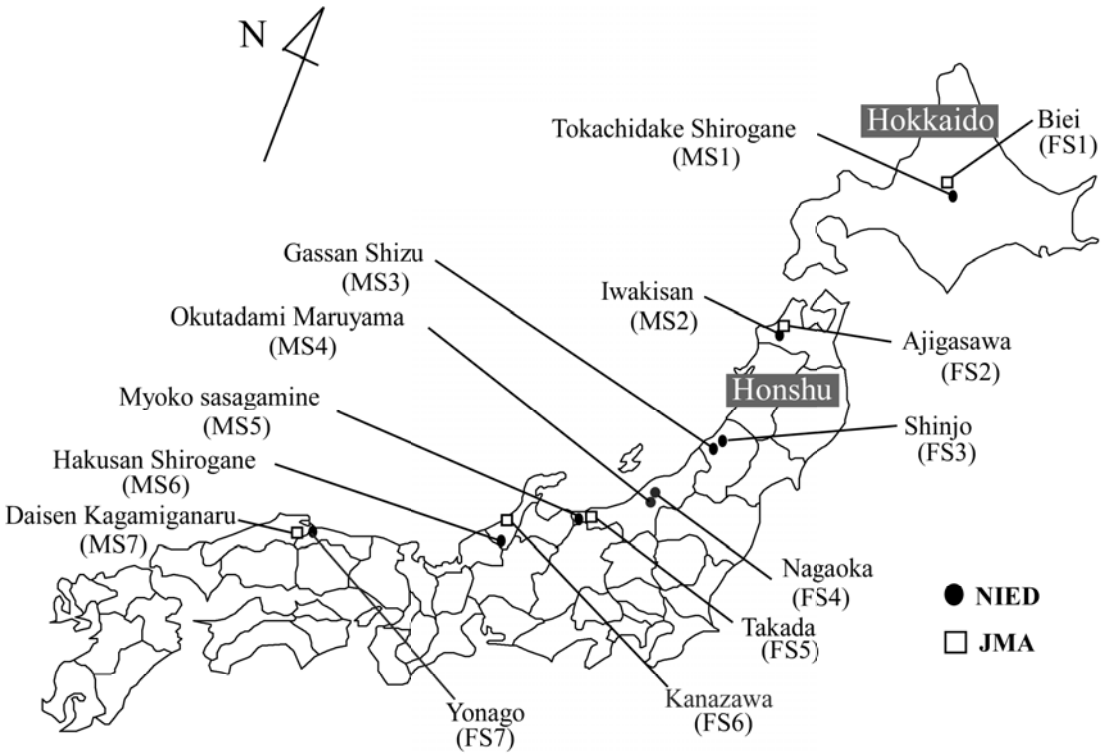

Fig. 1 Location of the observation sites.

Table 1 Locations of observation sites.

Site		Location	Horizontal separation† (km)	Altitude (m a.s.l.)	Altitude separation‡ (m)
Pair 1	MS1	43°29′N 142°36′E	14	520	270
	FS1*	43°35′N 142°30′E		250	
Pair 2	MS2	40°39′N 140°18′E	17	1238	1198
	FS2*	40°47′N 140°12′E		40	
Pair 3	MS3	38°29′N 140°00′E	43	710	583
	FS3	38°47′N 140°19′E		127	
Pair 4	MS4	37°09′N 139°14′E	42	1205	1108
	FS4	37°25′N 138°53′E		97	
Pair 5	MS5	36°52′N 138°05′E	31	1310	1297
	FS5*	36°06′N 138°15′E		13	
Pair 6	MS6	36°11′N 136°38′E	45	835	829
	FS6*	37°35′N 136°38′E		6	
Pair 7	MS7	35°20′N 133°35′E	17	875	869
	FS7*	35°26′N 133°20′E		6	

† Between mountain and flatland site. ‡ Station of the Japan Meteorological Agency.

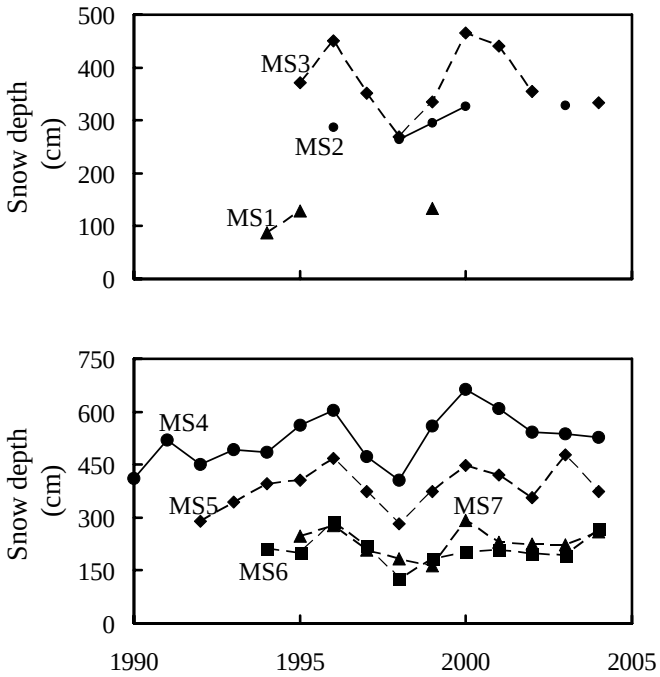

Fig. 2 Maximum snow depth at the mountain sites. The top plot shows the northern sites, the bottom plot shows the southern sites.

RESULTS

Snow depth, mean winter temperature, and winter precipitation in mountainous areas

The maximum snow depth at the mountain stations was found to have a trend distinct from that of the flatland stations. The data, plotted in Fig. 2, show that MS3, MS4, and

MS5 have two peaks of maximum snow depth, with one peak in 1996 and the other in 2000. In addition, there appears to be a third peak at MS5 in 2003, but this is produced by just one data point and thus we do not consider it. In contrast, MS6 and MS7, which are located in southern Japan, do not have a large interannual fluctuation and no remarkable tendency. Unfortunately, there were winter measurement problems in the two northernmost mountain sites (MS1, MS2), greatly reducing the amount of data and making it difficult to detect a trend from these stations. Thus most of the stations that had sufficient data showed peaks in 1996 and 2000.

The mean winter air temperature also showed several peaks that were consistent among the mountain stations. Peak temperature occurred in 1995, 1998, and 2002 at all stations except MS1 and MS2 in the north. The plots are shown in Fig. 3; like the snow depth plots in Fig. 2 the two northernmost stations had insufficient data to detect a trend.

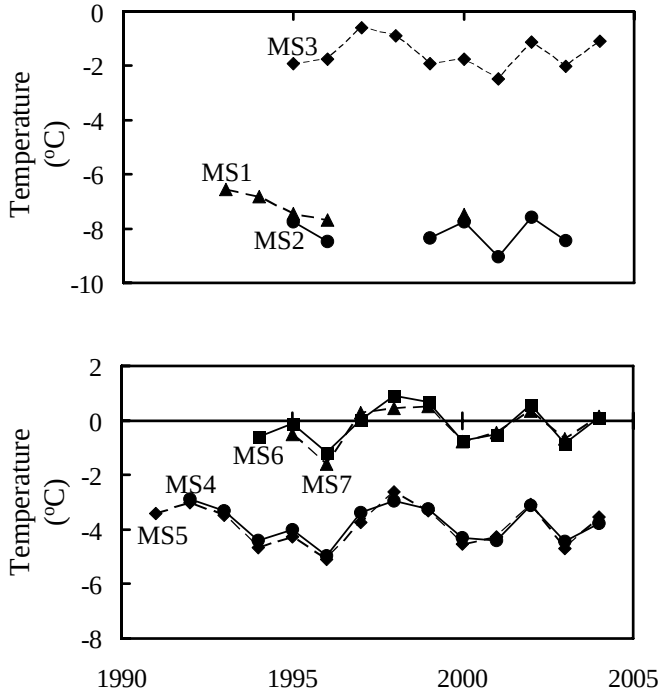

Fig. 3 Mean winter air temperature at the mountain site. Winter is defined as the period from December to March here and in other figures.

Figure 4 shows the total winter precipitation at three mountain stations. In the figure winter precipitation at MS5 and MS7 were measured directly, but winter precipitation at MS4 was not measured directly but was estimated from the snow mass changes, as air temperatures during the winter season were always below 0°C and thus most of the precipitation had to be snow. Therefore, some caution is necessary when the precipitation amount at MS4 is compared with that from the other two stations. Other stations (MS1, MS2, and MS3) did not have sufficient data of winter precipitation and snow mass. Their peaks are near 1996 and 2000, which are the same peak positions that occurred in the maximum snow depth.

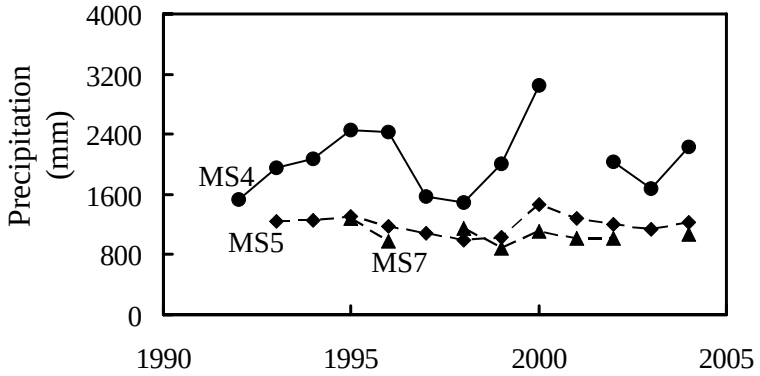

Fig. 4 Winter precipitation at the mountain sites.

Table 2 Correlations between adjacent flatland and mountain sites.

Pair of site	Number of samples	Correlation coefficient: Maximum snow depth	Mean air temperature	Precipitation
Pair 3	9	0.85	0.72	***
Pair 4	15	0.42	0.89	0.86
Pair 5	13	0.26	0.88	0.68
Pair 6	11	0.12	0.61	***
Pair 7	9	0.59	0.93	0.46

Lack of data is shown by ***.

Comparisons of flatland and mountain data

To better understand the relationship between the data from the mountain stations and that from the nearby flatland station, we determined the correlation coefficients for two sets of data. The results are summarized in Table 2. There is a good correlation between the temperatures, and precipitation also shows good correlation. Maximum snow depth has a wide range of correlations; Pair 3 in the north, and Pair 7 in the south have relatively high scores, especially Pair 3. However, the central pairs (4, 5, and 6) have coefficients below 0.5, even though their air temperatures and precipitation are relatively highly correlated.

These results suggest that it is difficult to estimate the snow cover in a mountainous area from snow cover in the nearby flatland areas.

Interannual fluctuations of degree-day factor

Degree-day factor, which indicates the relationship between melting rate and daily mean air temperature, is sometimes used to estimate the effect of global warming on the fluctuation of snow melting because it is much simpler than the heat balance method which exactly calculates the energy balance at the snow surface. Here we calculate the degree-day factor in mountainous areas using the variation of snow mass and the daily mean air temperature during the melt season. The melt season is defined as the uninterrupted period during which the daily mean air temperature is above 0°C

and the snow mass decreases. Table 3 lists the resulting degree-day factors at four observation sites in Honshu (MS4, MS5, MS6, and MS7) and air temperature averaged over each melt season. Standard deviations are also listed in brackets. The standard deviations of air temperature suggest that each degree-day factor was calculated under various temperature conditions, namely cool and warm melt seasons. However, although values of the degree-day factor vary by station, the standard deviations are all small. These observation results provide confidence that we can use the same present values of degree-day factor for estimating the fluctuation of snow melting under a small air temperature (±1°C).

Table 3 Degree-day factor at each site.

Site	Number of sample year	Degree-day factor ($mm\ °C^{-1}\ day^{-1}$) Mean value	Air temperature (°C) Mean value
MS4	11	6.7(±0.9)	8.5(±1.1)
MS5	10	5.5(±0.6)	6.7(±1.0)
MS6	6	5.3(±0.3)	4.6(±1.4)
MS7	4	5.2(±0.6)	6.2(±0.9)

Uncertainties are standard deviations.

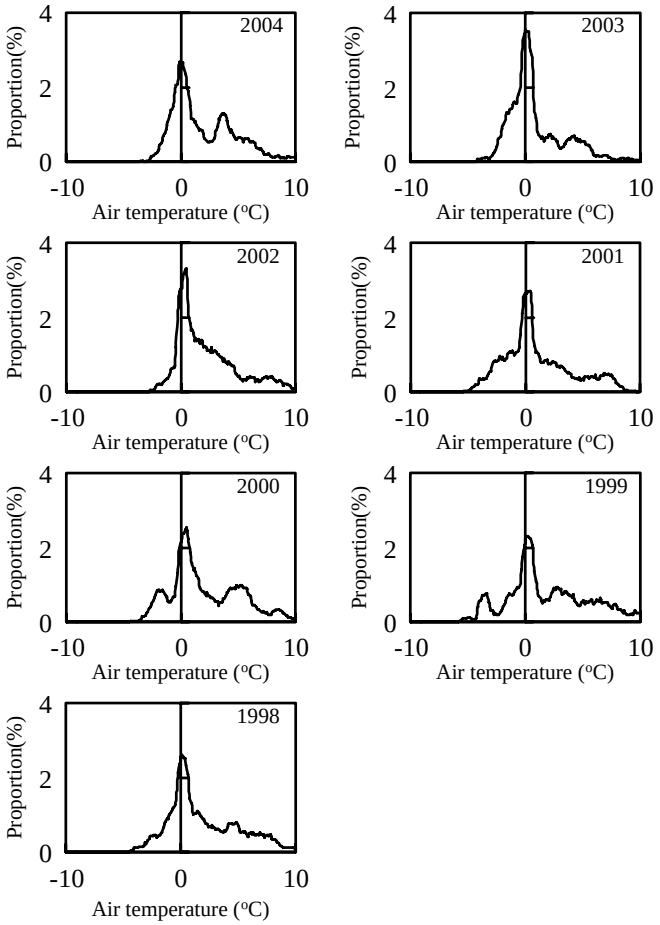

Fig. 5 Winter precipitation curve at a flatland station (FS4). The data in each graph show running mean of 11 data points.

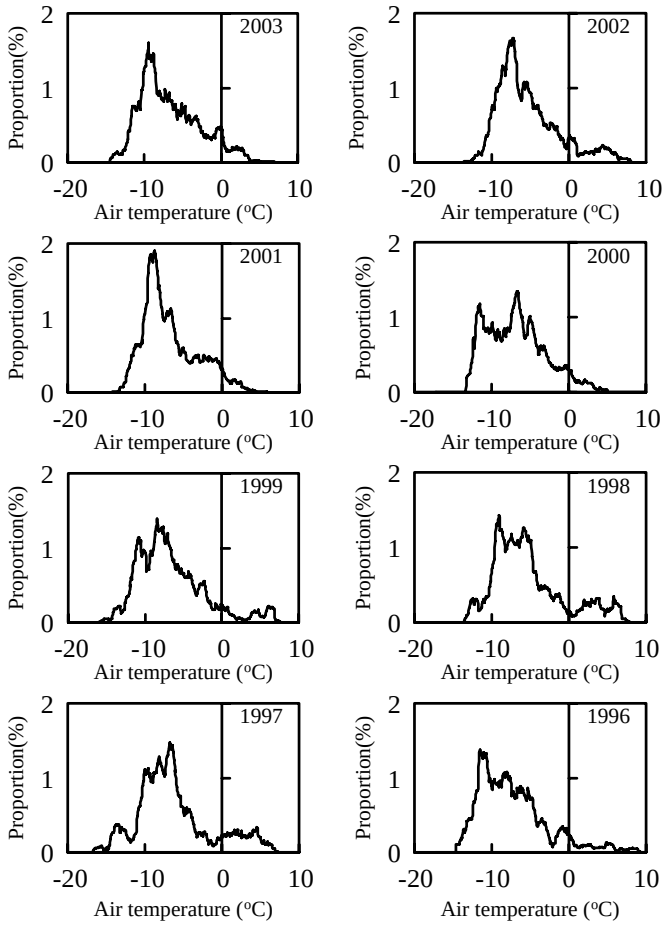

Fig. 6 Winter precipitation curve at a mountain station (MS5). The data in each graph show running mean of 11 data points.

DISCUSSION

Precipitation patterns of flatland and mountainous areas

We found a significant difference between the snow depth correlations and the winter precipitation correlations (as well as the temperature correlations). That is, the maximum snow depth at flatland and adjacent mountain stations in central Honshu (Pair 4, Pair 5, and Pair 6) had little correlation, whereas the winter air temperatures and precipitation had high correlations (Table 2). To investigate the cause of this difference, we analysed the relationship between air temperature and precipitation at a flatland area (FS4) and the same relationship for a mountainous area (MS5) that had small time resolution data (15 minutes).

Figure 5 and 6 show the distributions of precipitation with air temperature during each precipitation event. In the figures, resolution of air temperature is 0.1°C and sum of precipitation at each temperature has been normalized by dividing by total precipitation in the winter season (December–March).

Winter precipitation distributions at FS4 (Fig. 5) show that temperatures near 0°C were most likely to have precipitation (i.e. the peak is near 0°C). We assume, for simplicity, that precipitation below 0°C is snow, whereas that above 0°C is rain. Thus, the

fractional amount of precipitation that was snow is the fraction of area below the curves that are to the left of the 0°C line. For the flatland site FS4, these percentages fluctuate from 18 to 43% year by year (Table 4). This figure suggests that the amount of snowfall in FS4 (a typical flatland area in central Honshu) should be sensitive to climate changes.

Table 4 Percentage of rain and snow in the winter precipitation at a flatland station (FS4).

Data	Percentage (%)		Mean air temperature (°C)
	Rain	Snow	
1998	71.0	29.0	3.1
1999	69.1	30.9	2.9
2000	74.5	25.5	2.5
2001	59.1	40.9	2.0
2002	82.0	18.0	3.3
2003	57.4	42.6	2.1
2004	71.2	28.8	3.4
Average	69.2	30.8	2.8

Table 5 Percentage of rain and snow in the winter precipitation at a mountain station (MS5).

Data	Percentage (%)		Mean air temperature (°C)
	Rain	Snow	
1996	6.9	93.1	–5.1
1997	14.4	85.6	–3.8
1998	14.3	85.6	–2.6
1999	8.1	91.9	–3.3
2000	5.8	94.2	–4.5
2001	5.4	94.6	–4.3
2002	11.7	88.3	–3.1
2003	7.4	92.6	–4.7
Average	6.9	93.1	–3.9

In contrast with the flatland station, the precipitation peak at the mountain station MS5 is generally within a few degrees of –9°C (Fig. 6). Table 5 shows the proportion of winter precipitation that is snow and rain at MS5 for each year. The fluctuations of percentage of snow in MS5 are smaller than those of FS4, ranging from 86 to 95%, and this result indicates that the amount of snowfall in MS5, and by implication, other mountainous areas in central parts of Honshu, should not be sensitive to climate change.

The differences between the sensitivities of the snowfall amount at the flatland and mountain sites to the air temperatures may explain the difference in the correlations noted above. In particular, even if air temperature and precipitation fluctuations in both areas were the same, they would have a different change in the amount of snowfall.

Maximum snow depth variations in mountain areas for the air temperature fluctuations

In the previous section we only discussed the fluctuation of percentage of snow with air temperature change using precipitation curves, thus we neglected the effect of

change of precipitation amount. However, we argue here that a certain change of precipitation amount usually occurs with an increase of temperature. Nakamura & Shimizu (1996) reported a negative correlation between air temperature and precipitation. We found a similar negative correlation at MS4 and MS5. Thus, we chose air temperature as a description function of the snow depth change because of the negative correlation between air temperature and precipitation.

The results appear in Fig. 7. In the figure, the ordinate RSD is the value of the maximum snow depth in a given year divided by the average maximum snow depth for the years 1995 to 2004, and the abscissa ΔT is the value of the deviations of the mean winter temperature from the averaged mean winter temperature (1995–2004). This figure indicates that all sites have good correlations between RSD and ΔT. Moreover, gradients of variation in RSD against variation in ΔT at each site seem to be similar values.

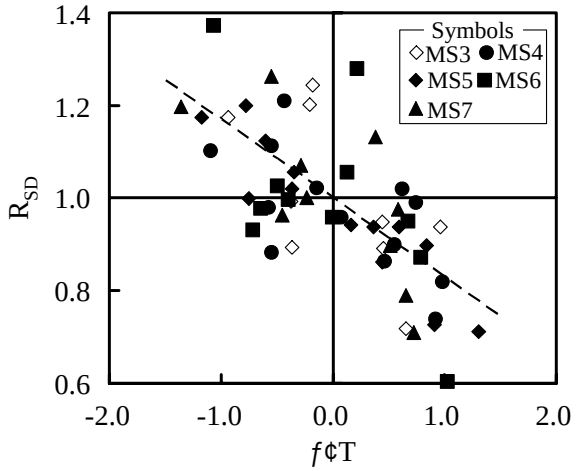

Fig. 7 Relationship between winter air temperature and maximum snow depth. RSD is proportional to the maximum snow depth and ΔT is a deviation of the mean winter temperature as defined in the text.

The least-squares linear fit to the RSD and ΔT data, which was constrained to pass through the point (0,1), is:

$$R_{SD} = -0.17\Delta T + 1 \quad (1)$$

This line has a correlation coefficient of –0.70 and a standard deviation of 0.11.

From equation (1), we can roughly estimate the change of maximum snow depth from the southernmost mountain areas near station MS7 to the mountain areas near the northernmost station MS3. That is, the water source from snow on mountainous areas in Honshu is predicted to decrease by approximately 23% in the next 100 years if the rate of winter temperature rise is the same as for the last 100 years (1.35°C/100 years).

CONCLUSIONS

We collected and analysed 10 years of data on winter precipitation, snow depth, and air temperature in mountain regions of Japan. To better understand the correlations

between these variables, data from each mountain station was compared to that from a nearby low-elevation station. The following results were obtained:

- The maximum snow depths depended on the mountain location; nevertheless, most stations had similar year to year changes. The estimated degree-day factors varied by site, but did not have large interannual changes.
- The relationship between precipitation and air temperature for given winter (precipitation curve) shifted from year to year but had a similar form. The precipitation curves indicated that the amount of snowfall in flatland areas is more sensitive to temperature changes than that in mountainous areas.
- The change ratio of maximum snow depth was correlated with the mean winter air temperature at all mountain sites. Moreover, the gradients of the variation in maximum snow depth against variation in mean winter air temperature at each site was approximately 17% $°C^{-1}$. Using this relation, the water source from snow on mountainous areas in Honshu was predicted to decrease by approximately 23% in the next 100 years.
- Although the data in this study covered 10 years, a longer period is needed to clearly determine the effects of climate change on mountain snowpack. For this reason, the mountain stations will continue to collect data.

Acknowledgments We thank the members of NIED, especially M. Shimizu, who maintained the observation sites in the mountain areas and arranged their data sets. We are also grateful for the useful suggestions of M. Ishizaka, T. Kobayashi, K. Nishimura, K. Iwamoto, and H. Hirashima of Nagaoka Institute of Snow and Ice Studies and T. Sato, K. Kosugi, and M. Nemoto of Shinjo Branch of Nagaoka Institute of Snow and Ice Studies.

REFERENCES

Ishizaka M. (1998) New categories for the climatic division of snowy areas in Japan. *Ann. Glaciol*. **26**, 131–137.

Nakamura, T. & Shimizu, M. (1996) Variation of snow, winter precipitation and winter air temperature during the last century at Nagaoka, Japan. *J. Glaciol.* **42**(140). 136–140.

Nakamura, H., Shimizu, M., Abe, O., Kimura, T., Nakawo, M. & Nakamura, T. (1997) A snow observation network for mountain area of NIED. In: *Snow Engineering: Recent Advances* (ed. by M. Izumi, T. Nakamura & R. L. Sack), 539–541. A. A. Balkema, Rotterdam, The Netherlands.

Shimizu, M. & Abe, O. (2001) Fluctuation of snow cover on mountainous areas in Japan. *Ann. Glaciol*. **32**, 97–101.

Glacier Mass Balance Changes and Meltwater Discharge (selected papers from sessions at the IAHS Assembly in Foz do Iguaçu, Brazil, 2005). IAHS Publ. 318, 2007.

Comparison of remote sensing derived glacier facies maps with distributed mass balance modelling at Engabreen, northern Norway

MATTHIAS BRAUN[1], THOMAS V. SCHULER[2,3], REGINE HOCK[3], IAN BROWN[3] & MIRIAM JACKSON[4]

1 *Center for Remote Sensing of Land Surfaces, University of Bonn, Germany*
matthias.braun@uni-bonn.de

2 *Department of Geosciences, University of Oslo, Norway*

3 *Department of Earth Sciences, Uppsala University, Sweden*

4 *Norwegian Water Resources and Energy Directorate, Oslo, Norway*

Abstract Calibration and validation of glacier mass balance models typically rely on mass balance data derived from measurements at individual points, often along altitudinal gradients, thus neglecting much of the spatial variability of mass balance. Remote sensing data can provide useful additional spatially distributed information, e.g. on surface conditions such as bare ice area, firn cover extent, or snow. We developed a semi-automated procedure to derive glacier-facies maps from Landsat satellite images, and applied it to Engabreen, an outlet glacier from the Svartisen ice cap in northern Norway. These maps, discriminating between firn, snow and ice surfaces, are then used as a reference for mass balance modelling. Facies information shows a general agreement with the available few field observations and results obtained by distributed mass balance modelling. We conclude that Earth Observation products provide a powerful, although as yet poorly exploited tool, for calibration and validation of distributed mass balance models.

Key words Engabreen; glacier facies; glacier mass balance; Landsat; modelling; Norway; remote sensing

INTRODUCTION

Glacier mass balance models are a basic requirement for climate sensitivity studies of glaciers. They are commonly calibrated and validated using measured mass balance (e.g. Braithwaite *et al.*, 2003) or discharge data (e.g. Hock, 1999). Such data are only available from a small number of glaciers due to constraints given by access, logistics and costs, particularly in remote areas. In addition, mass balance programmes generally suffer from a small number of *in situ* measurements upon which reported area-averaged mass balance and gradient values are based. Consequently, these data neglect much of the spatial small-scale variability typical for mass balance and, hence, they are of only limited value in validating the spatial pattern of mass balance as generated by distributed mass balance models. In recent years a trend towards fully distributed modelling can be observed, i.e. a mass balance is calculated for each grid cell of a digital elevation model (e.g. Klok & Oerlemans, 2003; Braun & Hock, 2004).

Remote sensing offers a powerful tool to provide enhanced spatial information as a base to validate and calibrate spatially distributed mass balance models and it also provides data for sites void of direct mass balance measurements. Repeated glacier

facies maps delineating the areas of firn, snow and ice can be used to validate modelled snow line retreat during the melt season. Glacier facies maps have been generated from optical and microwave satellite data for many years (e.g. Hall *et al.*, 1987; Hall *et al.*, 1988; Williams *et al.*, 1991; König *et al.*, 1999; Braun *et al.*, 2000), but rarely have such data been incorporated in calibration or validation of mass balance models. Heiskanen *et al.* (2003) have previously combined some glacier facies maps with *in situ* mass balance measurements (snow line and equilibrium line altitude) for the Engabreen site.

The purpose of this study is: (1) to develop a semi-automated processing chain to derive glacier facies maps; (2) to demonstrate their suitability to support the validation of a glacier mass balance model. As a test site we chose Engabreen, a steep outlet glacier from the Svartisen ice cap in northern Norway. We used satellite derived glacier facies maps to validate the results obtained from a distributed mass balance model. The model and its application to Engabreen are described in detail by Schuler *et al.* (2005).

STUDY SITE

Engabreen is located close to the northern Norwegian coast (66°40′N, 13°45′E) and parties an outlet glacier of the western Svartisen ice cap (Fig. 1). About 14% of the 38 km^2 glacier area is located in a channel-like narrow valley, whereas the main part is located on the rather flat plateau of the ice cap above 1100 m a.s.l. The glacier has an altitudinal range of about 1500 m, reaching almost down to sea level. Engabreen has shown considerable changes in mass balance and resulting frontal changes since the 1950s (Kjøllmoen *et al.*, 2003). Changes in glacier front position have been monitored since 1970, but sporadic measurements exist back to about 1900. During the 1990s the glacier advanced again, reaching the proglacial lake, but started retreating again in about 2000. The Norwegian Water Resources and Energy Directorate (NVE) have additionally operated an extensive mass balance programme, which started in 1970 (e.g. Kjøllmoen *et al.*, 2003).

METHODOLOGY

Facies maps

For this study, a total of eight Landsat Thematic Mapper (TM) and Enhanced Thematic Mapper (ETM+) scenes (30-m spatial resolution, seven spectral bands) acquired between 1984 and 2002 were available. Emphasis was given to data from the ablation period (summer). Table 1 gives an overview of the data sets. The few data available until 1999 also show the paucity of the previous operational acquisitions over glaciated areas. With the operation of Landsat-7 ETM+ since 1999 and its Long Term Acquisition Plan (LTAP) the amount of multi-temporal data sets within one season increased considerably. The theoretical repeat cycle of 16 days is even higher in high latitudes where satellite orbits converge and ground coverage of one area is

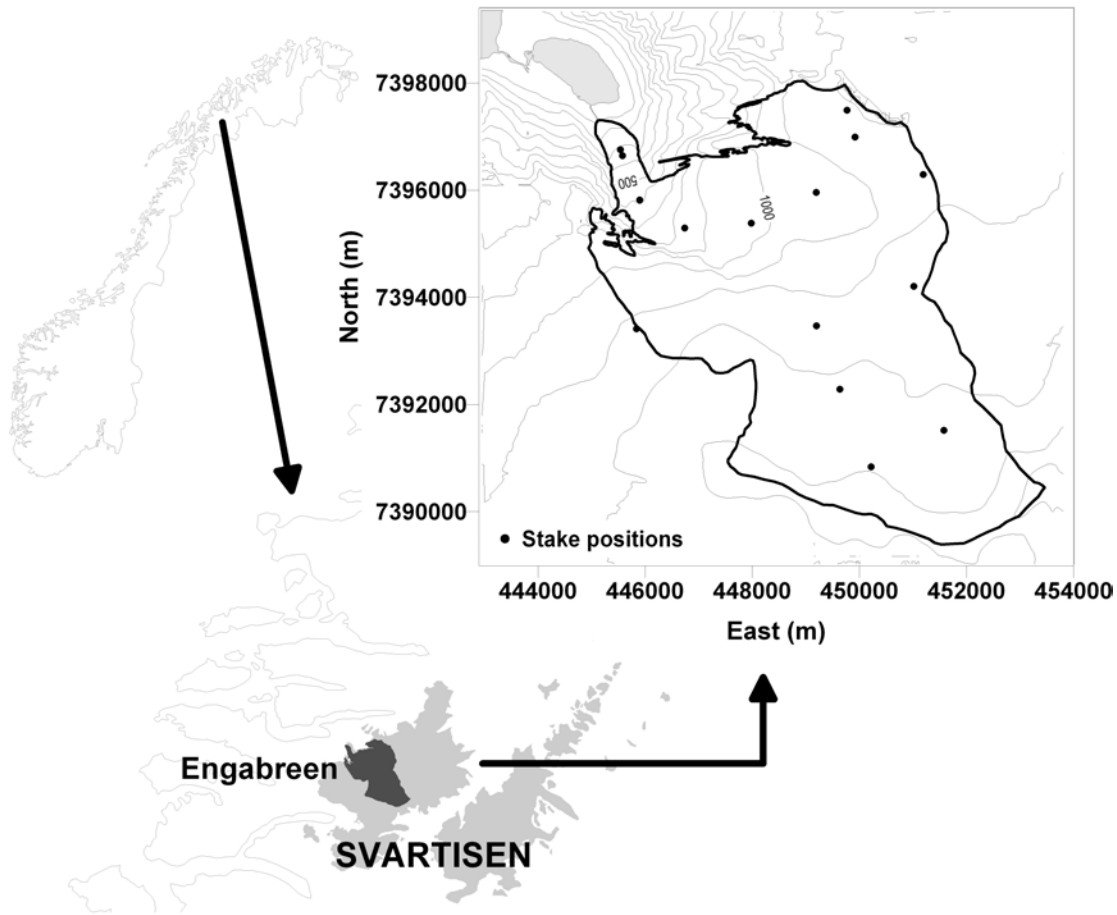

Fig. 1 Map of Engabreen and location in Norway.

Table 1 Overview of Landsat satellite data utilized in this study.

Sensor / Platform	Path	Row	Acquisition date	Centre longitude	Centre latitude
Landsat-5 TM	198	13	1984-08-13	15.20°E	66.56°N
Landsat-5 TM	198	13	1988-08-15	13.52°E	66.56°N
Landsat-5 TM	198	13	1994-08-25	15.16°E	66.56°N
Landsat-7 ETM+	198	13	1999-08-15	15.25°E	66.56°N
Landsat-7 ETM+	200	13	2001-07-17	12.13°E	66.56°N
Landsat-7 ETM+	198	13	2002-07-22	15.21°E	66.56°N
Landsat-7 ETM+	198	13	2002-08-07	15.21°E	66.56°N
Landsat-7 ETM+	198	13	2002-09-08	15.20°E	66.56°N

provided by various satellite tracks (images with different path/rows in the Landsat reference system). However, the theoretical improvement is still limited by the frequent cloud cover at our study site.

To extract the thematic information from the multiple Landsat satellite images a semi-automated procedure was developed (Fig. 2). The first step comprised the geo-correction and clipping of the data to a master scene (15-AUG-1999) by manual tie-point search in the imagery. A root mean square error below one pixel could be achieved for co-registration of all images, which was also proofed by the visual

inspection. Sidjak & Weathe (1999) previously reported the suitability of Principle Component Analysis (PCA) for facies mapping. In this study, a Tasseled Cap Transformation (Richards, 1995) was applied to reduce the data redundancy of the three visible channels as well as to increase the separation between clouds and snow surfaces. The resulting data set was classified into 10–15 classes using the unsupervised ISODATA algorithm (Richards, 1995). The ISODATA algorithm automatically generates a user-specified number of thematic classes based on the (spectral) information of the input image. Subsequently the output classes were merged for each image to generate masks to distinguish glacier and snow covered areas as well as clouds from other surfaces. The merging of the thematic classes was performed by visual inspection of an experienced operator. In the present study, cloud masking was slightly better in the Tasseled Cap imagery than in the PCA data. Using the snow and glacier mask the PCA data for the remaining area was then used to apply a second unsupervised classification (ISODATA) to extract the three facies types (bare ice, firn and snow). Snow refers to last winter's or fresh snow, and firn refers to snow that has survived at least one summer. In a first iteration 10 classes were used. In case operator inspection revealed no adequate separation of the surface types, an ISODATA run with 20 classes was performed. The final step comprised the export to the model format (ArcInfo ASCII). Results mainly rely on the visual interpretation of the operator but also some limited ground control data from direct observations were available for accuracy assessment.

Distributed mass balance modelling

We compare the satellite derived facies maps with surface types modelled by Schuler *et al.* (2006). They modelled the mass balance of Engabreen (and hence also surface

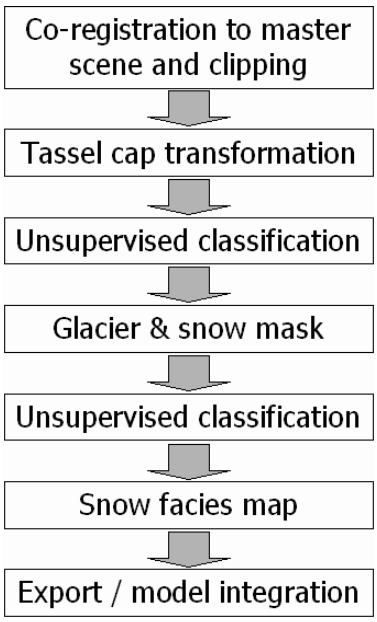

Fig. 2 Flowchart of the processing chain.

type) for the mass balance years 1974/1975–2001/2002 using a grid-based mass balance model utilizing a 25-m resolution digital elevation model and driven by daily temperature and precipitation data from Glomfjord (39 m a.s.l.), a meteorological station located about 20 km north of Engabreen. Snow accumulation was computed using a linear increase of precipitation with increasing elevation along with a fixed threshold temperature to discriminate snow from rain, while melt was modelled from a temperature-index approach incorporating potential direct solar radiation (Hock, 1999), thus considering topographic effects other than elevation. Model parameters were calibrated for the period 1993/1994 to 2001/2002 and left unchanged for the modelling of the remaining period (1974/1975–1992/1993) used for model validation. Schuler *et al.* (2005) used mass balance measurements (area-averaged mass balances, mass balance gradients and point data) for model calibration and validation. Using satellite glacier facies maps we provide additional data for model validation and test the performance of the model to reproduce the snow line retreat derived from the satellite images.

RESULTS AND DISCUSSION

We validate the satellite derived facies maps by comparison to direct surface observations taken during mass balance measurements. Such data are limited since field visits rarely coincided with satellite overpasses. However, based on all available data, observations at stake locations agreed with the satellite derived classification of the nearest grid cell in 35 out of 38 cases (92%) giving some confidence in the facies analysis, although more ground data would be desirable.

The comparison of the satellite derived facies maps and the modelled surface type maps reveals an overall reasonable agreement (Fig. 3), thus providing additional confidence in the results of the distributed mass balance model. The strong altitude dependence of the melt on Engabreen is clearly captured by both data sets. Bare ice areas coincide during both the model validation (especially e.g. 13 August 1984) and the model calibration period (especially e.g. 17 July 2001 or 07 August 2002). Generally, the model results show less small-scale spatial variability in facies types compared to the observations, which can be expected if we bear in mind the simple formulation of accumulation within the model. Redistribution of snow is not considered in the accumulation model, and only spatial effects related to elevation and solar radiation are incorporated in the melt model. In contrast, the satellite-based facies maps show a patchier pattern, including small-scale effects of lower accumulation on convex terrain form, crevasse patterns, etc. This is especially visible in the data from 15 August 1988 and 08 September 2002. The comparison of the firn areas is hampered due to lack of available detailed data; Schuler *et al.* (2005) ran the model with a constant firn line. The area above 1100 m a.s.l. was assumed to be underlain by firn once the winter snow cover has melted. For areas below this elevation an ice surface was assumed.

The bare ice areas can be classified with a high accuracy, whereas the spectral signatures in the wet snow areas leave more room for interpretation by the operator during the recoding of the unsupervised classification. The satellite based facies map in September 2002 shows snow on surfaces previously classified (August image 2002) as bare ice or firn. This is most likely due to late summer snowfalls that are not adequately

reproduced by the model. Although concurrent field observations are not available, field visits in late summer (20 August and 26 September) indicated snowfall events.

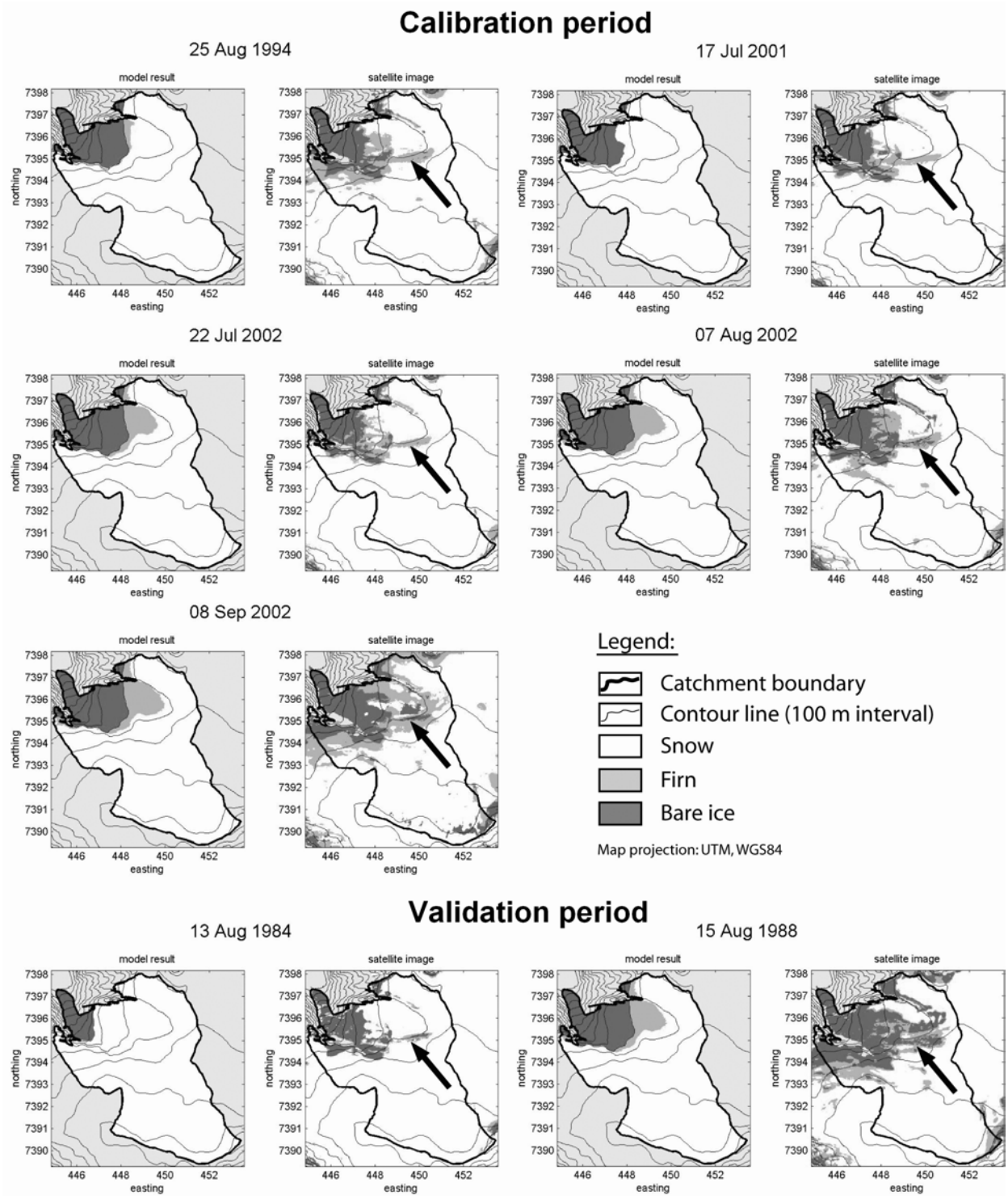

Fig. 3 Comparison of the satellite derived facies maps (right) and the results of the glacier mass balance model (left) for seven dates from 1984 to 2002. In 2002 three Landsat acquisitions enable more detailed model validation. Arrows mark feature discussed in the text.

The satellite data shows a narrow elongated feature (marked by an arrow in Fig. 3), which is persistent in all data sets. This striking pattern is not reproduced by the model results. However, the feature coincides with an area of enhanced topographic shading and reduced potential direct solar radiation (Fig. 4) compared to its immediate vicinity. This suggests that the feature detected in the satellite image may have been caused by illumination effect in the satellite data. Alternatively, the area accumulates less snow due to the topographic anomaly, and thus firn is exposed earlier than in the surroundings. In any case, the synergetic use of the distributed mass balance model also supports the interpretation of the satellite data and *vice versa*. For accurate topographic correction, radiative transfer modelling and an accurate DEM are needed. As the DEM quality was not considered sufficient, simpler approaches were taken into account. Hall *et al.* (1987) used a band ratio TM4/TM5 to improve the discrimination of facies in shadow areas and Dozier (1989) deployed a normalized differential snow index (TM2-TM5)/(TM2+TM5) to overcome illumination effects as well as pixel saturation over glaciated and snow covered areas. For the present study these measures did not reveal significant improvements in the classification. Heiskanen *et al.* (2003) confirm this indirectly. They applied a cosine correction to eliminate terrain effects at the Engabreen site; however, their pre-processing steps obviously could not remove the reported feature. This might be interpreted as a further indication for a real bare ice area due to reduced accumulation.

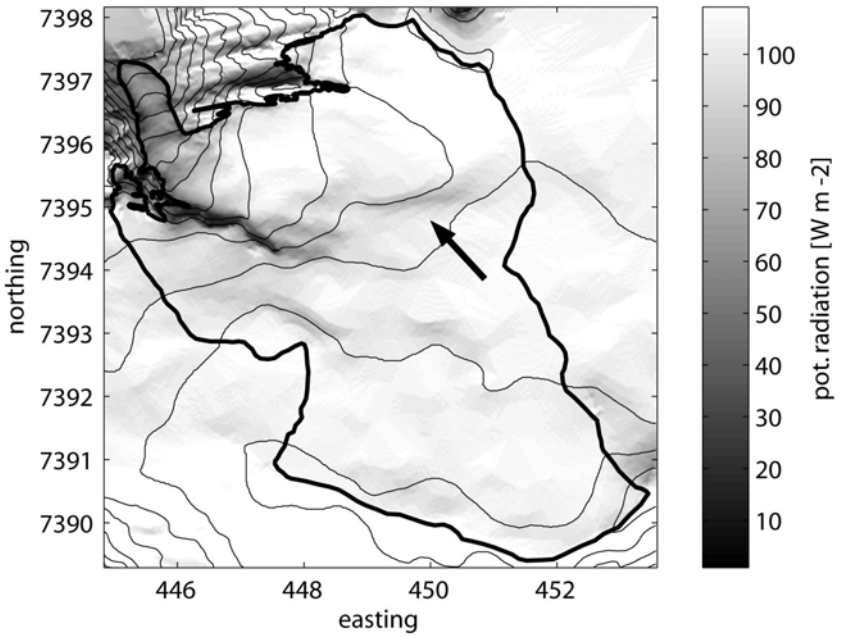

Fig. 4 Annual mean potential direct solar radiation for Engabreen as computed by the distributed mass balance model. Arrow marks feature discussed in the text.

In the lower right corner of the satellite facies maps partially outside Engabreen but on the ice cap, some bare and firn patches appear in some of the images. This is most likely a real feature related to blowing snow and resulting lower accumulation and consequently earlier bare ice appearance.

CONCLUSIONS AND OUTLOOK

We have presented a comparatively fast and efficient method to extract glacier facies maps from Landsat satellite data. As well as a suitable reference, an experienced operator is required for recoding of the unsupervised classifications. Some direct observations at various locations agreed well with the surface types derived for the closest pixel from the satellite images. Although more ground truth data would be needed to independently validate the glacier facies maps, the comparison with the model results suggests that the remote sensing products provide a valuable additional base to validate a distributed mass balance model. Agreement was generally reasonable, although some ambiguities arising from the spectral similarity of snow and firn in the remote sensing data still remain and require further refinement of the method. Furthermore the distributed modelling was limited by insufficient input data leading to the assumption of a fixed firn line at 1100 m altitude. Discrepancies between the model and remote sensing maps can be explained either by the complex pattern of snow accumulation, which is not captured by the model formulation, or by illumination effects which are difficult to extract from the Earth Observation data. The remote sensing product would certainly also support the validation of more complex accumulation routines incorporating other variables than altitude.

Although, as yet, remote sensing cannot provide quantitative information on, e.g. snow water equivalent, the summer facies maps enable highly valuable spatial information (difference between bare ice, snow and firn, and thus snowline retreat) for the validation of the mass balance models at different dates. At the same time the precisely co-registered satellite images can be used to extract and visualize changes in glacier front positions.

Future activities should also incorporate weather independent SAR data as a more frequent source of facies maps (or maps of radar glacier zones – terminology is ambiguous). The direct use of remote sensing products to initialise the model will also be analysed. Another option would be to investigate if the temporal evolution of SAR backscatter on the glacier over a season can be brought into a relationship or correlation with observed mass balance.

Acknowledgements This project is part of the Global Monitoring for Environment and Security (GMES) initiative “The Northern View” financed by the European Space Agency (ESA) under ESRIN/contract no. 17062/03/I-IW.

REFERENCES

Kjøllmoen, B. (ed.), Andreassen, L. M., Engeset, R. V., Elvehøy, H., Høivik, L.P. & Jackson, M. (2003) Glaciological investigations in Norway in 2001. NVE Report 1-2003.

Braithwaite, R. J., Zhang, Y. & Raper, S. C. B. (2003) Temperature sensitivity of the mass balance of mountain glaciers and ice caps as a climatological characteristic. Z. *Gletscherkd & Glazialgeol*. **38**(1), 35–61.

Braun, M. & Hock, R. (2004) Spatially distributed surface energy balance and ablation modelling on the ice cap of King George Island (Antarctica). *Glob. Plan. Change* **42**, 45–58.

Braun, M., Rau, F., Saurer, H. & Goßmann, H. (2000) The development of radar glacier zones on the King George Island ice cap (Antarctica) during the austral summer 1996/97 as observed in ERS-2 SAR data. *Ann. Glac.* **31**, 357–363.

Dozier, J. (1989) Spectral signature of Alpine snow cover from the Landsat Thematic Mapper. *Remote Sens. Env.* **28**, 9–22.

Hall, D. K., Chang, A. T. C. & Siddalingaiah, H. (1988) Reflectances of glaciers as calculated using Landsat 5 Thematic Mapper data. *Remote Sens. Env.* **25**, 311–321.

Hall, D. K., Xormsby, J. P., Bindschadler, R. A. & Siddalingaiah, H. (1987) Characterization of snow and ice reflectance zones on glaciers using Landsat TM data. *Ann. Glac*. **9**, 104–108.

Heiskanen, J., Kajuutti, K., Jackson, M., Elvehoy, H. & Pellikka, P. (2003) Assessment of glaciological parameters using Landsat satellite data in Svartisen, Northern Norway. *EARSeL e-Proc.* **2**(1), 34–42.

Hock, R. (1999) A distributed temperature index ice and snow melt model including potential direct solar radiation. *J. Glaciol.* **45**(149), 101–111.

Kjollmøen, B., Andreassen, L. M., Engeset, R. V., Elvehøy, H. & Jackson, M. (2003) Glaciological investigations in Norway in 2002. NVE Report 3-2003.

Klok, E. J. & Oerlemans, J. (2002) Model study of the spatial distribution of the energy and mass balance of Morteratschgletscher, Switzerland. *J. Glaciol*. **48**(163), 505–518.

König, M., Winther, J.-G. & Isaksson, E. (1999) Measuring snow and glacier ice properties from satellite. *Rev. Geophys.* **39**(1), 1–27.

Richards, J. A. (1995) *Remote Sensing Digital Image Processing. An Introduction*. Springer-Verlag, Berlin, Germany.

Schuler, T., Hock, R., Jackson, M., Elvehoy, H., Braun, M., Brown, I. & Hagen, J.-O. (2005) Distributed mass balance and climate sensitivity modelling of Engabreen, Norway. *Ann. Glaciol.* **42**, 395–401.

Sidjak, R. W. & Weathe, R. D. (1999) Glacier mapping of the Illecillewaet icefield, British Columbia, Canada, using Landsat TM and digital elevation data. *Int. J. Remote Sens.* **20**(2), 273–284.

Williams, R. S., Hall, D. K. Jr. & Benson, C. S. (1991) Analysis of glacier facies using satellite techniques. *J. Glaciol.* **37**, 120–127.

Glacier Mass Balance Changes and Meltwater Discharge (selected papers from sessions at the IAHS Assembly in Foz do Iguaçu, Brazil, 2005). IAHS Publ. 318, 2007.

Inventory of glacier-front positions using CBERS-2 data: a case study for the Bolivian Andes

RAFAEL R. RIBEIRO[1], JEFFERSON C. SIMÕES[1], JORGE ARIGONY-NETO[1,2] & EDSON RAMIREZ[3]

1 *Núcleo de Pesquisas Antárticas e Climáticas, Depto. Geografia, Instituto de Geociências, Universidade Federal do Rio Grande do Sul, Porto Alegre, Brazil*
jefferson.simoes@ufrgs.br; rrr.3@pop.com.br

2 *Institut für Physische Geographie, Albert-Ludwigs-Universität Freiburg, Germany*

3 *Universidad Mayor de San Andrés, IHH, La Paz, Bolivia*

Abstract For the first time, products of the China–Brazil Earth Resources Satellite (CBERS) are used for Andean glaciers studies. In this paper we compare results from previous ground studies with our observations using two scenes acquired by the High Resolution Charge Coupled Device (CCD) and the Infra-Red Multispectral Scanner (IRMSS) aboard the second Chinese–Brazilian satellite (CBERS-2), to establish an inventory of glacier frontal positions from 1975 to 2004 in the Cordillera Tres Cruces, Central Bolivia. All studied glaciers have retreated since 1974 (by up to 409 m) agreeing with ground studies. The use of CBERS-2 can contribute to establish an inventory of Andean glaciers as it covers the same area each 26 days.

Key words remote sensing; glacier inventory; CBERS-2

INTRODUCTION

Andean glaciers play an important role in the hydrological and social-economic systems of many countries. For example, they are essential to supply drinking water to local communities; produce energy in hydroelectric power plants; supply water for agriculture; and have scenic values in tourism. In La Paz (Bolivia), for instance, 70% of the water used by the population comes from glaciers.

Mountain glaciers, in general, lost mass during the 20th century (Dyurgerov & Meier, 2000). This is a process that can be attributed both to a general atmospheric warming and to regional climatic variability (Meier, 1984). Altogether, melting of mountain glaciers, ice caps and parts of the Antarctic and Greenland ice sheets, are the main contributors (70%) to sea level rise; the rest is mainly due to the thermal expansion of the ocean water (Church *et al.*, 2001). Though mountain glaciers constitute less than 1% of the cryosphere volume, it is estimated that they contributed with ¼ of the sea level increase between 1988 and 1998 (Dyurgerov, 2003). In short, mountain glaciers are considered by the Intergovernmental Panel on Climate Change (2001) as one of the main contributors to future sea level rise and key indicators of climate change.

Accurate determination of mountain glacier changes may be useful for assessing regional hydrological balance and water supply. One of the methods for these evaluations consists of measuring temporal differences in the frontal part of glaciers

(extent and altitude). Unfortunately, the great majority of mountain glaciers are in remote areas where traditional topographic surveys are expensive, if not impossible. The main solution is to integrate the scarce field data obtained by traditional methods with remote sensing data (Reinhardt & Rentsch, 1986).

In recent years, Landsat and Advanced Space Borne Thermal Emission and Reflection Radiometer (ASTER) images data have been used to create a glacier inventory (Kääb *et al.*, 2002), for example, through the Global Land Ice Measurement from Space (GLIMS) programme. Yet, some parts of the Andes do not have good imagery coverage. On the other hand, since 2001, a new opportunity arose from the launch of the China-Brazil Earth Resources Satellites (CBERS). In this paper we compare results from previous studies (Jordan, 1991, 1998) with two scenes acquired by the High Resolution Charge Coupled Device (CCD) and the Infra-Red Multispectral Scanner (IRMSS) aboard the second Chinese-Brazilian satellite (CBERS-2), to establish an inventory of glacier frontal positions over the last 30 years in the Cordillera Tres Cruces, Bolivia (67°22′–67°32′W and 16°47′–16°09'S, Fig. 1).

In this paper we show results of the first application of CBERS visible and near-infrared imagery for glaciological studies, integrating remote sensing data with the geographic information system (GIS) techniques. Glaciers' features, such as extent and

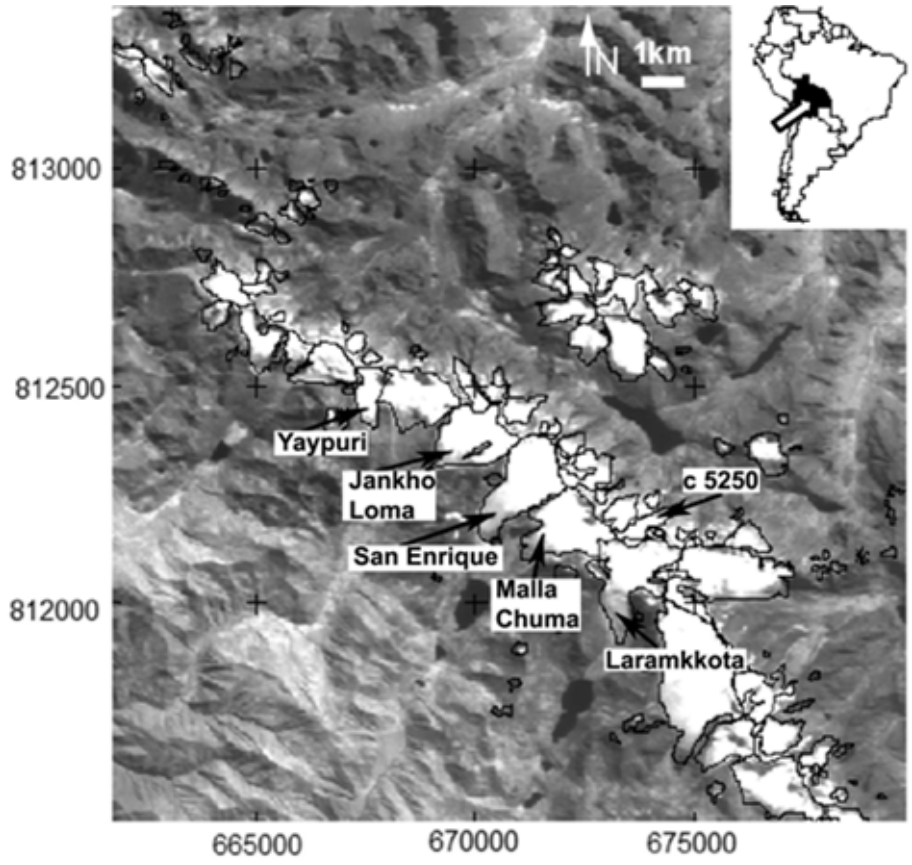

Fig. 1 A CBERS-2 CCD band 3 image (19 May 2004) of Tres Cruces Cordillera (Bolivia), thin black lines outline glacier drainage basins as identify in a 1975 topographic map (Jordan, 1991). The arrow in the inset locates this mountain range in South America (black area marks the Bolivian territory).

terminus altitude, and 30-year trends were computed. Results are then compared with glacier-front position manually digitized from the image.

STUDY AREA

The mountain range Tres Cruces (Quimsa Cruz in Aymara) is approx. 35 km long and 10 km wide; it is about 150 km east of the city of La Paz (16°30′S, 68°09′W). These mountains begin to the southeast of the La Paz River, extending up to the city of Ventillaque. In 1975, the total glacier area was 39 km^2 (Jordan, 1998), distributed in 156 drainage basins. Several peaks reach more than 5000 m above sea level; the highest are the Jachancuncollo (5900 m) and the Gigante Grande (5807 m). Several lakes exist in front of these glaciers, of which the most extensive are Huallatani, Laramkkota, Octa Kkota and Chatamarca. The source of the River Miguillas, where there are four small hydroelectric power plants, forms by melting of some glaciers in these mountains.

The regional climate is marked by two strongly distinct annual seasons (Kaser & Osmaston, 2002). In summer (October–May), the intertropical circulation influences the meteorological settings, precipitation occurring due to the humid air masses coming from the Amazonian region. Winter (June–September) is the dry season when air masses coming from the southwest predominates and do not bring precipitation. Therefore, the total summer precipitation is the main control of the glaciers annual mass balance.

REMOTE SENSING DATA

CBERS–2

The CBERS program results from a Brazilian–Chinese partnership in the space technical scientific segment. The launch of the CBERS-2 occurred on 21 October 2003. It carries three sensors: a CCD, an IRMSS, and a Wide Field Imager (WFI). Its orbit is helios-synchronous at 778 km of altitude, performs about 14 revolutions a day allowing a complete coverage of the Earth each 26 days (www.cbers.inpe.br). In this study, we use two CCD and IRMSS scenes acquired on 19 May 2004. The Brazilian Instituto Nacional de Pesquisas Espaciais (INPE) provides South American CBERS-2 images free of charge for registered researchers. Table 1 shows the characteristics of these two images.

Table 1 Specifications of CBERS-2 CCD and IRMSS sensors used in this work.

Cameras	Band/Name	Range (μm)	Spatial resolution (m)	Swath (km)
CCD	2	0.52–0.59 μm (green)	20	113
	3	0.63–0.69 μm (red)	20	113
	4	0.77–0.89 μm (near infrared)	20	113
IRMSS	1	0.50–1.10 μm (panchromatic)	80	120
	2	1.55–1.75 μm (middle infrared)	80	120

DEM

A digital elevation model (DEM), based on a topographic map, complements the study. DEM is a representation of the surface by a digital environment. In glaciology it is useful for detecting changes in glacier geometry (e.g. size, slope and orientation). Different algorithms of interpolation can be used to obtain a DEM; the final product quality depends on the density and distribution of reference points used to generate the model. It is important, therefore, to know which interpolation method results in the smallest error.

Digitized topographic data came from a 1:70 000 map, produced from 1975 aerial photographs using stereophotogrammetric methods (Jordan, 1991). It is a work produced by the Institut für Photogrammetrie und Ingenieur-Vermessungen e Geographisches, University of Hanover, Germany.

These data were used to "create" an elevation grid with 20 m of resolution. We tried two interpolation techniques, Triangulated Irregular Network and TOPOGRID (using Arc-Info^{TM} 8.0.1); the latter produced the smallest error (mean of ±4 m). To verify each model, we used control points not employed in the interpolation process, for example, fluvial drainage lines and other water bodies.

METHODOLOGY

The two satellite images used in this work (Table 1) were acquired at the end of the dry season, when the superficial snow pack is at its annual minimum, which facilitates the identification of the glacier limits. A thick seasonal snow cover makes a correct delineation of a glacier front position difficult, especially when rock outcrops are not spectrally identified because of radiative similarities. Furthermore, sensor calibration of the CBERS-2 data is not yet possible (calibrating coefficients, e.g. gain and slope, are not yet available to users).

The 1975 topographic map was taken as the reference for geometric corrections. We used the ERDASTM software for data co-registration, and the two CBERS-2 CCD and IRMSS images were georeferenced using 20 ground control points (GCP), with a first-degree polynomial transformation and nearest neighbour resampling (20 m and 80 m per pixel, respectively, for CCD and IRMSS data). The root-mean-square error (RMSE), obtained from the geometric correction procedure, is 1.88 pixel for CCD and 2.11 pixel to IRMSS image. After this correction, two different methods for glacier front position delimitation were tested (Fig. 2); their results were superimposed and compared with the manual delineation (discussed above).

Ratio bands, combined with the digital elevation model, were used to separate glaciers/snow features from surrounding land (Paul *et al.*, 2002). The DEM is particularly useful in shadowed areas where surface spectral variations are strongly reduced, resulting in difficult target discrimination. To apply this methodology with CBERS-2 data requires the following ratio segmentation: (first method) IRMSS channel 2 and CCD channel 4; (second method) IRMSS channels 1 and 2. To use ratio bands, in the first method, we integrated CCD with IRMSS data (the latter was resampled to 20 m) using bilinear interpolation.

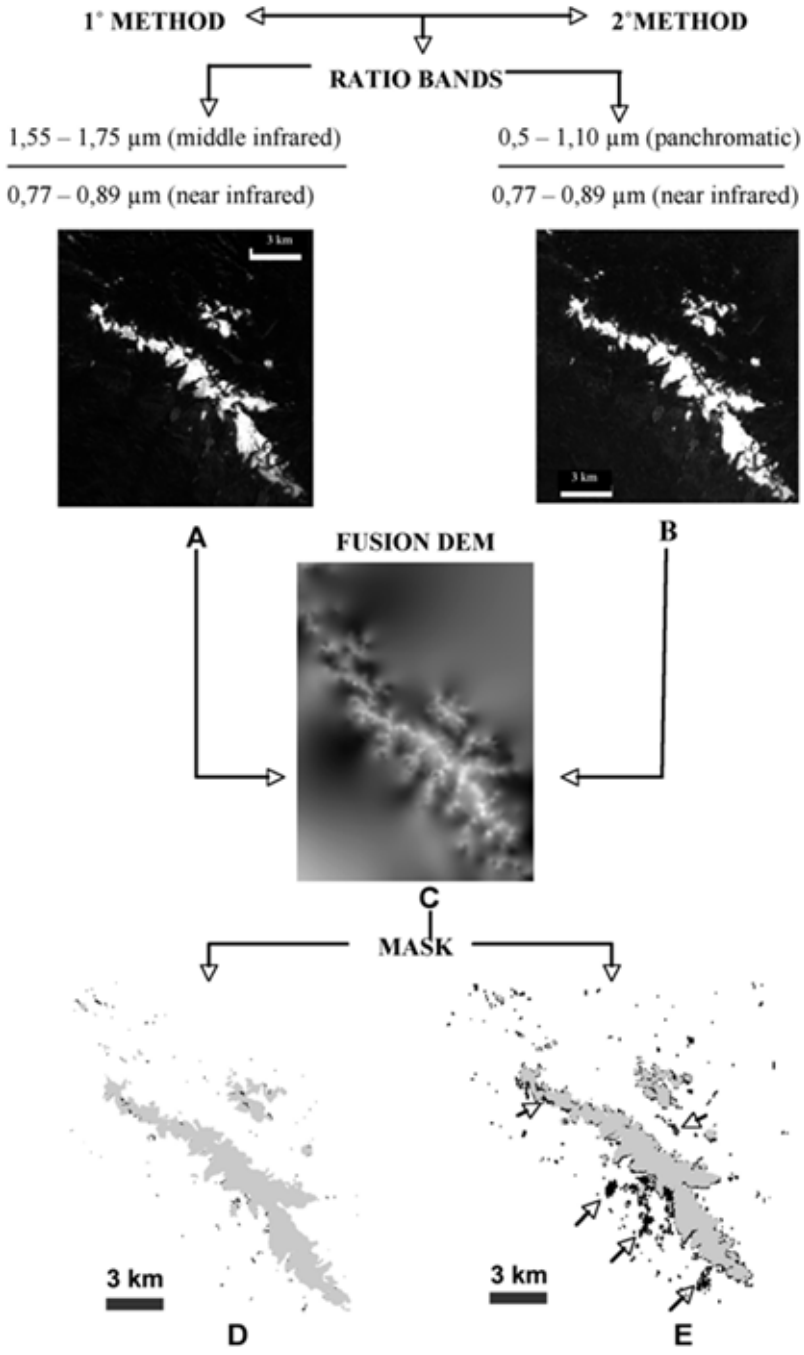

Fig. 2 Glacier masks workflow obtained from IRMSS band 2/CCD band 4 (a,c,d) and IRMSS band 1/IRMSS band 2 (b,c,e). Grey areas mapped by manual delimitation, only ratio bands map black ones. Arrows in "e" indicate where shadows and water were mapped as glacier area by the second method (only corrected identified by visual inspection of the image).

For each method, threshold values were estimated by visual inspection, using ratio bands with a DEM fusion to obtain a glacier mask. The margins of glaciers were identified by converting data from raster to vector format. Data were then transferred to Arcview^{TM} GIS 3.2 software, to construct polygons of glacier termini changes.

Glacier front positions changes can then be observed in the overlay map using different time polygons. Integration of glacier maps with the DEM allowed determination of a glacier terminus altitude. Figure 2 shows the workflow used in this work to determine glacier front position from CBERS-2 satellite image ratio bands.

RESULTS AND DISCUSSION

The difference of reflectivity between the visible (high for snow and ice) and middle infrared (low for the same targets) allows glacier classification from segmented glacier map CBERS–2 data, applying the methodology of Paul *et al.* (2002).

The two methods (Fig. 2) were superimposed and compared with the manual delineation results, in combination with band 3 CCD image equalized histograms, allowing us to determine termini position changes of six glaciers for the period 1975–2004: Yaypuri, Jankho Loma, San Enrique, Malla Chuma, Laramkkota and c 5250 (Fig. 1). The best results are provided by the use of IRMSS channel 3 with CCD channel 4 (Fig. 3). It is not possible to clearly discriminate shadows/water from ice/snow targets using the IRMSS band 2/CCD band 4 ratio due to the lower spatial resolution (80 m).

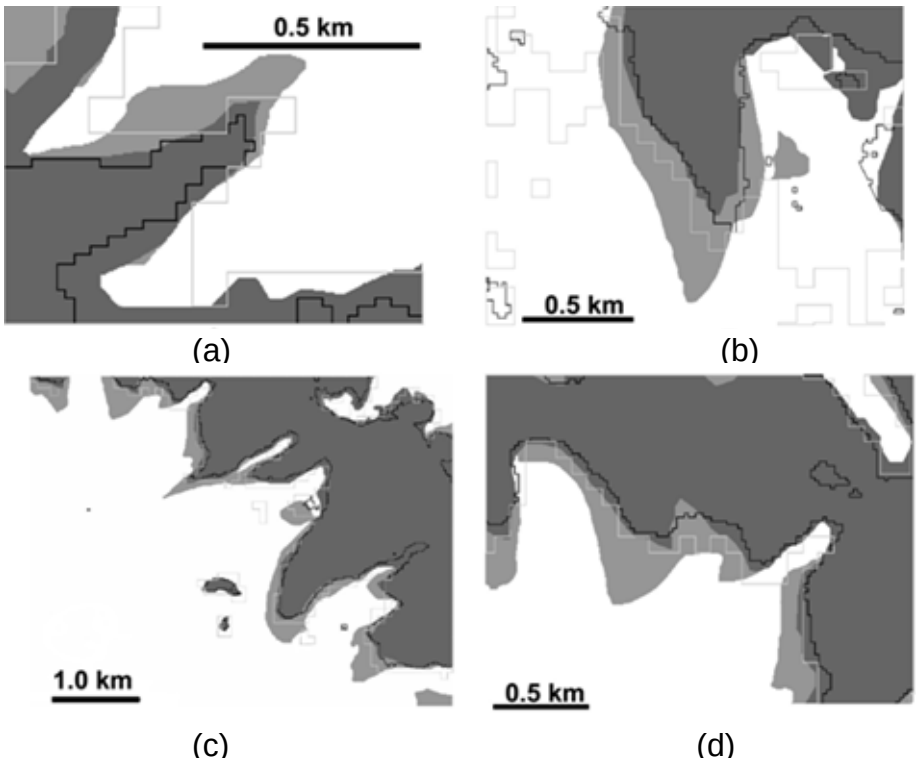

Fig. 3 The six glaciers fronts studied in this work: (a) c 5250; (b) Laramkkota; (c) Malla Chuma, San Enrique, Jankho Loma; (d) Yaypuri. Light grey areas are glacier terminus as found in 1975 (Jordan, 1991), manual delimitation over the 2004 CBERS-2 images are in dark grey. The thin light grey line represents ice front positions as determined by the band IRMSS band 2/CD band 4 ratio; the thin black line represents delimitation using IRMSS channel 3 with CD channel 4, used for the Tres Cruces Cordillera glaciers inventory.

For the first method we integrated CCD with IRMSS images, after a 20-m resampling of the latter. We estimated the uncertainty between the images (Table 2) using the formula by Hall *et al.* (1992), as we do not have any ground topographical survey which prevents verification of our results:

$$\text{Uncertainty} = (\text{IRMSS pixel resolution after resampling})^2 + (\text{CCD pixel resolution})^2]^{½} + \text{registration error}$$

We have:

$$\text{Uncertainty} = [(20)^2 + (20)^2]^{½} + 40 = 80 \text{ m}$$

Table 2 Uncertainty of the CBERS-2 CCD and IRMSS sensors.

Methods	Cameras/Channels			Uncertainty (m)
	IRMSS	IRMSS/Resampling 20 m	CCD	
1	–	2	4	±80
2	1	–	–	±160
	2	–	–	
DEM	–	–	–	±4

For the second method of construction of ratio bands no resampling of the images is needed, both have a spatial resolution of 80 m.

Table 3 shows the results of the glacial inventory for Tres Cruces Cordillera. All studied glaciers have retreated since 1974. On the east side of the Cordillera, glaciers retreated from 279 to 422 m (i.e. Malla Chuma Glacier); in general, the higher the 1974 ice front elevation, the greater the changes. The San Enrique Glacier is the only one on the west slope that does not follow this behaviour. The only glacier on the eastern slope (c 5250) had the smallest changes (an ice front retreat of 184 m), which is not an unexpected observation as the main source of precipitation is the Amazon basin. In all, our observations confirm results from other investigations concerning a general retreat of Bolivian glaciers during the last 30 years (Francou *et al.*, 2005).

Table 3 Changes in glacier length and terminus elevation between 1975 and 2004 in the Tres Cruces Cordillera (Bolivia).

Glacier	Year	Length (m)	Length Change	Elevation (m)	Elevation Change
Yaypuri	1975	1306	394 ± 80	4901	143 ± 4
	2004	912		5044	
Jankho Loma	1975	2263	409 ± 80	4890	135 ± 4
	2004	1854		5025	
San Enrique	1975	2443	279 ± 80	4943	128 ± 4
	2004	2164		5071	
Malla Chuma	1975	1727	422 ± 80	4946	182 ± 4
	2004	1305		5128	
Laramkkota	1975	2215	330 ± 80	4884	125 ± 4
	2004	1885		5009	
c 5250	1975	1248	184 ± 80	5050	62 ± 4
	2004	1064		5112	

CONCLUSIONS

This is the first application of CBERS data for glacier studies. The analysis of two satellite images gave satisfactory results in the ratio bands used (IRMSS channel 3 with CCD channel 4) for the delimitation of glacier frontal positions in Cordillera Tres Cruces. There is a 40-m mean difference between results using this method and those obtained from manual digitization. Normalized bands differences (e.g. Normalized Difference Snow Index) were not established because CBERS-2 calibrating coefficients are not yet available to users and we do not have ground observations.

The use of CBERS-2 can contribute to establishing an inventory of glaciers from space, through an integration of remotely sensed data with a GIS. The great advantage of using CBERS-2 data is the no-cost policy. Furthermore, CBERS-2 revisits the same area each 26 days, allowing monthly monitoring of Andean glaciers.

All glaciers studied in the Tres Cruces Cordillera, in Central Bolivia, have retreated since 1974 (up to 409 m until 2004). This observation agrees with ground monitoring studies that found a general reduction of the Bolivian glaciers over the last three decades.

REFERENCES

Burrough, P. A. & McDonnell, R. A. (1998) *Principles of Geographical Information Systems*. Oxford, Oxford University Press, Oxford, UK.

Church, J., Gregory, J. M., Huybrechts, P., Kuhn, M., Lambeck, K., Nhuan, M. T., Qin, D. & Woodworth, P. L. (2001) Changes in sea level. In: *Climate Change 2001, The Scientific Basis: Contribution of Working Group I to the Third Assessment Report of the Intergovernmental Panel on Climate Change* (ed. by J. Houghton, Y. Ding, D. J. Griggs, M. Nouguer, P. Van Der Linder & D. Xiaou), 639–694. Cambridge University Press, Cambridge, UK.

Dyurgerov, M. B. (2003) Mountain and subpolar glaciers show an increase in sensitivity to climate warming and intensification of the water cycle. *J. Hydrol.* **282**, 164–176.

Dyurgerov, M. B. & Meier, M. F. (2000) Twentieth century climate change: evidence from small glaciers. *Proc. Nat. Acad. Sci.* **97**, 1406–1411.

Francou, B., Ribstein, P. Wagnon, P. Ramirez, E. & Pouyaud, B. (2005) Glaciers of the Tropical Andes, indicators of the global climate variability. In: *Global Change and Mountain Regions: An Overview of Current Knowledge* (ed. by U. Huber, K. M. Harald & M. A. Reasoner). Springer, Berlin, Germany.

Hall, D. K., Williams, R. S. & Bayr, K. (1992) Glacier recession in Iceland and Austria. *EOS* (*Trans. Am. Geophys. U.*), **73**(12), 129–141.

INPE – Instituto Nacional de Pesquisas Espaciais (2006) http://www.cbers.inpe.br/pt/programas/cbers1-2_cameras.htm.

Jordan, E. (1991) Die Gletscher der bolivianischen Anden. PhD Thesis. Heinrich-Heine-Universitt, Stuttgart, Germany.

Jordan, E. (1998) Glaciers of Bolivia. In: *Satellite Image Atlas of Glaciers of the World: South America* (ed. by R. S. Williams Jr. & J. G. Ferrigno). US Geol. Survey. Professional paper, no.1386-I-5, I81–I108.

Kaser, G. & Osmaston, H. (2002) *Tropical Glaciers*. Cambridge University Press, Cambridge, UK.

Kääb, A., Huggel, C., Paul, F., Wessels, F., Raup, B., Kieffer, H. & Kargel, J. (2002) *Glacier Monitoring From ASTER Imagery: Accuracy and Applications* (Proc. EARSef-LISSIG-Workshop Observing our Cryosphere from from Space, Bern, 11–13 March).

Meier, M. F. (1984) Contribution of small glaciers to global sea level. *Science* **226**, 1418–1421.

Paul, F., Kääb, A. Maisch, M. Kellenberger, T. & Haeberli W. (2002) The new remote-sensing-derived Swiss glacier inventory: I. Methods. *Annals Glaciol.* **34**, 355–361.

Reinhardt, W. & Rentsch, H. (1986) Determination of changes in volume and elevation of glaciers using digital elevation models for the Vernagtferner, Otztal Alps, Austria. *Annals Glaciol.* **8**, 151–158.

Glacier Mass Balance Changes and Meltwater Discharge (selected papers from sessions at the IAHS Assembly in Foz do Iguaçu, Brazil, 2005). IAHS Publ. 318, 2007.

Recent glacier mass balance calculations at Volcán Mocho-Choshuenco (40ºS), Chilean Lake District

FRANCISCA BOWN[1], ANDRÉS RIVERA[1,2], CESAR ACUÑA[1] & GINO CASASSA[1]

1 *Centro de Estudios Científicos, Maipú 60, PO Box 1469, Valdivia, Chile*
fbown@cecs.cl

2 *Departamento de Geografía, Universidad de Chile, Santiago, Chile*

Abstract The majority of glaciers in the Chilean Lake District (38º–42ºS) have experienced shrinking and ice thinning during recent decades, presumably in response to climatic changes as observed at nearby meteorological stations. One of these glaciers is the southeastern basin of Volcán Mocho-Choshuenco (39°55′S, 72°02′W), a dormant volcano which has not experienced fumarolic activity since 1864. In order to analyse the glacier response to climatic conditions affecting this region, a monthly based mass balance programme was initiated in 2003. This paper presents new results and discusses the mass balance method applied during recent years. The 2004/2005 glacier average net mass balance yielded +0.36 ± 0.07 m w.e. year^{-1} (metres of water equivalent per year) with a winter balance of +4.04 m w.e. year^{-1} and a summer balance of –3.73 m w.e. year^{-1}. This positive mass balance is analysed in comparison to El Niño Southern Oscillation (ENSO) phenomena observed during recent years, as well as previous mass balance results.

Key words Chilean Lake District; climate changes; glacier mass balance; ice-capped volcanoes; precipitation

INTRODUCTION

The great majority of glaciers in the Chilean Lake District (Fig. 1(a)) are located on active volcanic cones (Rivera *et al.*, 2000), most of them showing retreating frontal tongues and ice thinning (Rivera *et al.*, 2002). Volcanic activity has been considered an important factor affecting glacier behaviour, especially when geothermal activity is enhancing ice melting at the bedrock (Björnsson, 1998). Glaciers are also considered an important factor when risk assessments are carried out on ice-capped active volcanoes, especially because of lahar generation during eruptive processes (Naranjo & Moreno, 2004). As a result of these glacier–volcano interactions, some glaciers might have experienced strong retreats due to volcanic activity (Casassa *et al.*, 2004), while other glaciers have been protected by thick ash-debris layer deposits which are insulating the ice from direct solar radiation (Rivera *et al.*, 2005).

This paper presents the mass balance results obtained for the 2004/2005 period at Volcán Mocho-Choshuenco (39°55′S, 72°02′W, Fig. 1), an active volcano during the Holocene but inactive in historical times since 1864 (González-Ferrán, 1995; Rodríguez *et al.*, 1999), having an important glacier over its depression or "caldera" (Echegaray, 2005).

This is the second year of mass balance data at the southeastern glacier since a monthly based monitoring programme was initiated in 2003. This glacier was selected

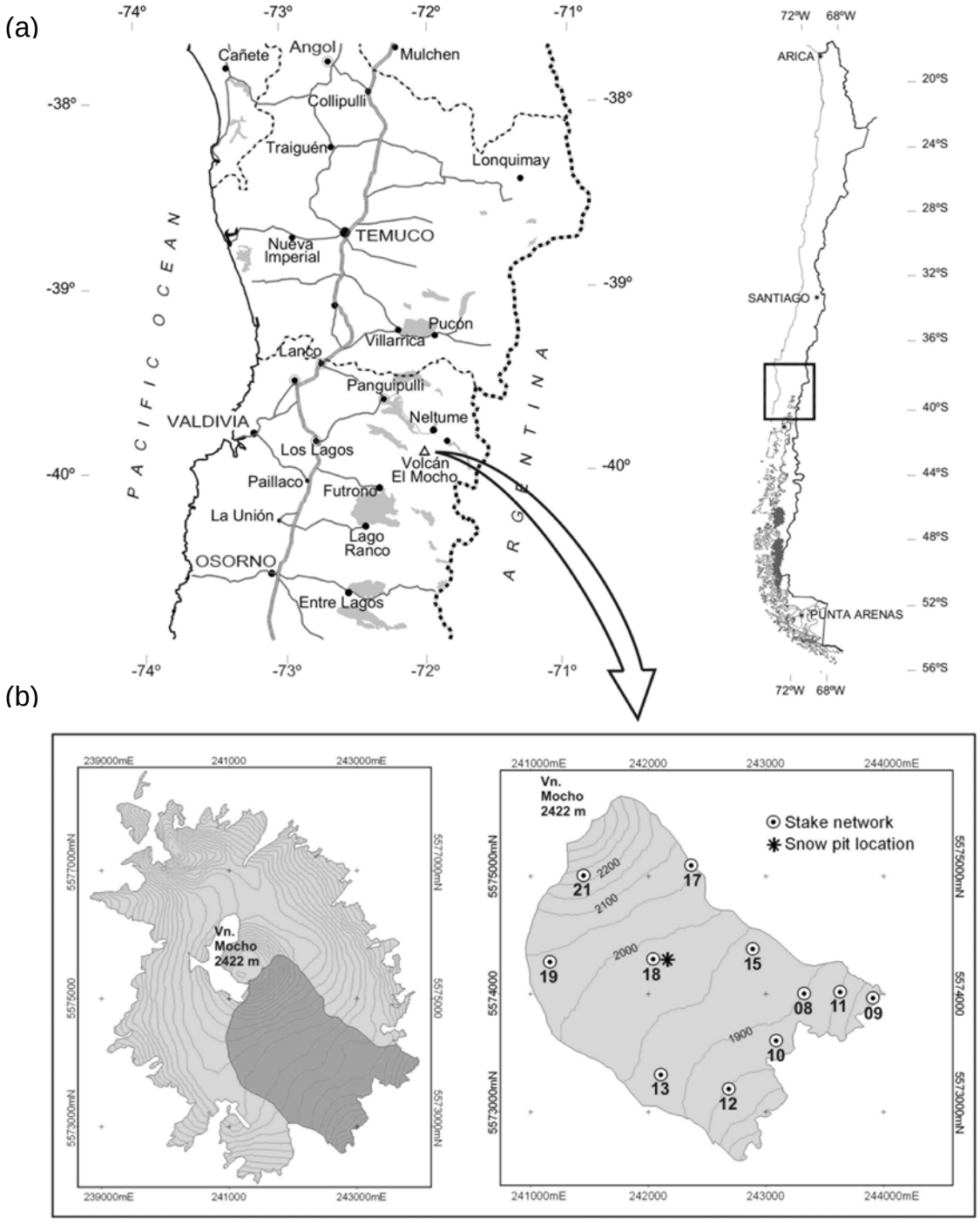

Fig. 1 Map of the Chilean Lake District showing the location of Volcán Mocho-Choshuenco (a). On (b), the ice limits of the whole volcano and the southeastern glacier are based on SRTM and geodetic GPS data (left). The stake network for mass balance measurements and snow pit location are shown on the right-hand side. Contour lines are expressed in m a.s.l. and coordinates in UTM-WGS 1984 system for all figures.

because of its accessibility and logistic facilities, being considered representative of glaciers located over volcanoes without present activity (Rivera *et al.*, 2005). The "glaciological" method was employed to account for the annual net glacier mass

balance, where a relatively dense stake-network was installed on the glacier and snow pits are periodically dug for measuring snow densities and surface snow structures.

Weather seasonality and maritime environment have been considered important factors when studying glacier mass balance (Holmlund & Schneider, 1997). Precipitation throughout the year in this part of the country varies according to the changing frequency of wind circulation and frontal systems from the Pacific Ocean. Thus, the annual as well as seasonal mass balances are estimated and compared with year to year fluctuations of precipitation and temperature, in order to discuss possible relationships between climatic trends and glacier responses.

METHODS

Glacier site and mass balance data collection

Glacier ice basins at Volcán Mocho-Choshuenco have been determined based upon SRTM data (Shuttle Radar Topography Mission) of 2000 and several geodetic quality GPS surveys carried out since 2003. The main glacier of the volcano was located in the southeastern flank of the cone, with a total area of 5.1 km^2 (Rivera *et al.,* 2005). However, due to deformations still remaining on steeper slopes of the volcanic cone, new resampling procedures were carried out recently with to date available data, allowing a more accurate determination of glacier area as 4.8 km^2 (Rivera *et al.,* 2006) (Fig. 1(b)).

Mass balance data have been collected almost continuously since the programme was initiated by Centro de Estudios Científicos in early 2003. A Chilean bamboo (coligüe) stake network was installed from the summit at 2422 m to 1750 m a.s.l., covering representative sectors of the glacier. Frequently many stakes located on steep flanks and at high altitude were missing due to strong westerly winds, or were buried beneath the surface because of avalanches and high snowfall affecting the volcano especially during the early ablation season. At lower sites, some coligües were complemented with 10 m-PVC (plastic) stakes drilled into the ice using a steam drill (Heucke, 1999). Some of these stakes drilled into the ice were totally covered by snow during the winter, but they emerged on the surface of the glacier during the summer season, allowing an annual estimation of ablation at each site. A total of 11 stakes were finally used for the analysis (Fig. 1(b)), where snow heights were measured on a monthly basis. Some missing snow-height values were derived by means of simple linear regression (>75% variance) between existing stakes.

In order to convert height differences (m) between successive dates into gains or losses of mass units, snow densities were measured throughout the year, mainly at a snow pit dug around stake #18 (Fig. 1(b)). Volume and weight of snow samples, as well as temperature and stratigraphic data were registered every 10 cm down to 100–120 cm depth using a 500 cm^3 metal device and a digital balance. Additionally, in late winter surface density measurements (upper 140-cm layer) were carried out with a "Mount Rose" sampling tube (Model 3600 "Federal") in every stake, including #18 (Fig. 1(b)). The inaccuracies of the snow pit data, when compared with Mount Rose densities at stake #18 at similar dates and depths were estimated to be 10%. Snow pit measurements were then used to calibrate density values per site/per date based on the resulting ratio of stake #18 and the snow pit data (Table 1).

Table 1 Surface snow/firn density (%) in September 2004 obtained with the "Mount Rose" sampling tube at several stakes and calculated density ratio with respect to stake #18.

Stake	Altitude (m a.s.l.)	Density (%)	Density ratio (density of stake/density of stake #18)
8	1917	45.0	1.02
9	1723	45.0	1.02
10	1908	45.0	1.02
11	1846	45.0	1.02
12	1853	54.5	1.24
13	1947	53.2	1.21
15	1947	50.0	1.14
17	2074	44.4	1.01
18	2013	44.0	1.0
19	2050	53.7	1.22
21	2169	47.3	1.08

Calculation of average glacier net mass balance

The hydrological year in this region of the country spans between the beginning of May and the end of the following April (Rivera *et al*., 2005). The "combined" net mass balance ($B_{n\ Combined}$) (Østrem & Brugman, 1991) for hydrological year 2004/2005, was calculated by the algebraic sum of the total annual accumulation (B_c) and ablation (B_a) considering the glacier as a whole. Due to the strong weather seasonality observed in this part of the country, the mass balance was separated into two main periods, i.e. the net winter and summer balances, B_w and B_s, respectively. The winter period was established when most of the accumulation takes place (May–October), with October marking the threshold between positive and negative height measurements, and the summer period being defined to take place between November and April, characterised by strong ablation and negligible accumulation.

According to Paterson (1994), the mass gain or loss of a glacier is an equivalent volume of water (w.e.) per area relative to the previous summer surface. Thus, the glacier average mass balance components mentioned above, e.g. net balance ($\overline{b_{n\ Combined}}$), net accumulation ($\overline{b_c}$), net ablation ($\overline{b_a}$), net winter balance ($\overline{b_w}$) and net summer balance ($\overline{b_s}$) are computed by dividing annual values of the whole glacier by the total area (A).

In order to obtain mass balance components (accumulation and ablation) for the glacier as a whole from discrete annual accumulated values obtained at each stake, several interpolation methods were applied, such as the Inverse Distance Weight (IDW), Triangular Irregular Network (TIN), Kriging and Bi-Cubic Spline. All these methods were based upon SRTM data for 2000 at 90-m resolution. The best interpolation method was determined using a "jack-knifing" procedure (Lythe *et al.*, 2001), yielding 15% inaccuracies on average when the TIN method was used.

RESULTS

In Table 1 density results obtained in September 2004 (spring time) are shown by using the "Mount Rose" device at 11 stakes. In all cases density values at stakes were

larger than the density at stake #18 and therefore, show ratios >1.0. Stakes located at lower altitude show generally higher density values, especially on the ablation season where ice density is expected (~90%), whilst upper sites show smaller but more homogeneous density ratio data throughout the year.

Accumulation obtained at stakes ranged from 3.0 to a maximum of 5.4 m w.e. year^{-1} (Table 2). The stakes were spatially distributed generally following a west–east trend, with maximum values near the western edge of the glacier at higher elevations (Fig. 2(a). At the steep summit cone (#21) accumulation decreases due to frequent snow avalanches. Minimum accumulation was detected on the lowermost northeastern side of the glacier.

Table 2 Mass balance components measured at the 11 stakes used for this study.

Stake	Altitude (m a.s.l.)	Accumulation (m w.e. year^{-1})	Ablation (m w.e. year^{-1})	Net winter balance (m w.e. year^{-1})	Net summer balance (m w.e. year^{-1})	Net balance (m w.e. year^{-1})
8	1917	3.1	–5.8	3.0	–5.7	–2.7
9	1723	3.3	–10.7	2.7	–10.1	–7.4
10	1908	3.5	–7.9	3.3	–7.7	–4.4
11	1846	3.0	–8.1	2.7	–7.8	–5.1
12	1853	5.3	–9.2	5.1	–9.0	–3.9
13	1947	5.3	–8.3	4.7	–7.7	–3.0
15	1947	4.3	–4.5	4.0	–4.2	–0.2
17	2074	4.5	–1.7	3.9	–1.1	2.8
18	2013	4.6	–1.2	3.9	–0.5	3.4
19	2050	5.4	–0.5	4.5	0.4	4.9
21	2169	4.3	–1.4	4.1	–1.2	2.9

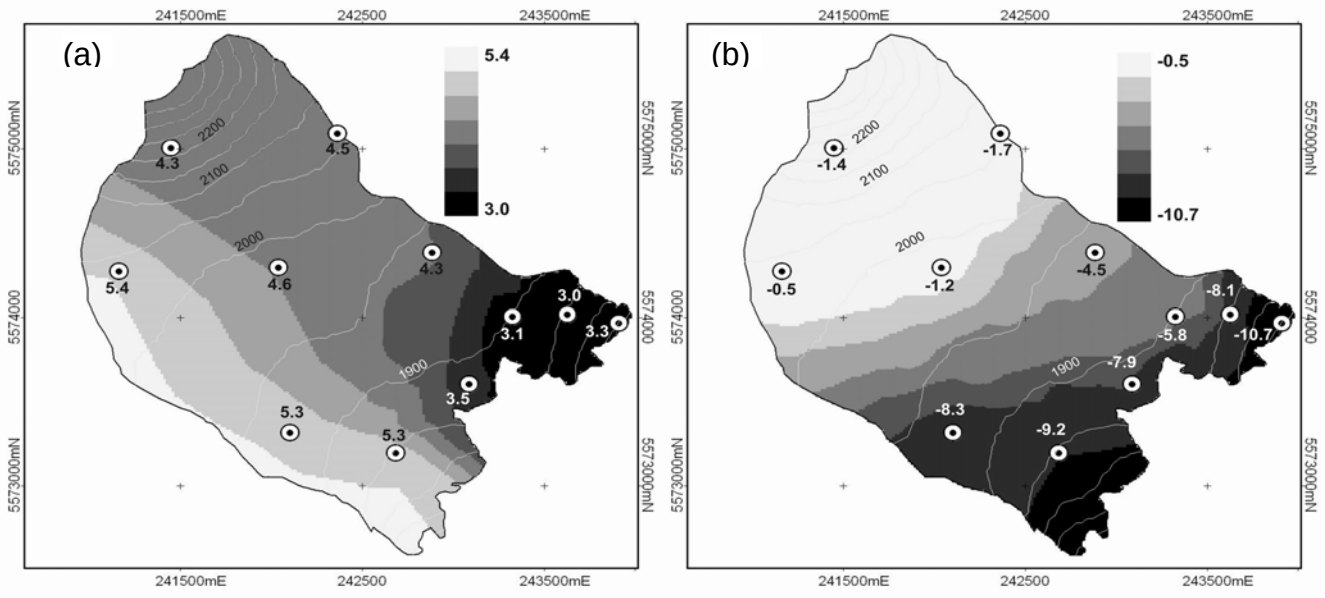

Fig. 2 Annual net accumulation (a) and ablation (b) in m w.e. year^{-1}. Individual values represent observations at each stake for all figures.

As expected, ablation measurements show a strong dependency on altitude, with the extreme negative value at lowermost stake #9 (–10.7 m w.e. year^{-1}) decreasing upstream up to a minimum of –0.5 m w.e. year^{-1} at stake #19 (Table 2). On steep flanks, some mass losses are enhanced by avalanches (Fig. 2(b)).

Seasonal mass balance components calculated per each stake are shown in Table 2. The winter balance showed a similar distribution to the annual accumulation, i.e. higher positive values at the southern side (>5 m w.e. year^{-1}) and progressive decrease towards the glacier front to the northeast (Fig. 3(a)). The summer balance showed negative values for almost the whole glacier area ranging from nearly "zero" m w.e. year^{-1} up to –10 m w.e. year^{-1}, except by the surroundings of stake #19 where there are small positive accumulations (Fig. 3(b)).

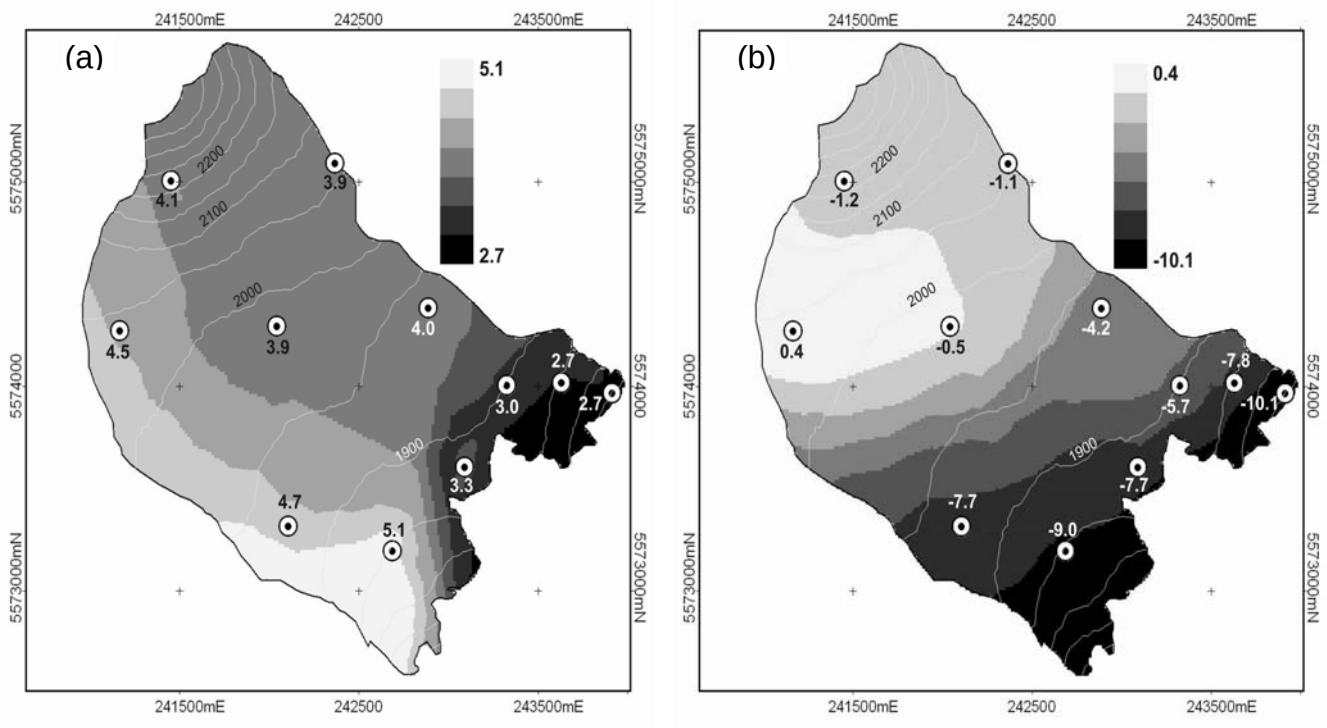

Fig. 3 Annual net winter (a) and summer (b) balance in m w.e. year^{-1}.

An average net mass balance of +0.36 ± 0.07 m w.e. year^{-1} was obtained at Volcán Mocho-Choshuenco in 2004–2005, with net accumulation and ablation of +4.48 and –4.12 m w.e. year^{-1}, respectively. The 20% uncertainty assigned to the net mass balance was calculated based upon the Root Mean Square (RMS) of independent errors, e.g. the snow-pit density measurements (10%) (Harper & Bradford, 2003), the stake-height field measurements (5%) and the selected interpolation method (15%). If the algebraic sum of seasonal balances is taken into account, a net mass balance of +0.31 ± 0.06 m w.e. year^{-1} is obtained, which is statistically equal to the net mass balance obtained by subtracting accumulation and ablation.

The Equilibrium Line Altitude (ELA) was estimated at 1961 ± 11 m a.s.l. defining an Accumulation Area Ratio (AAR) of 0.56.

Comparison to previous mass balance data

The final mass balance results are shown in Fig. 4. Table 3 summarizes average glacier values compared to the same parameters measured in 2003/2004 at glacier Mocho as well as Echaurren Norte, a glacier surveyed since the 1970s in central Chile.

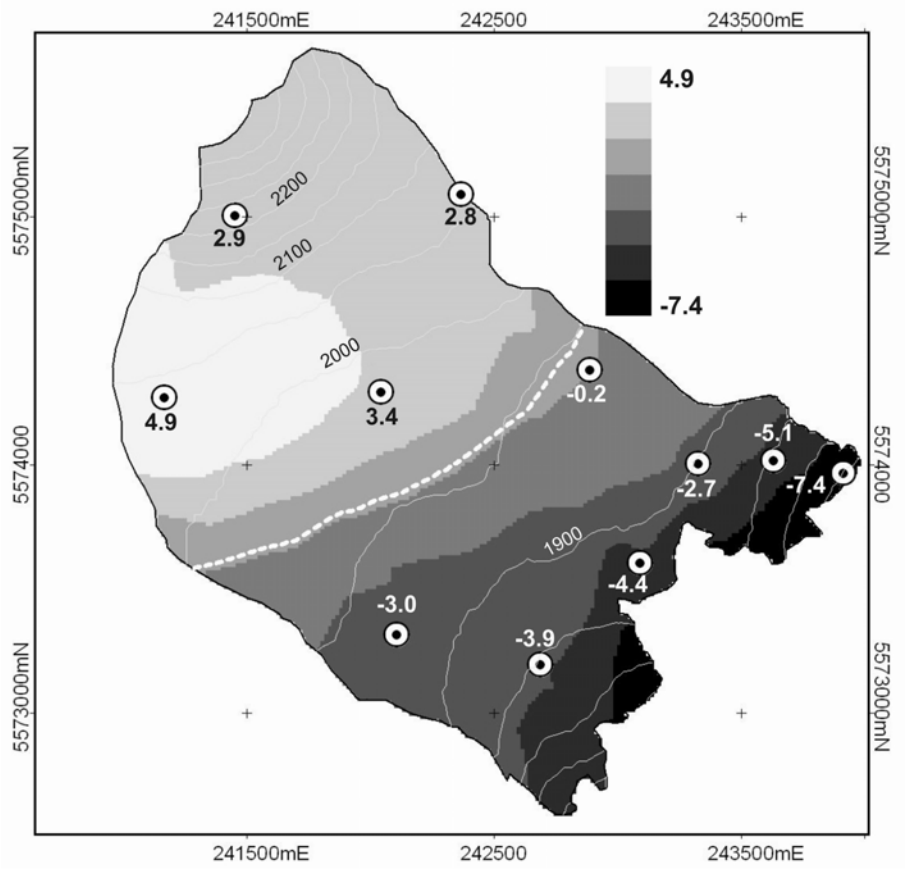

Fig. 4 Annual net mass balance in m w.e. year^{-1}. ELA location is shown as a dashed-white line.

Table 3 Average mass balance values at Glacier Mocho for the 2004/2005 period and its comparison with previous mass balance data.

Period	2003–2004		2004–2005
	Gl. Echaurren (33ºS)	Gl. Mocho (40ºS)	Gl. Mocho (40ºS)
Net accumulation (m w.e. year^{-1})	2.0	2.59	4.48
Net ablation (m w.e. year^{-1})	–2.57	–3.47	–4.12
Net winter balance (m w.e. year^{-1})	n/d	n/d	4.04
Net summer balance (m w.e. year^{-1})	n/d	n/d	–3.73
Net mass balance (m w.e. year^{-1})	–0.57	–0.88 ± 0.18	0.36 ± 0.07
ELA (m a.s.l.)	n/d	1956 ± 53	1961 ± 11
AAR	n/d	0.52	0.56
Sources	DGA, personal communication	Rivera *et al.*, 2005	This study

The most significant change experienced by the glacier between 2003/2004 and 2004/2005 was the higher accumulation rates in the latter period, which resulted in a positive annual mass balance. Higher ablation values were also detected in 2004/2005, particularly at lower altitudes, suggesting that 2004/2005 experienced a steeper mass balance gradient.

The ELA between both periods did not experience a significant change; however the AAR experienced a small increment from 0.52 to 0.56, which supports a more positive balance as measured during the last hydrological year.

DISCUSSION AND CONCLUSIONS

Long-term climate trends along the coast in southern Chile have shown a general near surface atmospheric warming, except for cooling detected in the Lake District (Rosenblüth *et al.*, 1997). However, in atmospheric levels above 850 hPa geopotential height (approximately at an altitude of 1500 m a.s.l., representing the mean elevation of glaciers in this region), temperatures exhibited a positive trend (Aceituno *et al.*, 1993; Bown & Rivera, 2007). Annual precipitation in the Chilean Lake District showed negative trends during the second half of the 20th century (Bown & Rivera, 2007), with the strongest decreases at Valdivia (–15 mm year^{-2}, 39º38′S) and Puerto Montt (–14 mm year^{-2}, 41º26′S).

These tropospheric warming and rainfall deficits, suggest negative long term glacier mass balances in the region. In spite of that, inter-annual variability could play an important role, especially in connection to El Niño Southern Oscillation (ENSO) events (Quintana, 2004).

The rainfall inter-annual variability in the Chilean Lake District has been teleconnected to the latitudinal migration of the southeastern Pacific Ocean anticyclonic cell (Montecinos & Aceituno, 2003), with reinforcement (weakness) of the southern edge of the anticyclonic cell during El Niño (La Niña) years, provoking dry (wet) summers. During recent years, however, ENSO phenomena have not shown any strong events, as illustrated by Sea Surface Temperature (SST) anomalies in El Niño region 3.4 (Trenberth, 1997) and the Southern Oscillation Index (Díaz & Markgraf, 2000). While a strong La Niña phase took place in 1999–2000, neutral and weak-to-moderate conditions have alternated thereafter, with the current period 2004–2005 being estimated as a weak El Niño year (Table 4).

Therefore these weak atmospheric–oceanic interactions are probably not the main driving factors affecting the glacier mass balance in the Chilean Lake District since 2003, and the occurrence of a negative mass balance in Glacier Mocho during 2003/2004 and a positive mass balance during 2004/2005, are probably responding to inter-annual variability of precipitation and temperature not related to ENSO. This behaviour is very distinctive when compared to the mass balance records obtained in central Chile, where the mass balance of Glacier Echaurren Norte is strongly dependent on the occurrence of ENSO events (Escobar *et al.*, 1995). For instance, during the moderate-weak El Niño year 2002/2003 the mass balance yielded +2.06 m w.e. year^{-1}, whereas in neutral ENSO year 2003/2004 the mass balance was –0.57 m w.e. year^{-1} (DGA, personal communication).

Table 4 Mean Sea Surface Temperatures (SST) in Region 3.4 and Southern Oscillation Index (SOI) standard deviations during the last 5 years*.

Year	Mean SST standard deviation Region 3.4	Mean SOI standard deviation	Classification
1999–2000	–1.08	0.70	Strong Niña
2000–2001	–0.42	0.60	Neutral
2001–2002	0.16	–0.28	Neutral
2002–2003	0.87	–0.80	Weak/moderate El Niño
2003–2004	0.29	–0.13	Neutral
2004–2005	0.61	–0.74	Weak Niño

* Monthly SST and SOI standard deviations obtained from NOAA-CIRES Climate Prediction Center and Australian Bureau of Meteorology, respectively. Annually-mean standard deviations and event classification obtained by this study.

Table 5 Annual precipitation in 2003 and 2004 at selected Chilean Lake District meteorological stations and deficit/surplus relative to the 1961–1990 climatological mean*.

Meteorological station	2003		2004	
	Precipitation (mm)	Deficit/surplus (%)	Precipitation (mm)	Deficit/surplus (%)
Temuco	917	–17	1149	4
Valdivia	1703	–6	1721	–5
Osorno	1075	–15	1290	2
Puerto Montt	1286	–24	1458	–14

* National Meteorological Office, personal communication.

The precipitation regime in the Chilean Lake District showed a clear deficit during 2003, especially significant in Puerto Montt, whilst 2004 exhibited “normal” behaviour (Table 5). No clear trends were observed regarding temperature between both years. However, the summer of 2004 was particularly dry and warm due to abnormal synoptic conditions, which were blocking frontal systems coming from the west, while the summer of 2005 was also dry, but not especially warm (National Meteorological Office, personal communication).

The above characterization of meteorological variables indicates that in the absence of strong ENSO events in the Pacific Ocean, the mass balance of Glacier Mocho is presumably more sensitive to rainfall variability and summer temperatures. Considering the synoptic circulation in this part of the country, the appearance of strong ENSO events should be reflected in opposed ways between central Chile and the Chilean Lake District, with positive (negative) mass balance in central Chile (Lake District) during El Niño years and *vice versa*.

Although measurements at the glacier located on Volcán Mocho-Choshuenco started only in 2003, the mass balance results seem to evidence climate driving factors. This suggests that volcanic activity plays a minor role on the glacier behaviour.

In spite of the above, further data are strongly needed to determine more accurate mass balance changes, as well as the relationships with climatic factors.

Acknowledgements This work was sponsored by Fondo Nacional de Ciencia y Tecnología of Chile (FONDECYT 1040515) and Centro de Estudios Científicos (CECS). CECS is a non-profit organization funded in part by the Millenium Science Initiative (ICM) and the Centro de Ingeniería de la Innovación. Marcos Rodríguez, Ronald Mella and Felipe Contreras surveyed the stake network and measured snow pits during monthly field campaigns. Jorge Quinteros performed "Mount Rose" snow density measurements. The logistic support of Víctor Petterman, Roberto Monroy and Ariel Amollado, from Fundo Huilo-Huilo, is acknowledged. Many thanks are given to the anonymous referees for their valuable recommendations.

REFERENCES

Aceituno, P., Fuenzalida, H. & Rosenblüth, B. (1993) Climate along the extratropical west coast of South America. In: *Earth System Responses to Global Change: Contrasts between North and South America* (ed. by H. A. Mooney, E. R. Fuentes & B. I. Kronberg) (Elsevier Science & Technology Books), 61–69. Academic Press Inc., San Diego, California, USA.

Björnsson, H. (1998) Hydrological characteristics of the drainage system beneath a surging glacier. *Nature* **395**, 771–774.

Bown, F. & Rivera, A. (2007) Climate changes and recent glacier behaviour in the Chilean Lake District. *Global Planet Change* **59,** 79–86.

Casassa, G., Acuña, C., Zamora, R., Schliermann, E. & Rivera, A. (2004) Ice thickness and glacier retreat at Villarrica Volcano. Boletín SERNAGEOMIN **61**, 53–60.

Díaz, H. & Markgraf, V. (2000) *El Niño and the Southern Oscillation. Multiscale Variability and Global and Regional Impacts*. Cambridge University Press, New York, USA.

Echegaray, J. (2005) Geological and geochemical evolution of the Mocho-Choshuenco Volcanic Center, Southern Andes, 40ºS. MSc Thesis, University of Chile, Santiago, Chile.

Escobar, F., Pozo, V., Salazar, A. & Oyarzo, M. (1995) Balance de masa en el glaciar Echaurren Norte, 1975 a 1992. Resultados preliminares. *Dirección General de Aguas*, H.A. y G., **95**(1).

González-Ferrán, O. (1995) *Volcanes de Chile*. Instituto Geográfico Militar, Santiago, Chile.

Harper, J. & Bradford, J. (2003) Snow stratigraphy over a uniform depositional surface: spatial variability and measurement tools. *Cold Reg. Sci. Technol.* **37**, 289–298.

Heucke, E. (1999) A light portable steam-driven ice drill suitable for drilling holes in ice and firn. *Geografiska Ann.* **81A**(4), 603–609.

Holmlund, P. & Schneider, Th. (1997) The effect of continentality on glacier response and mass balance. *Ann. Glaciol.* **24**, 272–276.

Lythe, M., Vaughan, D. & The Bed Map Consortum (2001) Bedmap: A new ice thickness and subglacial topographic model of Antartica. *J. Geophys. Res.* **106**(B6), 11335–11351.

Montecinos, A. & Aceituno, P. (2003) Seasonality of the ENSO-related rainfall variability in central Chile and associated circulation anomalies. *J. Climate* **16**(2), 281–296.

Naranjo, J. A. & Moreno, H. (2004) Laharic debris flows from Villarrica Volcano. In: *Villarrica volcano (39.5ºS), Southern Andes, Chile* (ed. by L. Lara & J. Clavero). Chilean Geological Survey, Bull. **61**, 28–38.

Østrem, G. & Brugman, M. (1991) *Glacier Mass Balance Measurements: A Manual for Field and Office Work.* Norwegian Water Resources and Energy Administration, and Environment Canada, National Hydrology Research Institute Science Report no.4, Saskatchewan, Canada.

Paterson, W. S. B. (1994) *The Physics of Glaciers*. Pergamon Press, London, UK.

Quintana, J. (2004) Study upon the factors explaining precipitation variability in Chile at the interdecadal timescale. MSc Thesis, University of Chile, Santiago, Chile.

Rivera, A., Casassa, G., Acuña, C. & Lange, H. (2000) Variaciones recientes de glaciares en Chile. *Rev. Invest. Geogr.* **34**, 29–60.

Rivera, A., Acuña, C., Casassa, G. & Bown, F. (2002) Use of remotely-sensed and field data to estimate the contribution of Chilean glaciers to eustatic sea-level rise. *Ann. Glaciol.* **34**, 367–372.

Rivera, A., Bown, F., Casassa, G., Acuña, C. & Clavero, J. (2005) Glacier shrinkage and negative mass balance in the Chilean Lake District (40ºS). *Hydrol. Sci. J.* **50**(6), 963–974.

Rivera, A., Bown, F., Mella, R., Wendt, J., Casassa, G., Acuña, C., Rignot, E. & Clavero, J. (2006) Ice volumetric changes on active volcanoes in Southern Chile. *Ann. Glaciol.* **43,** 111–122.

Rodríguez, C., Pérez, Y., Moreno, H., Clayton, J., Antinao, J., Duhart, P. & Martin, M. (1999) Geologic map of the Panguipulli-Riñihue area, Lake region, 1:100.000 scale. *Geologic maps series no. 10, Chilean Geological Survey*.

Rosenblüth, B., Fuenzalida, H. & Aceituno, P. (1997) Recent temperature variations in southern South America. *Int. J. Climatol.* **17**, 67–85.

Trenberth, K. (1997) The definition of El Niño. *Bull. Am. Meteorol. Soc.* **78**, 2771–2777.

Glacier Mass Balance Changes and Meltwater Discharge (selected papers from sessions at the IAHS Assembly in Foz do Iguaçu, Brazil, 2005). IAHS Publ. 318, 2007.

Crevasse detection in glaciers of southern Chile and Antarctica by means of ground penetrating radar

RODRIGO ZAMORA[1], GINO CASASSA[1], ANDRES RIVERA[1,2], FERNANDO ORDENES[1], GUILLERMO NEIRA[1,3], LUIS ARAYA[1,3], RONALD MELLA[1] & CLAUDIO BUNSTER[1]

1 *Centro de Estudios Científicos (CECS), Arturo Prat 514, PO Box 1469,Valdivia, Chile*
rzamora@cecs.cl

2 *Departamento de Geografia, Universidad de Chile, Chile*

3 *Centro de Estudios e Investigaciones Militares (CESIM), Chile*

Abstract Detection of crevasses is critical for safe travelling on glaciers. Here we present the use of a Ground Penetrating Radar (GPR) for crevasse detection. Experiments were made in temperate ice on Glacier Mocho, Volcán Mocho-Choshuenco, southern Chile (39°25′S) and in cold ice in East Antarctica (87°30′S). In southern Chile the radar was hand-carried 1.2 m in front of the operator who was walking over the glacier at a speed of ~0.5 m s^{-1}, while in Antarctica it was mounted on a 7-m long rod in front of a tractor convoy travelling at a speed of ~2 m s^{-1}. In both geographical sites profiles were made perpendicularly to crevasses ranging in width from 0.1 m to 1.0 m. Buried crevasses clearly show as apexes of diffraction hyperbolae, which could be detected down to a depth of 15 m. They show as discontinuities in the firn stratigraphy which have a width equal to the crevasse width, and associated diffraction hyperbolae to each side of the crevasse. The GPR proved to be a valuable tool for detecting crevasses, allowing for a reaction time of ~9 s (equivalent to ~4.5 m on the ground) in the case of the hand-carried system and ~5 s (or ~10 m on the ground) for the tractor system.

Key words Antarctica; crevasses; GPR; southern Chile; temperate ice

INTRODUCTION

Ground penetrating radar (GPR) has many subsurface applications, for example in mining, soil exploration, archaeology, groundwater exploration, detection of buried objects such as pipelines and mines, and forensic research (Daniels, 2004). Dry snow and ice are especially transparent to electromagnetic wave propagation at a wide range of frequencies from 1 MHz to 10 GHz, which allows studying in great detail the snow and glacier thickness, its internal stratigraphy and structure, and basal properties (Bogorodsky *et al*., 1985). Radar soundings at frequencies > ~100 MHz ($\lambda \approx 1.6$ m in ice) allows detection at sub-metre resolution and are especially adequate for studying the internal stratigraphy of seasonal snow cover and glaciers. The goal of this paper is to present results of GPR as a means to detect crevasses within glaciers.

The traditional view is that crevasses are formed perpendicular to the principal extending strain rate, in areas where the strain rate exceeds a critical threshold and the ice fractures as a brittle material (e.g. Vaughan, 1993; Pralong *et al*., 2003). This may happen at the margins of a glacier at shear zones in ice streams, at the front of a calving glacier, in steep areas of a glacier, or where the glacier flows over obstacles. At

depth (> ~20 m) the lithostatic (compressive) pressure of ice tends to close the crevasse, although much deeper crevasses have been found in Antarctica, and also in temperate glaciers with abundant meltwater. In the accumulation area of a glacier or during the autumn–winter–spring periods, crevasses may be covered by snow, with shallow/weak snow bridges, which can increase the risk of glacier travel. In large parts of Antarctica, crevasses might be snow covered at any time of the season. Numerous crevasse accidents have been reported in the literature, both in mountain glaciers and over ice sheets, including travel by foot (e.g. AAC, 2005) and by means of snow vehicles (http://news.bbc.co.uk/1/hi/world/americas/4297550.stm).

The GPR is a method of exploration based on the emission and propagation of electromagnetic waves in a dielectric media, with delayed reception of reflections that are produced in discontinuities within the substrate, as a result of sudden changes of the electromagnetic parameters, such as conductivity, dielectric permittivity and the magnetic permeability. In the last few decades GPRs have been used as the main method for studying ice depth, internal stratigraphy and also physical characteristics of the glacier bed, both in temperate and cold ice (Bogorodsky *et al*., 1985; Paterson, 1994).

The GPR method has also been applied successfully on glaciers for crevasse detection in support of selection of tractor traverse routes, both from the ground (e.g. Kovacs & Abele, 1974; Delaney *et al*., 2004) and from the air (e.g. Delaney & Arcone, 1995), as well as for the detection of buried objects and installations (e.g. Arcone *et al*., 1995). The ability of GPRs for crevasse detection has allowed very detailed studies of glacier dynamics (e.g. Retzlaff & Bentley, 1993; Clarke & Bentley, 1994) where the burial depth of crevasses has been linked to the glacier flow history.

This paper discusses the results of data collected using a GPR dragged on foot on Glacier Mocho-Choshuenco, Chilean lake district (39°25′S), and transported by means of a tractor in East Antarctica (87°30′S).

STUDY SITES

The data were collected at two locations, one in the Chilean Lake District and the other in east Antarctica. During May 2004 a radar survey was performed by two operators on foot on the eastern glacier of ice capped Volcán Mocho-Choshuenco (39º25′S, 71º57′W), Chilean Lake District (Fig. 1), where mass balance measurements are routinely carried out by Centro de Estudios Científicos (CECS), Chile. Measurements over the glacier are normally performed using a Pisten Bully 200 snow tractor, but sporadically with a snowmobile, or on foot when snow vehicles are not available. The Volcán Mocho-Choshuenco is active, although it has been dormant since the last eruption in 1864 (Gonzalez-Ferrán, 1995). This temperate glacier has been receding during the last few decades in response to regional warming and also partly to precipitation decrease (Rivera *et al*., 2005). It had an area of 5.1 km^2 in 2004, extending from an elevation of 1603 m a.s.l. to 2422 m a.s.l. with an equilibrium line altitude located at 1956 m in 2003/2004, when the mean net accumulation yielded 2.6 m w.e.$year^{-1}$, the mean net ablation was –3.5 m w.e.$year^{-1}$ and the net mass balance resulted in –0.88 m ± 0.09 m w.e.$year^{-1}$ (Rivera *et al*., 2005). Crevasses occur in several sectors of the glacier, both in the accumulation and in the ablation areas, being largely covered by

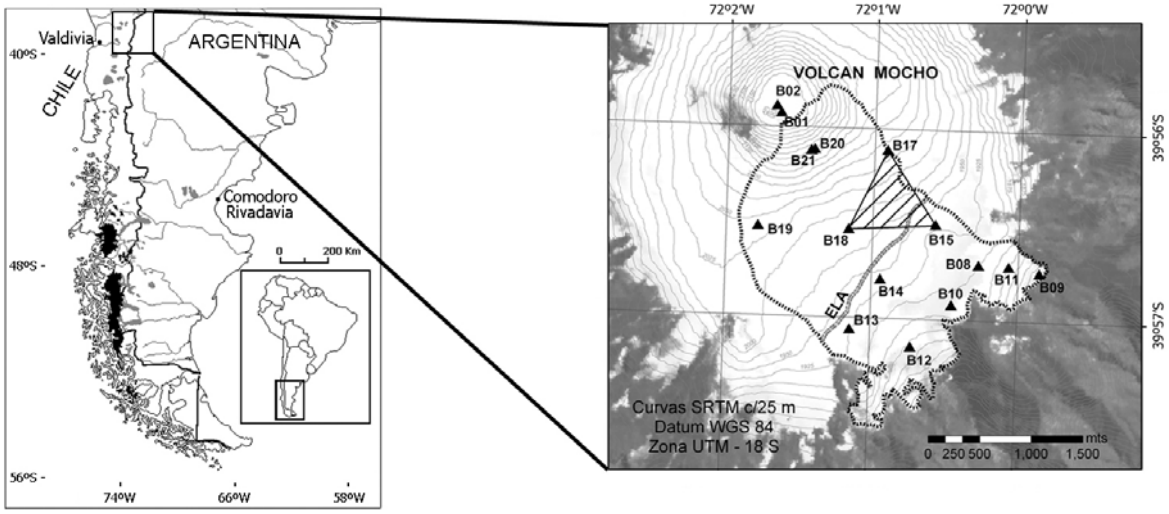

Fig. 1 Location map of the Chilean Lake District with an inset corresponding to the 2003 ASTER image of Volcán Mocho–Choshuenco (39º25′S, 71º57′W) showing the glacier basin. The black triangles correspond to the network of stakes used for measuring mass balance. The hachured area on the right corresponds to the crevasse area studied by GPR in the field. The dotted line indicates the equilibrium line altitude (ELA) of 2003–2004, with net accumulation above the ELA and net ablation below the ELA.

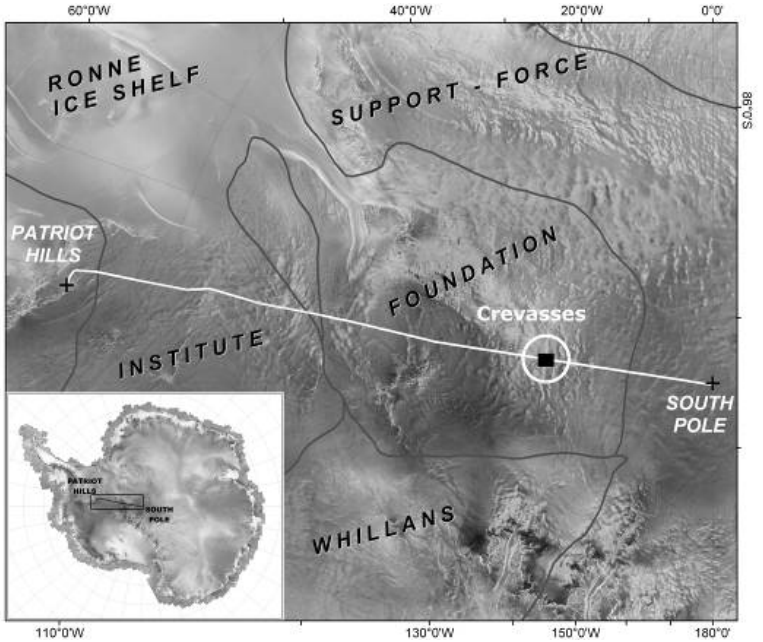

Fig. 2 RADARSAT image of Antarctica corresponding to the box indicated in the inset showing the convoy route as a white line. The crevasse location is indicated with a white circle and a box inside (87º30′S 82º25′W). The major glacier basins, corresponding to Ice Streams, have been added, obtained from Rignot and Thomas (2002) (Topographishe Karte vom Filchner – Ronne – Schelfeis, 1993).

the winter snow accumulation, with a maximum surface exposure at the end of the dry season (March–April). During the field observations (May 2004) crevasses were partly covered by a thin layer of about 20 cm of newly deposited snow.

In November and December 2004 a tractor traverse was carried out in East Antarctica (Fig. 2), during the Chilean South Pole Scientific Expedition. The traverse started at Patriot Hills, followed a route south between meridians 80–83°S, reaching the South Pole on 30 November and returning to Patriot Hills on 31 December. The route was chosen based on previous skiing traverses to the South Pole, and on a RADARSAT image at 25 m resolution (Jezek, 2002) where large crevasse fields were detected following a similar procedure used by the US Antarctic Program (Bindschadler & Vornberger, 2005). The radar was switched on at a few selected sites along the route. A large east–west trending crevasse was detected visually on 25 November across the route at 87º30′S, 82º25′W, within an area located over an east–west trending escarpment in the upper Foundation Glacier basin. The RADARSAT image showed a distinct crevasse field approx. 5 km east of the chosen route (Fig. 3), which was considered safe for the tractor traverse. The crevasse in the field was about 3 m wide at the point where it intersected the planned route, with an associated topographic depression of ~1 m in elevation, which was not detected in the RADARSAT image mainly due to its limited resolution and partly also to the high brightness of this part of the satellite image. At the point where the crevasse was finally crossed by the tractor convoy (Fig. 3) its width was 70 cm, being located over a homogeneously sloping surface with no significant topographic depression.

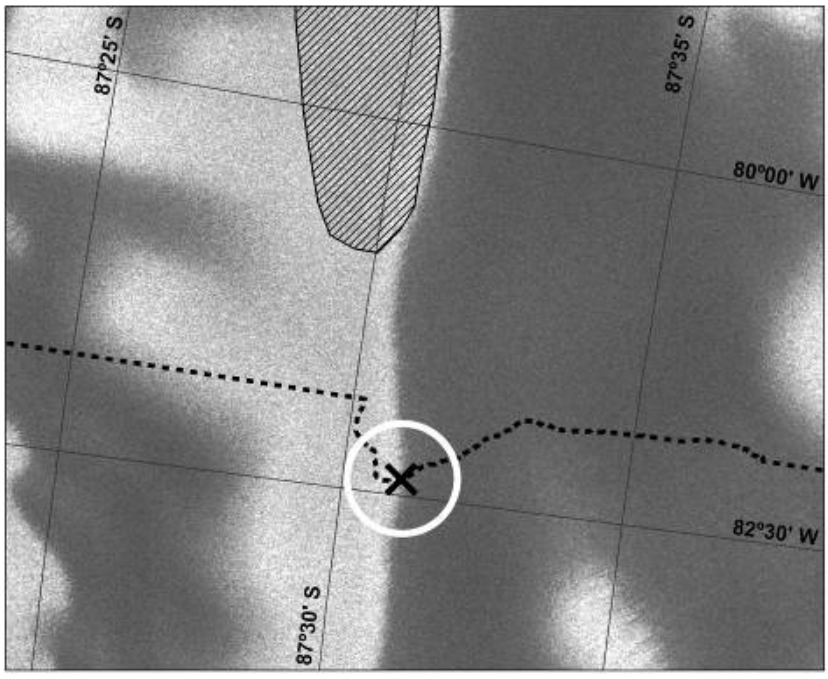

Fig. 3 1997 high resolution RADARSAT Antarctic Mapping Mission (AMM) image (Jezek, 2002) of the area of crevasses along the route to the South Pole at 87º30′S, 82º25′W, corresponding to the Foundation Ice Stream. This image is shown as a black box in Fig. 2. The hachured area corresponds to crevasses interpreted from the RADARSAT image. The black segmented line is the route followed by the tractor convoy. “X” is the crevasse crossed with the tractor convoy on 25 November 2004. The crevasse was oriented perpendicular to the route, following an E–W trend and running along the topographic escarpment which is seen on the image as the transition between the bright (steep) area on the left of the crevasse and the dark (more level) area to the right.

INSTRUMENTS AND METHODS

The GPR system is manufactured by Geophysical Survey Systems Inc. (GSSI), North Salem, USA, and is composed of a digital control unit (GSSI model SIR 3000) and a high frequency radar transducer (GSSI model 5103, 400 MHz). The transducer includes shielded dipole pairs, transmitter and receiver. The digital control unit of the radar triggers pulses at 100 kHz repetition rate. Data were recorded in 16 bit format, using 512 and 4096 samples per scan. The range was set between 100 and 240 ns to record subsurface reflection.

All data were processed using RADAN for Windows v5.0, specific software from GSSI, and REFLEXW developed by K. J. Sandmeier (www.sandmeier-geo.de). Both software allow display, editing and printing of the GPR data, in addition to performing mathematical operations (averaging, subtractions, products); Infinite Impulse Response (IIR) and Finite Impulse Response (FIR) filters, and signal processing such as migration, deconvolution and static correction, among others.

An electromagnetic signal transmitted into the glacier can be reflected at any discontinuity or interface in the medium which exhibits contrasting dielectric characteristics within the glacier, such as a horizontal snow/firn layer or a near-vertical crevasse wall. Energy losses will be produced in the transmission/reception stages, within the medium, and at the interfaces.

In the radar echogram the horizontal axis represents the distance covered on the ground, and the vertical axis represents the two-way travel time of the propagated wave. Based on the real part of the dielectric constant of the media and the two-way propagation time, the thickness can be obtained for a monostatic radar system as follows (Delaney & Arcone, 1995):

$$h = \frac{ct}{2\sqrt{\varepsilon}} = \frac{vt}{2} \tag{1}$$

where h is depth of the reflector in m; c is speed of electromagnetic waves in vacuum (0.3 m ns^{-1}); t is two-way travel time in ns; ε is dielectric permittivity of the medium; and v is speed of the electromagnetic wave in the medium (m ns^{-1}).

A crevasse can be detected in a radar image based on hyperbolae diffractions produced at any sharp discontinuities associated with the crevasse (Delaney *et al.*, 2004), such as the roughness on the bottom of a snow bridge, and the interface between a near-vertical crevasse wall and near-horizontal snow/ice layers, which act as natural diffractors. A crevasse cavity is also a discontinuity within the glacier stratigraphy, affecting the pattern of internal reflections of the glacier. In the case of an air-filled crevasse, it is seen in the radar image as an area without reflections.

At the Chilean location, the radar measurements were performed on foot by two operators, one person carrying the transducer ahead and the other person behind the digital control unit (Fig. 4). The transducer was mounted on a 1.4-m long fibreglass rod provided by GSSI.

In Antarctica the Berco TL6 tractor was equipped with a 7-m long rod composed of a metal frame with a wooden beam inside. The transducer was mounted at the end of the rod in the interior of a tire inner tube, which was pushed along the glacier surface in front of the tractor (Fig. 5). The tractor radar assembly followed the model

used by S. Arcone (Delaney *et al*., 2004). The operator carried the digital control unit inside the tractor cabin. At both sites (Volcán Mocho-Choshuenco and Antarctica) the radar records could be interpreted in real time by the operator.

Fig. 4 Ground penetrating radar used on Volcán Mocho-Choshuenco, Chilean Lake District. The operator on the left has the digital control unit, while the person on the right carries the transducer.

Fig. 5 Ground penetrating radar mounted on a 7-m long metal rod in front of the BERCO TL6 tractor, East Antarctica. The radar transducer is installed inside the rubber inner tube at the right end of the rod, which is connected with a cable to the digital control unit installed in the tractor cabin.

RESULTS

Part of the tests of the radar system for crevasse detection were made in May 2004 at the eastern part of the glacier of Volcán Mocho-Choshuenco, in the area between stations 15, 17 and 18 (Fig. 1), at a mean elevation of 2000 m a.s.l. Crevasses here are only obvious in steep places and close to stake 17, particularly at the end of spring and summer (Fig. 1). The radar records show that for the case of temperate firn in Volcán Mocho-Choshuenco the penetration depth of the 400 MHz radar is at least 15 m and can reach 35 m or more. The radar was able to detect internal layering and the location of surface and buried crevasses.

The speed of the electromagnetic wave in firn can be calculated based on the slope of the hyperbolic diffraction asymptotes, according to equation (2) (Daniels, 2004):

$$v = \sqrt{\frac{x_n^2 - x_{n-1}^2}{t_n^2 - t_{n-1}^2}} \tag{2}$$

where Δx is the horizontal distance on the ground corresponding to a segment of a diffraction hyperbola (abscissa on Figs 6, 7 and 8), n represent each one of the points of the hyperbola usually expressed in m, and Δt is the one-way time interval of the same hyperbola segment (left ordinate of Fig. 8 divided by a factor of 2).

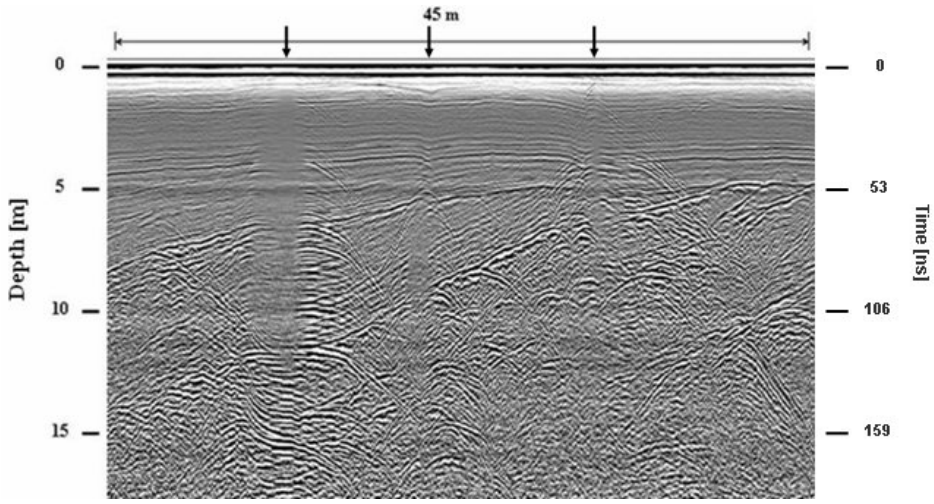

Fig. 6 Radar echogram from Volcán Mocho–Choshuenco corresponding to the crevassed area between stakes 15, 17 and 18 in Fig. 1. The vertical axis is depth (m) and the horizontal axis is a non calibrated measure of horizontal distance across the crevassed area, with a total length of approximately 45 m. The main crevasses interpreted from the image are shown by vertical arrows. The crevasse in the middle is buried while the other two reach the surface. Notice the distortions in the firn layers associated with the crevasses, particularly of the two crevasses on the right of the image. The left crevasse has a width of 0.5 m.

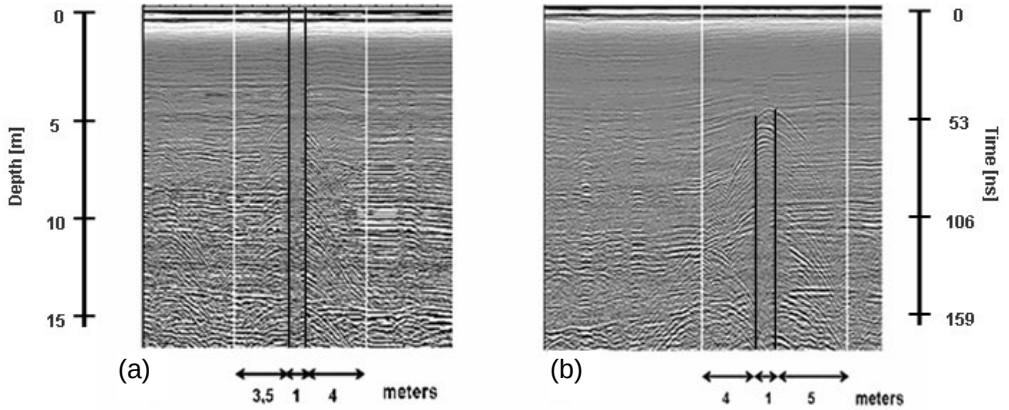

Fig. 7 Crevasses seen on radargrams from Volcán Mocho-Choshuenco. (a) Is an open crevasse, while (b) corresponds to a crevasse buried under a 5 m snow bridge. The vertical scale indicates depth in m. The vertical white lines show the area on the radar records where diffraction hyperbolae associated with prominent crevasses are clearly seen, detected to within a distance of 3.5 to 5 m away from the crevasse wall. The black vertical lines show the crevasse walls. The crevasses were 1 m wide in both cases.

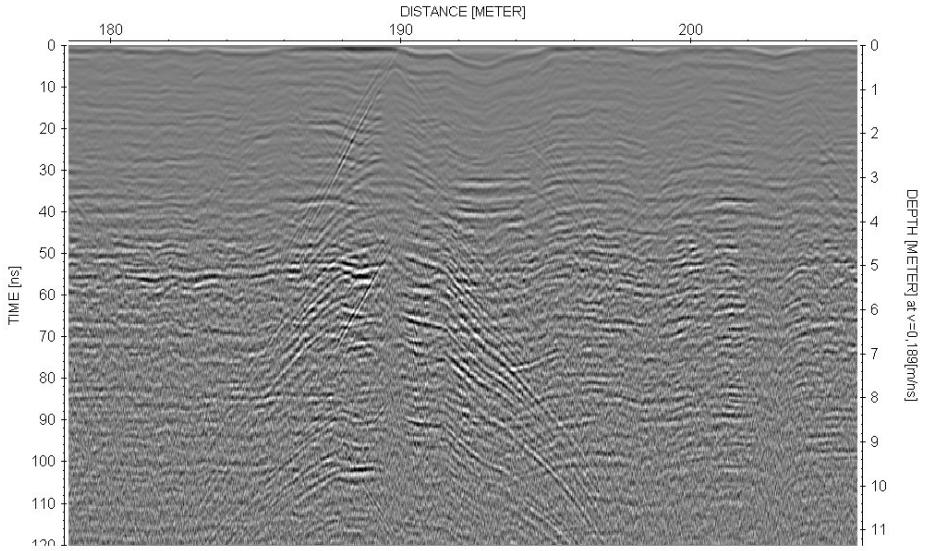

Fig. 8 Crevasse area detected during the traverse from Patriot Hills to the South Pole, East Antarctica (87º30′S, 82º25′W), corresponding to the area marked with an "X" in Figs 2 and 3. The horizontal axis is the horizontal distance scale across the crevassed area. The vertical axis on the left is two-way travel time in ns, while on the right a depth scale in m is indicated considering an airwave velocity in firn of 0.19 m ns^{-1}, obtained from a slope analysis of hyperbola segments as explained in the text. The sets of diffraction hyperbolae centred at approx. 190 m correspond to the prominent crevasse detected on the surface. Crevasse width is 0.7 m.

Based on equation (2) the mean electromagnetic wave speed in firn at Volcán Mocho-Choshuenco was 0.19 m ns^{-1} ± 0.03 (ε = 2.49 ± 0.16) for the upper 10 m of the glacier, derived from a set of five hyperbolae from one crevasse.

Three crevasses can be seen in Fig. 6 on Volcán Mocho-Choshuenco. It is possible to see how the crevasses interrupt the internal layers. For example the prominent crevasse on the left of Fig. 6 has a width of 0.5 m, presenting strong diffractions and a distinct area without reflections corresponding to the air-filled cavity. A similar case of an open crevasse can be seen in Fig. 7(a). In Fig. 7(b) a crevasse covered by a 5 m snow bridge is clearly seen, with good preservation of the snow stratigraphy above the crevasse.

Based on the experience gained at Volcán Mocho-Choshuenco and considering the satisfying results obtained by polar researchers who have used GPRs during tractor traverses as a means for detecting crevasses (e.g. Kovacs & Abele, 1974; Delaney *et al.*, 2004), it was decided to mount the radar system for crevasse detection on the Berco TL6 tractor along the route during the 2004 Chilean expedition to the South Pole.

In the radar profile of Fig. 8, recorded in East Antarctica, crevasses are clearly detected as apexes of diffraction hyperbolae. Similar to the case of Volcán Mocho-Choshuenco, the speed of the electromagnetic wave in the medium (firn) was calculated for a set of six hyperbolae of one crevasse from equation (2), yielding a mean value of 0.19 m ns^{-1} ± 0.03 (ε = 2.47 ± 0.16) for the upper 8 m of the glacier. This speed value is essentially equal to the speed in temperate firn measured at Volcán Mocho-Choshuenco, and is a representative value for glacier firn (Bogorodsky *et al.*, 1985). In principle a faster speed in firn in Antarctica would have been expected, since

temperatures are cold and firn density is in principle smaller than on temperate firn. The 10-m depth firn temperature at the site of the crevasse (2430 m a.s.l., 87°30′S) can be estimated approximately as –43°C based on 10 m firn temperatures of 45 ± 0.5°C and 36 ± 0.5°C (Simões, personal communication, 2005) measured along the tractor traverse with a thermistor in boreholes at 2621 m a.s.l., 88°01″S and 1621 m a.s.l., 86°00′S, respectively.

CONCLUSIONS

The GPR system used at Volcán Mocho-Choshuenco and Antarctica is capable of identifying surface and buried crevasses, which are characterized by distortions and diffractions in the upper firn layers of the glaciers. Crevasse widths and burial depths could be detected in the radar images.

The first diffraction hyperbolae are detected 3.5 m from the apex of the crevasse, which is a mean representative value for the crevasses found in Volcán Mocho Choshuenco and Antarctica. Considering an average ground speed of ~0.5 m s^{-1} (1.8 km h^{-1}) in the case of the hand-carried system, and a transducer distance of 1.2 m ahead of the operator (1.4 m rod with an inclination of 30°) plus the 3.5 m hyperbolae detection distance from above, a reaction time of ~9 s could be obtained prior to detecting a crevasse. For the tractor system, with an average ground speed of ~2 m s^{-1} (7.2 km h^{-1}) in the crevassed area, a transducer distance of 7 m ahead of the tractor plus the 3.5 m, the reaction time was ~5 s.

In Antarctica, within the 1084 km track, only one crevasse area of a total distance of about 100 m was detected with data analysed mainly in post processing. In the Chilean Andes the radar records were analysed in post processing. Therefore, in both geographic areas GPR signals were examined in detail only after post processing, with only an initial identification of the presence of crevasses. In the future this method should be applied as part of a real time decision-making process.

Although GPR proved to be an efficient tool in detecting crevasses, it should be used as a field component of an integral crevasse detection system, which should include detailed prior inspection of other information regarding the area such as satellite images (visible, near infrared and radar), digital terrain models and ice flow information at the highest available resolution. In the field, appropriate safety measures should be considered when crossing glacier areas where the presence of crevasses is probable.

Acknowledgements We thank Mr Steven Arcone, Cold Regions Research Engineering Laboratory for his valuable cooperation. CECS is a non-profit organization funded in part by the Millennium Science Initiative and grants from Fundación Andes and the Tinker Foundation. Institutional support to the Centro de Estudios Científicos (CECS) from Empresas CMPC is gratefully acknowledged. Guisela Gacitúa helped with post processing in Reflexw, Víctor Petterman, Roberto Monroy and Ariel Amollado from Fundo Huilo-Huilo provided logistic support during the field campaigns at Volcán Mocho-Choshuenco. In Antarctica the collaboration of

all members of the Chilean South Pole Expedition (Chilean Army, Chilean Air Force and CECS) is acknowledged, as well as the support from the Chilean Defense Ministry, Antarctic Logistics and Expeditions, National Science Foundation (USA) and Berco (Sweden). This work was also sponsored by Fondo Nacional de Ciencia y Tecnología of Chile (FONDECYT 1040515). Two anonymous referees made valuable recommendations.

REFERENCES

AAC (The American Alpine Club) (2005) *Accidents in North American Mountaineering*, 58th edn. New York, USA.

Arcone, S. A. & Tobiasson, W. & Delaney, A. J. (1995) Ground-penetrating radar investigation of the proposed dome–CARA tunnel route and utilities at South Pole Station, Antarctica. *CRREL, Special Report 95-24.*

Bindschadler, R. & Vornberger, P. (2005) Guiding the South Pole traverse with ASTER imagery. *J. Glaciol.* **51**(172), 179–180.

Bogorodsky, V. V., Bentley, C. R. & Gudmandsen, P. E. (1985) *Radioglaciology*, first edn. D. Reidel Publishing Company, Dordrecht, The Netherlands.

Clarke, T. S. & Bentley, C. R. (1994) High-resolution radar on Ice Stream B2, Antarctica: measurements of electromagnetic wave speed in firn and strain history from buried crevasses. *Annals Glaciol.* **20**, 153–159.

Daniels, D. D. (2004) *Ground Penetrating Radar*, 2nd edn. The Institution of Electrical Engineers, London, UK.

Delaney, A. J. & Arcone, S. A. (1995) Detection of Crevasses near McMurdo Station, Antarctica with Airborne Short-Pulse Radar. *CRREL Laboratory*, Special Report 95-7, 14 p.

Delaney, A. J., Arcone, S. A. & O'Bannon, J. W. (2004) Crevasse detection with GPR across the Ross Ice Shelf, Antarctica. In: *Proc. Tenth Int. Conf. on Ground Penetrating Radar* (Delft, The Netherlands, Volume II, 4 p.).

Gonzalez-Ferrán, O. (1995) *Volcanes de Chile*. Instituto Geográfico Militar, Chile, Santiago, Chile (in Spanish).

Jezek, K. (2002) RADARSAT-1 Antarctic Mapping Project: change-detection and surface velocity campaign. *Annals Glaciol.* **34**(1), 263–268.

Institut für Angewandte Geodäsie (IFAG) (1993) Topographishe Karte vom Filchner – Ronne – Schelfeis.

Kovacs, A. & Abele, G. (1974) Crevasse detection using an impulse radar system. *Antarctic J. United States* **9**(4).

Paterson, W. S. B. (1994) *The Physics of Glaciers.* Pergamon Press, London, UK.

Pralong, A., Funk, M. & Lüthi, M. P. (2003) A description of crevasse formation using continuum damage mechanics. *Annals Glaciol.* **37**(1), 77–82.

Retzlaff, R. & Bentley, C. (1993) Timing of stagnation of Ice Stream C, West Antarctica, from short-pulse radar studies of buried surface crevasses. *J. Glaciol.* **39**(133), 553–561.

Rinot, E. & Thomas, R. (2002) Mass balance of Polar Ice sheets. *Science* **297**(5586), 1502–1506.

Rivera, A., Bown, F., Casassa, G., Acuña, C. & Clavero, J. (2005) Glacier shrinkage and negative mass balance in the Chilean Lake District. *Hydrol. Sci. J.* **50**(6), 963–974.

Vaughan, D. G. (1993) Relating the occurrence of crevasses to surface strain rates. *J. Glaciol.* **39**(132), 255–266.

Glacier Mass Balance Changes and Meltwater Discharge (selected papers from sessions at the IAHS Assembly in Foz do Iguaçu, Brazil, 2005). IAHS Publ. 318, 2007.

Deriving glacier mass balance from accumulation area ratio on Storglaciären, Sweden

REGINE HOCK[1,2], DIRK-SYTZE KOOTSTRA[3] & CARLEEN REIJMER[4]

1 *Geophysical Institute, University of Alaska, Fairbanks, Alaska 99775-7320, USA*
regine.hock@gi.alaska.edu

2 *Department of Earth Sciences, Uppsala University, Villavägen 16, 75236 Uppsala, Sweden*

3 *Department of Physical Geography, Utrecht University, PO Box 80115, 3508 TC Utrecht, The Netherlands*

4 *Institute for Marine and Atmospheric Research, Utrecht University, PO Box 80005, 3508 TA Utrecht, The Netherlands*

Abstract Glacier net mass balance, b_n, tends to correlate well with accumulation area ratio (AAR). A method that substitutes the long term b_n – AAR relationship by the transient relationship, derived from repeated measurements during one ablation season, is tested on Storglaciären, a well-investigated glacier in Sweden. We use the 1946–2004 long term record, transient mass balance measurements in 2004, and results from a distributed energy-balance mass-balance model. The long term and transient relationships are in good agreement for negative and slightly positive mass balances corresponding to AAR of roughly 0.2 to 0.6, but progressively deviate from each other with increasing net balances and larger AARs. The modelling indicates that the deviation becomes smaller as winter mass balance increases. It is concluded that the transient $b_{n,t}$ – AAR_t relationship should: (a) be established during a highly negative mass balance year, and (b) exclude any data from the earlier part of the melt season. Deriving the relationship from mass balance modelling may provide a powerful alternative, circumventing the need for a highly negative mass balance year for the transient measurements.

Key words accumulation area ratio; glacier mass balance; Storglaciären; Sweden

INTRODUCTION

Monitoring glacier mass balance is important for understanding and predicting the response of glaciers to climate change and resulting impacts on sea level change, watershed hydrology, and glacier-related hazards. However, direct measurements are scarce (Dyurgerov, 2002) since traditional mass balance measurements are highly time- and labour-consuming, and glaciers tend to be located in remote areas. Hence, there is a need for alternative less expensive but accurate methods. Dyurgerov (1996) proposed a method that derives glacier mass balance from the accumulation area ratio (AAR) or the equilibrium line altitude (ELA). AAR is defined as the ratio of accumulation area at the end of the melt season and total glacier area. The purpose of this study is to test this method on Storglaciären, a well-investigated valley glacier in Sweden, where continuous mass balance measurements have been conducted since 1945/1946 (Holmlund *et al*., 2005). Elaborating on previous studies that use direct measurements of mass balance, we also investigate the method based on results from distributed energy-balance mass balance modelling.

DYUGEROV´S METHOD

The method proposed by Dyurgerov (1996) is based on the generally observed close relationship between annual area-averaged net mass balances, b_n, and ELA or AAR for glaciers with a distinct winter accumulation and summer ablation season. While such a relationship can be established from long term field measurements, Dyurgerov (1996) proposes that this relationship can be obtained from repeated mass balance measurements during only one summer. From these measurements so-called "transient" (current) area-averaged mass balances, $b_{n,t}$, can be computed and related to concurrent transient values of AAR and ELA (here referred to as AAR_t and ELA_t, respectively). Hence, the method assumes that the relationship between transient (current) values of mass balance ($b_{n,t}$) and ELA_t/AAR_t in the course of one season is identical to the relationship between b_n and ELA/AAR at the end of the mass balance year over many years. Once the relationship has been established b_n can be computed from the ELA or AAR obtained, e.g. from remote sensing, thus greatly facilitating mass balance determination. The method has been tested on a number of glaciers, mostly in Asia (e.g. Dyurgerov *et al*., 1996; Kamniansky & Pertziger, 1996). Since Storglaciären's equilibrium line is very irregular (deviating strongly from the course of contour lines) we focus on the relationship between b_n and AAR instead of ELA. On Storglaciären, the accumulation area generally coincides with the area above the snowline.

FIELD MEASUREMENTS AND DATA

Storglaciären holds a continuous mass balance record starting in 1945/1946 (Holmlund *et al.*, 2005), and thus is an ideal site for this study. The glacier's surface area has remained roughly constant at ~3.2 km^2 during the last three decades, and ranges in elevation from 1140 to 1730 m a.s.l. (Fig. 1). Winter mass balance is obtained from roughly 300 probings on a 100 × 100 m grid, while summer mass balance is derived from about 50–90 ablation stakes spread across the glacier. In 2004, detailed mass balance measurements were performed on nine occasions during the melt season in

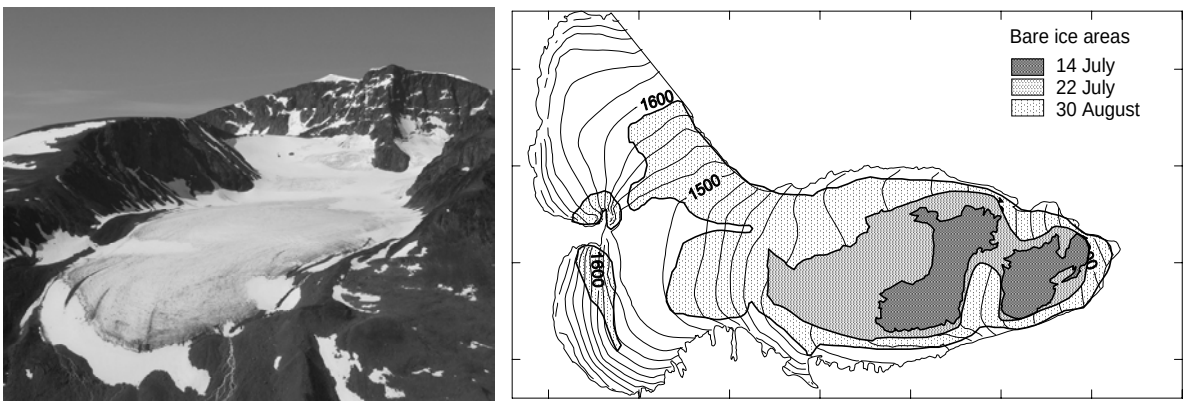

Fig. 1 Photograph taken on 29 July 2004 (left) and map of Storglaciären (right) showing the typically irregular pattern of snowline retreat. Bare ice areas as mapped on three of nine occasions on Storglaciären in 2004. Elevation contours with 20 m spacing. Tick mark spacing corresponds to 500 m horizontal distance.

order to establish the transient $b_{n,t} - \mathrm{AAR_t}$ relationship. A network of 88 ablation stakes was available for computation of the summer mass balance. Meltwater equivalent was computed considering changes in snow density during the season based on snow pit measurements and previous studies (Schytt, 1973). Concurrent with each mass balance measurement, the snow line retreat was mapped using a handheld GPS. From these data, $\mathrm{AAR_t}$ values were computed and compared to those obtained from the mass balance integrations. Since deviations between both data sets were negligible the latter values were used in further analysis. The mass balance (in water equivalent, w.e.) in 2004 was slightly negative (–0.19 m year^{-1}) and similar to the long term (1945/1946–2003/2004) average of –0.24 m year^{-1} (Kootstra, 2005).

MASS BALANCE MODELLING

In addition to the transient $b_{n,t} - \mathrm{AAR_t}$ relationship derived from the 2004 measurements, we investigate the relationship based on results from mass balance modelling. This has the advantage that the relationship can be obtained for the entire range of possible AAR values (0–1) by sufficiently manipulating the climate forcing to remove the winter snow cover by the end of the melt season. In contrast, the actual AAR recorded at the end of the season in 2004 only reached a minimum of 0.38. The mass balance model is based on a distributed surface energy balance model (Hock & Holmgren, 2005) coupled to a multi-layer snow model (Reijmer & Hock, 2007). Shortwave incoming and longwave radiation are computed considering the effects of slope, aspect and surrounding topography. Ice albedo is assumed constant in time while snow albedo is generated internally according to Zuo & Oerlemans (1996) and Oerlemans & Knap (1998). The turbulent fluxes are computed by the bulk aerodynamic approach correcting for atmospheric stability following Munro (1990) and using the non-linear stability functions by Beljaars & Holtslag (1991). The multi-layer snow model is a modified version of the model presented by Greuell & Konzelmann (1994) and Bougamont *et al.* (2005). It determines surface temperature, melt and runoff by calculating vertical profiles of temperature, density and water content down to 30 m below the surface taking the processes of melt, refreezing, meltwater percolation, slush formation and densification into account.

Computations are performed on a 30-m resolution grid and driven by hourly air temperature, humidity, wind speed, precipitation, shortwave incoming and reflected radiation, and longwave incoming and outgoing radiation. The model was run for the melt season 1999 when a detailed automatic weather station was operated on Storglaciären from 9 May to 2 September, providing the necessary input data to the model for an entire melt season (Hock *et al.*, 2000). Modelled mass balances, snow line retreat and snow temperatures generally agreed well with observations (Reijmer & Hock, 2006). The model was initialized with the measured winter mass balance (1.34 m w.e.). From the model run, transient mass balances and corresponding AAR values were extracted for every couple of days during the simulation period for which climate data were available. The mass balance in 1998/1999 was –0.21 m year^{-1} (AAR = 0.39), and thus similar to the one in 2003/2004 (–0.19 m year^{-1}, AAR = 0.38).

Three additional model experiments were conducted. The model was also run, shifting measured temperature uniformly by +2 and +4 K, in order to generate more

negative mass balances and lower AARs, and to investigate the effect of the melting "history" on the results. The perturbations reduced the AAR to 0.24 and 0.09, respectively, by the end of the simulation period. Finally, the winter mass balance was increased uniformly by 1 m w.e. in order to analyse the effect of winter balance on the $b_{n,t}$ – AAR_t relationship. For this run, temperature was shifted by +6 K to generate AARs that span the entire range of possible AAR values. It is emphasized that increasing both winter balance and temperature in the same run is not necessarily a realistic scenario, but it suffices for our purpose to investigate the effect of winter balance on the $b_{n,t}$ – AAR_t relationship. Without a temperature increase AAR would change only a little throughout the season.

RESULTS AND DISCUSSION

Figure 2(a) shows the relationship between net balance and AAR for both the 59-year record of Storglaciären and the transient values obtained from repeated mass balance measurements for the melt season 2004. As found on other glaciers (e.g. Dyurgerov *et al*., 1996; Kamniansky & Pertziger, 1996) there is a strong linear relationship between these quantities for the long term data set (r^2 = 0.88). However, in contrast to the underlying assumption of the method, the $b_{n,t}$ – AAR_t relationship for the transient data set of the year 2004 strongly deviates from the long term b_n – AAR relationship. Using

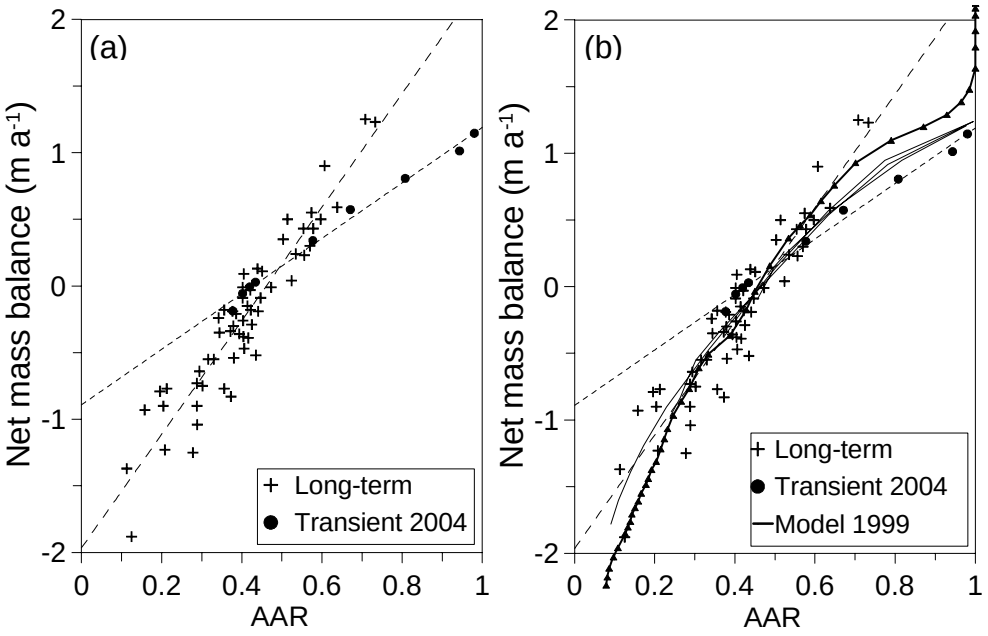

Fig. 2 Net mass balance *vs* accumulation area ratio (AAR) for: (a) the long term mass balance data of Storglaciären (1945/1946–2003/2004) and the transient data of 2004, and (b) including the results from four model runs (forced with measured temperatures, and temperatures shifted by 2 and 4 K (thin lines). Thick line (with triangles marking every second day) refers to model run with temperature shifted by 6 K in addition to increasing the measured winter balance by 1 m w.e.. The dashed lines are the linear regression lines for the long term (y = 4.26 × –1.97; r^2 = 0.88) and the transient data set (y = 2.08 × –0.89; r^2 = 0.99).

the $b_{n,t}$ – AAR_t relationship to estimate the net mass balance leads on average to an overestimation of 0.2 m ranging from up to 0.52 m underestimation to up to 0.83 m overestimation for individual years. In comparison, b_n is underestimated and overestimated by up to 0.37 m and 0.46 m, respectively, with no difference for the mean, when the long term b_n – AAR relationship is used. Sensitivity analysis was performed to investigate whether this discrepancy between the long term b_n – AAR and the transient $b_{n,t}$ – AAR_t relationship could be explained by uncertainties in the mass balance computations. Mass balances were computed using different assumptions on snow and firn densities as well as different methods of interpolating the point measurements across the glacier. Results indicated that the discrepancy could not be explained by uncertainties in the mass balance computations. Statistical tests indicate that the difference in slope between both regression lines is significant at 95% confidence interval.

We further investigate if a significant difference in slope between the annual and transient relationship (Fig. 2) is a coincidence for the year 2004, or to be expected for the entire record by adopting the following approach. For each year of the long term record the maximum slope, $\alpha_{t,max}$, of the transient $b_{n,t}$ – AAR_t linear regression line can be approximated by:

$$\alpha_{t,\max} = \frac{b_w - b_n}{1 - AAR} \tag{1}$$

where b_w and b_n are winter and net mass balance, respectively. Figure 3 illustrates schematically that α computed thus provides the maximum slope $\alpha_{t,max}$ for each year's transient relationship (provided that the glacier is entirely snow-covered at the beginning of the melt season, which is the case on Storglaciären). Unless snow-cover on at least part of the glacier immediately melts off exposing bare ice, the actual transient slope, α_t will be lower, because AAR remains 1 for an initial period of melting until the first ice is exposed at the surface. $\alpha_{t,max}$ was computed for each year of the 59-year mass balance record and compared to the slope of the long term b_n – AAR regression line (The years 1960 and 1963 had to be excluded due to lack of reported AARs). Mean maximum slope, $\alpha_{t,max}$, of the transient $b_{n,t}$ – AAR_t relationship (equation 1) is

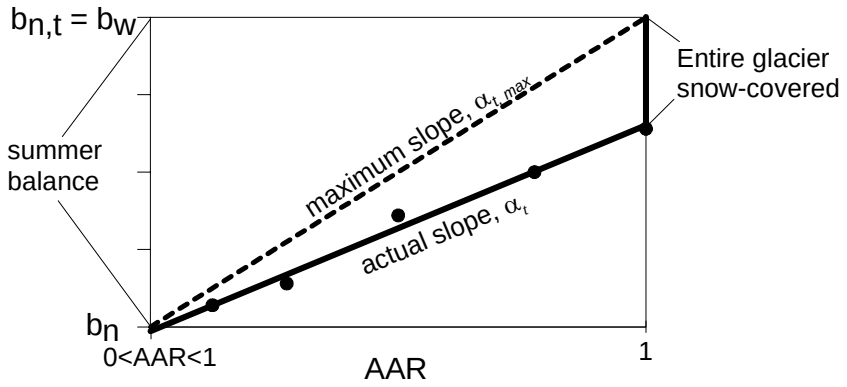

Fig. 3 Schematic sketch illustrating that the maximum possible slope, $\alpha_{t,\,max}$, for each year's transient $b_{n,t}$ – AAR_t relationship derived from the winter (b_w) and net balance (b_n) exceeds the actual slope, α_t, since the glacier will remain entirely snow-covered for an initial period before bare ice is first exposed and the AAR drops below 1.

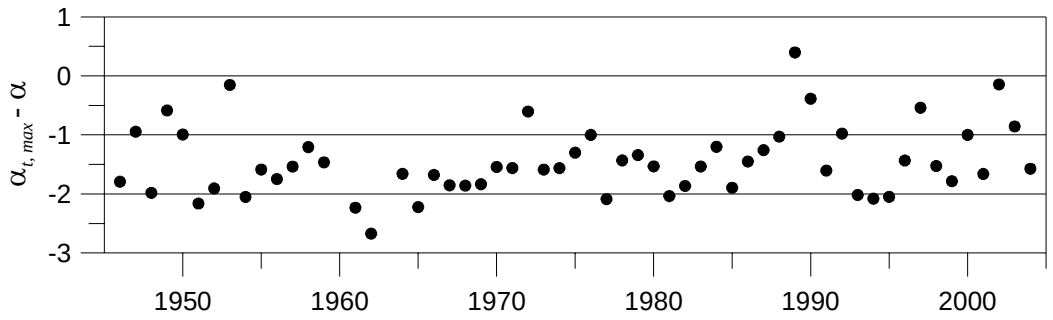

Fig. 4 Maximum slope, $\alpha_{t,max}$, obtained for each year from equation (1) minus the slope, α, derived from the b_n – AAR regression line based on the long term mass balance record of Storglaciären. The mean difference is -1.46. Mean $\alpha_{t,max}$ and α are 2.80 and 4.26, respectively.

2.80 ± 0.59, which is considerably lower than the slope α = 4.26 (Fig. 2) of the long term b_n – AAR regression line. Figure 4 shows that the maximum slope, $\alpha_{t,max}$, obtained by equation (1) for all but one year is lower than the slope, α, obtained from the long term b_n – AAR regression line. This indicates that the long term b_n – AAR and transient $b_{n,t}$ – AAR_t relationships generally differ from each other, and the different relationships obtained for t 2004 are not a coincidence. Figure 3 also illustrates that the method is only effective when AAR has dropped below 1. There is no correlation between b_n and AAR for both the long term and transient case, as long as the glacier is entirely snow-covered. The method also becomes insensitive in highly negative mass balance years with continued ablation after the AAR has reached 0.

Figure 2(b) shows the results from the mass balance modelling. All relationships derived from both data and modelling results largely coincide for AARs varying roughly between 0.2 and 0.6, but relationships progressively deviate from each other outside this range, in particular with increasing AAR. For overlapping ranges the results for the three model runs that were initialized with measured winter mass balance also largely coincide for large AARs. This indicates that the relationship is independent of the climate forcing applied. The +4 K and +6 K model runs span almost the entire range of possible AAR values and suggest a logarithmic $b_{n,t}$ – AAR_t relationship which is roughly linear for AARs varying between 0.2 and 0.6. The modelled transient $b_{n,t}$ – AAR_t relationships based on measured winter mass balance agree well with the one derived from the measurements, hence deviating from the long term b_n – AAR relationship for more positive mass balances and associated high AARs. However, results from the model run initialized with +1 m winter mass balance coincides more closely with the regression line for the long term relationship. This indicates that for large AARs the transient $b_{n,t}$ – AAR_t relationship depends on winter mass balance. With increasing winter balance the transient $b_{n,t}$ – AAR_t relationship tends to approach the long term b_n – AAR relationship.

A discrepancy between long term b_n – AAR and transient $b_{n,t}$ – AAR_t relationships has been found typical for all experiments run in the Tien Shan and the Pamir glaciers (Dyurgerov, 1996; Kamniansky & Pertziger, 1996). Long term mass balance data covers the climate conditions over about 50 years since the middle of the previous century. Due to relatively warm conditions during this period and associated general glacier retreat, observations including very high end-season AAR values are scarce. On

Storglaciären, AAR exceeded 0.7 only twice in the almost 60 year data record, and consequently the b_n – AAR relationship beyond this range is unknown. However, uncertainties in the b_n – AAR relationship for higher AARs are of decreasing practical importance in the light of generally predicted further glacier retreat.

CONCLUSIONS

Measurements and modelling results show that the b_n – AAR relationships derived from long term and transient values within one summer closely agree over the range of AARs roughly from 0.2 to 0.6. However, they progressively deviate from each other as AAR increases above 0.6, but modelling suggests that this deviation becomes less as winter mass balance increases. Hence, the transient relationship should preferably be established during a year of strongly above average winter balance, but also highly negative net mass balance to include lower AAR values. It is obvious that such conditions rarely occur. Nevertheless, our results suggest that a transient $b_{n,t}$ – AAR_t relationship intended to be used for long term mass balance determination can be acceptably established from transient measurements, irrespective of winter mass balance. However, it is essential that the net mass balance is highly negative and early season data are excluded. Due to acceleration of glacier wastage observed on a global scale, mass balances are likely to become more negative, accompanied by decreasing AARs, thus facilitating establishment of the $b_{n,t}$ – AAR_t relationship from transient measurements during only one year. The relationship, thus obtained, can then be used to substitute the long term b_n – AAR relationship. Once calibrated, this approach provides a powerful method for widely monitoring glacier contribution to regional and global water cycles and sea level rise, especially in the light of increasing availability of remote sensing products.

Our study indicates that use of mass balance modelling based on weather station data may provide an efficient alternative to transient field measurements since the $b_{n,t}$ – AAR_t relationship can be established for the full range of AAR values irrespective of annual mass balance. Further studies including more mass balance years and other glaciers are desirable to ascertain results.

Acknowledgements RH is a Royal Swedish Academy of Science Research Fellow supported by a grant from the Knut Wallenberg Foundation. Gratitude is expressed to the staff at Tarfala Research Station, especially Mart Nyman, who greatly assisted in collecting the transient mass balance measurements in 2004 and providing the mass balance record. Mark Dyurgerov is gratefully acknowledged for fruitful discussions and valuable comments on the manuscript. An anonymous reviewer, Bryn Hubbard and editor Jean-Emmanuel Sicart are acknowledged for their comments.

REFERENCES

Beljaars, A. C. M. & Holtslag, A. A. M. (1991) Flux parameterization over land surfaces for atmospheric models. *J. Appl. Meteorol.* **30**, 327–341.

Bougamont, M., Bamber, J. L. & W. Greuell, W. (2005) Development and test of a surface mass balance model for the Greenland ice sheet. *J. Geophys. Res*. **110**, F04018,doi:10.1029/2005JF000348.

Dyurgerov, M. (1996) Substitution of long term mass balance data by measurements of one summer. *Gletscherkd. Glazialgeol.* **32**, 177–184.

Dyurgerov, M. B. (2002) Glacier mass balance and regime: data of measurements and analysis. In: *INSTAAR Occasional Paper no. 55* (ed. by M. Meier & R. Armstrong).

Dyurgerov, M., Uvarov, V. N. & Kostjashkina, T. E. (1996) Mass balance and runoff of Tuyuksu glacier and the north slope of the Zailiyskiy Alatau Range, Tien Shan. *Z. Gletscherkd. Glazialgeol*. **32**, 41–54.

Greuell, W. & Konzelmann, T. (1994) Numerical modelling of the energy balance and the englacial temperature of the Greenland ice sheet. Calaculations for the ETH-camp location (West Greenland, 1155 m a.s.l.). *Glob. Planet. Change* **9**, 91–114.

Hock, R. (2005) Glacier melt – a review on processes and their modelling. *Progr. Phys. Geogr*. **29**(3), 362–391.

Hock, R. & Holmgren, B. (2005) A distributed energy balance model for complex topography and its application to Storglaciären, Sweden. *J. Glaciol.* **51**(172), 25–36.

Hock, R., Carrivick, J. & Jonsell, U. (2000) Glacio-meteorological investigations on Storglaciären 1999. Forsknings-rapport 111, 20–23. Department of Physical Geography, Stockholm University, Sweden.

Holmlund, P., Jansson, P. & Pettersson, R. (2005) An analysis of mass changes of Storglaciären over the last 58 years. *Ann. Glaciol*. **42**, 389–394.

Kamniansky, G. M. & Pertziger, F. I. (1996) Optimization of mountain glacier mass balance measurement. *Z. Gletscherkd. Glazialgeol.* **32**, 167–175.

Kootstra, D. (2005) Determining glacier mass balance from surrogate variables. A case study on Storglaciären using ELA and AAR. Exam thesis N-57, Department of Physical Geography and Quaternary Geology, Stockholm University, Sweden.

Munro, D. S. (1990) Comparison of melt energy computations and ablatometer measurements on melting ice and snow. *Arctic & Alpine Res.* **22**(2), 153–162.

Oerlemans, J. & Knap, W. (1998) A 1 year record of global radiation and albedo in the ablation zone of Morteratschgletscher, Switzerland. *J. Glaciol.* **44**(147), 231–238.

Reijmer, C. & Hock, R. (2007) Internal accumulation on Storglaciären, Sweden, in a multi-layer snow model coupled to a distributed energy and mass balance model. *J. Glaciol.* (in press).

Schytt, V. (1973) Snow densities on Storglaciären in spring and summer. *Geogr. Ann.* **54A**(3–4), 155–158.

Zuo, Z. & Oerlemans, J. (1996) Modelling albedo and specific balance of the Greenland ice sheet: Calculations for the Søndre Strømfjord, transect. *J. Glaciol.* **42**(141), 305–317.

3 Meteorology

Glacier Mass Balance Changes and Meltwater Discharge (selected papers from sessions at the IAHS Assembly in Foz do Iguaçu, Brazil, 2005). IAHS Publ. 318, 2007.

Constitution d'une base de données météorologiques sur un site andin de haute altitude: Le site du Charquini, 4795 m, Bolivie

YVES LEJEUNE[1], YANN L'HOTE[2], PIERRE ETCHEVERS[1], PATRICK WAGNON[2], JEAN-PHILIPPE CHAZARIN[2] & PIERRE CHEVALLIER[2]

1 *Météo-France, Centre National de Recherches Météorologiques, Centre d'Etudes de la Neige, Grenoble, France*
yves.lejeune@meteo.fr

2 *Institut de Recherche pour le Développement, Unité de Recherche GREAT-ICE (Glaciers et Ressource en Eau dans les Andes Tropicales, Indicateurs Climatiques et Environnementaux) Montpellier et Grenoble, France*

Résumé Cet article décrit la base de données météorologiques collectées entre octobre 2001 et juillet 2003 sur un bassin versant non englacé de la haute montagne andine, le site du Charquini (4795 m, 16°17′Sud, 68°32′Ouest) en Bolivie. Les données mesurées sont la température et l'humidité relative de l'air, les températures et les flux dans le sol à plusieurs profondeurs, les quatre termes du bilan radiatif, les vitesse et direction du vent, les cumuls des précipitations et la hauteur de neige. Par comparaison à la moyenne montagne des régions tempérées, ce site de haute montagne tropicale diffère principalement par le flux radiatif solaire incident très intense (ce qui le rend propice à la validation des modèles de sol ou de couvert neigeux développés dans les régions tempérées). Dans cet article sont aussi présentées les méthodes d'estimation des paramètres non mesurés, telles que la nébulosité N (couverture nuageuse totale du ciel) et la phase des précipitations, souvent changeante à l'altitude du site, ainsi que la méthode de reconstitution du rayonnement atmosphérique de grandes longueurs d'ondes.

Mots clés Andes tropicales; base de données météorologiques; nébulosité; phases des précipitations; rayonnement de grandes longueurs d'ondes

Meteorological data set build-up on a high Andean site: The Charquini site, 4795 m a.m.s.l., Bolivia

Abstract This paper describes the meteorological database collected between October 2001 and July 2003 on the Charquini site (4795 m, 16°17′S, 68°32′W) located in a non-glacierized catchment of the Bolivian Andes. This database provides air temperature and relative humidity, ground temperatures and fluxes at various depths, the four terms of the radiative balance, wind speed and direction, cumulated precipitation and snow depth. Compared to mid-latitude mountains, this site is very different, mainly because incident solar radiation is almost twice as high in the tropics (which makes the meteoro–logical database valuable to validate soil or snow models built for mid-latitude regions). This paper also presents methods to estimate non-measured parameters such as cloudiness or precipitation phase (snow or rain) and methods to re-calculate incoming long-wave radiation when missing.

Key words tropical Andes; meteorological data base; cloudiness; precipitation phase; incoming short-wave radiation

INTRODUCTION

De récentes études, telles que celles menées par Thompson *et al*. (2003) sur la composition en isotopes stables de l'oxygène (^{18}O), prélevées dans des carottes de glace extraites de plusieurs glaciers sud-américains (Huascaran et Quelccaya Ice Cap au Pérou, Sajama en Bolivie), attestent du réchauffement climatique (supérieur à +1.5°C) auxquelles ont été soumises au cours du siècle dernier les régions tropicales de haute altitude de l'hémisphère sud; réchauffement régionalement plus accentué qu'aux latitudes tempérées (de l'ordre de +0.6°C). Par ailleurs sur ces hautes régions, les prévisions des modèles climatiques de grande échelle (Bradley *et al*., 2004) évaluent à plus de 2.5°C l'accroissement de la température pour les quatre-vingt futures années. Parallèlement à ces études climatiques, des études de bilans d'énergie réalisées sur le glacier Zongo en Bolivie (Wagnon *et al*., 1999a,b, 2001; Sicart *et al*., 2005) ou sur le glacier Antizana en Equateur (Favier *et al*., 2004a,b) ont apporté une compréhension de plus en plus fine et complète sur le fonctionnement des glaciers tropicaux.

En revanche, l'évolution des couvertures neigeuses des zones non englacées n'a jusqu'alors que très peu été abordée. Pourtant, les ressources en eau, destinées à l'approvisionnement en eau potable ou à la production hydroélectrique des populations vivant au pied des cordillères andines, ne se limitent pas à la seule fonte (neige + glace) des glaciers, mais sont aussi issues de la fusion des couverts neigeux fréquents jusqu'à quelques centaines de mètres en dessous de leurs limites inférieures (Caballero, 2001). Bien que souvent peu conséquents et fugaces, ces manteaux neigeux influent sur les ressources en eau par réduction de l'évaporation et stockage de l'eau. Dans le contexte actuel de réchauffement climatique intense favorisant la disparition rapide des petits glaciers tels que celui de Chacaltaya en Bolivie (Francou *et al*., 2003), la faible connaissance de l'évolution du couvert nival des zones non englacées méritait d'être affinée et justifiait la conduite d'un projet national de recherches en hydrologie, le projet PNRH01-37, "Dynamique de la couverture neigeuse dans les Andes Tropicales". Par ailleurs sur les hauts bassins andins, l'alternance des précipitations sous forme de pluie ou de neige est fréquente, et cela principalement en saison humide, soit d'octobre à mars. La phase des précipitations n'y dépend pas uniquement de la température (souvent proche de 0°C) mais aussi de la nature de la masse d'air, de son état convectif, des inversions liées à la topographie. Etre capable de mieux évaluer la nature des phases (L'Hôte *et al*., 2004, 2005) était une condition préalable aux simulations de l'enneigement qui feront l'objet d'un autre travail non présenté ici.

Ces objectifs ne pouvaient être réalisés qu'à la seule condition de disposer localement de données, météorologiques et nivologiques bien documentées. A cet effet, une campagne de mesures a été réalisée durant dix-huit mois sur un site morainique (16°17′Sud; 68°32′Ouest; 4795 m) de la haute montagne andine (Bolivie). Dans cet article on s'appliquera: (a) à décrire le dispositif expérimental et les données collectées, (b) à définir le contexte climatique et ses particularités par rapport à celui d'un site alpin, (c) à développer les méthodes mises en œuvre pour construire la base de données.

LA STATION "CHARQUINI", LE SITE D'ETUDES ET LE DISPOSITIF INSTRUMENTAL

Localisé dans le massif du Charquini (16°17′Sud; 68°32′Ouest; 4795 m) à 30 km au Nord de La Paz (Bolivie), le site, bien représentatif des zones non englacées de la haute montagne tropicale (Fig. 1) est facilement accessible malgré son altitude élevée, permettant ainsi son suivi. Ce massif appartient à la Cordillère Royale, limite naturelle d'orientation NW–SE entre le haut bassin amazonien et l'Altiplano. La station automatique a été installée au milieu d'un ancien cirque glaciaire ouvert sur la vallée du Zongo. Autour de la station située sur une plate-forme naturelle, la pente d'une inclinaison de 15° environ est d'orientation Nord–Est. En surface, le sol est recouvert d'éboulis de différentes tailles et de végétation rase (mousses et herbes) occupant moins de 30% de la surface. Les 50 premiers centimètres de sol sont constitués d'environ 70% de sable, 20% de limon et 10% d'argile.

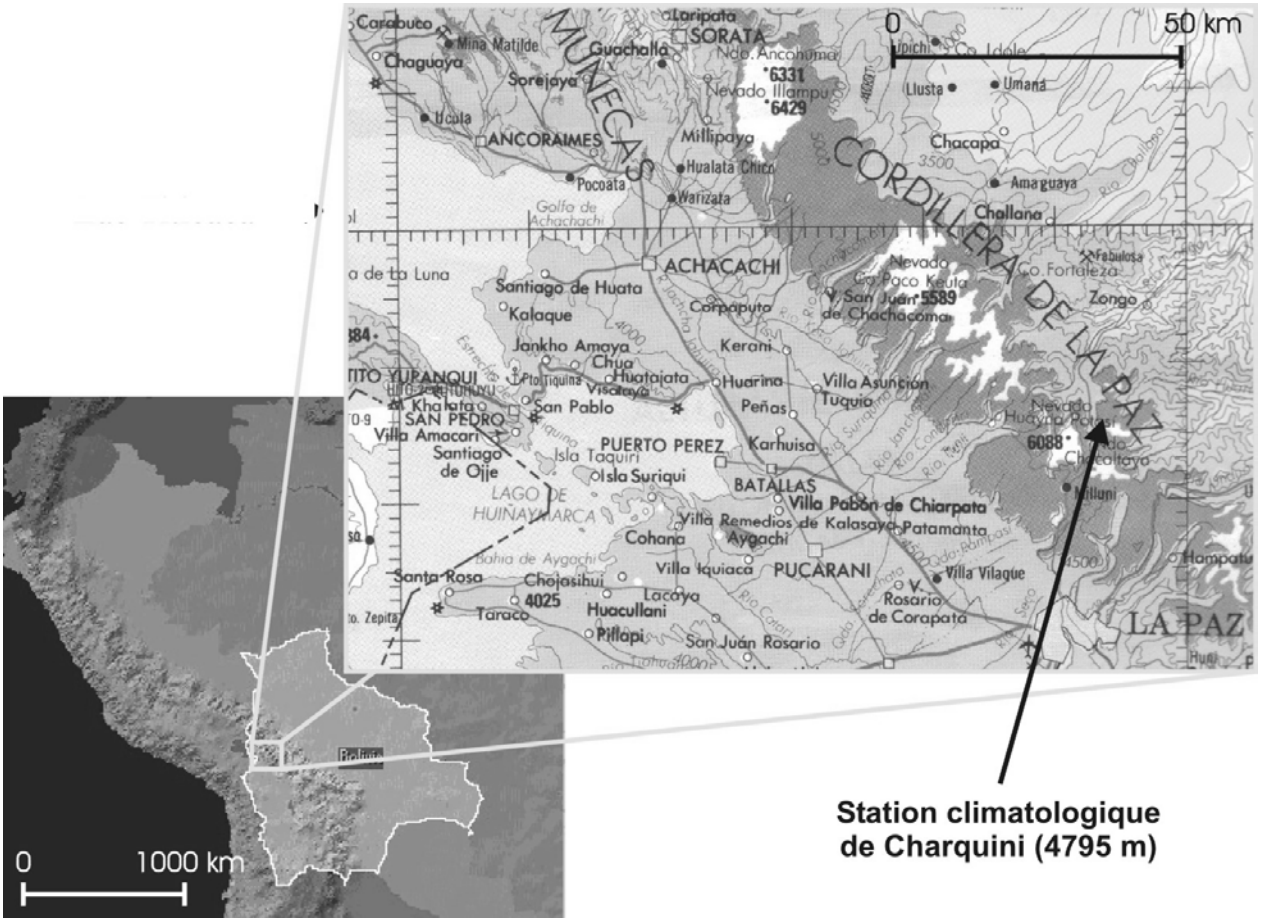

Fig. 1 Localisation géographique du site de mesures Charquini.

La campagne de mesures s'est déroulée du 24 octobre 2001 au 16 juillet 2003 (durée définie par le projet PNRH01-37). Durant cette période, deux centrales de mesures ont collecté: toutes les 10 secondes la température et l'humidité de l'air à 1.50 m

du sol, la lame d'eau des précipitations (pluviomètre totalisateur), les quatre termes du bilan radiatif, la vitesse et la direction du vent à 2.05 m du sol, la hauteur de neige, les températures (–3 cm, –10 cm, –20 cm, –43 cm) et les flux (–3 cm, –43 cm) dans le sol, ainsi que toutes les dix minutes le cumul des précipitations (pluviomètre à augets basculants). La base de données a été constituée à partir des moyennes demi-horaires de ces paramètres, exceptions faites pour la direction du vent et la hauteur de neige pour lesquelles ont été retenues les valeurs instantanées demi-horaires. La pression, non mesurée sur le site, a été évaluée à partir de celle de l'aéroport de La Paz (4071 m). Les caractéristiques du dispositif expérimental et la précision des capteurs sont récapitulées dans le tableau 1. Le fonctionnement de l'instrumentation (pannes, mesures suspectes) est détaillé dans Lejeune *et al*. (2003).

Tableau 1 Caractéristiques du dispositif expérimental.

Quantité mesurée (unité de mesure)	Hauteur capteur (+ spécificité abri)	Type matériel	Précision constructeur
Centrales d'acquisition	… …	Campbell CR23X Campbell CR23X	… …
Précipitations (mm)	175 cm 160 cm	Pluviomètre Géonor T-200B Pluviographe Hobo	0.1 mm …
Température de l'air (°C)	150 cm (ventilé) 100 cm (non ventilé)	Vaisala HMP45 Thermocouple Campbell	± 0.2°C à 20°C …
Humidité relative (%)	150 cm (ventilé)	Vaisala HMP45	± 1% à 20°C
Vitesse (ms^{-1}) et direction (°) du vent	205 cm	Anémomètre-Girouette Young 05103	± 3 ms^{-1} (vit.), ± 3° (dir.)
Radiations "in et out" courtes longueurs d'ondes (Wm^{-2})	90 cm	Kipp & Zonen CM3 jusqu'au 18/04/2002 Pyranomètre Schenk depuis le 15/05/2002	± 10% sur les cumuls journaliers … résolution 1 Wm^{-2}
Radiations "in et out" grandes longueurs d'ondes (Wm^{-2})	90 cm	Kipp & Zonen CG3 jusqu'au 18/04/2002	± 10% sur les cumuls journaliers
Radiations "in et out" globales (Wm^{-2})	90 cm	Pyrradiomètre Schenk depuis le 15/05/2002	… résolution 1 Wm^{-2}
Températures dans le sol (°C)	–3 cm, –10 cm, –20 cm –43 cm	Thermocouples cuivre-constantan	…
Flux du sol (Wm^{-2})	–3 cm, –43 cm	Fluxmètres Hukseflux HFP01	Sensibilité, environ 60 $\mu V/Wm^{-2}$
Hauteur de neige (cm)	115 cm	Sonde Ultrasons Campbell UDG01	± 1cm ou ± 4% distance à la cible

CONTEXTE CLIMATIQUE

Le climat des Andes boliviennes, typique des tropiques externes, est caractérisé par une quasi-absence de saisonnalité des températures et par l'alternance d'une saison humide d'octobre à mars et d'une saison sèche de mai à août (Vuille, 1999, 2000; Kaser & Osmaston, 2002).

Les conditions météorologiques à la station Charquini

Pour les mois d'octobre 2002 à mars 2003 de la saison humide 2002–2003 (Fig. 2), le cumul de précipitations de 1079 mm représente 85% de celui de l'année complète (juillet 2002–juin 2003); les moyennes des températures de +2.1°C et de l'humidité relative de 87%, sont respectivement supérieures de 0.5°C et de 14% à celles de l'année complète; celle du vent de 1.1 m s^{-1} est légèrement plus faible que celle de 1.3 ms^{-1} de l'année complète. La saisonnalité, saison sèche (mai à août) – saison humide (octobre à mars) est donc bien appréhendée par les mesures de la station Charquini. De plus on peut retenir que du 24 octobre 2001 au 16 juillet 2003, 84% du cumul des lames d'eau et 75% des occurrences de précipitations se sont produites entre –1°C et +3°C, soit dans une gamme de températures où l'alternance des phases pluie ou neige est très fréquente.

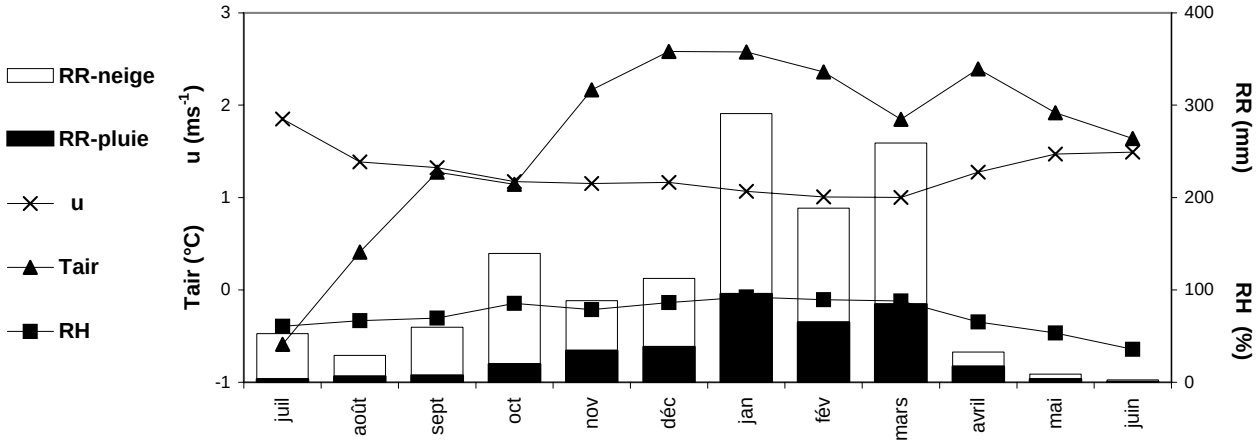

Fig. 2 Moyennes mensuelles des: température de l'air (Tair), humidité relative (RH), vitesse du vent (u), et cumuls mensuels des précipitations (RR, pluie ou neige) à la station Charquini (juillet 2002–juin 2003).

Par ailleurs, Bourqui (2003) a réalisé un travail de comparaison entre les données pluviométriques de la station Charquini et celles de la station Plataforma (4750 m) éloignée de 2 km. Cette étude, effectuée sur treize mois de novembre 2001 à décembre 2002, montre que si le pluviomètre de la Plataforma minore les lames d'eau réelles des précipitations (Sicart, 2002), les cumuls mensuels des deux sites sont en revanche très bien corrélés (R^2 = 0.908). Ainsi il est légitime de faire référence à la pluviométrie (climatologie de trente années de la Plataforma) pour critiquer celle des saisons humides 2001–2002 et 2002–2003 de la station Charquini. Le travail de Bourqui (2003) a été étendu à toute la période de mesures sur les données pluviométriques Charquini. Il montre que si avec 811 mm, le cumul des mois de novembre à mars de la saison humide 2001–2002 est légèrement déficitaire, celui de 1079 mm des mois d'octobre à mars de la saison 2002–2003 est quant à lui un peu excédentaire. Ces cumuls, proches de la valeur de 1000 mm évaluée par Caballero (2001) pour cette tranche d'altitude, confirment par ailleurs l'absence d'occurrence Niño ou Niña au cours des saisons hydrologiques 2001–2002 et 2002–2003 (Wagnon *et al*., 2001).

Forçages météorologiques de la haute montagne andine: comparaison avec la moyenne montagne alpine, le cas du Col de Porte

Le Col de Porte (CDP), localisé à une altitude de 1320 m dans le massif de la Chartreuse (45°30′Nord, 5°77′Est) dans les Alpes françaises est le site de référence du Centre d'Etudes de la neige (CEN) de Météo-France pour le suivi du couvert nival saisonnier (Lejeune & Martin, 1995). Les conditions météorologiques du Charquini pour les mois de novembre à mars de l'été austral, saison humide et période préférentielle de chutes de neige sur la haute montagne andine, ont été comparées à celles du CDP, pour les mois de décembre à avril de l'hiver boréal, saison d'accumulation hivernale sur les Alpes. Les moyennes mensuelles, de la température T_{air} et de l'humidité relative RH de l'air, de la vitesse du vent u, des précipitations RR (Fig. 3), et des flux radiatifs (Fig. 4) des mois d'hiver (boréal) du CDP ont été évaluées sur les 10 années de la période 1996–2005. Celles de l'été austral du Charquini ont été établies sur les deux saisons humides 2001–2002 et 2002–2003 de la campagne de mesures. On peut noter qu'il fait un peu plus froid au CDP (moyennes des T_{air} de +0.9°C au CDP et +2.3°C au Charquini) et que la variabilité inter-mensuelle de la T_{air} est plus marquée sur le site alpin que sur le site andin (amplitudes de 4.4°C au CDP et 0.6°C au Charquini). Les précipitations (quantité et phase), l'humidité relative RH et la force du vent u, comme les rayonnements atmosphériques de grandes longueurs d'ondes LW_{in} sont sur les deux sites très comparables. En revanche, sur le site du Charquini, le rayonnement solaire incident SW_{in} est en moyenne deux fois plus fort que sur le CDP (gain moyen d'environ 90 W m^{-2}) et sa variabilité inter-mensuelle est moins marquée que sur le site alpin. Parallèlement, on peut retenir: (a) que sur le CDP l'accumulation du manteau neigeux débute mi-octobre, que le maximum d'épaisseur est atteint en mars (125 m), que la disparition du couvert saisonnier se produit au cours de la première décade de juin (statistiques 1961–2004), et, (b) qu'en saison humide sur le Charquini le sol est plus fréquemment déneigé qu'il n'est enneigé; les couvertures neigeuses les plus conséquentes (de l'ordre de 20 cm d'épaisseur) ne recouvrent pas le site plus de 2 à 5 jours consécutifs.

En saison humide, des premières évaluations du bilan énergétique de surface sur le site du Charquini montrent que les flux turbulents sont faibles en raison d'un vent faible. De plus la chaleur latente perdue par sublimation des grains de surface des couvertures neigeuses est largement compensée par l'apport de chaleur sensible issu de l'air circulant au dessus de ces couvertures. Ce constat s'accorde bien aux résultats obtenus sur le glacier Zongo par Wagnon (1999a,b) et Sicart (2005). Pour cette même saison humide, les longues périodes de déneigement du site du Charquini et l'importance des flux solaires auxquels il est exposé favorisent le stockage dans son sol de quantités de chaleur importantes, là où celui du CDP, rapidement enneigé en début d'hiver de manière persistante, ne cesse ensuite de se refroidir par transfert de chaleur vers le manteau neigeux jusqu'à sa disparition. Ces différences d'apports de chaleur du sol vers la couverture neigeuse, probablement très conséquentes, s'ajoutent à celles quantifiées précédemment sur les flux solaires pour expliquer la vulnérabilité des manteaux neigeux tropicaux au regard des manteaux neigeux alpins. Il sera essentiel d'en tenir compte pour simuler correctement l'évolution de l'enneigement du Charquini.

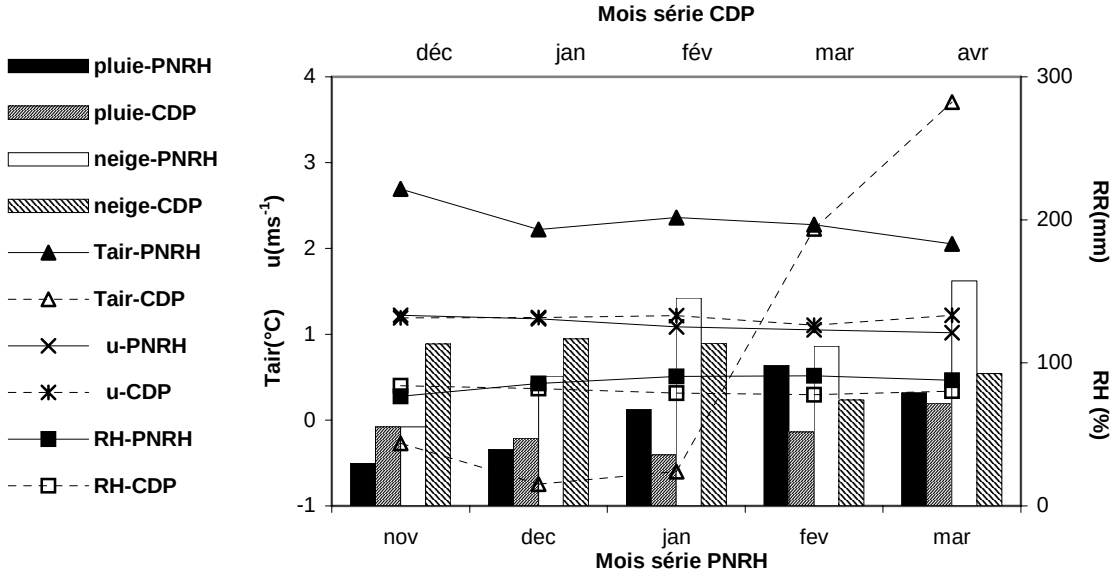

Fig. 3 Moyennes mensuelles des: température de l'air (Tair), humidité relative (RH), vitesse du vent (u), cumul des précipitations de pluie et de neige (RR) du PNRH Charquini (2 années, mois de novembre à mars) et du Col de Porte CDP (9 années, mois de décembre à avril).

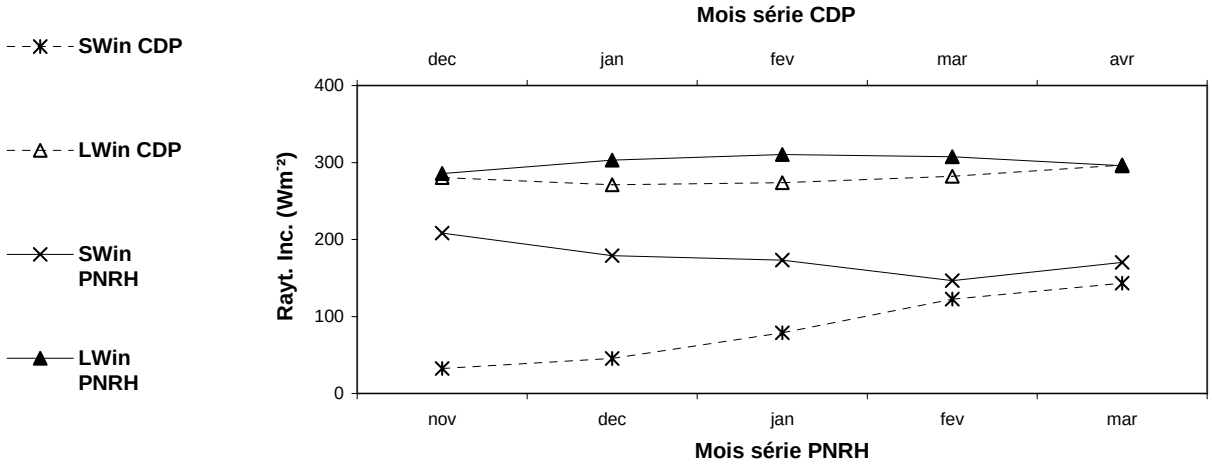

Fig. 4 Moyennes mensuelles des rayonnements incidents de courtes (SWin) et grandes longueurs d'ondes (LWin) du PNRH-Charquini (2 années, mois de nov.–mars) et du Col de Porte CDP (9 années, mois de décembre à avril).

LA CONSTITUTION DE LA BASE DE DONNEES

La méthodologie de constitution des jeux de données Charquini et ses différents algorithmes sont relatés en détail dans Lejeune *et al*. (2003). Dans la suite de cet article seront abordés les développements les plus conséquents de ce travail. Ils se rapportent à l'évaluation de la couverture nuageuse (ou nébulosité) N, à la reconstitution du rayonnement incident de grandes longueurs d'ondes LW_{in} sur les périodes de dysfonctionnement du pyrgéomètre (1501/2002–23/03/2002 et 15/05/2002–16/07/2003) et aux traitements des précipitations. L'interruption des mesures, du 18/04/2002 au

14/05/2002, suite au remplacement des capteurs de rayonnements nous a conduits à traiter les données en deux séries distinctes: 20/10/2001–18/04/2002 et 15/05/2002–16/07/2003.

Evaluation de la nébulosité N et reconstitution du rayonnement incident de grandes longueurs d'ondes (LWin)

Un des objectifs de la constitution de la base de données Charquini était l'évaluation (au pas de temps demi-horaire) de la nébulosité N, paramètre d'entrée du modèle de neige CROCUS (Brun *et al*., 1989, 1992) que l'on utilisera pour simuler l'enneigement du site. Plusieurs auteurs, tel que Berliand (1952) (formulation (1) détaillée par la suite), proposent des expressions calibrées qui explicitent le lien physique existant entre LW_{in}, RH, T_{air} et N. Sur le Charquini, en raison des dysfonctionnements du pyrgéomètre, N n'a pu d'une part être extraite d'une telle expression, et d'autre part devait être déterminée en premier lieu pour ensuite pouvoir reconstituer les mesures erronées de LW_{in}. N a donc été évaluée (au pas de temps demi-horaire) par la méthode suivante (méthode pw). Cette méthode, décrite en détail par ce qui suit, diffère le jour et la nuit:

(a) Le jour, le rayonnement solaire SW_{in}, somme du rayonnement direct $SW_{in\text{-}dir}$ du disque solaire non occulté par les nuages et du rayonnement diffus $SW_{in\text{-}diff}$ provenant de la voûte céleste (sauf disque solaire) et des nuages, fluctue en fonction de N. Le modèle SAFRAN (Durand *et al*., 1998, 1999), module éprouvé de fourniture de données météorologiques à la chaîne SAFRAN-CROCUS-MEPRA, outil opérationnel de Météo-France d'aide à la prévision des risques d'avalanches, évalue pour un lieu donné les flux solaires SW_{in} (et leur répartition en SW_{indir} et SW_{indiff}). Pour contrôler cette évaluation il utilise un schéma de rayonnement solaire théorique basé sur les travaux de Perrin de Brichambaut et Vauge (1981). Les rayonnements théoriques (et leur partition direct-diffus) issus de ce schéma dépendent de N et des caractéristiques géographiques (latitude et longitude) et topographiques (altitude, orientation et inclinaison) du lieu. Sur Charquini, à chaque pas de temps, ce schéma nous a permis de simuler les rayonnements $SW_{in}(N)$ théoriques pour onze nébulosités N du ciel clair (N = 0) au ciel couvert (N = 1). La nébulosité N_{pw} estimée est, de ces onze nébulosités N, celle qui permet de minimiser l'écart entre les rayonnements SW_{in} mesuré et théoriques.

(b) La nuit, l'évaluation de la couverture nuageuse a été appréhendée à partir des valeurs ou (et) des évolutions temporelles des paramètres, précipitations, T_{air}, et RH qui, dépendantes de N, sont caractéristiques en cas de couverture totale du ciel (N = 1). A partir des mesures disponibles, des critères objectifs ont été établis afin d'identifier les périodes pour lesquelles le site se trouvait, soit noyé dans le nuage, soit sous un ciel totalement couvert. Les justifications physiques de ces critères (séparés ici dans un souci de lisibilité mais souvent concomitants) et leurs valeurs seuils, spécifiques au site, sont: (a) le site est complètement couvert ou "dans le nuage", si l'air est proche de la saturation (RH > 98%) ou si une précipitation significative se produit ($\geq$0.6 mm h^{-1}), (b) le site couvert au pas de temps précédent

le reste si RH est forte (>97%) et si la variation de T_{air} sur le pas de temps est faible (≤0.1°C), (c) le site non couvert au pas de temps précédent le devient sur le pas de temps si RH est forte (>96%) et si le refroidissement nocturne s'est ralenti (baisse de T_{air} plus faible de 0.3°C sur le pas de temps que celle mesurée au cours du pas de temps précédent). L'établissement des valeurs seuils du pas de temps et celles des variations entre deux pas de temps, de T_{air}, RH, et des précipitations, a été réalisé par comparaison des N_{pw} ainsi estimées aux N_{berl} estimées par la formule de Berliand (1) (sur les périodes de bon fonctionnement du pyrgéomètre). Sur toute la période de mesures environ 12% des nébulosités nocturnes ont ainsi été estimées comme celles d'un ciel couvert. Celles restant indéterminées ont été interpolées linéairement à partir des valeurs de jour et de nuit déjà définies. Telle interpolation se justifie par le fait qu'invasions et disparitions des masses nuageuses sur ces hauts reliefs sont le plus souvent lentes et progressives (Wagnon, 1999).

La validation de la méthode a été réalisée par comparaison des N_{pw} aux observations (140) réalisées lors des campagnes de mesures. La moyenne de 0.64 des nébulosités observées est très proche de celle de 0.63 des nébulosités N_{pw} estimées. L'écart quadratique moyen (RMS) des deux populations est de 0.26. Cette méthode est donc satisfaisante même si elle mériterait d'être validée sur un plus grand échantillon d'observations.

Chaque année sur le site du CDP (Lejeune & Martin, 1995) un jeu de données météorologiques d'entrée du modèle de neige CROCUS (Brun *et al*. 1989, 1992) est constitué. La nébulosité N, paramètre d'entrée du modèle non mesurée sur le site, est extraite (par encadrements successifs) de la formule de Berliand (1952) qui s'énonce:

$$LW_{in} = \varepsilon \sigma T_{air}^{4} \quad (1)$$

avec:

$$\varepsilon = 0{,}58+0.9\ k\ N_{berl}^{2} + 0{,}06\ e_{air}^{-0{,}5}\ (1 - k\ N_{berl}^{2}) \quad (2)$$

et

$$k = 0.09 + 0.2\ N_{berl} \quad (3)$$

où: LW_{in} s'exprime en W m^{-2}, T_{air} et e_{air} (tension de vapeur de l'air) mesurées à une hauteur standard, s'expriment respectivement en Kelvin et en hpa. σ (= 5.67 10^{-8} W m^{-2} K^{-4}) est la constante de Stefan Boltzmann. N_{berl} est la nébulosité (en $1/10^{ème}$ de 0 à 1), k est une fonction de N_{berl}.

Sur Charquini, disposant de la nébulosité N_{pw} au pas de temps demi-horaire, LW_{in} a été reconstitué avec la formule de Berliand (1) sur toutes les périodes de dysfonctionnement du pyrgéomètre.

Une telle estimation de LW_{in} à partir de N_{pw}, paramètre lui-même estimé, nécessitait aussi d'être discutée. Sur les périodes de bon fonctionnement du pyrgéomètre, méthode pw d'évaluation de N puis méthode d'estimation de LW_{in} par la formule de Berliand ont successivement été appliquées. Les valeurs diurnes et nocturnes des LW_{inpw} ainsi estimés ont été comparées à celles des LW_{in} mesurés (tableau 2). Les moyennes (jour + nuit) des écarts (ou biais moyen) sont de 9 W m^{-2} (4%) du 20/10/2001 au 15/01/2002 et de 1 W m^{-2} (0%) du 24/03/2002 au 18/04/2002, les RMS sont pour ces deux périodes de 33 W m^{-2} et 35 W m^{-2}. En outre, le flux moyen quotidien LW_{inpw} estimé a été comparé à celui LW_{in} mesuré et à ceux LW_{in-10} et

LW_{in+10} mesurés affectés de l'incertitude constructeur (± 10% sur le cumul quotidien, cf. tableau 1). Sur la Fig. 5 (20/10/2001-15/01/2002) le flux estimé suit correctement les fluctuations journalières du flux mesuré et reste à quelques exceptions près compris dans l'intervalle d'incertitude de la mesure. L'ensemble de ces comparaisons nous permet donc de considérer que la méthode pw, qui évalue LW_{in} à partir des seules données météorologiques du dispositif expérimental sans aucune connaissance des profils verticaux d'humidité et de température de la masse d'air située au dessus du site d'études, est satisfaisante.

Tableau 2 Comparaison des moyennes, des écarts relatifs moyens et des écarts quadratiques moyens (RMS) des rayonnements grandes longueurs d'ondes LWin mesurés (LWmes) et estimés par la méthode pw (LWpw) durant les périodes de bon fonctionnement du pyrgéomètre.

Périodes	Jour				Nuit				Jour et nuit			
	moy. (W m^{-2})		écart relatif (%)	RMS (W m^{-2})	moy. (W m^{-2})		écart relatif (%)	RMS (W m^{-2})	moy. (W m^{-2})		écart relatif (%)	RMS (W m^{-2})
	LW_{mes}	LW_{pw}			LW_{mes}	LW_{pw}			LW_{mes}	LW_{pw}		
20/10/01–15/01/02	307	287	7	35	286	283	1	31	296	285	4	33
24/03/02–18/04/02	304	292	4	33	281	294	–5	36	292	293	0	35

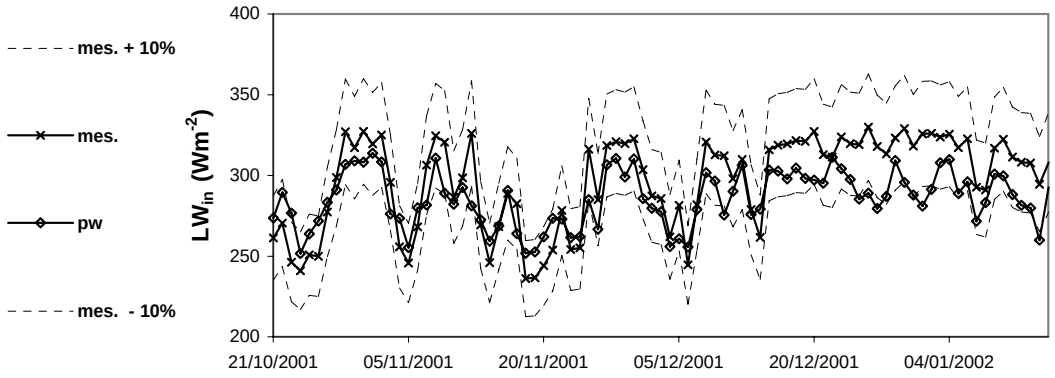

Fig. 5 Moyennes quotidiennes des rayonnements grandes longueurs d'ondes incidents LWin mesurés (mes.) et estimés par la méthode pw (pw), et enveloppes LWin+10 (mes. + 10%) et LWin-10 (mes. –10%) d'incertitude de la mesure, au cours de la première période de bon fonctionnement du pyrgéomètre (87 jours).

Estimation de la phase des précipitations et correction de la lame d'eau mesurée

Les variations d'épaisseur du manteau neigeux sont un critère très utile d'estimation des phases Cependant sur Charquini, les mesures de hauteur de neige sont très incomplètes et peu fiables et seules quelques valeurs supérieures à 2 cm ont été retenues (avec une précision de ±2 cm). Leur trop petit nombre ne nous a pas permis d'en tenir compte dans l'algorithme de discrimination des phases. La méthode développée est donc la suivante:

Au delà de +3°C la phase est pluie, en deçà de –1°C la phase est neige. Entre ces deux seuils de température, des critères de discrimination ont été établis à partir de toutes les mesures disponibles. Ceux qui prévalent d'une discrimination sous forme de neige sont: (a) par rapport au pas de temps précédent, un accroissement de l'albédo (>

0.1), un refroidissement marqué des premiers centimètres de sol (baisses du flux du sol à –3 cm (>15 W m^{-2}) et de T_{sol} à –3 cm (> 1.5°C)), (b) sur le pas de temps, une perte de chaleur du sol au profit de la surface (traduit par convention de signe par un flux de sol négatif), un sol "froid" (T_{sol} à –3 cm < +1.5°C), la présence d'une pellicule de neige sur la coupelle du capteur SW_{in} (albédo mesuré supérieur à 1), une intensité de précipitation susceptible de refroidir localement la masse d'air (>1 mm h^{-1}), et enfin un air plus ou moins froid (T_{air} < 0°C ou 0°C < T_{air} < +2°C ou T_{air} > +2°C). La manifestation de chacun de ces critères, leur intensité et leur caractère discriminant dépendent de l'état d'enneigement (ou non) du sol en début de pas de temps et de l'occurrence de précipitations, et en ce cas de leur phase, lors du pas de temps précédent. L'algorithme de la méthode a été construit en ce sens (les seuils détaillés précédemment sont ceux utilisés pour un sol déneigé au début du pas de temps, sans chutes de neige au cours du pas de temps précédent; à contrario les critères et les seuils utilisés diffèrent).

Comme pour la nébulosité, la campagne de terrain de février 2002 nous a permis d'observer sur le site les phases de 54 événements précipitants. Ces observations et les estimations correspondantes ont été comparées dans une table de contingence (tableau 3). En considérant que les mauvaises estimations sont celles de pluie pour neige et inversement, que les bonnes estimations sont neige pour neige, pluie pour pluie, ou pluie et neige mélangée pour pluie et neige mélangée, et que les estimations moyennes sont trivialement les autres, le score des mauvaises estimations est de 2, celui des bonnes est de 32, celui des moyennes est de 20. Le biais le plus conséquent de la méthode est de privilégier la phase liquide: pluie estimée pour un mélange de pluie et neige observé (13 cas) ou mélange de pluie et neige estimé pour neige observée (4 cas). Ce biais toujours observé pour des températures supérieures à +1°C devrait peu influer sur les simulations de l'enneigement, mais cela est d'autant plus difficile à appréhender que l'observation d'un mélange de pluie et neige n'en définit pas la partition réelle de la phase liquide et de la phase solide. On peut donc considérer que la méthode, bien que testée sur un petit échantillon d'observations est globalement concluante et que les simulations d'enneigement permettront d'en parfaire l'évaluation pour les cas les plus discutables.

Tableau 3 Table de contingence des phases observées et estimées.

		Observations		
		Pluie	Pluie et neige	Neige
Simulations	Pluie	22	13	1
	Pluie et neige	2	0	4
	Neige	1	1	10

Comme le recommande l'organisation mondiale de la météorologie, l'OMM, la non captation par les pluviomètres d'une part des lames d'eau de précipitation, d'autant plus importante en cas de chutes de neige froides et ventées, nécessite que les cumuls mesurés soient réévalués. Ces corrections sont dépendantes du type de pluviomètre, de la température de l'air, de la vitesse du vent et de la phase (Forland *et al.*, 1996). Sur le jeu de données Charquini, après estimation des phases, le cumul des

précipitations a ainsi été majoré de 5%; majoration relativement faible puisque la plupart des chutes de neige se sont produites pour des vents faibles et des températures de l'air voisines de 0°C.

CONCLUSIONS ET PERSPECTIVES

La méthodologie développée pour l'estimation des données non mesurées et pour la reconstitution des mesures manquantes pourra être appliquée, moyennant quelques adaptations, sur le site de l'ORE-Glacioclim (Observatoire de Recherche en Environnement – Les GLACIers, un Observatoire du CLIMat; Wagnon et Vincent, 2003) du glacier Zongo (6000–4900 m), situé en face du Charquini. Des forçages atmosphériques complets pour des modèles physiques de neige et de sol et des données de validation ont ainsi pu être constitués à l'échelle locale sur la haute montagne tropicale pour les deux périodes 24/10/2001–17/04/2002 et 15/05/2002–16/07/2003. Un tel jeu de données est inusuel sur ces régions dont une des caractéristiques climatiques est d'être soumises à des flux solaires très intenses permettant à leurs sols de stocker en absence de neige de grandes quantités de chaleur. Le jeu Charquini nous permettra de tester les capacités des modèles de sol ISBA (Noilhan *et al*., 1989, 1996) et du modèle de neige CROCUS (Brun *et al*., 1989, 1992) de METEO-France (modèles développés et validés sur les montagnes des régions tempérées) à représenter le couvert neigeux du site Charquini. Ces futures modélisations devraient contribuer à affiner la compréhension des processus d'évolution du couvert nival des hautes régions tropicales. Le travail décrit précédemment en était donc le préambule indispensable.

Remerciements Cette étude a été réalisée grâce à un financement du Programme National français de Recherche en Hydrologie. On remercie Joel Noilhan et Florence Habets du Groupe de Modélisation Moyenne Echelle du CNRM de METEO-France pour leurs collaborations actives au projet PNRH 01-37 ainsi que Pierre Ribstein, Robert Gallaire, Rolando Fuertes, Alvaro Soruco, Etienne Berthier, Bernard Francou de l'IRD (GREAT-ICE), ainsi que tous les représentants de l'IRD et leurs collaborateurs locaux à La Paz (Bolivie).

REFERENCES

Berliand, M. E. & Berliand, T. G. (1952) Measurement of the effective radiation of the earth with varying cloud amounts, Izv. Akad. Nauk SSR, Ser. Geofiz., 1, (in Russian).

Bourqui, M. (2003) Forçages climatiques et précipitations en très haute montagne tropicale, comparaison sols nu et englacé-Vallée du Rio Zongo (Cordillère Royale, Bolivie). Mémoire de DEA, Université Montpellier II, 55p.

Bradley, R. S., Keimig, F. T. & Diaz, H. F. (2004) Projected temperature changes along the American Cordillera and the planned GCOS Network. *Geophys. Res. Lett.* **31**(16), doi:10.1029/2004GL020229.

Brun, E., Martin, E., Simon, V., Gendre, C. & Coleou, C. (1989) An energy and mass model of snow cover suitable for operational avalanche forecasting. *J. Glaciol*. **35**(121), 333–342.

Brun, E., David, P., Sudul, M. & Brunot, G. (1992) A numerical model to simulate snow-cover stratigraphy for operational avalanche forecasting. *J. Glaciol*. **38**(128), 13–22.

Caballero, Y. (2001) Modélisation des écoulements d'origine pluvio-nivo-glaciaire en contexte de haute montagne tropicale – application à la haute vallée du Zongo (Bolivie), Thèse de doctorat, Univ. Montpellier 2, France.

Durand, Y., Giraud, G. & Mérindol, L. (1998) Short-term numerical avalanche forecast used operationally at Météo-France over the Alps and Pyrenees. *Ann. Glaciol*. **26**, 357–366.

Durand, Y., Giraud, G., Brun, E., Mérindol, L. & Martin, E. (1999) A computer-based system simulating snowpack structures as a tool for regional avalanche forecasting. *J. Glaciol*. **45**(151), 469–484.

Favier, V., Wagnon, P., Chazarin, J. P., Mashinsho, L. & Coudrain, A. (2004a) One-year measurements of surface heat budget on the ablation zone of Antizana glacier 15, Ecuadorian Andes. *J. Geophys. Res*. **109**(D18, D18105), doi: 10.1029/2003JD004359.

Favier, V., Wagnon, P. & Ribstein, P. (2004b) Glaciers of the inner and outer tropics: a different behaviour but a common response to climatic forcing. *Geophys. Res. Lett*. **31**(L16403), doi:10.1029/2004GL020654.

Forland, E. J., Allerup, P., Dahlström, B., Elomaa, E., Jonsson, T., Madsen, H., Perälä, J., Vedin, H. & Vejen, F. (1996) Manual for operational correction of Nordic precipitation data. Klima Report N°24/96, DNMI, Nordic Working Group on Precipitation (NWGP).

Francou, B., Vuille, M., Wagnon, P., Mendoza, J. & Sicart, J. E. (2003) Tropical climate change recorded by a glacier in the central Andes during the last decades of the 20th century: Chacaltaya, Bolivia, 16°S. *J. Geophys. Res.* **108**(D5), ACL 1.1–1.12.

Kaser, G. & Osmaston, J. (2002) *Tropical Glaciers*. Int. Hydrology Series, UNESCO and Cambridge University Press, Cambridge, New York, USA.

L'Hôte, Y., Chevallier, P., Etchevers, P., Lejeune, Y. & Wagnon, P. (2004) Pluie ou neige? Dispositif de mesures pluviographiques dans les Andes de Bolivie et interprétation des enregistrements. *Hydrol. Sci. J.* **49**(2), 273–281.

L'Hôte, Y., Chevallier, P., Coudrain, A., Lejeune, Y. & Etchevers, P. (2005) Relationship between precipitation and air temperature: comparison between the Bolivian Andes and the Swiss Alps. *Hydrol. Sci. J.* **50**(6), 989–997.

Lejeune, Y. & Martin, E. (1995) Application du modèle CROCUS aux données de la saison 93/94 du Col de Porte et de la campagne LEADEX 92. Météo-France, Centre National de Recherches Météorologiques – Centre d'Etude de la Neige, Note de Centre no. 6, France.

Lejeune, Y., L'Hôte, Y. & Chevallier, P. (2003) Instrumentation et constitution d'une base de données météorologiques et nivologiques dans les Andes; Station Charquini, 4795 m, Bolivie. Météo-France, Centre National de Recherches Météorologiques – Centre d'Etude de la Neige, Note de Centre N°21, France. (Disponible sur: http://www.mpl.ird.fr/hydrologie/pch/documents/PNRH01-37/pdf/PNRH0137_note_charquini.pdf).

Noilhan, J. & Planton, S. (1989) A simple parametrization of land surface processes for meteorological models. *Mon. Weath. Rev*. **117**, 536–549.

Noilhan, J. & Mahfouf, J. F. (1996) The ISBA land surface parametrization scheme. *J. Global & Planetary Change* **13**, 145–159.

Perrin de Brichambaut, C. & Vauge C. (1981) Le gisement solaire: Evaluation de la ressource énergétique. Technique et documentation, ed. Lavoisier, Paris, France.

Sicart, J. E. (2002) Contribution à l'étude des flux d'énergie, du bilan de masse et du débit de fonte d'un glacier tropical: Le Zongo, Bolivie. Thèse de doctorat, Université Paris VI – Pierre et Marie Curie, Paris, France.

Sicart, J. E., Wagnon, P. & Ribstein, P. (2005) Atmospheric controls of the heat balance of Zongo Glacier (16°S, Bolivia), *J. Geophys. Res.* **110** D12106, doi:10.1029/2004JD005732.

Thompson, L. G., Mosley-Thompson, E., Davis, M. E., Lin, P. -N., Henderson, K. & Mashiotta, T. A. (2003) Tropical glacier and ice core evidence of climate change on annual to millennial time scales. Highest Volume. *Climatic Change* **59**(1–2), 137–155.

Vincent, C., Ribstein, P., Wagnon, P., Francou, B., Favier, V., Le Meur, E. & Six, D. (2005) Glacier fluctuations in the Alps and in the tropical Andes. *CR Geosci*. **337**, 97–106.

Vuille, M. (1999) Atmospheric circulation over the Bolivian Altiplano during dry and wet period and extremes phases of the Southern Oscillation. *Int. J. Climate* **19**, 1579–1600.

Vuille, M. (2000) Interannual climate variability in the Cental Andes and its relation to Tropical Pacific and Atlantic forcing. *J. Geophys. Res*. **105**(12),447–460.

Wagnon, P. (1999) Analyse du bilan d'énergie d'un glacier tropical, Application à la relation glacier-climat. Thèse de doctorat de l'Université Joseph Fourier, Grenoble, France.

Wagnon, P., Ribstein, P., Francou, B. & Pouyaud, B. (1999a) Annual cycle of energy balance of Zongo Glacier, Cordillera Real, Bolivia. *J. Geophys. Res*. **104** D4, 3907–3923.

Wagnon, P., Ribstein, P., Kaser, G. & Berton, P. (1999b) Energy balance and runoff seasonality of a Bolivian glacier. *Global & Planetary Change* **22**, 49–58.

Wagnon, P., Ribstein, P., Francou, B. & Sicart, J. E. (2001) Anomalous heat and mass budget of Zongo Glacier, Bolivia during the 1997-98 El Niño year. *J. Glaciol*. **47**(156), 21–28.

Wagnon, P. & Vincent, C. (2003) Climate change as recorded by glaciers. *IGBP Global Change News Lett*. **56**, 13–16.

Glacier Mass Balance Changes and Meltwater Discharge (selected papers from sessions at the IAHS Assembly in Foz do Iguaçu, Brazil, 2005). IAHS Publ. 318, 2007.

Temperature lapse rates and surface energy balance at Storglaciären, northern Sweden

KEIKO KONYA[1,2,3]**, REGINE HOCK**[4,5] **& RENJI NARUSE**[2]

1 *Graduate school of Environmental Earth Science, Hokkaido University, Japan*

2 *Institute of Low Temperature Science, Hokkaido University, Kita19 Nishi8, Kita-ku, Sapporo, Hokkaido 060-0819, Japan*

3 *Institute of Observational Research for Global Change, Japan Agency for Marine-Earth Science and Technology, Japan*
conya@jamstec.go.jp

4 *Department of Earth Sciences, Uppsala University, Villavägen 16, 75236 Uppsala, Sweden*

5 *Geophysical Institute, University of Alaska, Fairbanks, Alaska 99775-7320, USA*

Abstract A detailed meteorological experiment, including the operation of several automatic weather stations on and outside the glacier, was performed on Storglaciären, a valley glacier in Sweden, in summer 2003. On average, near surface air temperature lapse rates derived from several weather stations on the glacier were –6.0 ± 3.5°C km^{-1}, indicating strong temporal variability. We found no correlation with meteorological variables as a base for parameterization in melt modelling. Surface energy balance computations showed that, on average, net radiation is the largest contributor to melt energy, in agreement with previous studies. Latent heat fluxes were positive throughout the simulation period indicating condensation. It was not possible to constrain roughness lengths within several orders of magnitudes, since the differences in modelled melt for all cases were still within the range of uncertainty pertinent to the melt measurements during the 13-day period of coincident meteorological and melt measurements.

Key words ablation; automatic weather stations; glacier; modelling; surface energy balance; temperature lapse rate

INTRODUCTION

Glacier melt is determined by the surface energy balance (e.g. Takeuchi *et al*., 1999; Oerlemans, 2001), but detailed glacio-meteorological studies are relatively scarce (see e.g. summary in Hock, 2005) as operation of automatic weather stations on glaciers still provides a challenge due to continuously changing surface conditions and, typically, harsh weather conditions. In this paper, we report some first analyses of a detailed glacio-meteorological experiment conducted on Storglaciären, a small valley glacier in northern Sweden (67°55′N, 18°35′E, Fig. 1) in summer 2003. The experiment included the operation of several automatic weather stations (AWS) on and outside the glacier, and detailed profile measurements at one site. The glacier (3 km^2, 1120 to 1730 m a.s.l.) is well investigated and has one of the longest mass balance records in the world (Holmlund *et al*., 2005). Previous studies on surface energy balance on Storglaciären (Hock & Holmgren, 1996) and distributed energy balance modelling (Hock & Holmgren, 2005) have shown that the turbulent fluxes are significant contributors to the energy available for melt providing roughly one third to about half of the melt energy.

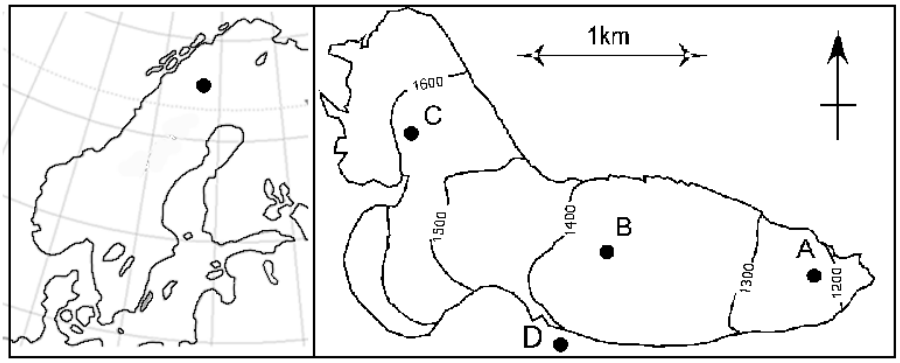

Fig. 1 Storglaciären and location of the automatic weather stations (A–D) operated in summer 2003. Station B included profile measurements. The contour lines are in m.

Mass balance modelling often relies upon the assumption of a constant temperature lapse in order to distribute measurements of air temperature to or across the glacier (e.g. Braithwaite & Zhang, 2000; Hock & Holmgren, 2005; de Woul & Hock, 2005), although lapse rates are known to vary with location and time. Hence most accurately, temporally variable lapse rates are applied in mass balance modelling but often such data are not available.

Our specific objectives are: (1) to analyse air temperature lapse rates based on near-surface air temperature data from several weather stations across the Storglaciären, and (2) to compute the surface energy balance from the meteorological data and investigate energy partitioning. An analysis of the profile measurements will be given in a forthcoming paper.

METHODOLOGY

Field measurements

One detailed and several less-equipped AWS were operated on and outside the glacier between mid July and mid September, 2003 (Konya & Hock, 2003). The detailed station was operated close to the centre of the glacier, where the surface is relatively smooth, with slopes less than 3°, and included profile measurements of air temperature (Vaisala HMP45D, accuracy 0.3°C), relative humidity (Vaisala HMP45D) and wind speed (Lastem 034S, accuracy 0.4 m s^{-1}) with sensors mounted at 0.5, 1, 2 and 4 m above the surface. Shortwave incoming and reflected radiation and longwave incoming and outgoing radiation were recorded at roughly 1.5 m above the surface using CNR1-sensors (Kipp and Zonen). Surface lowering was measured by an ultrasonic device (Campbell Scientific SR50), in order to derive hourly melt rates. Sensors were mounted to masts drilled into the ice, and the stations were visited every couple of days to adjust the instrument heights to surface lowering. Air temperature and humidity sensors were artificially ventilated. These and the wind sensors were calibrated relative to each other on the glacier. Measurements were taken every 10 minutes (radiation) and 1 minute (remaining instruments) and stored on data loggers (DATAMARK, Hakusn Co. Ltd). Three less-equipped stations were run on the glacier during shorter

periods, including air temperature, humidity and wind speed measurements at one level. An additional station was installed on the top of the southern ridge of the glacier (D in Fig. 1). Bare ice was exposed at the surface around stations A and B (Fig. 1) during the measurement period except for short periods following summer snowfall.

Energy balance calculation

The energy available for melt Q_M was computed by:

$$Q_M = Q_R + Q_H + Q_L \quad (1)$$

where Q_R is net radiation, and Q_H and Q_L are the sensible and latent heat fluxes, respectively. The sensible heat by rain and the ice heat flux were neglected. Also the flux by advection of warm air from adjacent valley slopes was assumed negligible, considering the distance of more than 1 km to the glacier margin in the dominant upwind direction. Net radiation was computed from the measurements of the individual components. Following Hock & Holmgren (2005) the sensible and latent heat fluxes were calculated by the bulk aerodynamic method considering atmospheric stability based on Monin-Obukhov similarity theory (Stull, 2001). Q_H, and Q_L were estimated from the following equations using the data measured at 2 m above the surface:

$$Q_H = \frac{k^2}{[\ln(z\ / z_0) - \Psi_m(z/L)][\ln(z/z_T)\Psi_T(z/L)]} \rho C_p U_z (T_z - T_0), \quad (2)$$

$$Q_L = \frac{k^2}{[\ln(z\ / z_0) - \Psi_m(z/L))][\ln(z/z_q)\Psi_q(z/L)]} \rho L_v U_z (q_z - q_0), \quad (3)$$

where k is the von Karman constant (0.4), ρ is the air density, C_p is the specific heat capacity of air, L_v is the latent heat of evaporation, z is observation height (2 m), U_z is wind speed, q is specific humidity at height z (q_z), and at the glacier surface (q_0), T_z is air temperature and T_0 is surface temperature, and z_0, z_T and z_q are the roughness lengths for wind, temperature and humidity, respectively. Ψ_m, Ψ_T and Ψ_q are the corresponding stability functions depending on the Monin-Obukhov length L. For the stable case the non-linear stability functions by Beljaars & Holtslag (1991) were applied; for the less frequent unstable case the commonly used Businger-Dyer expressions (see Paulson, 1970) were applied. The stability functions were computed using an iterative procedure following Munro (1990). We computed the turbulent fluxes for different values of roughness lengths (z_0) taken from a range of values reported in the literature (Brock *et al.*, 2006), aiming at maximum agreement between total modelled and measured melt over the period 4–12 August, for which detailed ablation measurements were available and no snowfall occurred. Roughness lengths z_T and z_q were assumed 1/100 of z_0 following Ambach (1986). The surface temperature was computed for every hour from the measurements of longwave outgoing radiation assuming an emissivity $\varepsilon = 1$. Q_M, if positive, was converted to water equivalent melt for comparison with measured melt rates assuming ice density of 900 kg m^{-3}. For $Q_M \leq 0$, Q_M was set to 0. The energy balance was computed for a 33-day period between 29 July and 9 September 2003, excluding a data gap between 13 and 22 August.

RESULTS AND DISCUSSION

Temperature lapse rates

Temperature differences between station B and the other three stations were analysed. We derived hourly lapse rates, defined as the negative ratio of the temperature difference and the altitude difference between two stations, using the measurements at equal heights above the surface. Mean lapse rates including standard deviations are summarized in Table 1. Average lapse rates follow the moist adiabatic lapse rate but standard deviation is large. Figure 2 shows that the lapse rates strongly vary in time. They also vary spatially across the glacier since the lapse rates derived from the glacier station data do not follow each other well. Lapse rates falling below –10°C km^{-1} or positive lapse rates occur more often when deriving lapse rates from the station outside the glacier (Fig. 3(c)) instead of exclusively using the data from the glacier (Fig. 3(a) and (b)). This can be attributed to the different energy exchange processes outside and on the glacier. Positive lapse rates may be caused by strong warming of near-surface air masses at station D due to surface warming of the rocks, while such warming is subdued on the glacier because the ice temperature cannot exceed 0°C, thus cooling near-surface air masses.

Braun & Hock (2004) found a strong dependence of lapse rates on the synoptic weather patterns on King George Island, Antarctica, with below average lapse rates

Table 1 Average temperature lapse rates, Γ, derived from hourly data at stations A (1219 m a.s.l.), B (1384 m a.s.l.), C (1612 m a.s.l.), and D (1700 m a.s.l.; Fig. 1). σ is standard deviation, Δh is elevation difference, z is measurement height above surface and n is number of cases.

Stations	Γ(°C km^{-1})	σ	Δh (m)	z (m)	n	Period
B-A	–6.0	2.9	165	1	424	21 Aug–8 Sep
B-C	–6.0	3.5	228	1	399	19 Aug–5 Sep
B-D	–7.1	4.8	316	2	407	21 Aug–7 Sep

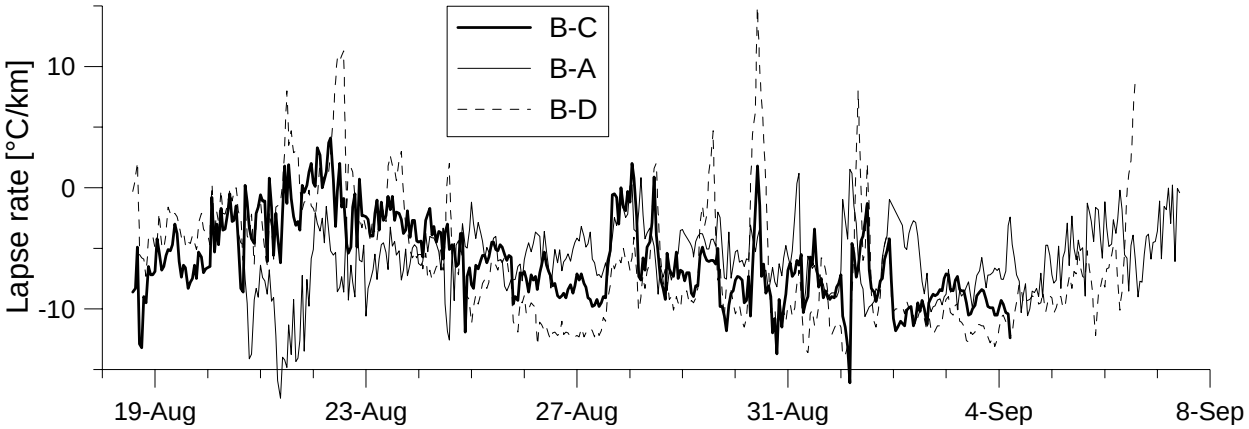

Fig. 2 Hourly surface air temperature lapse rates between 18 August and 7 September, 2003. Lapse rates are derived from (a) stations B and C, (b) stations B and A, (c) and stations B and D (outside glacier). (a) and (b) are based on the data at 1 m, while (c) is based on the data at 2 m in order to derive lapse rates from data at the same heights above the surface.

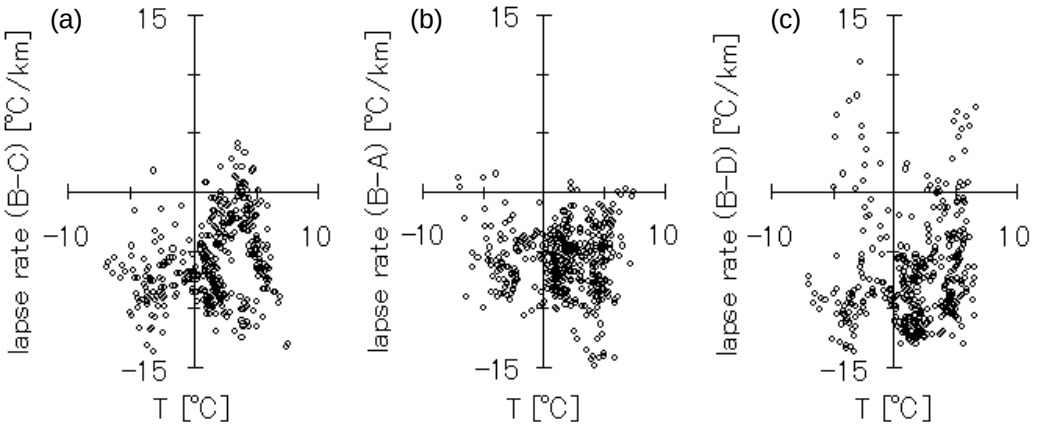

Fig. 3 Hourly surface air temperature lapse rates *vs* air temperature, *T*, at station B. Lapse rates are derived from (a) stations B and C, (b) stations B and A, and (c) stations B and D (outside glacier). (a) and (b) are based on the data at 1 m, while (c) is based on the data at 2 m in order to derive lapse rates from data at the same heights above the surface.

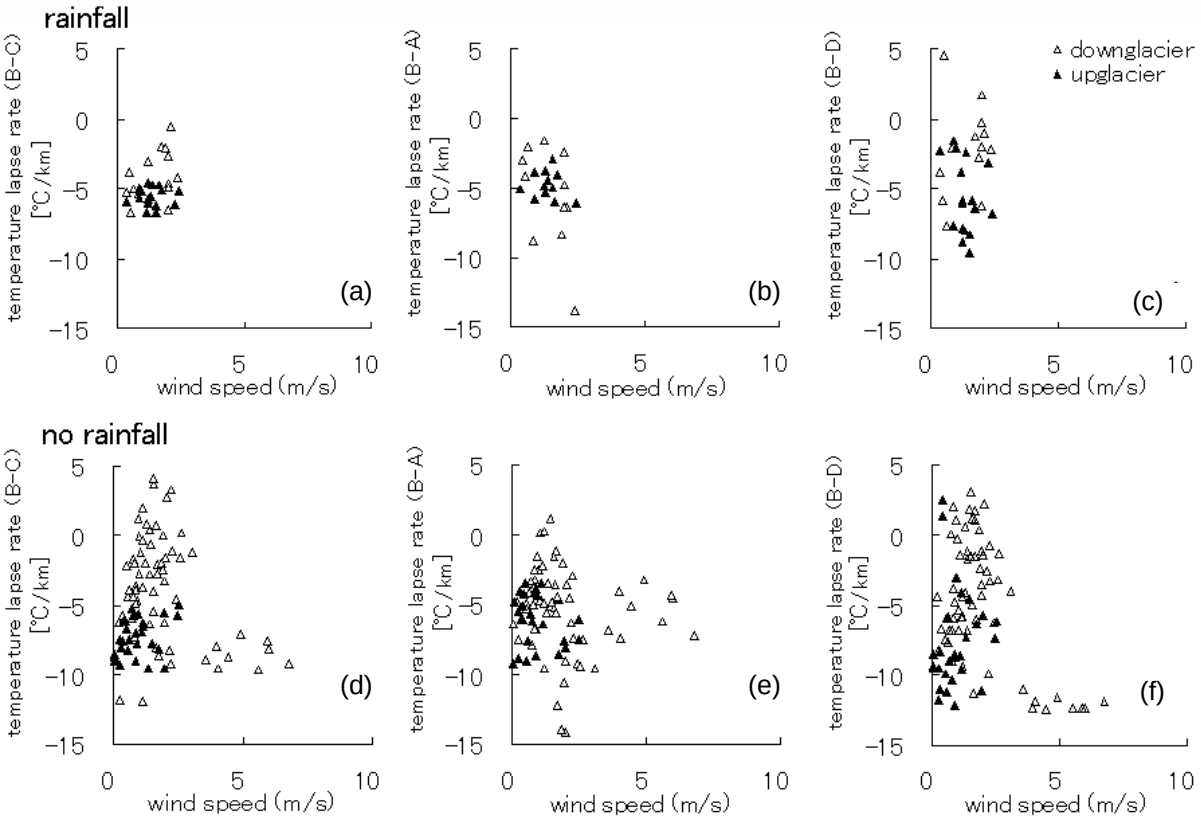

Fig. 4 Hourly surface air temperature lapse rates *vs* wind speed, *u*, at station B. Lapse rates are derived from ((a), (d)) stations B and C, ((b), (e)) stations B and A and ((c), (f)) stations B and D (outside glacier). Cases with wind direction between 250 and 290 ("downglacier") are distinguished from cases with wind direction between 70 and 110 ("upglacier"), both with ((a)–(c)) and without ((d)–(f)) precipitation.

during periods of strong melt associated with warm humid air advection and above average lapse rates during periods of low melt and cold air advection. We explore the

application of variable lapse rates dependent on meteorological conditions as base for their parameterization in mass balance models in order to elaborate on the generally made assumption of constant lapse rates. We plot lapse rates against air temperature (Fig. 3) and wind speed (Fig. 4). For the latter, cases with downglacier and upglacier wind direction and cases with and without precipitation are distinguished. Overall, we did not find any significant correlation between lapse rate and any of the meteorological variables studied. Hence, there seems no simple way to parameterize lapse rates for melt modelling, and preferably data from several weather stations on the glacier is used as input to the modelling.

Surface energy balance

Mean energy fluxes and energy partitioning based on different assumptions on roughness lengths, z_0, are listed in Table 2. Assuming z_0 = 0.001 mm yields 228 mm melt and hence the melt total measured during the 13-day period of coincident meteorological and detailed melt measurements. Such z_0 is suspiciously low and we increased z_0 values by up to three orders of magnitudes, which lies within the range of roughness lengths reported in the literature (Brock *et al*., 2006). If z_0 values of 0.01, 0.1 and 1 mm are adopted for calculating the turbulent fluxes, the model overestimates melt by 4%, 11% and 23%, respectively, compared to the melt derived from the measurements (Table 2)

Table 2 Energy balance components (in Wm^{-2} and % of Q_M) and modelled melt on Storglaciären for two periods in 2003 and for different assumptions on roughness length, z_0. Q_N is net radiation, Q_H and Q_L are the sensible and the latent heat flux, respectively, Q_M is the sum of Q_N, Q_H and Q_L, i.e. the energy available for melt and changes in internal energy. *A* is modelled ablation (cm) and *OE* (%) is the overestimation of melt compared to the ablation derived from the continuous record of surface lowering (22.8 cm in this study).

Period	z_0 mm	Q_N W m^{-2} *(%)*	Q_H W m^{-2} *(%)*	Q_L W m^{-2} *(%)*	Q_M W m^{-2}	*A* cm	*OE* %
4–16 Aug 2003	0.001	75 (*84*)	10 (*11*)	4 (*5*)	89	22.8	0.0
	0.01	75 (*80*)	13 (*14*)	6 (*6*)	94	23.7	4
	0.1	75 (*73*)	19 (*19*)	8 (*8*)	102	25.2	11
	1	75 (*64*)	30 (*26*)	13 (*11*)	118	28.1	23
29 Jul–9 Sept. 2003*	0.001	56	8	5	69	69	–**
	0.01	56	11	6	73	72	–
	0.1	56	16	9	81	77	–
	1	56	25	14	95	88	–
19 July–Aug 28, 1994***	2.7	73 *(66)*	33 *(29)*	5 *(5)*	111	126	–10
5 July–Sept. 6, 1994****	10	49 *(58)*	36 *(42)*	0 *(0)*	85	–	–
June 7–Sept. 17, 1993****	10	18 *(39)*	20 *(43)*	8 *(17)*	46	–	–

*33-day period excluding data gap 13–22 Aug.; **melt measurements unreliable due to frequent snow fall; ***Hock & Holmgren (1996); ****Hock & Holmgren (2005, note: values refer to glacier-wide averages).

Deviations between modelled and measured melt may be attributed to uncertainties in the conversion of surface lowering to melt and small-scale differences in melt between the site of the weather station and the site of the melt measurements. Even though these sites were less than 10 m apart, observations indicated that surface characteristics such as albedo or roughness varied between both sites and may have caused spatial melt variations of the order of the results. Braithwaite *et al.* (1998) found small-scale differences in melt of >10% caused by variations in surface albedo. The assumption of a full emitter, thus neglecting reflection of longwave radiation, affects the computation of the surface temperature by up to a few degrees, and hence the turbulent fluxes. Further uncertainties arise from neglect of energy fluxes other than included in equation (1), uncertainties in underlying assumptions in the calculation of the turbulent fluxes (Hock, 2005) and from measurement uncertainties (Rolstad & Oerlemans, 2005). Differences between resulting turbulent fluxes when changing the roughness, z_0, by one order of magnitude roughly correspond to an assumed measurement uncertainty of ±10 W m^{-2} for the radiation measurements (see Table 2). For example, an overestimation of net radiation by 10 W m^{-2} due to measurement errors combined with an underestimation of measured melt by 6% due to uncertainties in density changes and surface lowering, requires a 100-fold larger roughness length (z_0 = 0.1 instead of z_0 = 0.001) to close the energy balance.

These qualitative considerations suffice to conclude that it is not possible from the data available in this study to determine z_0 from closing the energy balance based on melt measurements. Nevertheless, some general conclusions on energy partitioning and surface energy fluxes can be drawn. Net radiation contributes 84% to 64% of the energy available for melt and changes in internal energy, assuming z_0 = 0.001 mm to 1 mm, respectively. Earlier studies yielded averages of 39–66% (Hock & Holmgren, 1996, 2005; Table 2). Variations in energy partitioning to melt energy between different studies may result from averaging over different periods and lengths of time and from varying prevailing weather conditions. In accordance with previous studies the average latent heat flux is positive indicating condensation. In fact energy is provided by condensation throughout the modelling period (Fig. 5). Mean measured radiation components generally compare well with results from previous studies on Storglaciären (Table 3). Net longwave radiation was negative on average. During several nights net radiation turned negative (Fig. 5).

Table 3 Mean radiation (W m^{-2}) on Storglaciären. *G* is global radiation, *SWB* is shortwave radiation balance, $L\downarrow$ and $L\uparrow$ are incoming and outgoing longwave radiation, respectively, and Q_N is net radiation. The results for 1–3 are derived from measurements at an automatic weather station on the glacier; row 4–5 refer to glacier-averaged results from a distributed energy balance melt model.

	Period	*G*	*SWB*	$L\downarrow$	$L\uparrow$	$L\downarrow + L\uparrow$	Q_N	Reference
1	4–16 Aug. 2003	145	88	280	–309	–30	75	This study
2	29 July–9 Sept. 2003*	106	65	290	–308	–17	56	This study
3	19 July–27 Aug. 1994	169	97	–	–	–	73	Hock & Holmgren (1996)
4	5 July–6 Sept. 1994	169	77	271	–299	–28	49	Hock & Holmgren (2005)
5	7 June–17 Sept. 1993	147	37	277	–297	–20	18	Hock & Holmgren (2005)

*33 day period excluding data gap 13–22 August.

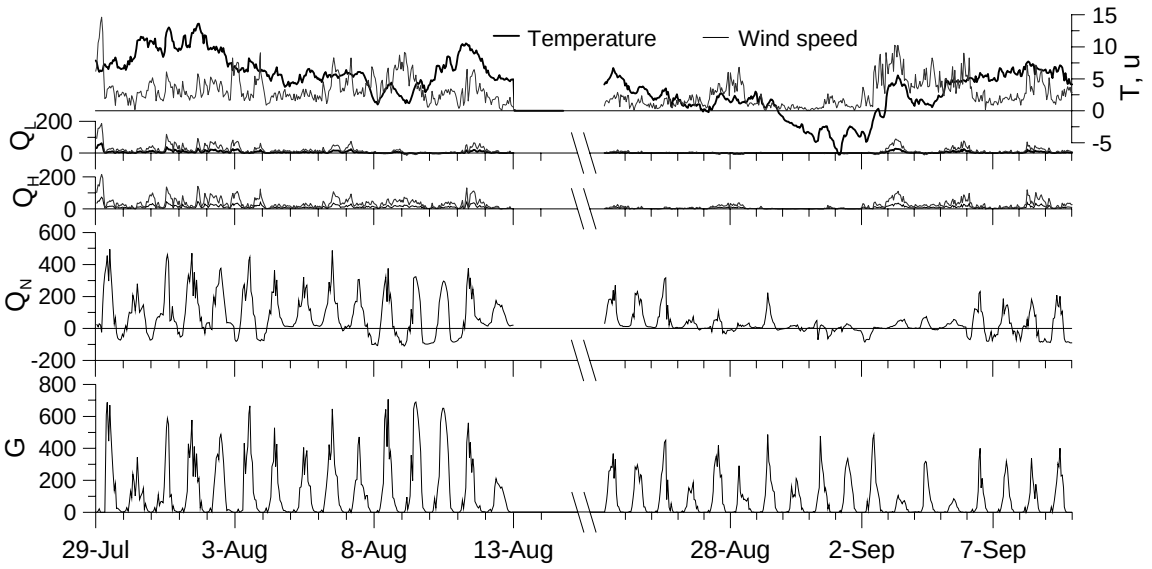

Fig. 5 Hourly energy balance components (W m^{-2}), air temperature, T (°C) and wind speed, u (m s^{-1}, 2 m level) at station B on Storglaciären, 29 June to 9 September, 2003. Note data gap 13–22 August. Q_N is net radiation, G is global radiation, Q_H and Q_L are the sensible and the latent heat flux, respectively, all in W m^{-2}. Q_H and Q_L are shown for two assumptions on roughness length, z_0 = 0.001 mm (thin line) and z_0 = 1 mm (thick line).

CONCLUSIONS

Analysis of hourly air temperature data collected at various locations on and outside the glacier indicates that surface air temperature lapse rates vary strongly in time, although on average values are close to the moist adiabatic value. The standard deviation is higher when lapse rates are derived from data on and outside the glacier than when they are computed exclusively from data from the glacier. This is to a large extent due to differences in surface energy exchange processes on and outside the glacier. We could not detect any correlation between temperature lapse rates and meteorological variables, and hence could not find a simple way to parameterize lapse rates for use in melt modelling.

Net radiation was the main contributor of melt during a 33-day period between 29 July to 9 September 2003, excluding a data gap between 13 and 22 August. However, more precise energy partitioning was hampered by lack of sufficient coincident meteorological and melt measurements. It was not possible to derive realistic values of roughness lengths from tuning the model by closing the energy balance since variations of roughness lengths by several orders of magnitude resulted in melt rates within the range of uncertainty for the melt measurements. Results emphasize the difficulties in using meteorological and melt measurements over limited periods of time for determining the energy balance over glaciers.

Acknowledgements Mart Nyman and others at Tarfala Research Station are acknowledged for their logistic support. Discussion with staff of Stockholm University and J. O. Hagen was very helpful to this study. This study was financially supported by

the Sasakawa Scientific Research Grant from the Japan Science Society, the Inoue Fund of Field Science by the Japanese Society of Snow and Ice and the 21st century COE program “Prediction and avoidance of an abrupt change in the bio-geosphere system” of Graduate School of Environmental Earth Science, Hokkaido University. R. Hock is Royal Swedish Academy of Science Research Fellow supported by a grant from the Knut Wallenberg Foundation.

REFERENCES

Ambach, W. (1986) Nomographs for the determination of meltwater from snow and ice surfaces. *Berichte des naturwissenschaftlich medizinischen Vereins in Innsbruck* **73**, 7–15.

Beljaars, A. C. M. & Holtslag, A. A. M. (1991). Flux parameterization over land surfaces for atmospheric models. *J. Appl. Meteorol.* **30**, 327–341.

Braithwaite, R. J. & Zhang, Y. (2000) Sensitivity of mass balance of five Swiss glaciers to temperature changes assessed by tuning a degree-day model. *J. Glaciol.* **46**(152), 7–14.

Braithwaite, R., Konzelmann, T., Marty, C. & Olesen, O. B. (1998) Errors in daily ablation measurements in northern Greenland, 1993-94, and their implications for glacier climate studies. *J. Glaciol.* **44**(148), 583–588.

Braun, M. & Hock, R. (2004) Spatially distributed surface energy balance and ablation modelling on the ice cap of King George Island (Antarctica). *Glob. Plan. Change* **42**(1–4), 45–58. doi 10.1016/j.gloplacha.2003.11.010.

Brock, B., Willis, I. C. & Sharp, M. J. (2006) Measurement and parameterization of aerodynamic roughness length variations at Haut Glacier d´Arolla, Switzerland. *J. Glaciol*. **52**(177), 281–297.

de Woul, M. & Hock, R. (2005) Static mass balance sensitivity of Arctic glaciers and ice caps using a degree-day approach. *Ann. Glaciol.* **42**, 217–224.

Hock, R. (2005) Glacier melt – a review on processes and their modelling. *Progr. Phys. Geogr.* **29**(3), 362–391.

Hock, R. & Holmgren, B. (1996) Some aspects of energy balance and ablation of Storglaciären, Northern Sweden. *Geogr. Ann.* **78A**(2–3), 121–131.

Hock, R. & Holmgren, B. (2005) A distributed energy balance model for complex topography and its application to Storglaciären, Sweden. *J. Glaciol*. **51**(172), 25–36.

Holmlund, P., Jansson, P. & Pettersson, R. (2005) An analysis of mass changes of Storglaciären over the last 58 years, *Ann. Glaciol.* **42**, 389–394.

Konya, K. & Hock. R. (2003) Meteorological observations on Storglaciären in 2003. In: *Tarfala Research Station Annual Report 2002–2003* (ed. by P. Klingbjer). Reports from the Department of Physical Geography and Quaternary Geology, Stockholm University 3, 21–25.

Munro, D. S. (1990) Comparison of melt energy computations and ablatometer measurements on melting ice and snow. *Arctic Alp. Res.* **22**(2), 153–162.

Oerlemans J. (2001) *Glaciers and Climate Change*. A.A. Balkema Publishers, Lisse, The Netherlands.

Paulson, C. A. (1970) The mathematical representation of wind speed and temperature profiles in the unstable atmospheric surface layer. *J. Appl. Meteorol.* **9**, 857–861.

Rolstad, C. & Oerlemans, J. (2005) The residual method for determination of the turbulent exchange coefficient applied to automatic weather station data from Iceland, Switzerland and West Greenland. *Ann. Glaciol.* **42**, 367–372.

Stull, R. B. (2001) *An Introduction to Boundary Layer Meteorology*. Kluwer Academic Publishers, Dordrecht, The Netherlands.

Takeuchi, Y., Naruse, R., Satow K. & Ishikawa, N. (1999) Comparison of heat balance characteristics at five glaciers in the Southern Hemisphere. *Glob. Plan. Change* **22**, 201–208.

Glacier Mass Balance Changes and Meltwater Discharge (selected papers from sessions at the IAHS Assembly in Foz do Iguaçu, Brazil, 2005). IAHS Publ. 318, 2007.

Precipitation variations on different slopes of Tien Shan

TIANDING HAN, YONGJIAN DING, CHANGWEI XIE, BAISHENG YE & YONGPING SHEN

Tianshan Glaciological station/Key Laboratory of Cryosphere and Environment, Cold and Arid Regions Environmental and Engineering Research Institute, CAS, Lanzhou 730000, China

tdhan@lzb.ac.cn

Abstract Based on monthly and annual precipitation of the southern and northern slopes of the Tianger Range in the Tien Shan Mountains of China, the spatial-temporal variations of precipitation and their trends were analysed. The analysed precipitation series from the 1950s to 2002 was collected from nine meteorological and hydrological stations (i.e. hydro-meteorological stations), which scatter over the south and north slopes of the Tianger Range in Tien Shan. The statistical analysis shows an increasing trend of precipitation at the north and south slopes of the Tianger Range. The variable coefficient of precipitation is larger at the southern slope, particularly in winter and spring compared with summer and autumn. A decreasing trend of precipitation was found at the Yingxiongqiao Station in the Urumqi River basin. There is a significant inverse correlation in April–May and June–August at the Daxigou Station at the headwater of the Urumqi River, with correlation coefficients of –0.475 and –0.376, respectively.

Key words climate change; precipitation; Tien Shan

INTRODUCTION

In recent decades the global climate has shown a quite obvious warming trend. Climate warming and the speeding up of water circulation in velocity and frequency led to a decreasing tendency to global precipitation (Shi & Chen, 2002). The spatio-temporal variability of precipitation increases, and the differences in precipitation intensity, and daily and monthly variations in different regions become distinct (Kutiel, 1988; Kiely *et al*., 1998; Serrano *et al*., 1999; Groisman *et al*., 2001). However, the precipitation is generally affected by the Westerly current in the Tien Shan of Xinjiang, China, and exhibited an increasing trend in the plain regions and the mountain regions from the mid-1970s and mid-1980s, respectively (Shi *et al*., 2002; Han *et al*., 2003). In this research the characteristics of precipitation on the south and north slopes of the Tianger Range of Tien Shan were studied (Fig. 1). The yearly (monthly) variations and variability of precipitation, its relation to global precipitation changes and the precipitation effects in the climatic transition processes in northwest China, and the response features of precipitation at different aspects and elevations of the Tien Shan, were analysed.

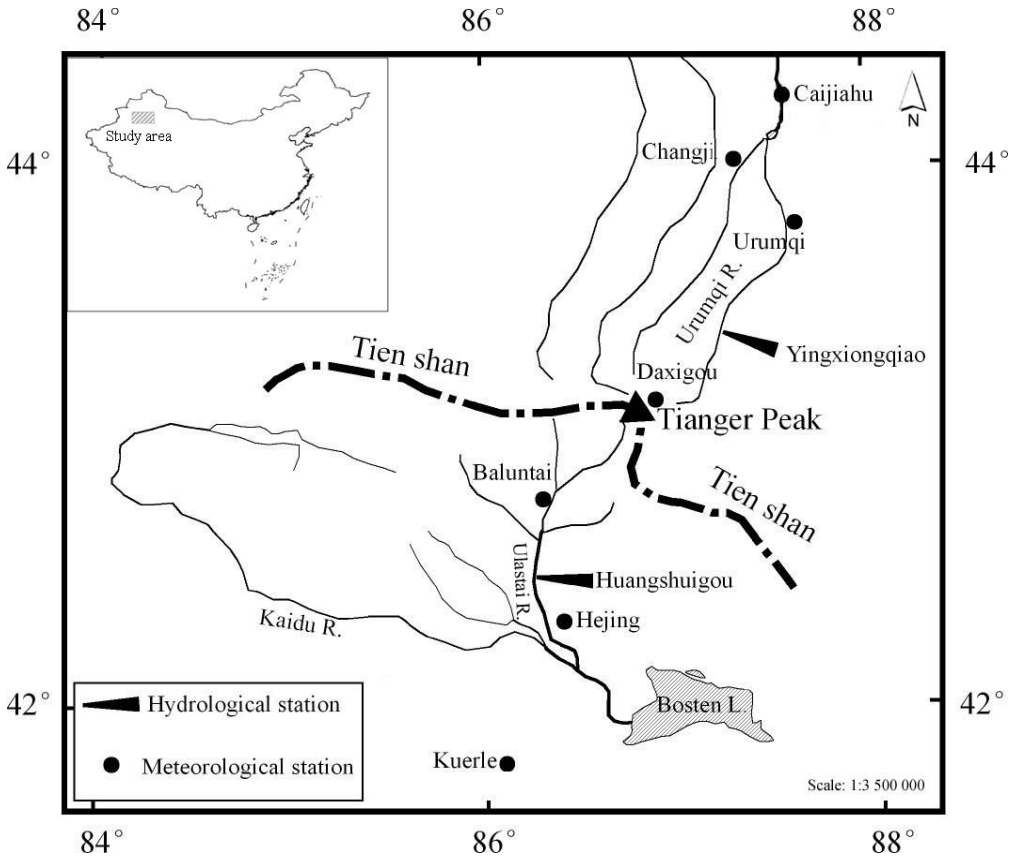

Fig. 1 Sketch map of the studied area and locations of precipitation stations on the north and south slopes of the Tianger Range in Tien Shan.

DATA AND METHODS

The precipitation data at the hydro-meteorological stations at different elevations on the north and south slopes of the Tianger Range of the Tien Shan in the Urumqi and Ulastai River basins are shown in Fig. 1. The stations were selected for statistical analysis, the variations of precipitation at different elevations of the north and south slopes, and at seasonal and annual resolution. Furthermore, the changes in precipitation were correlated with major atmospheric circulation patterns observed between 1950 and 2000. The stations selected on the south slope of the Tianger Range precipitation analysis include Baluntai (1958–2000), Huangshuigou (1958–2001), Hejing (1960–1995) and Kuerle (1959–2000) stations. The stations on the north slope include Yingxiongqiao (1959–2001), Urumqi (1951–2000), Changji (1953–1996); Caijiahu (1959–2000), and Daxigou (1958–2002) stations (Fig. 1). All selected stations have over 20 years of observations. Their average observed precipitation values are basically stable (Li, 2002) and their trend analysis can represent 20 to 50 years climatic variability.

We carried out trend analyses by the trend and correlation analytical method for the long-term precipitation data to examine precipitation variation on the south and north slopes at different elevations, and the seasonal (annual) variation features at all the above stations.

ANNUAL PRECIPITATION AT DIFFERENT ASPECTS AND ELEVATIONS

Variation trend

As seen in Fig. 2, the precipitation values recorded at various stations on the north (Fig. 2(a)) and south slopes (Fig. 2(b)) of the Tianger Range showed an obvious increasing trend. The shifts in time of precipitation from decrease to increase occurred in 1978 and 1987 in the plain regions (e.g. the Urumqi station) and the mountain regions (e.g. the Daxigou station), respectively. Among them, the trend coefficient of precipitation increase at the stations, such as Caijiahu, Urumqi, Daxigou, Baluntai, and Hejing, reached a confidence level of 0.05, while the trend coefficient of precipitation increase at the Huangshuigou station of south slope reached 0.48 (confidence level 0.01). Although the trend coefficient of precipitation increase at Changji station in the plain region of the north slope and the Kuerle station on the south slope did not reach the confidence level of 0.05, the precipitation also showed a slight increasing trend. According to the statistical data, only the precipitation recorded at Yingxiongqiao station in the Urumqi River basin exhibited a slightly decreasing trend (the trend coefficient is –0.20). Han Ping *et al*. (2003) suggested that the regional precipitation in parts of the plain regions exhibited a decreasing trend. However, the decreasing trend of precipitation in the plain regions (includes Urumqi) was less evident, and such a decreasing trend only occurred at the Yingxiongqiao station in the canyon zone of the Urumqi River, and it was most likely this related to the topographic features of the station.

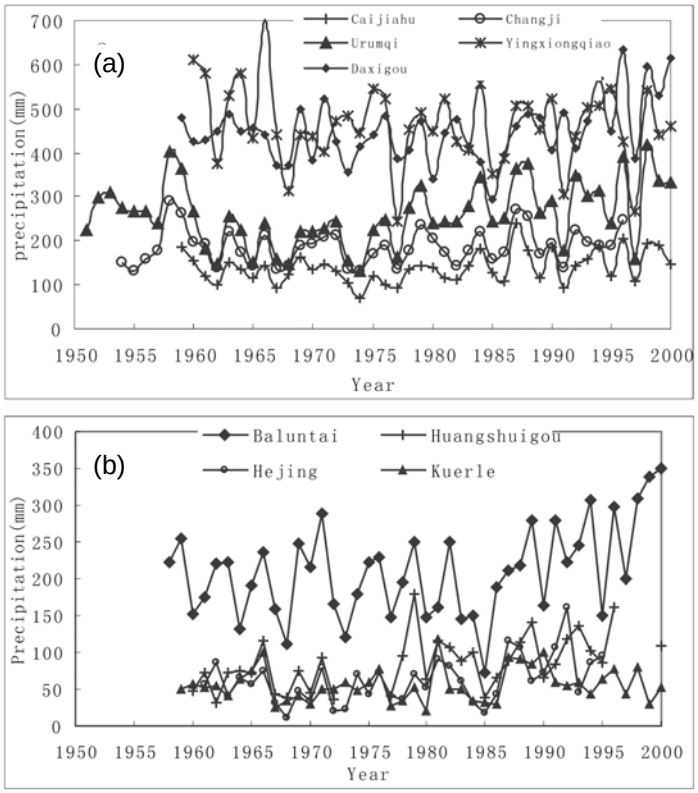

Fig. 2 Changes of annual precipitation on the north (a) and south (b) slopes of the Tianger Range in Tien Shan.

Since the precipitation in Xinjiang mainly comes from the westerly circulation, the north slope of the Tien Shan is its windward slope and receives the moist airflow from the west, and the south slope is the leeward slope; in addition, the local re-evaporated moisture is very important in producing the local precipitation. The precipitation in the Urumqi River basin on the north slope exceeds the precipitation in the Ulastai River basin on the south slope.

Variability analysis

Table 1 lists the station names selected in this study, their elevations and average annual precipitation; these stations are distributed on the south and north slopes of the Tianger Range at 441–3539 m a.s.l. The precipitation shows obvious variation differences on the north and south slopes. They basically reflect the variation characteristics of precipitation with the elevation and aspect in the Urumqi River and Ulastai River basins. Figure 3 shows the increasing trend of precipitation with elevation. Such a trend is even more prominent on the south slope of the Tianger Range; the largest precipitation occurs at the Yingxiongqiao station, on the north slope at the largest precipitation elevation (1600–2100 m) (Ling, 1995).

The annual precipitation variability (Cv) and annual precipitation show an obvious reversed correlation (Fig. 3) and the correlation coefficient is –0.82 (confidence level

Table 1 Elevation and annual precipitation of the stations on the south and north slopes of the Tianger Range, Tien Shan.

Aspect	north slope					south slope			
Station	Caijiahu	Changji	Urumqi	Yingxiongqiao	Daxigou	Baluntai	Huangshui gou	Hejing	Kuerle
Altitude (m)	441	577	918	1920	3539	1739	1313	1102	934
Annual average precipitation (mm)	139.4	186.7	259.9	468.5	449.4	210.0	86.3	62.7	55.9
Recording periods	1959–2000	1953–1996	1951–2000	1959–2001	1958–2002	1958–2000	1958–2001	1960–1995	1959–2000

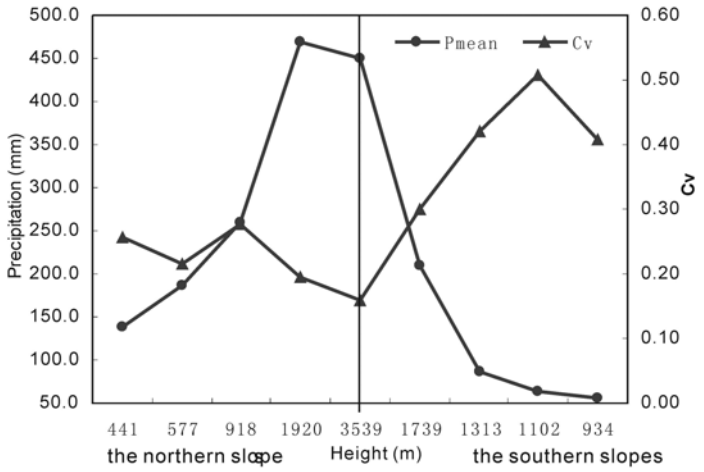

Fig. 3 Annual mean precipitation and variable coefficient at different elevations.

0.01). The Cv on the south slope is significantly larger than that on the north slope, while the Cv in the low mountain (1000–2000 m a.s.l) and the plain zone (<1000 m a.s.l) are larger than that in the middle (2000–3500 m a.s.l) and high mountains (>3500 m a.s.l). The Cv at the Daxigou station at the headwater of the Urumqi River is only 0.16, showing that the variation amplitude of the precipitation in the mountain regions is far smaller than that in other regions.

The correlation of annual precipitation at the stations

Results show that precipitation in the plains regions on the north or south slopes have good correlation among different stations (Table 2); while the correlation between the Daxigou and Yingxiongqiao station is weak. On the contrary, the precipitation at the stations of different elevation on the south slope and the Daxigou station show a favourable correlation. Preliminary analysis shows that the precipitation variations in the middle mountain zone are not entirely synchronous with the low and high mountain zones. The correlation between Yingxiongqiao station and other stations (except Kuerle station) is weak, and unique precipitation variations are often exhibited. These may cause local precipitation by the local re-evaporated moisture, and this might be the reason why the precipitation at Yingxiongqiao station shows a decreasing trend and the first largest precipitation occurs in Tien Shan (Ling, 1995). It seems to be correlated to the precipitation of the same aspect; their correlation coefficient reaches a significance level of over 95% and basically reflects the congeneric character and the consistency of the precipitation south and north of Xinjiang.

ANALYSIS OF MONTHLY PRECIPITATION TREND

Precipitation variation

It can be seen from Fig. 4 that the regional difference in monthly precipitation on the south and north slopes of the Tianger Range are evident: in the area of roughly the

Table 2 The correlation coefficient of annual precipitation on the south and north slopes.

Station	Caijiahu	Changji	Urumqi	Yingxiong qiao	Daxigou	Baluntai	Huangshui gou	Hejing	Kuerle
Caijiahu	1								
Changji	0.828**	1							
Urumqi	0.832**	0.824**	1						
Yingxiong qiao	0.359*	0.463**	0.369*	1					
Daxigou	0.456**	0.383*	0.526**	0.195	1				
Baluntai	0.367*	0.339*	0.464**	0.051	0.863**	1			
Huangshui gou	0.370*	0.494**	0.662**	0.292	0.584**	0.596**	1		
Hejing	0.234	0.353*	0.410*	0.147	0.485**	0.459**	0.457**	1	
Kuerle	0.241	0.270	0.272	0.467**	0.342*	0.151	0.441**	0.511**	1

Note: *indicates the confidence level of 0.05 and ** indicates the confidence level of 0.01.

same elevation, the precipitation on the north slope (Fig. 4(a)) further exceeds that on the south (Fig. 4(b)). In addition, the seasonal difference is large. On the north slope of the Tianger Range, the precipitation is larger in May and June. The largest precipitation occurs in July. The monthly variation processes of the precipitation at Daxigou and Baluntai stations especially are entirely consistent. Research shows that the annual variations of air temperature at these two stations also exhibit a significant correlation (correlation coefficient 0.63) and reach a confidence level of 0.01 (Han, 2002). This demonstrates the similarity of climatic variations in the middle mountain zone of the south slope and in the high mountain zone of the north slope. The precipitation in autumn is a little more than that in spring (from February to April). In winter (from November to January) the precipitation is very sparse.

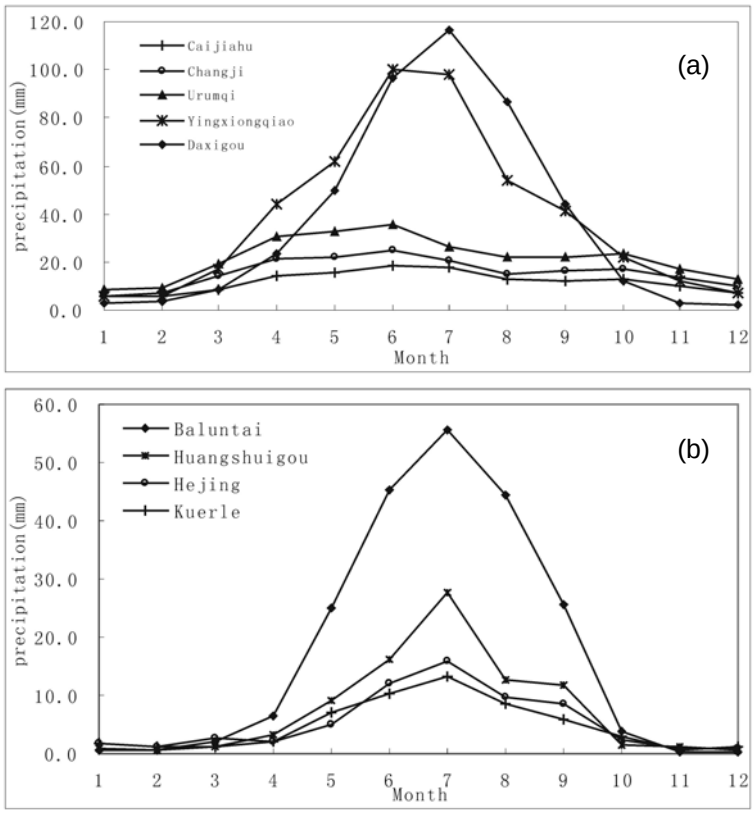

Fig. 4 Monthly precipitation changes on the north (a) and south (b) slopes of the Tianger Range in Tien Shan.

Since the Tien Shan blocks the penetration of the cold air from the north, coupling with the strong cooling effect of the Gobi and underlying desert surface, temperature inversion layer often develops steadily in the Urumqi River basin on the north slope in winter, and its upper limit may reach an elevation of over 2200 m or more (Han, 2002). The intense development of the temperature inversion layer leads to the lowering of the height of vapour condensation (Aizen *et al*., 1996; Han, 2002). Accordingly the precipitation in the plain zone of the north slope of Tien Shan in winter (especially

between November and December) is larger than that in the middle and high mountain zones. Such a precipitation variation tends to become normal as the temperature inversion layer disappears and the precipitation once again shows an increasing trend with the increasing height, but such a variation feature of precipitation is not found on the south slope in winter.

Precipitation variability

The monthly precipitation variability on the south and north slopes of Tien Shan exhibits an obvious regional difference (Fig. 5). Similar to the annual variations of the precipitation variability, the monthly precipitation variability is much larger on the south slope than on the north slope, and it also shows a large seasonal difference. The precipitation variability on the north slope is relatively small and its seasonal difference is also small. The precipitation variability at the Yingxiongqiao and the Daxigou on the north slope is smaller in summer (from May to September) than that in other seasons. The precipitation variability at the Daxigou on the north slope in winter is the largest. The precipitation variability on the south and north slopes in summer is smaller than that in other seasons.

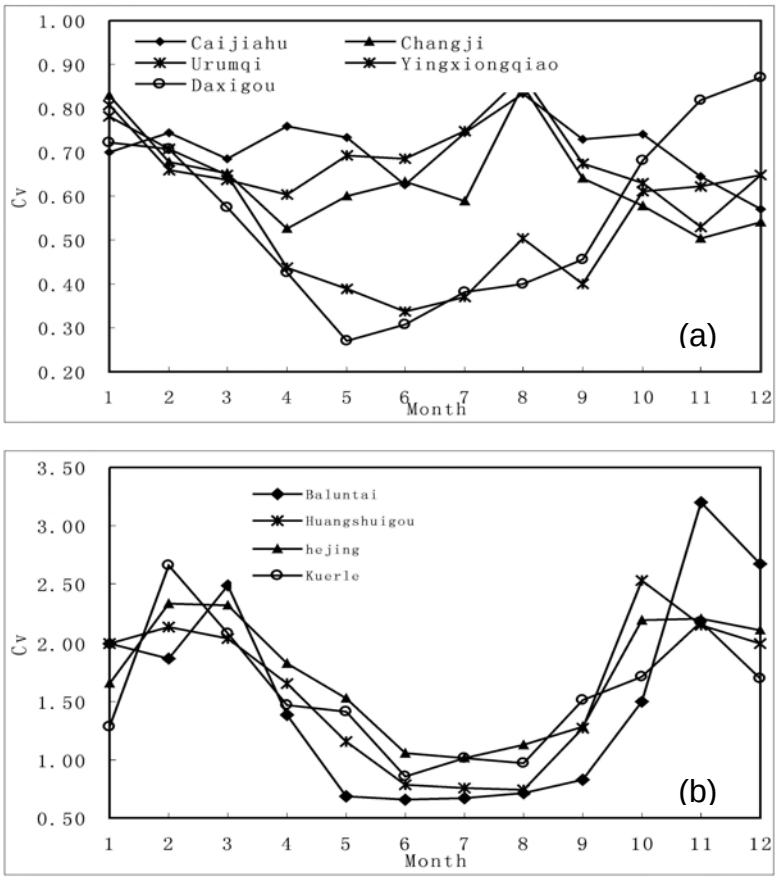

Fig. 5 Monthly precipitation variable coefficient on the north (a) and south (b) slopes of the Tianger Range in Tien Shan.

Trend analysis of precipitation

The precipitation at Yingxiongqiao station on the north slope of the Tien Shan shows a slightly increasing trend in winter. But in other months it exhibits a decreasing trend, which is especially evident in March (Fig. 6), with a trend coefficient of –0.325. The precipitation at Caijahu station in almost all months exhibits an increasing trend, but in March it exhibits an obvious decreasing trend (Fig. 6), and the trend coefficient is –0.315. They all reach the confidence level of 0.05. Similarly, the monthly precipitation at Hejing station on the south slope of Tien Shan shows a less evident variation trend, but in November it significantly decreases (Fig. 6); the trend coefficient is –0.335, and it also reaches the confidence level of 0.05.

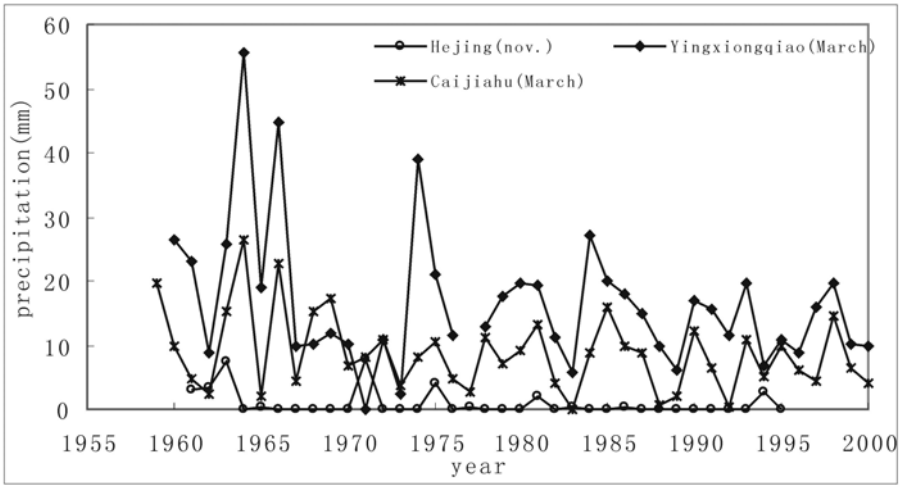

Fig. 6 Decreasing trend of the monthly precipitation on the south and north slopes of the Tianger Range in Tien Shan.

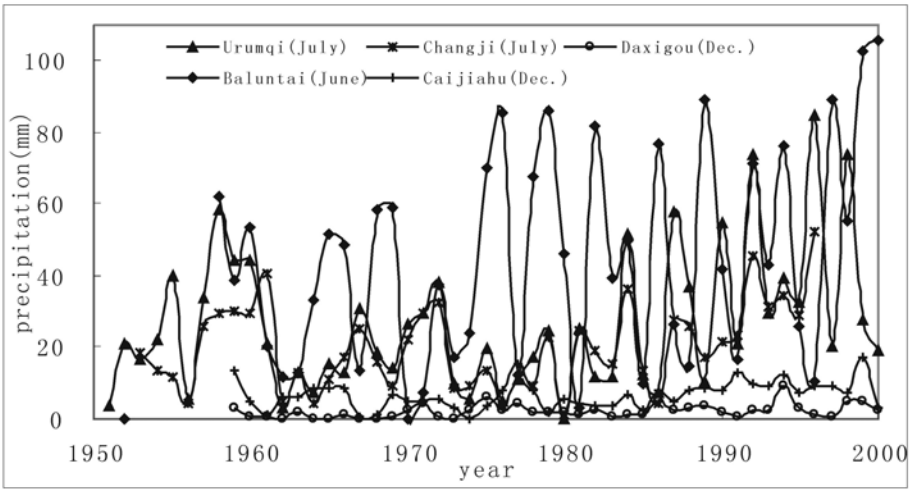

Fig. 7 Increasing trend of the monthly precipitation on the south and north slopes of the Tianger Range in Tien Shan.

The monthly precipitation at various stations mainly shows an obvious increasing trend (Fig. 7). The months in which the monthly precipitations trend coefficient reaches confidence levels of over 0.05 include: June at Baluntai; July at Caijiahu, Urumqi and Huangshuigou; January at Urumqi; November and December at Daxigou; and December at Caijiahu stations. The statistical results show that the increasing trend of monthly precipitation is mainly concentrated in summer and winter. In the plain regions the increase in precipitation mainly occurs in summer, but in the high mountain zone the winter precipitation exhibits an even more obvious increasing trend. The trend coefficient of precipitation increase at Daxigou station in December is 0.40 (the confidence level is 0.01). Furthermore, it corresponds to the obvious winter warming processes at the headwater of the Urumqi River in the Tien Shan (Han, 2002).

ANALYSIS OF CORRELATION OF INTERMONTHLY PRECIPITATION VARIATIONS

In the analysis of annual precipitation variations, the distribution proportion and difference of the monthly (seasonal) precipitation in the annual total precipitation are mostly considered, but their correlations are seldom analysed. Therefore, we made a correlation analysis on the month to month data at different stations. The analytical results show that the monthly precipitation, on the whole, is positively correlated to the precipitation in various months of a year, but also to existing obvious negative correlation. Since the precipitation on the south slope of the Tien Shan is mainly concentrated in summer, and spring and winter often have no precipitation at all in a whole month, the monthly correlation analysis therefore has no substantial climatic significance, so no detailed analysis is given here. The correlation analysis mainly focuses on the variations of precipitation on the north slope.

The winter and spring precipitation on the north slope of Tien Shan is obviously positively correlated to summer precipitation. The selected stations which reach the confidence level of 0.01 include: Urumqi (April–July and May–July), Caijiahu (Jan.–July and April–July). The stations that reached the confidence level of 0.05 include: Caijiahu (July–Nov. and July–Dec.), Changji (Jan.–Sept.), Yingxiongqiao (Feb.–March and June–Dec.) and Daxigou (Feb.–March and June–Dec.). It can be seen that the monthly precipitation in winter and spring partly pre-indicate the precipitation in July of the current year, and such a relationship is even more evident in the plain region.

Besides the positive correlation of the precipitation, there is also obvious negative correlation between the precipitation in April and May, as well as in June and August at Daxigou station in the high mountain zone on the north slope of the Tien Shan (Fig. 8). Their correlation coefficients are –0.475 and –0.376, respectively, and their confidence levels reach 0.01 and 0.05, respectively.

CONCLUSIONS

Annual precipitation recorded at various stations on the south and north slopes of the Tianger Range exhibit increasing trend. The shifts time of precipitation from decrease

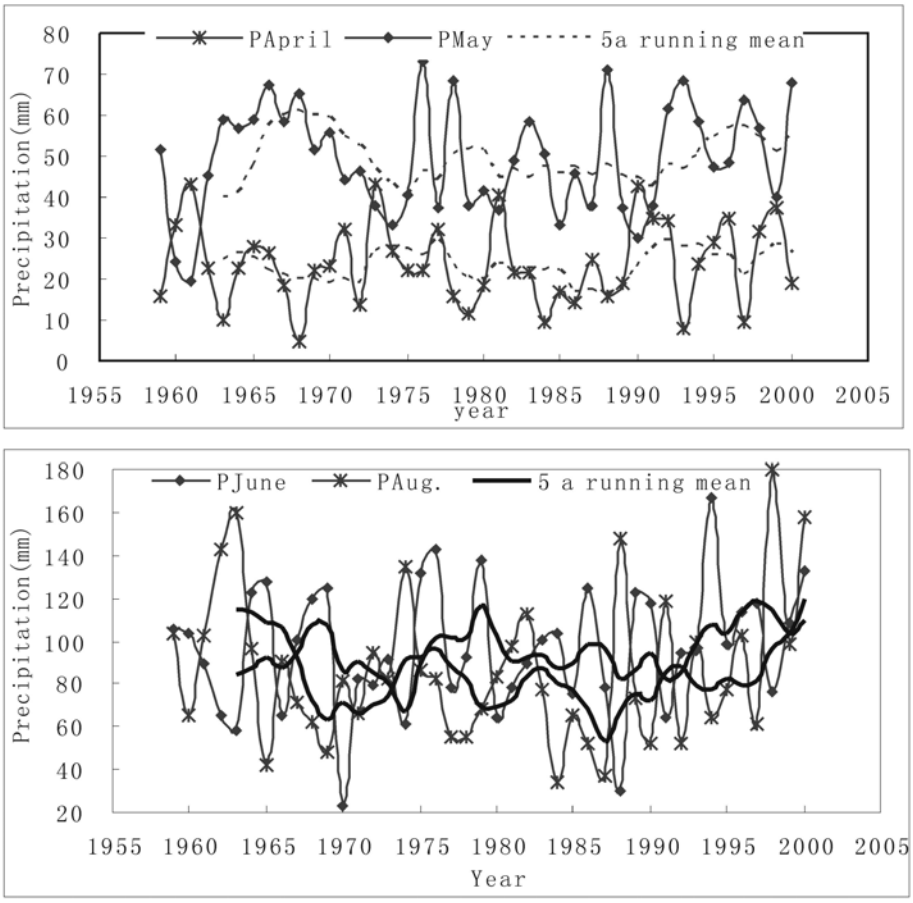

Fig. 8 The inverse correlation of monthly precipitation at the Daxigou station in the headwaters of the Urumqi River.

to increase is around the mid-1970s and mid-1980s at different elevations, respectively.

Annual precipitation variability (Cv) and annual precipitation amounts at different aspects and elevations exhibit an obvious reverse correlation. The Cv is significantly larger on the south slope than that on the north slope. Its seasonal difference is also larger than that of the north slope. The seasonal characteristics of the precipitation on the south slope are similar to those of the high mountain zone (e.g. Daxigou station).

Precipitation in winter (especially in Nov. and Dec.) is larger in the plain zone than that in the middle and high mountain zones. The largest monthly precipitation in the plain of the north slope generally occurs in May to June. The precipitation at Daxigou Station in April and May, as well as in June and August, exhibits an obvious negative correlation.

Acknowledgements This research was supported by National Basic Research Program of China (973 Program) no. 2007CB411500, the Knowledge-Innovation Program of Chinese Academy of Sciences (KZCX3-SW-345) and the project of National Natural Science Foundation of China (40371026). We thank Vladimir Aizen for his valuable

comments and suggestions, and Patrick Ginot, the Scientific Editor. We also thank Zhang Weimin, Sun Liangying and Shangguan Donghui for suggestions.

REFERENCES

Aizen, V. B., Aizen, E. M. & Melack, J. M. (1996) Precipitation, melt and runoff in the northern Tien Shan. *J. Hydrol.* **186**, 229–251.

Groisman, P. Y., Knight R. W. & Karl, T. R. (2001) Heavy precipitation and high streamflow in the contiguous United States: trends in the twentieth century. *Bull. Am. Met. Soc.* **82**(2), 219–246.

Kiely, G., Albertson, J. D. & Parlange, M. B. (1998) Recent trends in diurnal variation of precipitation at Valentia on the west coast of Ireland. *J. Hydrol.* **207**, 270–279.

Kutiel, H. (1988) Rainfall variations in the Galilee (Israel): variations in the temporal distribution between 1931–1960 and 1951–1980. *J. Hydrol.* **99**, 179–185.

Han, P., Xue, Y. & Su, H. (2003) Precipitation signal of the climatic shift in Xinjiang Region. *J. Glaciol. & Geocryol*. **25**(2), 179–182.

Han, T., Ye, B. & Jiao, K. (2002) Temperature variations in the southern and northern slopes of Mt. Tianger in the Tianshan Mountains. *J. Glaciol. & Geocryol*. **24**(5), 567–570.

Li, S., Cheng, G., Li, Y. *et al.* (2002) *Water Resources Rational Utilization and Environments Protect in the HEXI Corrido Huanghe River*, 17–27. Hydraulic Publishing House, Zhengzhou, China.

Ling, Z. (1995) *Climatology of Orographic Precipitation*, 26–32. Science Press, Beijing, China.

Serrano, A., Mateos, V. L. & Garcia, J. A. (1999) Trend analysis of monthly precipitation over the Iberian Peninsula for the period 1921–1995. *Phys. Chem. Earth (B)* **24**(1–2), 85–90.

Shi, N. & Chen, L. (2002) Precipitation fluctuation over globe land area in 1948–2000. *Chinese Sci. Bull.* **47**(21), 1671–1674.

Shi, Ya., Shen, Y. & Hu, R. (2002) Preliminary study on signal, impact and foreground of climate shift from warm-dry to warm-humid in northwest China. *J. Glaciol. & Geocryol.* **24**(3), 219–226.

Xue, Y., Han, P. & Feng, G. (2003) Change trend of the Precipitation and air temperature in Xinjiang since recent 50 years. *Arid Zone Res.* **20**(2), 127–130.

Yang, L. (2003) Climate change of extreme precipitation in Xinjiang. *Acta Geographica Sinica* **58**(4), 577–583

International Association of
Hydrological Sciences

Association Internationale
des Sciences Hydrologiques

IAHS AISH

www.iahs.info

IAHS Publication 318 ISBN 978-1-901502-39-8 ISSN 0144-7815